Doctoral Thesis

SOLAR PHOTO-FENTON TREATMENT OF EU PRIORITY SUBSTANCES
–
PROCESS PARAMETERS AND CONTROL STRATEGIES

DI Wolfgang Gernjak

Vienna, March 2006

Universität für Bodenkultur Wien
University of Natural Resources
and Applied Life Sciences, Vienna

Department für Wasser-Atmosphäre-Umwelt

Institut für Siedlungswasserbau, Industriewasserwirtschaft und Gewässerschutz

SOLAR PHOTO-FENTON TREATMENT OF EU PRIORITY SUBSTANCES

–

PROCESS PARAMETERS AND CONTROL STRATEGIES

Dissertation
zur Erlangung des Doktorgrades
an der Universität für Bodenkultur Wien

Betreuerin: AO.Univ.Prof.DI.Dr.nat.techn. Maria Fürhacker

Eingereicht von: DI Wolfgang Gernjak

Wien, März 2006

Deutsche Kurzfassung

In Zusammenhang mit der europäischen Wasserrahmenrichtilinie (EU Direktive 2000/60) und der sogenannten IVU-Richtlinie (EU Direktive 1996/61) besteht Bedarf an flexiblen Abwasserbehandlungsverfahren imstande mit toxischen Substanzen belastete Industrieabwässer zu klären. Unter den chemisch-oxidativen Verfahren sind die sogenannten Advanced Oxidation Processes (AOP) bekannt dafür, nahezu alle organischen Schadstoffe behandeln zu können.

Die vorliegende Arbeit berichtet über die Anwendung des solaren Photo-Fenton-Verfahrens, einer der genannten AOPs, zur Behandlung von Modellabwässern, welche elf verschiedene Schadstoffe enthalten, allesamt durch die Europäische Wasserrahmenrichtlinie als prioritäre Substanzen klassifiziert. Sämtliche experimentelle Arbeiten wurden in Pilotanlagen durchgeführt, deren Solarkollektoren auf der "Compound Parabolic Collector" Technologie basieren.

Sieben Pestizide (Alachlor, Atrazin, Chlorfenvinphos, Diuron, Isoproturon, Lindan, Pentachlorophenol) wurden erfolgreich in Metabolite umgewandelt (Konzentration zu Beginn der Behandlung 20 – 50 mg L^{-1}, je nach Löslichkeit). Der vollständige Abbau bis zu CO_2 wurde im Fall von Alachlor, Chlorfenvinphos, Lindan und Pentachlorophenol erreicht. In Übereinstimmung mit berichteten Ergebnissen von anderen oxidativen Verfahren konnten Atrazin, Diuron und Isoproturon nicht vollständig abgebaut werden. Drei nicht biologisch abbaubare chlorhaltige Lösungsmittel (Dichlormethan, Trichlormethan, 1,2-Dichlorethan, Anfangskonzentrationen von 50 mg L^{-1}) konnten vollständig abgebaut werden. Ein Tensidmetabolit (4-Nonylphenol, Anfangskonzentration 2 mg L^{-1}) wurde ebenfalls erfolgreich abgebaut.

Im Rahmen dieser Arbeit wurde eine neue Pilotanlage errichtet, in welcher im Sonnenkollektor Absorberrohre mit erhöhtem Innendurchmesser eingesetzt wurden (46,4 mm anstelle von 29,2 mm in vorhergehenden Anlagen). Es wurde theoretisch und experimentell gezeigt, dass der erhöhte Innendurchmesser zu besseren Resultaten führt. Erstens war der Reaktordurchsatz pro Quadratmeter Sonnenkollektor höher; zweitens wurden praktische und ökonomische Vorteile aufgezeigt bezüglich der Konstruktionsmaterialen und Instandhaltung. Schliesslich können aufgrund der erhöhten optischen Weglänge niedrigere Katalysatorkonzentrationen eingesetzt werden

(<20 mg L^{-1}), welche eine Eisenabtrennung nach der oxidativen Behandlung und vor Einleitung in eine biologische Kläranlage obsolet machen.

Alachlor wurde als Modellsubstanz ausgewählt (Anfangskonzentration 100 mg L^{-1}) um den Einfluss von drei Prozessparametern (Eisenkonzentration, Temperatur, Verhältnis von beleuchtetem zu nicht beleuchtetem Volumen) zu untersuchen. Zu diesem Zweck wurde ein faktorielles Design ohne Sternpunkte durchgeführt (Eisenkonzentration 2 – 20 mg L^{-1}, Temperatur 20 – 50ºC, Anteil des beleuchteten Volumens 11,9 – 59,5%).

Eine Erhöhung von Temperatur, Eisenkonzentration oder Anteil des beleuchteten Volumens vom minimalen zum maximalen untersuchten Wert bewirkte eine Verringerung der Behandlungszeit zur Erlangung von 80% Reduzierung des gelösten Gesamtkohlenstoffes (DOC) um einen Faktor von ca. jeweils 5, 6 oder 2. Wurden mehrere Parameter gleichzeitig geändert, so multiplizierten sich diese Faktoren miteinander, was insgesamt zu Abbauzeiten von 20 bis 1250 Minuten führte.

Mithilfe der „Response Surface Methodology" (RSM) wurden mathematische Modelle entwickelt, um die Zeit vorherzusagen, die der Abbau des DOC um 50 bzw. 80% benötigt. Ein weiteres Modell - basierend auf der „Logistic Dose Response" Gleichung - wurde entwickelt, welche die gesamte DOC Abbaukurve vorhersagt. Die drei variierten Prozessparameter sind jeweils unabhängige Eingangsparameter in den Modellen.

Mehrere Analyseparameter, welche ökonomisch online gemessen werden können, wurden auf ihre potentielle Anwendbarkeit für Prozesskontrollzwecke geprüft. UV/Vis Absorbanzmessungen zeigten, dass im Fall von aromatischen Schadstoffen die Absorbanz zu Beginn der oxidativen Behandlung zunimmt. Dies ist bedingt durch die Formierung von Zwischenprodukten im oxidativen Abbau, die Phenol-, Hydroquinon- und Quinonstrukturen enthalten. Wenn diese Zwischenprodukte weiter oxidiert werden, sinkt die Absorbanz wieder. Der gelöste Sauerstoff (DO) zeigt einen charakteristischen Anstieg zu übersättigten Werten, sobald die Konzentration der gelösten organischen Substanzen gering ist. Wenig Nutzen für Prozesskontrollzwecke konnte aus dem Oxidations-Reduktions Potential (ORP) gezogen werden. Ausschließlich zu Beginn zeigte der ORP Wert die Umwandlung von zweiwertigem zu dreiwertigem Eisen. Die Messung des pH-Werts zeigte sich als nützlich aufgrund seiner intrinsischen Bedeutung für den Prozess. Weiters konnten Veränderungen des pH-Werts während der Behandlung beobachtet werden, welche die chemische Umwandlung der Schadstoffe widerspiegelten - z.B. Ansäuerung durch die Formung von Salzsäure aus chlorierten Verbindungen. Der Wasserstoffperoxidverbrauch zeigte sich als direkt korreliert mit

dem Fortschritt des DOC-Abbaus unabhängig von anderen Abbauparametern. Somit kann durch seine Messung der DOC-Abbaugrad bestimmt werden. Die Konzentration des Wasserstoffperoxides in der Pilotanlage konnte mittels Anwendung eines Proportional-Integral (PI) Controllers, welcher die Dosierrate einer Wasserstoffperoxidpumpe steuerte, erfolgreich kontrolliert werden.

Abstract

Regarding the European Water Framework directive (EU directive 2000/60) and the IPPC directive (EU directive 1996/61) flexible wastewater treatment methods are required, which are able to treat industrial waste water contaminated with toxic substances. Among chemical-oxidative treatments the so-called Advanced Oxidation Processes (AOP) are well-known for their potential to be capable of treating almost all organic contaminants.

This work reports upon the application of solar photo-Fenton treatment, an AOP, on model waste waters containing eleven different contaminants, all classified as Priority Substances by the European Water Framework Directive. All experimental work was performed in solar pilot-plants, whose solar collector is based on Compound Parabolic Collector technology.

Seven pesticides (alachlor, atrazine, chlorfenvinphos, diuron, isoproturon, lindane and pentachlorophenol) were degraded successfully at initial concentrations from 20 to 50 mg L^{-1}, depending on their solubility. Mineralisation of the compound was complete in the case of alachlor, chlorfenvinphos, lindane and pentachlorophenol. Atrazine, diuron and isoproturon could not be mineralized completely as reported before for other oxidative treatments. Three non-biodegradable chlorinated solvents (dichloromethane, trichloromethane and 1,2-dichloroethane) could be degraded and mineralized completely at an initial concentration of 50 mg L^{-1}. One surfactant metabolite (4-nonylphenol) was successfully degraded at an initial concentration of 2 mg L^{-1}.

In the course of the work a new pilot-plant was constructed, in which increased absorber tube diameters were used in the Compound Parabolic Collector (46.4 mm inner diameter instead of 29.2 mm in previous plants). It was theoretically and experimentally proved that the increased absorber tube diameter had a better performance compared to the one used previously. First, the plant throughput per square metre solar collector under otherwise identical conditions is higher with the bigger diameter. Second, there are several practical and economical advantages regarding construction material and maintenance. Finally, lower catalyst concentration (<20 mg L^{-1}) can be applied, which makes iron separation after the oxidation step before discharge into a common biological treatment plant obsolete.

Alachlor was chosen as a model contaminant (initial concentration 100 mg L^{-1}) to assess the influence of three process parameters (iron concentration, temperature, ratio

between illuminated and dark volume). An experimental design following a Central Composite Design without star points was performed (iron concentration 2-20 mg L^{-1}, temperature 20-50ºC, illuminated volume 11.9 – 59.5% of total volume).

An increase in temperature, iron concentration and illuminated volume from minimum to maximum value reduced the time required for 80% degradation of initial Dissolved Organic Carbon (DOC) by approximate factors of 5, 6 and 2, respectively. When process parameter changes were made simultaneously, these factors multiplied each other, resulting in degradation times between 20 and 1250 minutes.

Models were designed to predict the time necessary to degrade 50% or 80% of the initial DOC applying Response Surface Methodology (RSM). Another model based on the Logistic Dose Response curve was also designed, which predicted the whole DOC degradation curve over time. The three varied process parameters (temperature, iron concentration and illuminated volume) were independent variables in all the models.

Several parameters, which can be measured economically on-line, were assessed for their potential application for process control purposes. UV/Vis absorbance measurements indicated that in the case of aromatic pollutants during the initial phase of the oxidative treatment the absorbance increases. This is due to the formation of intermediate degradation products containing phenol, hydroquinone and quinone structures. When these intermediates are further oxidised the absorbance decreases again. Dissolved Oxygen (DO) evolution inside the plant showed a characteristic increase reaching supersaturation levels, when the organic content inside the plant was low. Oxygen Reduction Potential (ORP) provided little valuable information for process control. Only, in the initial stages the ORP value reflected the transformation of ferrous to ferric iron. The measurement of the pH value proved to be useful due to its intrinsic importance in the process. Moreover, changes in the pH value during the treatment were observed, which were related to the chemical transformation of the contaminants, e.g. acidification by the formation of hydrochloric acid from chlorinated compounds. Hydrogen peroxide consumption was found to be directly correlated with the process progress independent of other process variables. Thus, by measuring its consumption the degree of oxidation of the waste water can be determined. Hydrogen peroxide concentration inside the pilot-plant could be successfully controlled by applying a proportional-integral (PI) controller acting upon the dosage rate of a hydrogen peroxide administering pump.

Acknowledgements

A doctoral thesis means quite a time of dedication and considerable effort. One can feel lucky, if looking back after such a period, it becomes obvious how many people gave their support willingly. I would like to take the opportunity to thank some of them.

- AO Prof Dr. Maria Fürhacker, who accepted my pledge for tutoring this doctoral thesis under the special circumstances of this Ph.D.
- Dr. Sixto Malato, who, without doubt, resolved many of my big and small problems, no matter if of administrative, scientific or sometimes also personal character.
- José Domingo Álvarez and Luis Yebra, whose help with the control topics was essential.
- Martín Vincent from Ecosystem S.A., who did a great job in all the set-up of the pilot plant.
- Tom, Georg and Ana, who helped to reduce the countless errors in the manuscript.
- Eva Augsten and Remedios Berruezo, who helped me with much of the experimental work.
- Agustín, Nacho, Pilar, Isa, Leo, Cosima, Bella, Diego and Julián, my colleagues from the "Environmental Applications of Solar Energy and Characterisation of Solar Radiation" at PSA, but also all the other colleagues at PSA.
- The institutions supporting my Ph.D. by awarding me grants, which are the "Austrian Academy of Sciences" (DOC grant), the "Österreichische Studienbeihilfenbehörde" and, once more, the "Plataforma Solar de Almería" within the framework of the agreement with the University of Almería. Financing of the experimental work through the "CADOX" project (European Commission, 5th Framework Programme, contract no. EVK1-CT-2002-00122) is acknowledged as well.

Finally, what would be life without friends and family? Well, to cut it short… Thanks to everybody supporting me and special thanks to my parents, who had to accept that their little son thought that he should be happy so far away from home.

Table of contents

1 Introduction

1.1 Water stress – Most relevant European Union legislation and related policies

Water, pre-requisite for life and key resource of humanity, is abundant on earth (about 1400 million km^3). However, 97.5% is salt water. Of the remaining 2.5% that is fresh water, 70% is frozen in the polar icecaps; the rest is mainly present as soil moisture or in inaccessible subterranean aquifers. Only less than 1% of the world's fresh water resources are readily available for human use; and even this resource is very unevenly distributed [1].

On the "blue planet" in the year 2002 around 1.1 billion people still lacked access to improved sources of water, and about 2.6 billion had no access to any form of improved sanitation. As a consequence, 1.6 million people in developing countries, more of 90% of them children, die every year from diseases associated with lack of safe drinking water, inadequate sanitation and poor hygiene [2].

While in developing countries the problems linked to lack of safe drinking water supply and improved sanitation are tremendous, within the so-called developed countries these infrastructures are fairly well built-up (coverage 98% in 2002 [2]). Therefore, in these regions concerns related to the water cycle focus on water stress caused by anthropogenic influences such as industrial, agricultural or human dwelling activities and the whole range of its impact on health associated, environmental and socio-economical issues.

Within the European Union (EU) pressure on water supply is especially high in arid regions with scarce fresh water resources such as the Mediterranean Basin [3]. Contamination by refractory organic substances significantly affects the viability of sustainable water re-use strategies applying treated municipal or industrial water effluents as potential alternative water sources. Since long, plant protection products, substituted phenols, non-biodegradable chlorinated solvents (NBCS) and surfactants are recognised as examples for relevant substances [4]. More recently, pharmaceuticals and personal care products (PPCPs) and especially endocrine disrupting chemicals (EDCs) are considered as emerging contaminants, which are still unregulated or in process of regularisation [5].

Adverse health and other potential effects of many contaminants present in water are still uncertain and lacking investigation. EU legislation takes into account increasing knowledge and continuously adapts the legal framework to protect and improve the quality of Europe's fresh water resources. The most recent update was the European Water Framework Directive (WFD) [6]. Therein, one of the most important instruments applied is the identification of Priority Substances (PS) and Priority Hazardous Substances (PHS) [7] that are considered of crucial impact concerning the future situation of the pollution of Europe's aquatic environment. Depending on the classification the identified substances are subject to strict regulation (PS) or to a planned complete phase-out of their application until 2020 (PHS). 23 PS and 10 PHS have been identified up-to-now [8].

Prior to the WFD, EU water legislation is set out in the following main directives: the Dangerous Substances Directive [4] and its daughter Directives controlling pollution of surface waters with dangerous substances from industrial installations; the Integrated Pollution Prevention and Control Directive (IPPC) [9] controlling pollution of surface water with dangerous substances from large industrial installations; the Drinking Water Directive [10] safeguarding human health by establishing strict standards for the quality of water intended for human consumption; the Urban Waste Water Treatment Directive [11] controlling pollution, in particular, eutrophication of surface water with nutrients (particularly nitrogen and phosphorus) from urban waste water; the Nitrates Directive [12] controlling nitrate pollution from agricultural sources, complementing the Urban Waste Water Treatment Directive and the Bathing Water Directive [13] safeguarding the health of bathers and maintaining the quality of bathing waters.

In the Lisbon strategy the EU set itself the goal of becoming "*the most competitive and dynamic knowledge-based economy in the world, capable of sustained economic growth with more and better jobs and greater social cohesion*" [14, 15]. Later, at the Gothenburg European Council in 2001 [16] and enlarged to a global scale in the Johannesburg Summit on Sustainable Development in 2002 [17] the EU committed itself to the EU sustainable development strategy. The EU sustainable development strategy is based on the principle that economic growth and environmental protection should go hand in hand. In other words, development and application of environmental technologies help to meet increased demands for a cleaner environment at lower costs. Thereby, environmental technologies play an important role in de-coupling environmental impacts from economic growth [18]. To promote enhanced market

penetration of environmental technologies the EU set up the so-called Environmental Technologies Action Plan (ETAP) [19]. Within the ETAP the role of the EU as a global player and the resulting possibilities for economic growth and positive global environmental and social impact are well acknowledged.

To meet the internal goals set by EU legislative framework and diminish contamination and environmental risks throughout the EU water bodies, pollutant sources have to be identified and appropriate environmental technologies developed and implemented, among them sustainable mitigation strategies as suggested by the ETAP. A series of innovative processes and process combinations with great potential benefit compared to state-of-the-art water technologies have been identified, e.g. Advanced Oxidation Processes (AOP), the combination of AOP and biological treatment and the application of solar radiation as a driving force of the AOP process stage [20, 21].

1.2 The addressed problem

Since the first European directive in 1976 [4], much progress has been made in tackling point source contamination of Europe's waters, but severe pressure remains regarding Priority Substances (PS). There are also a number of additional wastewater problems regarding non-biodegradable waste water, such as PPCP, dyes or certain agricultural waste waters, which have to be dealt with. Therefore, human health is threatened by pesticides, heavy metals, hydrocarbons, chlorinated hydrocarbons, etc. dissolved in water whose source is usually industrial wastewaters containing these PS at low-medium concentration (<500 mg L^{-1}). In this context, the IPPC Directive [9] has requested the development of technologies and management practices for specific industrial sectors (see Annex I of the Directive) for the minimisation of pollution and for the development of water recycling. Due to the lack of available on-site treatment technologies, a large quantity of the industrial activities included in Annex I of IPPC Directive are not treating their wastewaters appropriately. As a consequence, simple, low cost and at-hand technologies are strongly necessary to treat non-biodegradable wastewater. Oxidation technologies, among them AOPs (e.g. photo-Fenton treatment), are considered an interesting option to solve this problem, because of their versatility.

1.3 Objectives of this work

The objective of this Ph.D. thesis is to enhance the available knowledge on solar photo-Fenton treatment. On the basis of solar pilot-plant experimentation the viability of photo-Fenton technology shall be proved for a variety of waste water containing different contaminants. Special emphasis will be laid on medium/ highly soluble substances classified as PS by the EU within the WFD. The process shall be investigated, so that conclusions may be drawn how to implement and operate the process in a more cost-efficient way leading in the end to commercialisation.

Specific objectives are:

- The installation of a pilot-plant with new solar collector technology, on-line measurement and the development of a tailor-made Supervisory Control and Data Acquisition (SCADA) system.

- To prove the process feasibility and identify eventual problems a variety of model waste water containing Priority Substances (PS) will be treated by the photo-Fenton process. These are pesticides and mixtures of pesticides at low to medium concentration $(50 - 150 \text{ mg L}^{-1})$, non-biodegradable chlorinated solvents (NBCS, 50 mg L^{-1}) and 4-nonylphenol solutions at low concentration (2 mg L^{-1}).

- To assess the influence of process parameters such as catalyst concentration and solution temperature.

- To assess how the plant configuration (share of illuminated volume in the solar collectors, share of volume in the tanks) affects the process performance.

- To perform a screening for parameters, which could be measured on-line and check their usefulness for application in automated process control strategies.

2 Fundamentals

2.1 Solar resources and solar technology for water treatment

2.1.1 Solar resources

The earth receives about 1.7×10^{14} kW of solar radiation, meaning 1.5×10^{18} kWh per year. Extraterrestrial radiation has an intensity of 1367 W m^{-2} [22] and a wavelength of between 0.2 μm and 50 μm, which is reduced to between 0.28 μm and 4.0 μm when reaching the planet's surface due to the absorption of the rest by different atmospheric components (mainly ozone, oxygen, carbon dioxide, aerosols, steam, clouds). The solar radiation that reaches the ground without being absorbed or scattered is called direct beam radiation; radiation that reaches the ground but has been dispersed before is called diffuse radiation, and the sum of both is called global radiation.
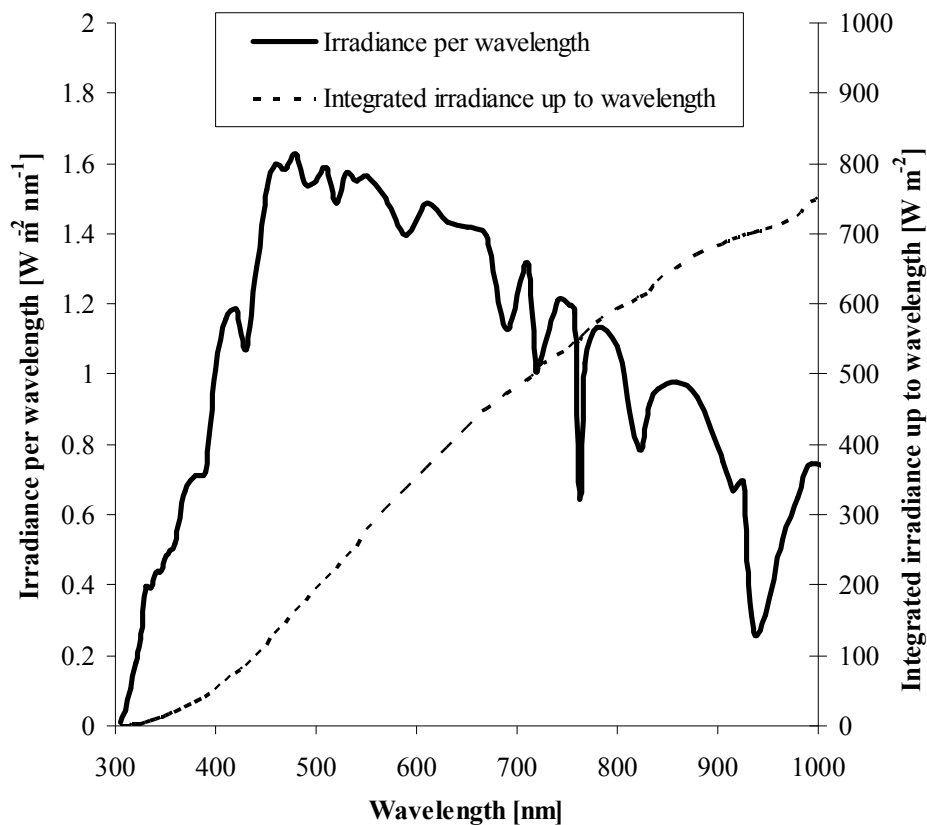
Figure 2.1: ASTM global irradiance standard solar spectrum (AM 1.5) up to a wavelength of 1000 nm, incident on a plane tilted 37º facing the sun, normalised to 1000 W m^{-2} for the whole spectrum (up to a wavelength of 4000 nm) [23]

Figure 2.1 shows the standard solar radiation spectrum [23] at sea level on a clear day for a standard atmosphere. The spectral irradiance data is for the sun at a solar zenith angle of 48.19°. This zenith angle corresponds to an air mass (AM) of 1.5, which is the ratio of the direct-beam solar-irradiance path length through the atmosphere at a solar zenith angle of 48.19° to the path length when the sun is in the zenith. AM = 1 when the sun is directly overhead (zenith). The AM 1.5 global irradiance is shown for a flat surface facing the sun and tilted 37° from the horizontal. The 37° tilt angle is used because it corresponds to the latitude of the Plataforma Solar de Almería.

The radiation effectively reaching the ground level varies strongly due to several factors, such as geographic latitude, date, time of day, atmospheric conditions (aerosols, humidity, etc.) or simply cloudiness. **Figure 2.2** shows the global UV irradiance measured at Plataforma Solar de Almería on a plane tilted 37° on cloudless days in different seasons.
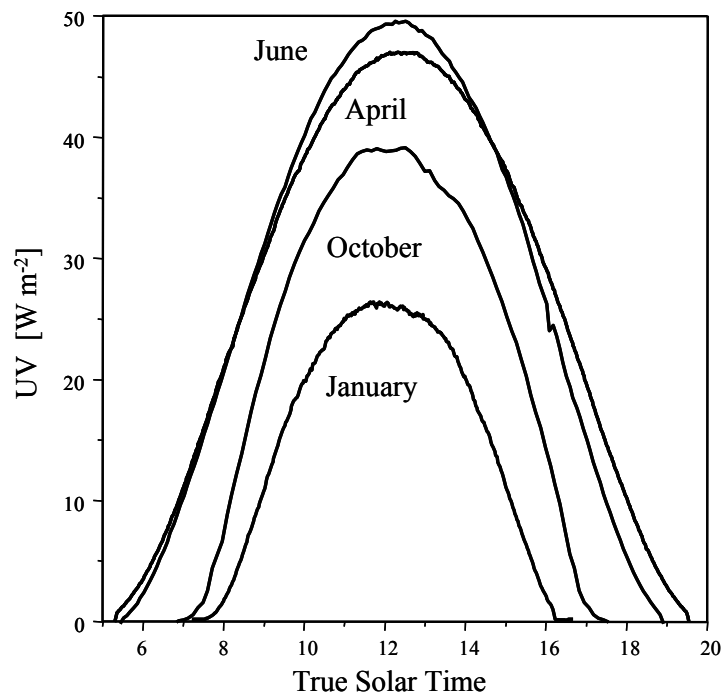
Figure 2.2: UV irradiance during a typical cloudless day at Plataforma Solar de Almería on plane tilted 37°.

To judge the feasibility and profitability of a solar application at a specific site, studies have to be performed to measure or estimate the amount of radiation actually available at the site in question along the year. Due to the large variability of radiation conditions from year to year such studies have to be based on data collected from at least five years

to be considered statistically significant [24]. **Figure 2.3** gives an idea of how world solar resources are distributed, although solar irradiance can vary strongly locally due to microclimates etc.
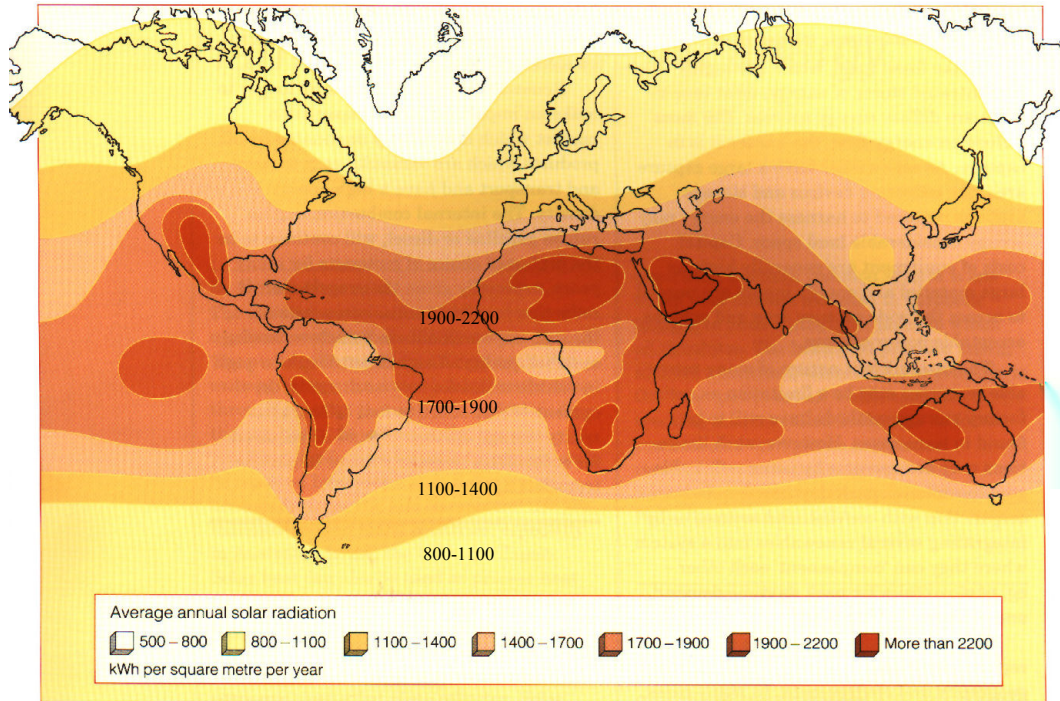
Figure 2.3: World Solar Radiation Map

2.1.2 Solar irradiance– Geometric and physical fundamentals

The average earth-sun distance during the year is called Astronomic Unit (AU) and its value is $1.496 \, 10^{11}$ m [24]. The earth receives an amount of radiation indirect proportional to the square of its distance to the sun. The earth-sun distance is smallest on the 3rd of January (perihelion, 0.983 AU) and highest on the 4th of July (aphelion, 1.017 AU), because the earth revolves around the sun on an elliptical orbit, called the eclipse.

The earth not only revolves around the sun but also rotates around its own axis, which is inclined 23.5º with respect to the perpendicular of the eclipse during the whole year. The angle between the terrestrial equatorial plane and the line joining the centres of the sun and the earth varies during the year between +23.5º and –23.5º (summer and winter solstice as referred to in the northern earth hemisphere). This angle is called declination (δ) and due to its annual variation the amount of radiation locally received varies during the year causing the seasons.

The day angle (Γ), Eq. (2.1), expresses the date of the year. n is the number of the day in the year. February is always assumed with 28 days, which causes a variation of exactness of the estimation of δ with a cycle of four years. δ can then be estimated on the basis of Γ with Eq. (2.2).

$$\Gamma = \frac{2\pi(n-1)}{365} \tag{2.1}$$

$$\delta = 0.006918 - 0.399912\cos\Gamma + 0.070257\sin\Gamma + 0.006758\cos 2\Gamma + \\ 0.000907\sin 2\Gamma + 0.002697\cos 3\Gamma + 0.00148\sin 3\Gamma \tag{2.2}$$
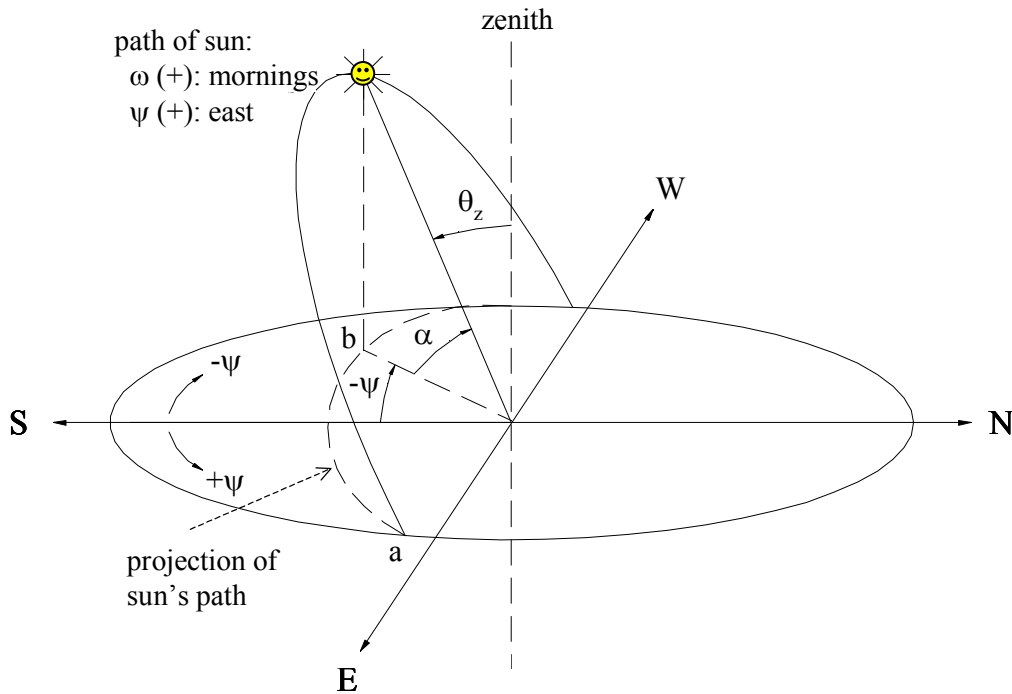
Figure 2.4: Main angles determining the solar position

Figure 2.4 shows the main angles determining the solar position during a day with reference to a horizontal plane. The sun's position can be described by two angles; the zenith angle (θ_z) and the azimuth angle (ψ). Other important angles are the sun altitude ($\alpha = 90° - \theta_z$), the complementary angle to the zenith angle, and the hour angle (ω). The zenith angle is 90° minus the local latitude and the declination at solar midday. The hour angle is 0° at solar midday and changes 15° every hour from positive (morning) to negative (evening). Solar midday is referring to the true solar time, which can be calculated from the local standard time, the local longitude and the day angle. In true

solar time the moment when the sun altitude is highest during a day is referred to as midday. The position of an inclined plane (which is the case of most solar collectors) is determined by two more angles; the inclination with respect to a horizontal plane (β) and the orientation with respect to the azimuth angle (γ). Detailed equations how to calculate all relevant geometric relationships can be found in [24].

Solar radiation can be divided into direct beam radiation (I_B) passing the atmosphere without being scattered or re-directed and diffuse radiation (I_D). The sum of both is called global radiation (I_G). The solar irradiation incident on a surface is not only dependent on geometric relationships but also on atmospheric conditions. It is therefore essential that a mathematical model estimating solar radiation incident on a sun collector take into account both aspects to be able to yield reliable results. It should be especially remarked that calculations based only on estimation or measurement of direct beam radiation and geometric relationships regarding the sun position and the sun collector orientation are insufficient due to the large share of diffuse radiation even under cloudless skies. This is particularly true for short wavelength calculations because the efficiency of atmospheric radiation scattering processes strongly increases towards shorter wavelengths (e.g. Rayleigh scattering is proportional to λ^{-4}).

The beam irradiance $I_{Bn\lambda}$ at wavelength λ received at ground level by a surface normal to the sun's rays (or "beam normal irradiance") at wavelength λ is given by Eq. (2.3)

$$I_{Bn\lambda} = I_{on\lambda} \cdot T_{R\lambda} \cdot T_{o\lambda} \cdot T_{n\lambda} \cdot T_{g\lambda} \cdot T_{w\lambda} \cdot T_{a\lambda} \qquad (2.3)$$

where $I_{on\lambda}$ is the extraterrestrial irradiance corrected for the actual sun-earth distance and the other factors are the transmittances for the different extinction processes: Rayleigh scattering ($T_{R\lambda}$), absorption by ozone ($T_{o\lambda}$), NO_2 ($T_{n\lambda}$), uniformly mixed gases ($T_{g\lambda}$) and water vapour ($T_{w\lambda}$), and finally, aerosol extinction ($T_{a\lambda}$).

Terrestrial diffuse radiation results from the complex radiance field of the sky and should theoretically be calculated as an integration of radiance over the whole sky vault, but this method implies extensive computer calculations. Simplified models obtain the diffuse irradiance from the same transmittance functions used to determine the direct beam irradiance. This is an approximation justified by theory because the transmittance function at the same time predicts the scattered radiation and it is possible to estimate the share of the scattered photons redirected downwards. Diffuse irradiance on an

arbitrarily oriented tilted surface is considered as the sum of four components: diffuse irradiance caused by Rayleigh scattering, aerosol scattering and sky and ground backscattering.

Furthermore, for arbitrarily oriented tilted surfaces all corresponding geometric considerations have to be taken into account, such as the cosine decrease regarding the angle of incidence of the beam irradiance or that a tilted surface receives diffuse radiation only of a part of the sky vault. For tilted surfaces not only the atmospheric conditions but also the spectral ground albedo has to be provided to the model.

2.1.3 Solar collectors for photochemical applications

2.1.3.1 Concentrating collectors

The first solar photoreactor designs for photochemical applications were based on line-focus parabolic-trough concentrators (PTCs). In this type of concentrators an absorber tube is placed in the focus of a parabolic reflector. The reflector redirects radiation parallel to the axis of the parable towards the absorber tube in the focus. Consequently, this type of concentrator has to track the sun and can use only parallel direct beam radiation (I_B). One-axis and two-axis tracking systems can be used for this purpose. The first engineering-scale solar photochemical facility for water detoxification in Europe was developed by CIEMAT [25] using twelve two-axis tracking PTCs (32 m^2 collector surface per PTC), each consisting of a turret and a platform supporting four parallel PTCs, with an absorber tube at the focus of each collector.

PTC concentrators represent a mature engineering concept due to their former similar development for solar thermal applications. They can be easily set-up and scaled-up due to the simple engineering concepts involved (tubular plug-flow photoreactor with turbulent flow conditions). Turbulent flow ensures good mass-transfer and maintains TiO_2 particles in suspension in case of TiO_2 slurry photocatalysis. Another advantage is that the photoreactors are closed systems. Therefore, no vaporization of volatile compounds takes place. A disadvantage of PTCs is, that due to their geometry they can use only direct beam radiation, which makes them practically useless, when the sky is clouded. They also are rather expensive systems due to the necessary sun tracking system. This applies to the investment as well as to the maintenance costs, because moving parts are prone to require enhanced maintenance effort. Another aspect that has

to be taken into account is the possibility of overheating water in large-scale installations with residence times in the concentrating collectors in the range of several minutes.

2.1.3.2 Non-concentrating collectors

The elevated prices of PTCs have encouraged the search for cheaper reactor concepts with non-concentrating geometry. Some different types of non-concentrating solar reactors reported are:

- Free-falling film: the process fluid falls slowly over a tilted plate with a catalyst attached to the surface, which faces the sun and is open to the atmosphere [26, 27].

- Pressurized flat plate: consists of two plates between which the fluid circulates using a separating wall [28].

- Solar ponds: Small, shallow, on-site pond reactors [29].

As stated non-concentrating or one-sun collectors are, in principle, cheaper than PTCs as they have no moving parts or solar-tracking devices. They do not concentrate radiation so that efficiency is not reduced by factors associated with concentration and solar tracking. A major advantage is that they harvest not only direct beam but also diffuse radiation. Consequently, they can as well be operated under cloudy sky conditions, although of course with reduced efficiency compared to sunny conditions. Depending on the type of collector vaporization of contaminants can occur. One problem common to non-concentrating collectors is mass transfer problems caused by laminar flow in non-concentrating systems. So, although non-concentrating collectors potentially present several important advantages their scale-up can be difficult due to reasons such as high pressure drop, inhomogeneous flow conditions etc.

2.1.4 Compound Parabolic Collectors (CPC)

CPCs are an interesting cross between PTCs and non-concentrating collectors without their respective disadvantages. CPCs are static collectors with a reflective surface formed by two connected parabolic mirrors with an absorber tube in the focus and have been found to provide the most efficient light-harvesting optics for low concentrating systems [30]. They have no tracking system and the design permits the solar rays to be reflected onto the absorber tube attaining a low concentration factor. The concentration

factor is defined as the ratio of the collector aperture to the absorber tube perimeter and is usually between 1 and 1.5 depending on the type of application. Thanks to the reflector design, almost all the radiation (not only direct, but also diffuse) incident at the CPC aperture area can be collected and is available for the process in the reactor. The light reflected by the CPC is distributed around the back of the tubular photoreactor (see **Figure 2.5**). The absorber tubes are closed system photoreactors, in which the waste water can be circulated under turbulent flow conditions. They can be easily up-scaled due to the simple engineering concepts involved. All these factors contribute to excellent performance of CPC collectors in solar photochemical and photocatalytic applications [31].

Incident radiation

photocatalytic reactor
(Pyrex glass tube)

reflecting surface
(electropolished aluminium)
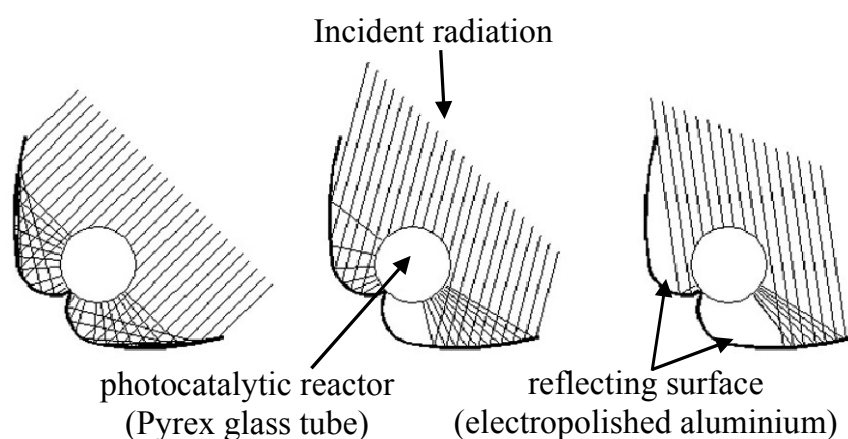
Figure 2.5: Geometric principle of Compound Parabolic Collector (CPC)

The photochemical reactor must contain the working fluid, including the catalyst or the sensitizer, and must transmit solar UV-light efficiently with minimal pressure drop across the system. It must also provide good mass transfer from the fluid stream to an illuminated photocatalyst or a sensitizer surface. Adequate flow distribution inside the reactor must be assured. Furthermore, reactor material must be inert to chemicals and resistant to high or low pH. The choice of materials that are both transparent to UV light and resistant to its destructive effects is limited to quartz glass, fluoropolymers and borosilicate glass. Low-iron-content borosilicate glass has good transmissive properties in the solar range to about 285 nm, is cheaper than the others and therefore, seems to be the most adequate [32]. The ideal reflective surface for solar photochemical applications must be highly UV-reflective, weather-resistant to guarantee long lifetime and reasonably priced. The materials currently available that best fit these requirements are

electropolished anodised aluminium and organic plastic films with an aluminium coating [32].

2.2 Treatment of biorecalcitrant waste water

2.2.1 Advanced Oxidation Processes (AOP)

Activated sludge biological treatment [33] is recognised as the Best Available Technology (BAT) by the EU for many applications. One of the main obligations for urban wastewater treatment imposed by EU [11, 34] is that wastewater collecting and treatment systems (generally involving biological treatment) must be provided by 31 December 2005 in all agglomerations of between 2000 and 10000 population equivalents. As a consequence this technology was widely implemented during the last 15 years. Yet, this technology can only cope with biodegradable waste water, which usually applies to urban waste water. Nevertheless, there exists a great number of anthropogenic activities that generate waste water containing non-biodegradable or even toxic substances, which cannot be treated with biological treatment methods. Examples for such activities are agriculture [27, 35], industry (see Annex I of IPPC directive [9]) or the household use of PPCPs [5].

Among alternative treatments are adsorption technologies, air stripping or extraction technologies. Yet, they are only phase-transfer technologies, which do not destroy the contaminant. Chemical-oxidative treatments chemically attack the pollutant, alter its chemical structure and thus ultimately remedy the waste problem. Conventional oxidation technologies include the application of oxidants such as chlorine, chlordioxide, peracetic acid, hydrogen peroxide, permanganate and ozone for either disinfection of pathogenic contamination or the oxidation of pollutants.

There is another group of chemical-oxidative processes, called Advanced Oxidation Processes (AOP) or Advanced Oxidation Treatments. AOPs are characterised by the generation of hydroxyl radicals. Second to fluorine the hydroxyl radical is the strongest known oxidant (2.8 V vs. Standard Hydrogen Electrode, see **Table 2.1**). It is therefore able to oxidise and mineralise almost every organic molecule yielding in the end CO_2 and inorganic ions. Rate constants for most reactions involving hydroxyl radicals in aqueous solution are usually in the order of 10^6 to 10^9 M^{-1} s^{-1} [37, 38].

Table 2.1: Oxidation potential against Standard Hydrogen Electrode of some relevant oxidants [39].

Oxidant	E° [V]
Fluorine	3.03
Hydroxyl radical	2.80
Singlet oxygen	2.42
Ozone	2.42
Hydrogen peroxide	1.78
Perhydroxyl radical	1.70
Permanganate	1.68
Chlordioxide	1.57
Hypochloric acid	1.45
Chlorine	1.36
Bromine	1.09
Iodine	0.54

Different techniques exist to generate hydroxyl radicals. The most important groups of AOPs are:

- Direct photolysis of oxidants (H_2O_2, O_3) or water with high energy UV radiation [39, 40].
- Heterogeneous photocatalysis illuminating a semiconductor [39, 41, 42].
- Fenton and Fenton-like processes with transition metals [40, 41, 43]
- Cavitation techniques (hydrodynamic and ultrasound) [40, 41].

The photochemical reactions for the generation of the hydroxyl radical in the most common AOPs involving radiation are given in **Table 2.2**. Production of UV radiation by lamps is expensive. Therefore, investigation is focusing increasingly on the two AOPs, which can be powered by solar radiation, i.e. light with a wavelength greater than 300 nm, which are homogeneous catalysis by the photo-Fenton reaction and heterogeneous catalysis by the UV/TiO_2 process [44, 45]. The first one is known for its high reaction rates and the application of environmentally benevolent reagents (iron salts at low concentrations, hydrogen peroxide is being decomposed to water and oxidising species being consumed during the treatment), which is why it could be considered the most promising photon-driven AOP for the remediation of contaminated waters [46, 47]. Therefore, the present work is focusing on this process.

Table 2.2: Hydroxyl radical generation by photochemical reactions [39, 43]

AOP	key reactions	Eq.	wavelength
UV/ H_2O_2	$H_2O_2 + h\nu \rightarrow 2\ OH^{\bullet}$	(2.4)	$\lambda < 300$ nm
UV/ O_3	$O_3 + h\nu \rightarrow O_2 + O\ (^1D)$	(2.5)	$\lambda < 310$ nm
	$O\ (^1D) + H_2O \rightarrow 2\ OH^{\bullet}$	(2.6)	
UV/ H_2O_2/ O_3	$O_3 + H_2O_2 + h\nu \rightarrow O_2 + OH^{\bullet} + OH_2^{\bullet}$	(2.7)	$\lambda < 310$ nm
UV/ TiO_2	$TiO_2 + h\nu \rightarrow TiO_2\ (e^- + h^+)$	(2.8)	$\lambda < 390$ nm
	$TiO_2(h^+) + OH^-_{ad} \rightarrow TiO_2 + OH^{\bullet}_{ad}$	(2.9)	
photo-Fenton	$H_2O_2 + Fe^{2+} \rightarrow Fe^{3+} + OH^{\bullet} + OH^-$	(2.10)	$\lambda < 580$ nm
	$Fe^{3+} + H_2O + h\nu \rightarrow Fe^{2+} + H^+ + OH^{\bullet}$	(2.11)	

2.2.2 Photo-Fenton

2.2.2.1 Aquatic iron chemistry

Behind oxygen, silicon and aluminium, iron is the fourth most abundant element in the earth's crust. It occurs in oxidation numbers from –II to +VI with coordination numbers of 3 to 8 [48]. Desert sands, dust and ash make iron omnipresent in the environment and practical all natural water contains iron at least in traces. In clouds, fog, lakes and rivers the iron concentration is around 10^{-5} M [49]. Iron is as well an vital element for life present in the whole biosphere. It is also an essential nutrient in aerobic biological wastewater treatment [33].

In aqueous solution the most abundant iron species have an oxidation number of +II (ferrous iron) and +III (ferric iron). Other iron species are highly unstable and are therefore not dealt with here in detail. Dissolved ferrous and ferric iron species are present in octahedral complexes with six ligands in water. Iron is complexed by water and hydroxyl ligands provided that no other complexing substances are present. How many of these ligands are hydroxyl ions, depends on the solution's pH, which influences directly the acid/base equilibrium of the aquo complex. Ferric iron is the more critical iron species in the photo-Fenton process, because its hydroxides precipitate at lower pH than those of ferrous iron. Consequently, only the acid/base equilibrium for the ferric iron aquo complex is described here, Eq. (2.12) - (2.14). For simplification, coordinated water molecules in the coordinate sphere will not be included in the chemical formulae from hereon. Formation of dimers, Eq. (2.15), and

oligomeres is possible as well, with the dimere being the most important at pH below 3 [50].

$$[Fe(H_2O)_6]^{3+} \rightleftarrows [Fe(H_2O)_5(OH)]^{2+} + H^+ \qquad K = 6.3 \ 10^{-3} \ M \qquad (2.12)$$

$$[Fe(H_2O)_5(OH)]^{2+} \rightleftarrows [Fe(H_2O)_4(OH)_2]^+ + H^+ \qquad K = 3.2 \cdot 10^{-4} \ M \qquad (2.13)$$

$$[Fe(H_2O)_4(OH)_2]^+ \rightleftarrows [Fe(H_2O)_3(OH)_3] + H^+ \qquad K = 1 \cdot 10^{-6} \ M \qquad (2.14)$$

$$2 \ Fe_{aq}^{3+} \rightleftarrows Fe_2(OH)_2^{4+} + 2 H^+ \qquad K = 1.3 \cdot 10^{-3} \ M \qquad (2.15)$$
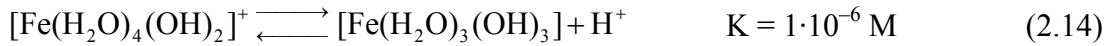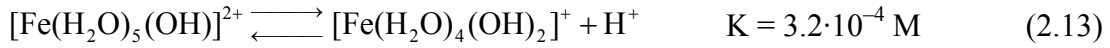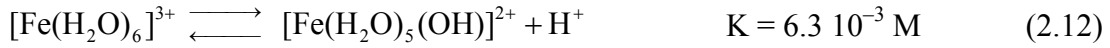
Figure 2.6 shows the equilibrium concentrations of the most important ferric iron aquo complexes in the absence of further complexing substances at different pH for a ferric iron concentration of 20 mg L^{-1}. The dimer concentration is rather low at this ferric iron concentration. As the formation of the dimer is a process of second order, the relative amount of this species augments at higher iron concentrations. It is evident that between pH 2.5 and 3 $[Fe(H_2O)_5(OH)]^{2+}$ is the dominant species.
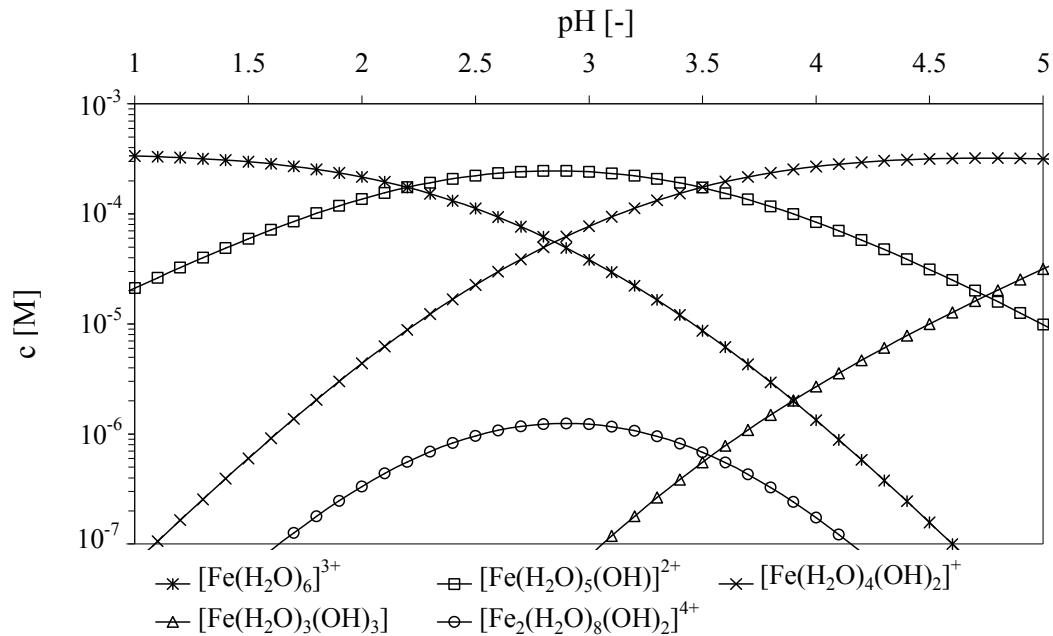
Figure 2.6: Ferric iron species present in aqueous solution at different pH at a concentration of 20 mg L^{-1}, calculated with equilibrium constants from [50], T = 20 ºC.

Because of the low solubility product of ferric iron hydroxide ($K_S(Fe(OH)_3) \approx 10^{-37}$), precipitation starts at pH 2.5-3.5 depending on the iron concentration and the temperature. The precipitation process starts with the formation of dimers and oligomeres, which at continuation gradually polymerise further and lose water until forming finally insoluble iron hydroxides (e.g. goethite or hematite). This aging process is slow and can take up to a hundred days [50, 51]. The precipitation and aging processes are also temperature dependent and more and faster precipitation takes place at higher temperatures [52]. The resulting precipitate is of red brown colour (absorption over the whole UV/Vis spectral range) and not stoichiometric. It contains a lot of water and has a strong cationic character, thus co-precipitating a lot of other ions but also organic substances. Therefore, ferric iron is often used as coagulant [33]. The precipitate is difficult to re-dissolve through acidification (insoluble above pH $\approx$ 1-1.5), but it can be re-dissolved by complexing substances (e.g. oxalic acid) [53] or photoleaching processes [54]. Photoleaching refers to photoreduction of ferric to ferrous iron and subsequent leaching of the ferrous iron from the precipitate.

2.2.2.2 Fenton chemistry - reactions of Fe^{2+}, Fe^{3+} and H_2O_2 in aqueous solution

Hydrogen peroxide is decomposed to water and oxygen in the presence of iron ions in aqueous solution. Two reaction pathways have been proposed in literature [55], the first formulating a radical chain reaction (Haber-Weiss mechanism) [56 - 59], the other an ionic mechanism (Kremer-Stein mechanism) [60 - 62]. After the work of Walling [59], the radical mechanism has been broadly accepted for reactions in acidic milieu. Yet, it should be mentioned that discussion is still on-going and the occurrence of ferrate and ferryl iron (+IV and +V), at least in intermediate complexes, has been proposed [63, 64].

Mixtures of ferrous iron and hydrogen peroxide are called Fenton reagent. If ferrous is replaced by ferric iron it is called Fenton-like reagent. The Fenton reaction, Eq. (2.16), was first reported by H.J.H. Fenton in 1894 [65]. Eq. (2.16) - (2.22) show the reactions of ferrous iron, ferric iron and hydrogen peroxide in the absence of other interfering ions and organic substances. The regeneration of ferrous iron from ferric iron by Eq. (2.19) - (2.21), is the rate limiting step in the catalytic iron cycle, if iron is added in small amounts. The listed rate and equilibrium constants for Eq. (2.16) - (2.25) were reported in [55].

$$Fe^{2+} + H_2O_2 \rightarrow Fe^{3+} + OH^- + OH^\bullet \qquad k = 53 - 76\ M^{-1}\ s^{-1} \qquad (2.16)$$

$$Fe^{2+} + OH^\bullet \rightarrow Fe^{3+} + OH^- \qquad k = 2.6 - 5.8 \cdot 10^8\ M^{-1}\ s^{-1} \qquad (2.17)$$

$$Fe^{2+} + HO_2^\bullet \rightarrow Fe^{3+} + HO_2^- \qquad k = 0.75 - 1.5 \cdot 10^6\ M^{-1}\ s^{-1} \qquad (2.18)$$

$$Fe^{3+} + H_2O_2 \rightarrow Fe^{2+} + HO_2^\bullet + H^+ \qquad k = 1 - 2 \cdot 10^{-2}\ M^{-1}\ s^{-1} \qquad (2.19)$$

$$Fe^{3+} + HO_2^\bullet \rightarrow Fe^{2+} + O_2 + H^+ \qquad k = 0.33 - 2.1 \cdot 10^6\ M^{-1}\ s^{-1} \qquad (2.20)$$

$$Fe^{3+} + O_2^{\bullet-} \rightarrow Fe^{2+} + O_2 \qquad k = 0.05 - 1.9 \cdot 10^9\ M^{-1}\ s^{-1} \qquad (2.21)$$

$$OH^\bullet + H_2O_2 \rightarrow H_2O + HO_2^\bullet \qquad k = 1.7 - 4.5 \cdot 10^7\ M^{-1}\ s^{-1} \qquad (2.22)$$
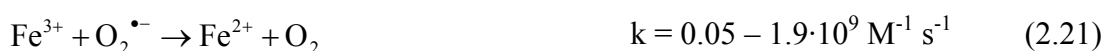
Furthermore, radical-radical reactions have to be taken into account:

$$2\,OH^\bullet \rightarrow H_2O_2 \qquad k = 5 - 8\ 10^9\ M^{-1}\ s^{-1} \qquad (2.23)$$

$$2\,HO_2^\bullet \rightarrow H_2O_2 + O_2 \qquad k = 0.8 - 2.2\ 10^6\ M^{-1}\ s^{-1} \qquad (2.24)$$

$$HO_2^\bullet + OH^\bullet \rightarrow H_2O + O_2 \qquad k = 1.4\ 10^{10}\ M^{-1}\ s^{-1} \qquad (2.25)$$

Finally, the following equilibriums have to be regarded [66, 67]:

$$H_2O_2 \rightleftarrows HO_2^- + H^+ \qquad K = 2.63\ 10^{-12}\ M \qquad (2.26)$$

$$[Fe]^{3+} + H_2O_2 \rightleftarrows [Fe(HO_2)]^{2+} + H^+ \qquad K = 3.1\ 10^{-3}\ M \qquad (2.27)$$

$$[Fe(OH)]^{2+} + H_2O_2 \rightleftarrows [Fe(OH)(HO_2)]^+ + H^+ \qquad K = 2\ 10^{-4}\ M \qquad (2.28)$$

$$HO_2^\bullet \rightleftarrows O_2^{\bullet-} + H^+ \qquad K = 3.55\ 10^{-5}\ M \qquad (2.29)$$

$$OH^\bullet \rightleftarrows O^{\bullet-} + H^+ \qquad K = 1.02\ 10^{-12}\ M \qquad (2.30)$$

$$HO_2^\bullet + H^+ \rightleftarrows H_2O_2^{\bullet+} \qquad K = 3.16 - 3.98\ 10^{-12}\ M \qquad (2.31)$$
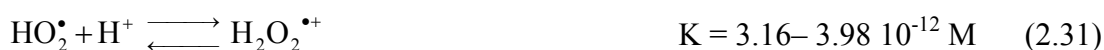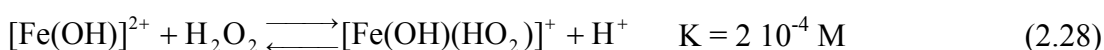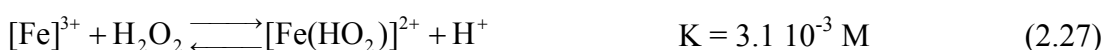
2.2.2.3 Fenton reaction in the presence of inorganic and organic substances

If organic substances (quenchers, scavengers or in the case of wastewater treatment pollutants) are present in the system $Fe^{2+}/\ Fe^{3+}/\ H_2O_2$, they react in many ways with the generated hydroxyl radicals. Yet, in all cases the oxidative attack is electrophilic and the

rate constants are close to the diffusion-controlled limit [37, 38, 45]. The following reactions with organic substrates have been reported [37, 39]:

- Hydrogen abstraction from aliphatic carbon atoms, Eq. (2.32).
- Electrophilic addition to double bonds or aromatic rings, Eq. (2.33).
- Electron transfer reactions, Eq. (2.34).

$$OH^{\bullet} + RH \rightarrow R^{\bullet} + H_2O \tag{2.32}$$

$$R - CH = CH_2 + OH^{\bullet} \rightarrow R - C^{\bullet}H - CH_2OH \tag{2.33}$$

$$OH^{\bullet} + RX \rightarrow RX^{\bullet+} + OH^- \tag{2.34}$$

The generated organic radicals continue reacting prolonging the chain reaction. Depending on the oxidation-reduction potential of the organic radical generated, reactions (2.35) - (2.38) can take place. The organic peroxide generated in reaction (2.38) can further react with ferrous iron similar to the Fenton reaction, (2.39) [68]. Of special interest is the reaction with dissolved oxygen (Dorfman-mechanism), Eq. (2.40) and (2.41) [69, 70], because the peroxyl radical can regenerate hydrogen peroxide by reaction (2.18) and thereby contribute to reduce the consumption of oxidant in wastewater treatment by Fenton and photo-Fenton method.

$$R^{\bullet} + Fe^{3+} \rightarrow R^+ + Fe^{2+} \tag{2.35}$$

$$R^{\bullet} + Fe^{2+} \rightarrow R^- + Fe^{3+} \tag{2.36}$$

$$R^{\bullet} + R^{\bullet} \rightarrow R - R \tag{2.37}$$

$$R^{\bullet} + HO_2^{\bullet} \rightarrow RO_2H \tag{2.38}$$

$$Fe^{2+} + RO_2H \rightarrow Fe^{3+} + OH^- + OR^{\bullet} \tag{2.39}$$

$$R^{\bullet} + O_2 \rightarrow RO_2^{\bullet} \tag{2.40}$$

$$RO_2^{\bullet} + H_2O \rightarrow ROH + HO_2^{\bullet} \tag{2.41}$$

In the case of aromatic pollutants the ring system usually is hydroxylated before it is broken up during the oxidation process. Substances containing quinone and hydroquinone structures are typical intermediate degradation products, e.g. produced by reactions equivalent to Eq. (2.42) and (2.43). These are especially worth mentioning because they provide an alternative, quicker pathway for ferrous iron regeneration

through Eq. (2.44) and (2.45) accelerating thereby the process. Resulting benzoquinone structures can also be reduced as in Eq. (2.46). Thereby, each molecule can reduce several ferric iron ions in a catalytic cycle. Anyway, sooner or later this catalytic cycle is interrupted, because in competition with reactions (2.42) - (2.46) also ring opening reactions occur, which further carry on the mineralisation of the molecule [71].

$$k = 7.3 \ 10^9 \ M^{-1} \ s^{-1} \qquad (2.42)$$

$$k = 1.5 \ 10^9 \ M^{-1} \ s^{-1} \qquad (2.43)$$

$$k = 4.4 \ 10^2 \ M^{-1} \ s^{-1} \qquad (2.44)$$

$$k = 4.4 \ 10^4 \ M^{-1} \ s^{-1} \qquad (2.45)$$

$$k = 3.7 \ 10^9 \ M^{-1} \ s^{-1} \qquad (2.46)$$
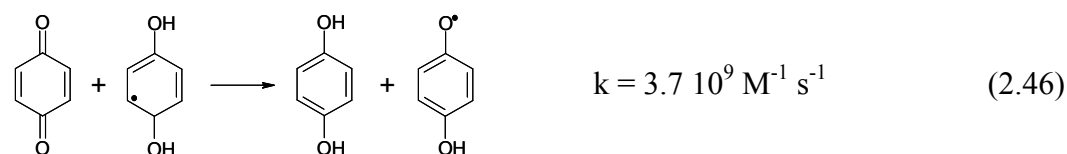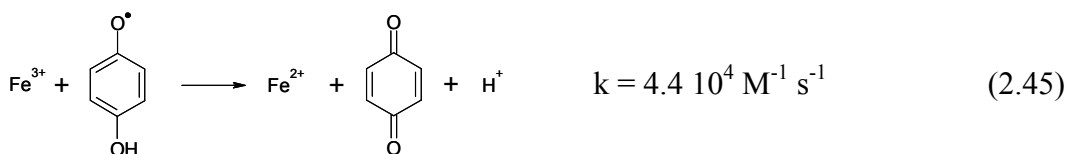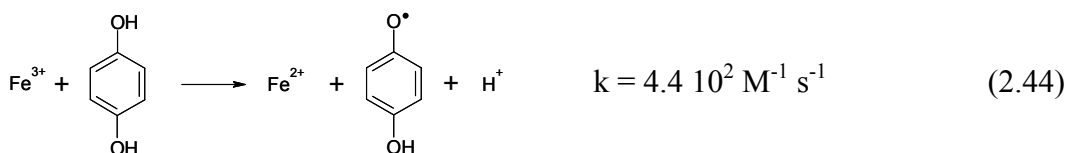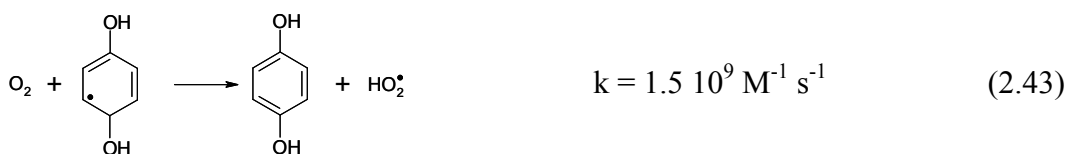
There is one great setback of the Fenton method. Especially when the treatment goal is the total mineralisation of organic pollutants, carboxylic intermediates cannot be further degraded. Carboxylic and dicarboxylic acids are known to form stable iron complexes, which inhibit the reaction with peroxide [72]. Hence, the catalytic iron cycle reaches a standstill before total mineralisation is accomplished, Eq. (2.47).

$$Fe^{3+} + n \ L \rightarrow [FeL_n]^{x+} \xrightarrow{H_2O_2, \ dark} \text{ no further reaction} \qquad (2.47)$$
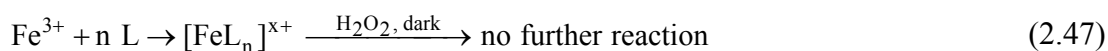
L: Mono- and Dicarboxylic acids

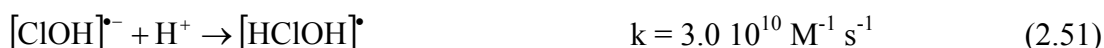Due to the high oxidation potential of the hydroxyl radical, it can also react with inorganic ions present in the solution. Several authors have described the strong negative effect of the presence of carbonate and phosphate in the Fenton reaction, while the effect of other ions such as chloride or sulphate is not as strong [70, 73 - 77]. Phosphate has a double detrimental effect; first, it precipitates iron and second, it scavenges hydroxyl radicals. Carbonate ions can scavenge hydroxyl radicals by reactions (2.48) and (2.49). The resulting carbonate radicals are particularly ineffective in the degradation of organic matter [70].

$$OH^\bullet + HCO_3^- \rightarrow H_2O + CO_3^{\bullet-} \qquad\qquad k = 8.5\ 10^6\ M^{-1}\ s^{-1} \qquad\qquad (2.48)$$

$$OH^\bullet + CO_3^{2-} \rightarrow OH^- + CO_3^{\bullet-} \qquad\qquad k = 3.9\ 10^8\ M^{-1}\ s^{-1} \qquad\qquad (2.49)$$

De Laat and co-workers [76] recently presented a rather comprehensive review of the additional reactions and equilibriums of importance in the presence of significant amounts of chloride and sulphate. Both ions are capable of complexing ferric as well as ferrous iron. They can thereby hinder reactions or also open completely new reaction pathways for the decomposition of hydrogen peroxide in the presence of dissolved iron. Also, hydroxyl radicals generated can react with these ions, creating chlorine radicals and sulphate radicals. Some representative reactions have been chosen from [76] and are shown in Eq. (2.50) - (2.53).

$$OH^\bullet + Cl^- \rightarrow [ClOH]^{\bullet-} \qquad\qquad k = 4.3\ 10^9\ M^{-1}\ s^{-1} \qquad\qquad (2.50)$$

$$[ClOH]^{\bullet-} + H^+ \rightarrow [HClOH]^\bullet \qquad\qquad k = 3.0\ 10^{10}\ M^{-1}\ s^{-1} \qquad\qquad (2.51)$$

$$[HClOH]^\bullet + Cl^- \rightarrow Cl_2^{\bullet-} + H_2O \qquad\qquad k = 8.0\ 10^9\ M^{-1}\ s^{-1} \qquad\qquad (2.52)$$

$$OH^\bullet + HSO_4^- \rightarrow H_2O + SO_4^{\bullet-} \qquad\qquad k = 3.5\ 10^5\ M^{-1}\ s^{-1} \qquad\qquad (2.53)$$

De Laat and co-workers [76] further calculate, that below pH = 4 practically all hydroxyl radicals end up in chlorine radicals (calculations done for 100 mM NaCl solution). In the presence of sulphate the conversion of hydroxyl radicals is considerable at acidic pH as well. Yet, it should be mentioned that these calculations were performed for solutions without any other scavenging substances (e.g. organic pollutants). There are two negative effects; first, the chlorine and sulphate radicals are potentially weaker

oxidants and the overall process efficiency becomes diminished and second, chlorine radicals can electrophilically add themselves to double bonds similar to hydroxyl radicals and generate undesired chlorinated intermediate reaction products, such as detected by Kiwi and co-workers [75].

2.2.2.4 Photochemical reactions

Irradiation with light up to 580 nm leads to photoreduction of dissolved ferric iron to ferrous iron [44]. The primary step is a ligand-to-metal charge-transfer (LMCT) reaction. Subsequently, intermediate complexes dissociate as shown in reaction (2.54) [78]. The ligand can be any Lewis base able to form a complex with ferric iron (OH^-, H_2O, HO_2^-, Cl^-, $R-COO^-$, $R-OH$, $R-NH_2$ etc.). Depending on the reacting ligand, the product may be a hydroxyl radical such as in Eq. (2.55) and (2.56) or another radical derivated from the ligand. The direct oxidation of an organic ligand is possible as well as shown for carboxylic acids in Eq. (2.57). The omnipresence of iron makes the photo-Fenton reaction an important factor for the autopurification capacity of lakes, rivers [54] and atmospheric water droplets [49].

$$[Fe^{3+}L] + h\nu \longrightarrow [Fe^{3+}L]^* \longrightarrow Fe^{2+} + L^\bullet \qquad (2.54)$$

$$[Fe(H_2O)]^{3+} + h\nu \longrightarrow Fe^{2+} + OH^\bullet + H^+ \qquad (2.55)$$

$$[Fe(OH)]^{2+} + h\nu \longrightarrow Fe^{2+} + OH^\bullet \qquad (2.56)$$

$$[Fe(OOC-R)]^{2+} + h\nu \rightarrow Fe^{2+} + CO_2 + R^\bullet \qquad (2.57)$$

Depending on the ligand the ferric iron complex has different light absorption properties and reaction (2.54) takes place with different quantum yields and also at different wavelengths. Consequently, the pH plays a crucial role in the efficiency of the photo-Fenton reaction, because it strongly influences which complexes are formed (e.g. see Eq. (2.12) - (2.15), **Figure 2.6**). Thus, pH 2.8 was frequently postulated as an optimum pH for photo-Fenton treatment (e.g. [43, 74]), because at this pH precipitation does not take place yet and the dominant iron species in solution is $[Fe(OH)]^{2+}$, the most photoactive ferric iron – water complex.
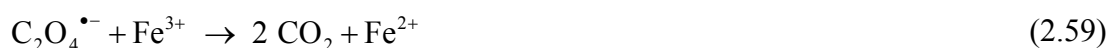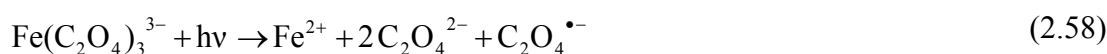
In fact, as shown in its general form in Eq. (2.54), ferric iron can form complexes with many substances and undergo photoreduction. Of special importance are carboxylic acids because they are frequent intermediate products in an oxidative treatment. Such

ferric iron – carboxylate complexes can have much higher quantum yields than ferric iron – water complexes. It is therefore a typical observation that a reaction shows an initial lag phase, until intermediates are formed, which can regenerate more efficiently ferrous iron from ferric iron accelerating the process. This can either happen through a photochemical pathway, Eq. (2.57), a thermal pathway, e.g. Eq. (2.42) - (2.46), or a combination of both.

Figure 2.7 illustrates the quantum yield of several complexes at different wavelengths by some examples from literature. Consequently, the addition of oxalate has been proposed to overcome the initial lag phase [79 - 81]. Thereby, the wastewater throughput in a photo-Fenton plant can be raised, but these gains have to be compared to the increased reagent cost due to the addition of oxalate, because oxalate is not acting as a catalyst, as it is as well degraded during this photochemical reaction. Other chelating agents have been proposed as well with the additional aim of working at neutral pH [82, 83]. The photolysis of ferric iron – oxalate complexes has been known for a long time and is used in actinometry for its high quantum yield, Eq. (2.58) and (2.59) [84, 86, 87].
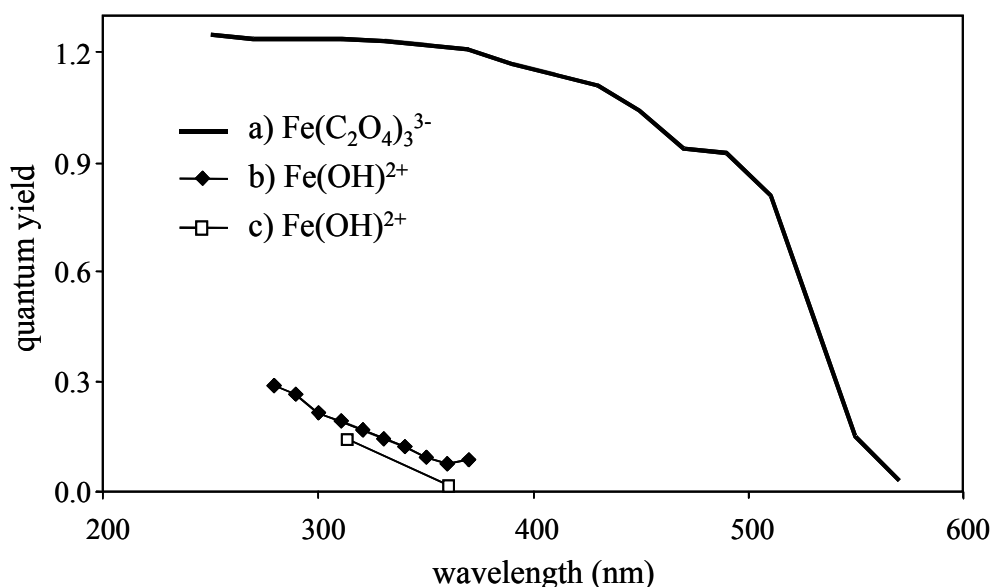
Figure 2.7: Quantum yields from literature. a) [84] is for the reaction in Eq. (2.58) and (2.59), b) [85] and c) [49] are for the reaction in Eq. (2.56)

$$Fe(C_2O_4)_3^{3-} + h\nu \rightarrow Fe^{2+} + 2C_2O_4^{2-} + C_2O_4^{\bullet-} \tag{2.58}$$

$$C_2O_4^{\bullet-} + Fe^{3+} \rightarrow 2\,CO_2 + Fe^{2+} \tag{2.59}$$

Finally, another photochemical reaction should be mentioned, which is the photoreduction of quinones to semiquinones, Eq. (2.60) [88]. By this reaction intermediate quinonic reaction products can be reduced and can further contribute to accelerate the reduction of ferric iron by Eq. (2.45). As a side product even a hydroxyl radical is generated.

$$H_2O + \text{(quinone)} \xrightarrow{h\nu} \text{(semiquinone)} + OH^\bullet \qquad (2.60)$$

2.2.2.5 Application to wastewater treatment

While the Fenton reaction has been known for more than a hundred years [65], it has only been in 1968 that it has been first suggested as means for wastewater treatment [89]. The photo-Fenton reaction was at first investigated by atmospheric researchers to clarify natural mechanisms of hydrogen peroxide production and oxidation of several pollutants in atmospheric water droplets [49]. At the beginning of the 1990s it was introduced in wastewater technology [74, 90 - 93].

Later on it was applied to waste water containing many different pollutants, such as pesticides [94 - 97], chlorophenols [98, 99], natural phenolic pollutants [27, 100], pharmaceuticals [101, 102], etc. It was also successfully applied to waste water with high organic load in the order of $10 - 20 \, g \, L^{-1}$ total organic carbon [103, 104]. Originally toxic waste water has been proven to lose its toxicity upon treatment by photo-Fenton process before total mineralisation has been achieved [96, 97]. Loss of toxicity usually is accompanied by an enhancement of biodegradability of the treated waste water [105, 106]. Consequently, photo-Fenton process and AOPs in general have been proposed as a pre-treatment to biological treatment [107, 108].

Several studies have discussed the influence of iron concentration and its catalytic behaviour [99, 109 - 112] and temperature [99, 113]. Within the investigated limits (maximal iron concentration 2.6 mM, maximal temperature 70 ºC) an increase of the respective parameter meant also an increase in reaction rate. Only one study examines the result of alternating time intervals with and without illumination [100]. It suggests the formation of pre-cursors in the dark prone to rapid photolysis upon irradiation.

Consequently, by alternating dark and illumination periods a decrease of necessary number of photons can be achieved compared to permanent illumination.

Other studies deal with the application of iron as a heterogeneous catalyst, e.g. in the form of suspended oxides [114], fixed on a support structure [115, 116] or even a combination of both [117]. While an easy separation and the possibility of working without pH adjustments are advantages of this approach, the drawback are generally diminished reaction rates compared to the homogeneous photo-Fenton process. This is mainly related with mass transfer limitations of the heterogeneous process and worsened light penetration into the photoreactor [101].

Whereas industrial applications of the photo-Fenton process are still very scarce, **Figure 2.8** illustrates the growing interest of the scientific community.
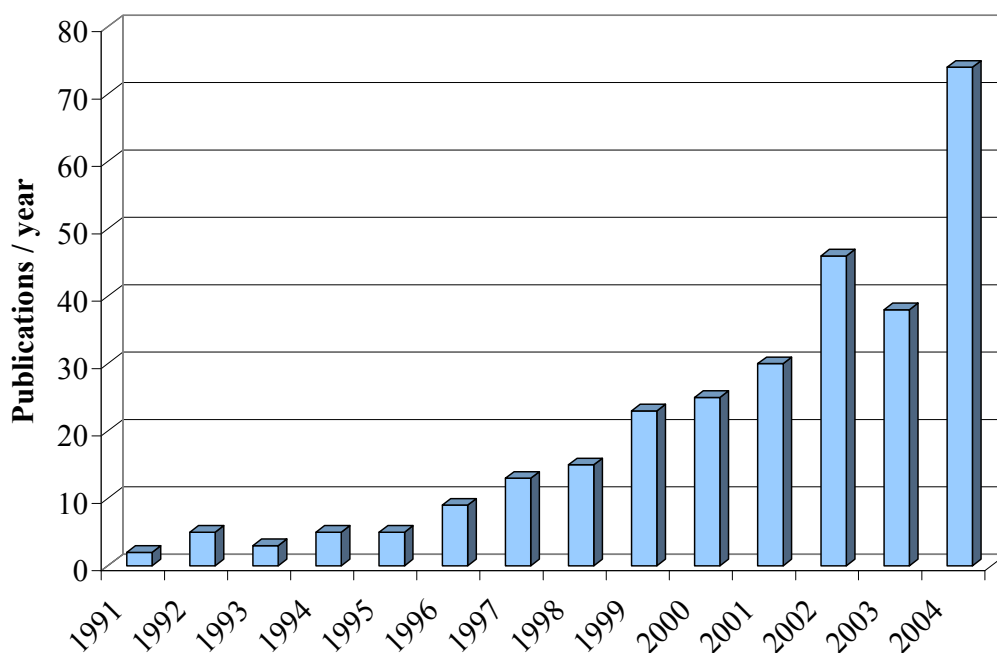

Figure 2.8: Number of publications on photo-Fenton in peer-reviewed journals (source: www.scopus.com, November 2005)

2.3 Model building

2.3.1 Experimental Design

Scientific research is a process of guided learning. The objective of experimental design is to optimise the experimentation process to obtain as much information as possible

from as few experiments as possible without disregarding correct statistical practice, so that statistically significant statements can be formulated. In an experimental design it is convenient to assess the effects of several variables at the same time to be able to quantify interaction between different input process variables (factors), especially if a maximum system response is searched by variation of input process variables. The reason is, that in classical one-variable-at-a-time strategy, very often the maximum cannot easily be found [118]. An example is given for an arbitrarily assumed correlation between reaction rate and the process factors temperature and iron concentration symbolized by the medians in **Figure 2.9**. In the example in the first try a series of experiments is conducted at 30°. Then, a second series is conducted at the established maximum at 11 mg L^{-1} Fe. The established maximum after two experiment series and 13 experimental runs is 67, and its coordinates are 11 mg L^{-1} Fe and 40°. The second approach begins with a series at 40° and continues with a second series at 8 mg L^{-1} Fe. The maximum found in this case is 70 and its coordinates are 8 mg L^{-1} Fe and 40 - 45°. In both approaches the maximum is different and in none the true maximum within the experimental region under investigation is found (73 at Fe = 5 mg L^{-1} and T = 50°).
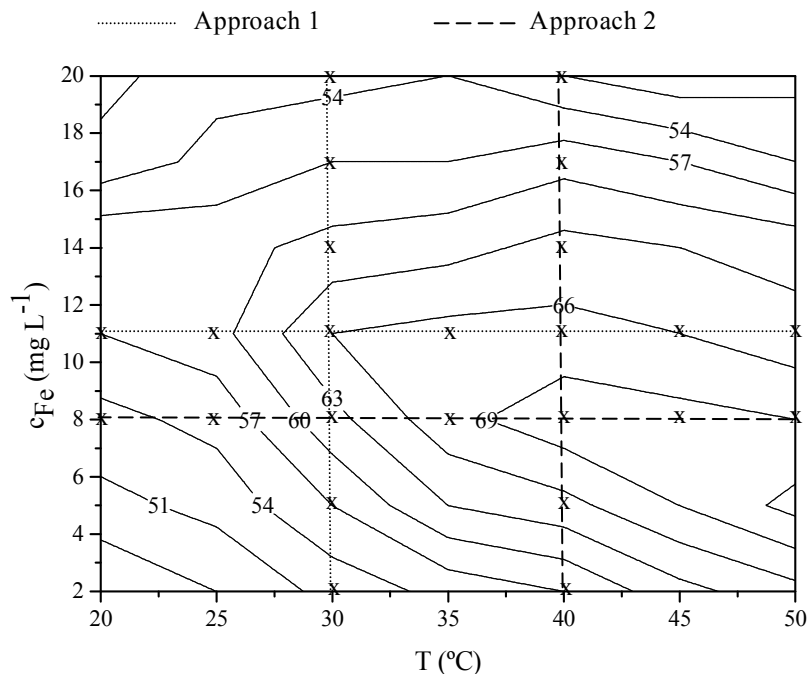
Figure 2.9: Arbitrary possible response surface for reaction rate in photo-Fenton system dependent on temperature and iron concentration. Points shown for two different one-variable-at-a-time approaches with the aim to detect the maximum reaction rate.

The example clearly shows that a good experimental design should cover the whole experimental region of interest respecting correct statistical practices and allowing calculating a model predicting the system response. Only that way the true maximum can be found with a small number of experiments.

There are several designs to adequately cover the experimental region. Among the most common are central composite and uniform shell designs [118, 119]. It has to be decided on a case-by-case basis, which one is the most appropriate.

2.3.1.1 Central composite design

The most common design is a full factorial design at two levels or central composite design [119]. In such a design each input variable (factor) is varied at two levels, which roughly present the minimum and the maximum values of the region of interest. The factors are usually standardised so that for each factor this maximum value is 1 and the minimum value -1, but this is not compulsory. A system with n factors will produce 2^n different experiments to vary each factor, while the others are kept constant. In analogy to the three factor case these experiments are called cube experiments, because in the three factor case, they represent a cube in the three dimensional factor space (after standardising the input factors). For a better covering of the experimental region and to generate additional experimental data for the posterior model building, so-called star points are added. In star-point experiments the values of all factors except one are set to the mean between minimum and maximum of the corresponding factor. The remaining factor is varied at two levels between $\pm\alpha$, where $1 \leq \alpha \leq n^{1/2}$ (if the factors are standardised as described). Again in analogy to the three factor case the design with $\alpha = 1$ is called a face centred design and the other extreme with $\alpha = n^{1/2}$ a spherical design. Consequently, if star points are added their number is two times the number of factors. Furthermore, so-called centre experiments are performed, in which all factors are set to the mean between minimum and maximum of the investigated factor region. The centre points are repeated 2 to 5 times to enhance the stability of the model. A second advantage of the repetition of the centre point is the possibility of calculating a standard deviation of the results of the centre point experiments, which gives a statistical measure of the repeatability of the experiments and their inherent experimental error. This can be interpreted as the maximum possible accuracy of the model.

More complex designs and procedures like fractional designs or blocking of variables are typically applied, when more than 3 to 4 factors are investigated at the same time to prevent excessive increase of number of experiments (e.g. 47 experiments in a full fractional design with n = 5). These designs were not considered here, but are explained elsewhere [118, 119]. Several examples for full factorial designs applied to photo-Fenton systems can be found in literature (e.g. [81, 111, 117]).

2.3.1.2 Uniform shell design

[120] proposed a design for systems with n different factors, which consists of $n^2 + n$ experimental runs uniformly spaced on an n-dimensional sphere (after standardisation of factors) plus one experimental run at the centre of the sphere. For n = 2 this is a regular hexagon (or six equidistant points on a circle) and for n = 3 a regular cuboctahedron (or twelve equidistant points on a sphere) plus the experiment at the centre. The main attractive feature of this design is its uniformity. The lack of coverage of the space between the origin and the surface of the sphere is a disadvantage as for any spherical design. The problem can be solved by placing a second sphere with a different radius between the origin and the first sphere. This has the drawback of doubling thereby the number of total experiments performed. If done so, the two spheres should be rotated regarding to each other to improve spacing of the points. Shell uniform designs are not recommended for systems with many factors due to the strong increase of experimental runs (e.g. 31 runs for n = 5). Several authors applied them to photo-Fenton systems [109, 110, 112].

2.3.2 Response Surface Methodology (RSM)

The study of a process often focuses on the relationship between the system response and the input factors. Typical motivations for such a study are the need for optimisation of a process or the intent of understanding the underlying mechanisms in the system. To describe the relation between a system response and input factors typically a mathematical model is formulated. The combination of experimental design and formulation of a mathematical model to yield a quantitative description of the response over a whole experimental region in a system with n continuous input factors is called Response Surface Methodology (RSM), because the system response can be described by a continuous surface in the n dimensional factor space [118]. Usually, the input

factors are scaled in such a way that the minimum value of the respective factor of the investigated region is -1 and the maximum value is +1, but from the mathematical point of view this is not compulsory.

Experimental design was described above (see chapter 2.3.1). Hence, here some considerations shall be given concerning the mathematical models employed. In the most general case neither reliable knowledge on the system mechanisms nor a set of mathematical equations readily fitting the correlations between input factors and system response are available beforehand. Then, polynomials provide a versatile approach for modelling the system response. Depending on the complexity of the system and the desired accuracy of the model first order or second order polynomials are usually employed including cross product terms and offset such as in Eq. (2.61) and (2.62),

$$y = \sum_{i=1}^{n} b_i x_i + \sum_{i=1}^{n-1} \sum_{j=i+1}^{n} c_{ij} x_i x_j + d \qquad (2.61)$$

$$y = \sum_{i=1}^{n} a_i x_i^2 + \sum_{i=1}^{n} b_i x_i + \sum_{i=1}^{n-1} \sum_{j=i+1}^{n} c_{ij} x_i x_j + d \qquad (2.62)$$

where $x_1 \ldots x_n$ are the n input factors and a_i, b_i, c_{ij} and d the different coefficients to be fitted in the modelling process. Consequently, for a model following Eq. (2.62) the number of coefficients to be adjusted is $(n+1)(n+2)/2$. Previous studies on photo-Fenton employing RSM usually applied this model [81, 109, 111, 112, 117].

The application of polynomials has further useful aspects. First, the cross-product terms are a direct measure for the degree of interaction of two factors. Second, not necessarily all coefficients of the general polynomial equations are to be taken into account in the final model. Different algorithms exist, which can distinguish significant from insignificant influences. A simple algorithm doing the task is the Yates algorithm [121]. The algorithm furthermore differentiates linear from curved response surfaces and thereby helps to decide if a first or second order polynomial model is required.

Nowadays, with computers and statistical software being standard tools of modern science many different algorithms are available and easily implemented, which can optimise a model distinguishing significant from not significant factors. The application of such variable selection techniques is especially important for studies, in which the number of observations is relatively small compared to the number of input factors. In this case many input factors to the model rapidly decrease the degrees of freedom and

negatively affect the quality of the model by causing, what is called over-fitting of the model. This term is used to describe the fact, that the model adapts too well to the experimental data and loses its ability of generalisation [122]. Particularly, the need for variable selection applies strongly to RSM, because its objective is precisely to minimise the experimental runs by optimising the experimental design. Consequently, having relatively few available observations is inherent to RSM.

One process of variable selection is called Forward Selection [122]. Forward Selection is a method to find the "best" combination of factors to optimise a criterion used to assess the quality of the model. To this end forward selection uses an iterative procedure by adding more and more factors to the model. In the case of multiple linear regression (MLR) the Fisher's value (F value) is used as the criterion to be maximised. The method is started by first selecting the factor, which correlates strongest with the system response (and yields the highest F value). Next, this factor is selected to test all combinations with the remaining factors in order to find the best model with two factors. In each further step another factor is added to the previously selected best combination in the same way until either all factors are integrated in the model or a maximum is found in the criterion, the F value.

Generally speaking, the ideal case of a model is the type of model, which is based on first principles, because these models best integrate physical/ chemical knowledge of the process, and, once set-up properly, tend to have the best performance and extrapolation qualities [123]. Accordingly, in RSM it is not compulsory to use polynomial equations to build a model based on the results of the experimental design. Induction of physical/ chemical background might be applied as well to find a set of mathematical functions more appropriate than polynomials to fit the experimental data.

2.3.3 Dynamic Modelling

RSM is a modelling approach, which assesses the change of system response due to variation of process input factors, which are maintained constant during the experiment. The system response is a single output such as a reaction rate constant, a degree of conversion during a defined time interval or the time needed to complete a process. RSM does not provide a model, which describes the process in the time interval between starting and ending the experiment. Such a modelling approach is called static modelling.

In a real application the process input factors often are not constant, e.g. in a solar photo-Fenton application sun irradiance cannot be maintained constant. In such a case a dynamic modelling approach is necessary, if the process development has to be predicted on-line based on simultaneous input from measuring devices and knowledge about the system. Such models are especially useful in automated process control strategies, where they can be implemented in the controller.

The two extreme cases for dynamic models are models based on first-principles and black box models. The approach based on first-principles is via the statement of non-linear differential equations from mass and energy balances. In the particular case of photo-Fenton and in general in wastewater treatment high uncertainties exist concerning these first-principle methods due to the complexity of the wastewater matrix. So, the application of such models is limited only to very special cases [124]. On the other hand black box models are usually a successful approach because of their capability of adaptation. Neural networks modelling non-linear systems [125] are such black box systems and their application has been proposed for photochemical processes [126] and photo-Fenton in particular [110]. Another black box model is the application of transfer function blocks for linear systems [127]. For control engineering purposes, classic approach for design of control systems requires a definition of the plant to control based on input/output transfer function blocks. These blocks define the dynamic behaviour of the plant to be controlled assuming that it is in steady state conditions, and it can be linearized around these conditions behaving as a linear dynamic system modelled by differential equations. For the control design approach modelling based on transfer functions is considered a more useful approach, although the model predictions are not as accurate as those of the non-linear neural network approach. The black box model based on the application of transfer function blocks can be enhanced by introduction of physical/ chemical knowledge about the process. Such an enhanced approach is then called grey-box modelling [128].
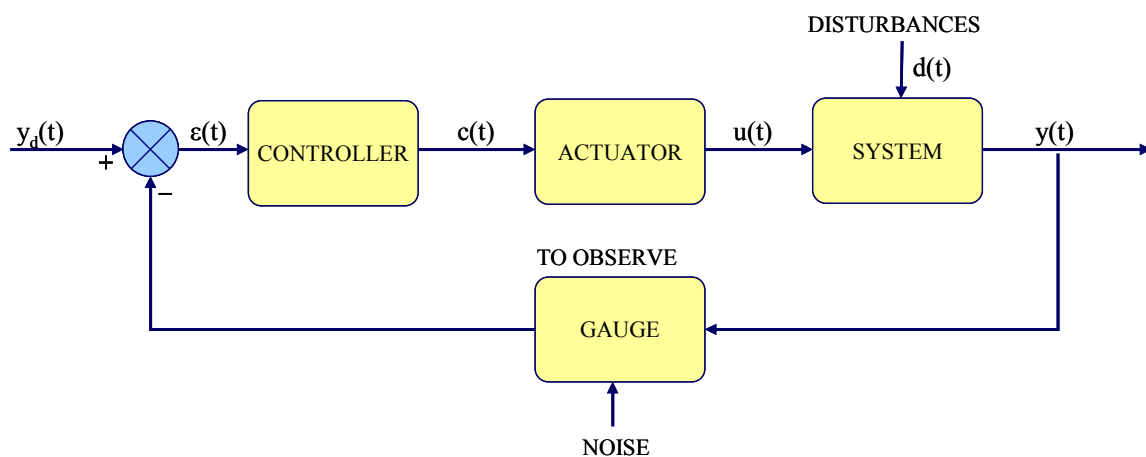
2.4 Process control

2.4.1 Feedback process control

Process control means that actions are taken, which affect a process with the goal to maintain a process in defined conditions. The desired conditions are typically defined

by one or more set-points of process variables. Feedback process control is probably the most common control strategy [127]. A feedback control system (**Figure 2.10**) consists of at least of four elements:

- Gauge: The gauge can be any measurement system, e.g. a pH sensor, which transfers the measured value to the comparator.

- Comparator: The comparator compares the value measured by the gauge with the set-point and generates an error function stating the difference between set-point and actual system output as measured by the gauge.

- Controller: The controller processes the error function and the implemented control algorithm determines an action to be taken by the control system.

- Actuator: The actuator is a device acting upon the system, e.g. a valve, which can be opened and closed.

The system is called feedback control because the control system continuously supervises the measurement values of the gauge and takes actions accordingly. The feedback control system is easy to implement and acts directly upon a deviation from the desired system output. It does not require an accurate model of the process, which makes it a very rugged control approach. On the other hand traditional feedback control is a rather slow control system, because it acts only after the disturbances have already affected the system.

Figure 2.10: General block diagram of a feedback control system. $y_d(t)$: set-point; $\varepsilon(t)$: error function; $c(t)$: controller command signal; $u(t)$: process input variable; $y(t)$: process output variable; $d(t)$: disturbances.

2.4.2 PID control

The classical proportional-integral-derivative (PID) controller is by far the most commonly used feedback controller [129]. As indicated by its name a PID controller's action is due to the sum of three terms, which are given in Eq. (2.63) - (2.65).

$$\text{Proportional term:} \quad K_c\, \varepsilon(t) \tag{2.63}$$

$$\text{Integral term:} \quad \frac{K_c}{\tau_I} \int_0^t \varepsilon(t')\, dt' \tag{2.64}$$

$$\text{Derivative term:} \quad K_c\, \tau_D\, \frac{d\,\varepsilon(t)}{dt} \tag{2.65}$$

where K_c is the proportional gain, τ_I the integral time and τ_D the derivative time constant. The tuning of these three parameters is essential for the correct action of the PID controller [130].

$c(t)$, the controller command signal regarding the corrective action to be taken, is then defined by Eq. (2.66), which is a differential equation. After application of the Laplace transformation, Eq. (2.67), we obtain a simple non-differential expression for the control command, which is not anymore dependent on the time t, but on the Laplace transformation s, Eq. (2.68).

$$c(t) = K_c \left(\varepsilon(t) + \frac{1}{\tau_I} \int_0^t \varepsilon(t')\, dt' + \tau_D\, \frac{d\,\varepsilon(t)}{dt} \right) \tag{2.66}$$

$$c(s) = \int_0^\infty c(t)\, e^{-st}\, dt \tag{2.67}$$

$$c(s) = K_c \left(1 + \frac{1}{\tau_I\, s} + \tau_D\, s \right) \varepsilon(s) \tag{2.68}$$

A phenomenon common to PID controllers is the so-called reset windup phenomenon [129]. This happens when the error function is so high that the corrective action suggested by the controller is higher than the maximum possible action by the actuator, i.e. the actuator is being saturated due to its physical limitations. This is a very typical situation for the start-up phase of a process, where the system output is far away from the set-point. Consequently, in such a case the feedback error will persist much longer

than usual. As long as the error persists the integrative part of the controller will simply continue to integrate the error contributing further to generate a strong corrective action. When the error is finally reduced, it might take a long time for the "wound up" integral error to return to a correct value and the actuator continues its action. This causes that the system output overshoots the set-point and the overall time to achieve a set-point is high for a conventional PID controller.

To avoid reset windup the error integral update has to be stopped, when the actuator is saturated. One possibility of implementing antireset windup is shown in **Figure 2.11**. In this strategy an additional feedback path is provided, which returns the actuator error ε_a (the difference between command of the control system and the actual actuator output) to the integrative part of the PID controller, with the final purpose to make ε_a equal to zero [127]. The integral is reset this way at a rate equal to the so-called tracking time constant τ_t, which has to be tuned for each control problem. Obviously, if the actuator is not acting beyond its maximum, ε_a is zero, the additional feedback loop is inactive and normal PID control is effectuated.
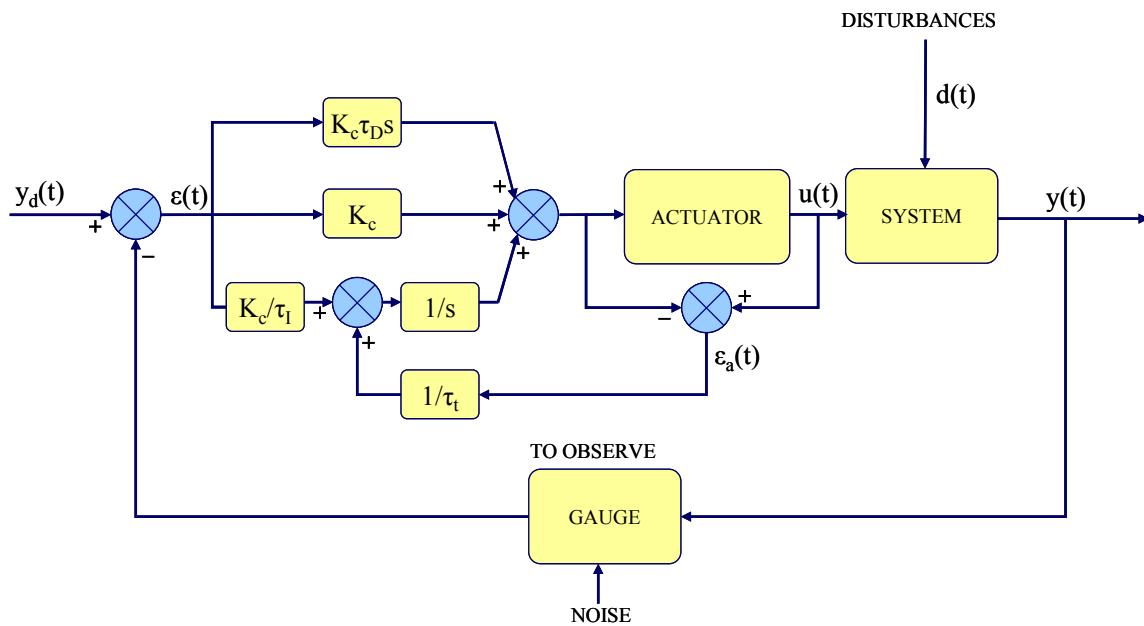
Figure 2.11: General block diagram of a feedback control system with antireset windup implemented in the PID feedback controller. For symbol descriptions refer to text.

# 3 Experimental

3.1 Model pollutants and reagents applied

3.1.1 Model pollutants

The non-biodegradable chlorinated solvents (NBCS) used were dichloromethane (DCM, 99.8%, Panreac, p.A.), 1,2-dichloroethane (DCE, 99.5%, Panreac, p.A.) and trichloromethane (TCM, 99.4%, Merck, p.A.). 4-Nonylphenol (4-NP) was obtained from Fluka (85%, technical grade) and is a mixture of different branched isomers. The pesticides used in the study were alachlor (ALC, 95%, Aragonesas Agro S.A., technical grade), atrazine (ATZ, 95%, Ciba-Geigy, technical grade), chlorfenvinphos (CFVP, 93.2%, mixture of E/Z-isomers, Aragonesas Agro S.A., technical grade), diuron (DIU, 98.5%, Aragonesas Agro S.A., technical grade), isoproturon (IPR, 98%, Aragonesas Agro S.A., technical grade), lindane (LIN, 90%, Rhône-Poulenc Exagama 90, commercial formulation) and pentachlorophenol (PCP, 98%, Sigma-Aldrich, p.A.), Some physical-chemical data on the model pollutants is listed in **Table 3.1** and their chemical structure is depicted in **Figure 3.1**.

Table 3.1: Physical-chemical data of model pollutants [131].

Pollutant	CAS	Formula	Solubility [mg L^{-1}]	K_{OW}	Boiling point
DCM	75-09-2	CH_2Cl_2	13000	1.25	39.8
TCM	67-66-3	$CHCl_3$	7590	1.97	61.7
DCE	1300-21-6	$C_2H_4Cl_2$	5100	1.83	80.4
4-NP	84852-15-3	$C_{15}H_{24}O$	7	5.92	-
ALC	15972-60-8	$C_{14}H_{20}ClNO_2$	240	3.52	-
ATZ	1912-24-9	$C_8H_{14}ClN_5$	35	2.61	-
CFVP	470-90-6	$C_{12}H_{14}Cl_3O_4P$	124	3.81	-
DIU	330-54-1	$C_9H_{10}Cl_2N_2O$	42	2.68	-
IPR	34123-59-6	$C_{12}H_{18}N_2O$	65	2.87	-
LIN	58-89-9	$C_6H_6Cl_6$	7	3.72	-
PCP	87-86-5	C_6HCl_5O	14	5.12	-

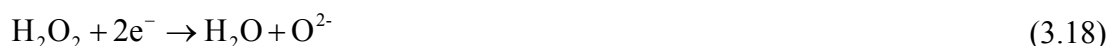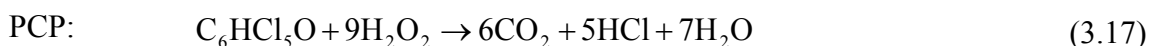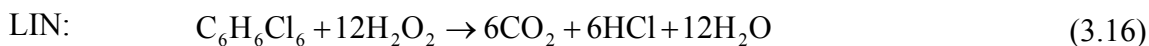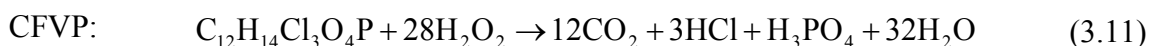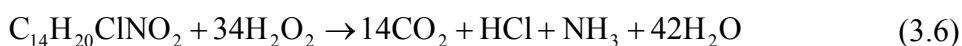All solubility data refers to 25 ºC and pH 7, boiling points to standard atmospheric pressure (1 bar).
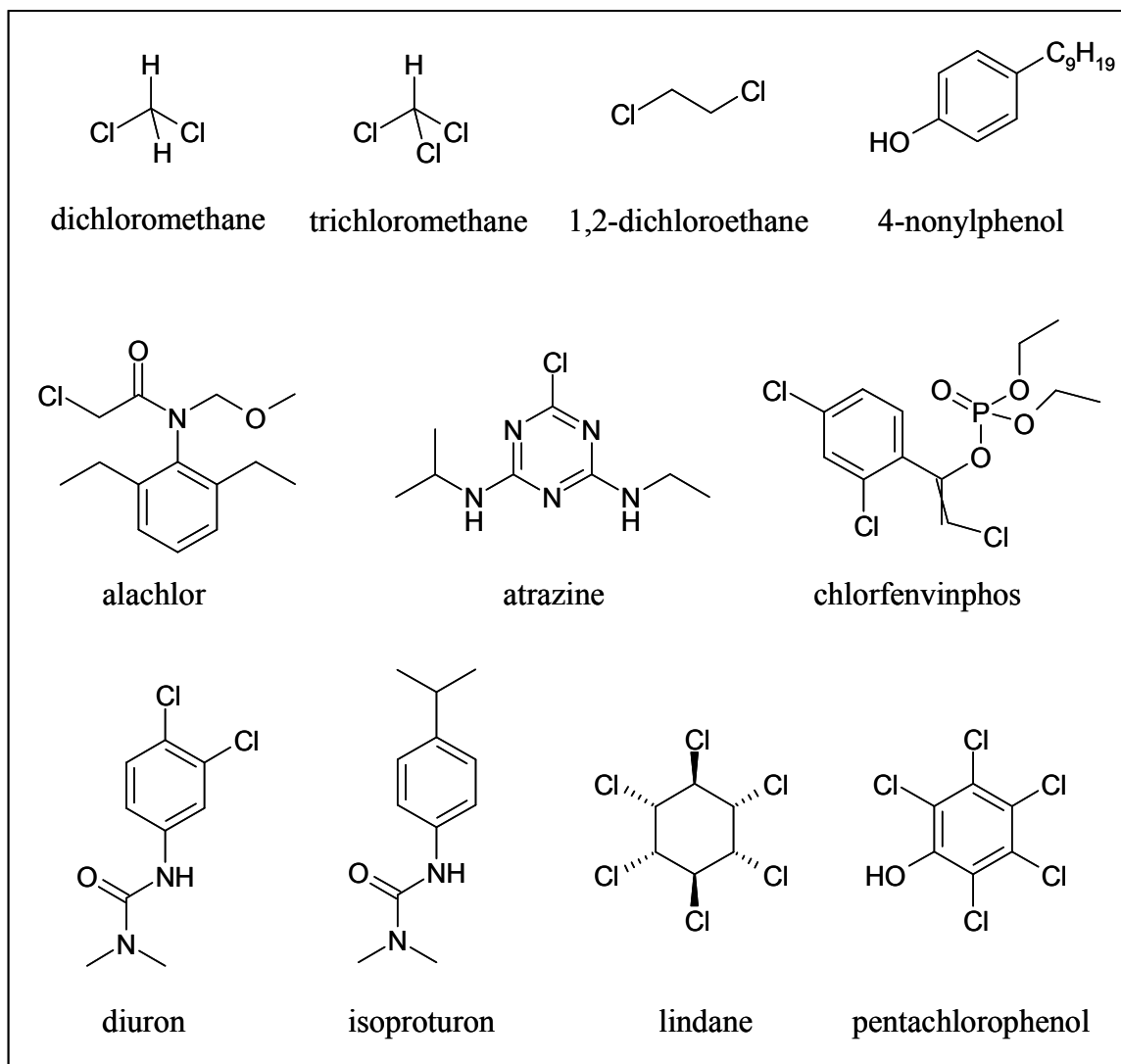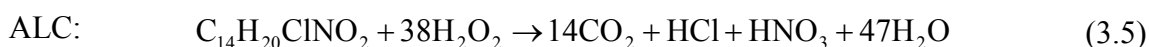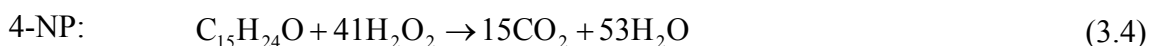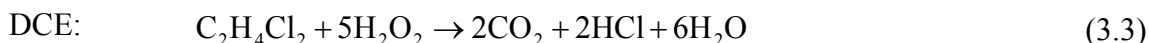
Figure 3.1: Chemical structure of model pollutants.

The stoichiometry of the oxidation of the model pollutants by hydrogen peroxide is listed in Eq. (3.1) - (3.17). From these reactions the theoretical chemical oxygen demand of a pollutant solution can be calculated directly taking into account the molecular weight and the concentration of the pollutant and that the reduction of one hydrogen peroxide molecule requires two electrons, the same as the reduction of one oxygen atom, Eq. (3.18) and (3.19). In the case of nitrogen containing compounds the fate of the nitrogen in the photo-Fenton process is unclear. Consequently, for these compounds both possible stoichiometries were listed (formation of ammonia and nitric acid). Also, atrazine is a special case, because it has been reported that its total mineralisation by hydroxyl radicals is impossible, leading instead to cyanuric acid as final product [132]. Consequently, not only the stoichiometries for total mineralisation are reported here in Eq. (3.7) and (3.8), but also the corresponding stoichiometries for

the formation of cyanuric acid, Eq. (3.9) and (3.10). Note, that the amount of oxidant needed is the same in Eq. (3.8) and (3.10), because the carbon atoms contained in cyanuric acid are already fully oxidised, which is as well the reason for the stability of this substance against an oxidative attack.

DCM: $$CH_2Cl_2 + 2H_2O_2 \rightarrow CO_2 + 2HCl + 2H_2O \tag{3.1}$$

TCM: $$CHCl_3 + H_2O_2 \rightarrow CO_2 + 3HCl \tag{3.2}$$

DCE: $$C_2H_4Cl_2 + 5H_2O_2 \rightarrow 2CO_2 + 2HCl + 6H_2O \tag{3.3}$$

4-NP: $$C_{15}H_{24}O + 41H_2O_2 \rightarrow 15CO_2 + 53H_2O \tag{3.4}$$

ALC: $$C_{14}H_{20}ClNO_2 + 38H_2O_2 \rightarrow 14CO_2 + HCl + HNO_3 + 47H_2O \tag{3.5}$$

$$C_{14}H_{20}ClNO_2 + 34H_2O_2 \rightarrow 14CO_2 + HCl + NH_3 + 42H_2O \tag{3.6}$$

ATZ: $$C_8H_{14}ClN_5 + 35H_2O_2 \rightarrow 8CO_2 + HCl + 5HNO_3 + 39H_2O \tag{3.7}$$

$$C_8H_{14}ClN_5 + 15H_2O_2 \rightarrow 8CO_2 + HCl + 5NH_3 + 14H_2O \tag{3.8}$$

$$C_8H_{14}ClN_5 + 23H_2O_2 \rightarrow$$
$$C_3H_3N_3O_3 + 5CO_2 + HCl + 2HNO_3 + 27H_2O \tag{3.9}$$

$$C_8H_{14}ClN_5 + 15H_2O_2 \rightarrow$$
$$C_3H_3N_3O_3 + 5CO_2 + HCl + 2NH_3 + 17H_2O \tag{3.10}$$

CFVP: $$C_{12}H_{14}Cl_3O_4P + 28H_2O_2 \rightarrow 12CO_2 + 3HCl + H_3PO_4 + 32H_2O \tag{3.11}$$

DIU: $$C_9H_{10}Cl_2N_2O + 26H_2O_2 \rightarrow 9CO_2 + 2HCl + 2HNO_3 + 29H_2O \tag{3.12}$$

$$C_9H_{10}Cl_2N_2O + 18H_2O_2 \rightarrow 9CO_2 + 2HCl + 2NH_3 + 19H_2O \tag{3.13}$$

IPR: $$C_{12}H_{18}N_2O + 37H_2O_2 \rightarrow 12CO_2 + 2HNO_3 + 45H_2O \tag{3.14}$$

$$C_{12}H_{18}N_2O + 29H_2O_2 \rightarrow 12CO_2 + 2NH_3 + 35H_2O \tag{3.15}$$

LIN: $$C_6H_6Cl_6 + 12H_2O_2 \rightarrow 6CO_2 + 6HCl + 12H_2O \tag{3.16}$$

PCP: $$C_6HCl_5O + 9H_2O_2 \rightarrow 6CO_2 + 5HCl + 7H_2O \tag{3.17}$$

$$H_2O_2 + 2e^- \rightarrow H_2O + O^{2-} \tag{3.18}$$

$$\frac{1}{2}O_2 + 2e^- \rightarrow O^{2-} \tag{3.19}$$

3.1.2 Reagents applied in experiments and analysis

All experiments were performed in distilled water matrix. The distilled water was obtained from the PSA distillation plant (electric conductivity $< 10 \ \mu S \ cm^{-1}$, $Cl^- = 0.2$-$0.3 \ mg \ L^{-1}$, $SO_4^{2-} = 0.2$-$0.3 \ mg \ L^{-1}$, $DOC < 0.5 \ mg \ L^{-1}$). Ultrapure water was obtained from a Millipore Milli-Q® system. Milli-Q® water was applied for preparation of all analytical standards and for eluent preparation and sample dilution in chromatography.

Iron sulphate ($FeSO_4 \cdot 7H_2O$, p.A.), hydrogen peroxide (reagent grade, 30% w/v), sulphuric acid (96% w/w, p.A.) and NaOH (p.A.) were provided by Panreac. Ferric nitrate ($Fe(NO_3)_3 \cdot 9H_2O$, p.A.) and nitric acid (65% w/w, p.A.) were obtained from Merck.

Chromatographic standards of alachlor, atrazine, chlorfenvinphos, diuron and isoproturon were obtained from Riedel - de Häen (Pestanal® product series). In the case of PCP and 4-NP the reagents applied in the degradation experiments were also applied for standard preparation.

All solvents applied in chromatography were HPLC grade. Sodium hydroxide solutions for ionic chromatography were prepared with Baker 50% w/w NaOH solution ("Baker analyzed" grade).

All other reagents employed for determination of dissolved iron and hydrogen peroxide concentration were of p.A. grade.

3.2 Analytical Methods

3.2.1 UV radiation measurement

3.2.1.1 Equipment description and measurement principle

As described above (see **Figure 2.1**) the intensity of the solar spectrum is dependent on the wavelength [22 - 24]. Nevertheless, to characterise solar irradiation or the power input into a solar collector usually figures are employed, which describe the irradiance power within a defined spectral range. These numbers commonly are obtained by broadband measurements, contrarily to spectral intensity measurements. The first type of measurement is performed with so-called broadband radiometers, the second one with spectroradiometers. In this work measurement of global UV irradiance inclined 37º (local latitude) and oriented towards the equator the same way as the solar pilot plants

was considered the most appropriate way to describe the solar power input to the solar collector. The choice of the measurement position of the radiometer is obvious and global radiation measurement is more adequate than direct radiation measurement, because of the nature of the CPC collectors, which are able to utilize global radiation. The choice of the UV spectral range has two principal reasons; first, UV radiometers adjust themselves in their spectral range best to the active radiation of the photo-Fenton process ($\lambda < 580$ nm, [44]) considering the common broadband radiometers available on the market, and second, scientists working on photo-Fenton (e.g. [94]) and related disciplines, such as solar photocatalysis [45] or solar disinfection [133], often choose the same spectral range to evaluate experimental results. Consequently, comparison of results is greatly simplified.
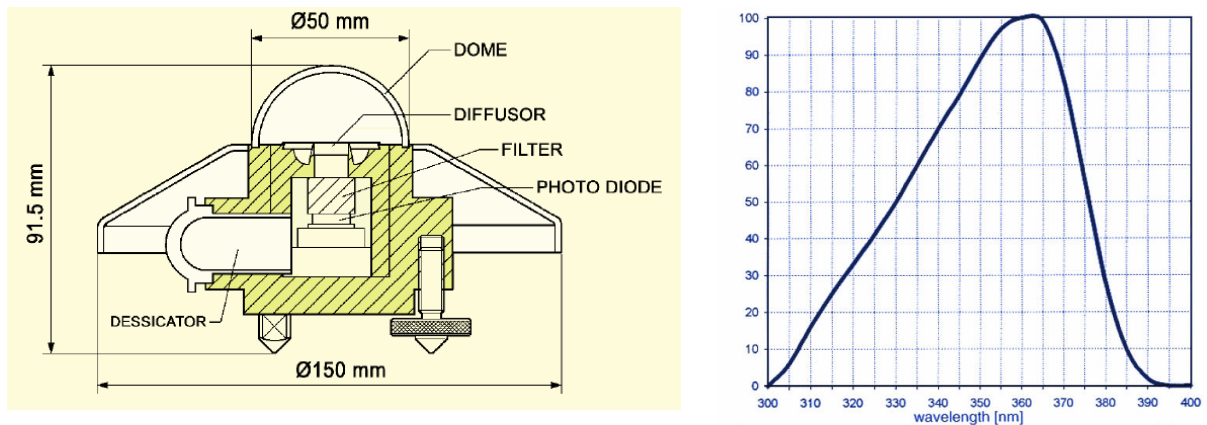
Figure 3.2: a) Drawing and b) relative spectral response of the Kipp & Zonen CUV3 broadband UV radiometer.

The radiometer applied in this work is a Kipp & Zonen CUV3 broadband UV radiometer. The instrument has sensitivity across the entire naturally occurring UV range (285 – 400 nm). The design is based on a combination of diffusor, filter and photodiode (see **Figure 3.2**.a). The diffusor ensures the correct angular response. The filter is the main component responsible for the spectral response (see **Figure 3.2**.b). The photodiode generates a voltage output linearly proportional to the number of incident photons, but each wavelength has its own attenuation factor caused by the filter. Furthermore, the incident photons have a wavelength distribution according to the solar spectrum and the photons of different wavelengths reaching the photodiode are each counted as one photon regardless of their actual energy. The calibration takes these facts into account and calculates the final value of global UV intensity in the spectral

range of 285 - 400 nm, basing itself thereby on the characterisation of the filter and a spectral distribution corresponding to a tungsten-halogen lamp as recommended by ISO 9847, Annex A.3.1 [134]. Due to the intrinsic uncertainties about the spectral distribution and other difficulties related to the measurement (e.g. cosine error) the error margin of the measurement is around 5%.

3.2.1.2 Quality control parameters

Once installed, the radiometer is practically maintenance free. The glass dome is cleaned weekly. To identify abnormal drifts of the measurement the obtained data under clear skies is periodically compared with data of the same annual season from previous years.

3.2.2 Dissolved Organic Carbon (DOC)

3.2.2.1 Equipment description and measurement theory

The DOC was determined to evaluate the degree of mineralisation of the contaminants during the AOP process. To this end an analyser, model Shimadzu TOC-5050A equipped with a Shimadzu ASI-5000A autosampler, was used. This analyser measures Total Carbon (TC) and Total Inorganic Carbon (TIC). The TOC is the difference between TC and TIC of the aqueous samples.

The TC measurement is based on combustion of the aqueous sample on a platinum catalyst supported on aluminium oxide spheres thereby converting all carbon into CO_2. The temperature in the combustion chamber is 680 ºC. The combustion off-gas is then transported by a carrier gas (CO_2 free air at a flow of 150 mL min^{-1}) and fed into a non-dispersive infrared detector common for analysis of CO_2 in gaseous samples. The detector generates an analogue signal, whose shape depicted against time is a peak similar to a Gaussian normal distribution. After being converted by a standard D/A converter the area of this peak is evaluated by the equipment's software.

For the TIC measurement the sample is injected into 25% w/v phosphoric acid. Thereby, carbonate and bicarbonate are liberated as CO_2 and stripped from the reactor by CO_2 free air (150 mL min^{-1}) as a carrier gas. The same detector and signal processing devices are used as for the TC measurement.

For quantification a linear relationship between the peak area and the carbon concentration (for TC and TIC) in the sample exists, which is quantified by calibration

with standard solutions prepared in ultrapure water (Milli-Q® system). The TC measurement is calibrated using potassium hydrogen phthalate (Panreac ACS-ISO) standard solutions, which contain sulphuric acid to avoid contamination by dissolution of atmospheric CO_2. Five linear regression curves were established for the concentration ranges $1 - 10$, $10 - 50$, $50 - 250$, $250 - 1000$ and $1000 - 4000$ mg L^{-1}. For TIC measurement standards were used, which contained half of the carbon as sodium carbonate and the other half as sodium hydrogen carbonate (both analytical grade from Nacalai Tesque). Similarly, five linear regression curves were established for the concentration ranges $0.5 - 2.5$, $2.5 - 15$, $15 - 75$, $75 - 250$ and $250 - 1000$ mg L^{-1}.

To be able to measure carbon contents in such a wide dynamic range the equipment has two separate control mechanisms. First, the sample injection volume can be varied between 4 and 250 µL (depending on the size of the installed syringe) by a precision injection system. Second, the electronic signal can be attenuated by a factor up to 30. The standard deviation of the equipment is around 1% of the measured value. Furthermore, the analyser has automatic statistical quality control based on standard deviation limits set prior to the analysis by the operator for measurements with multiple sample injections. If the criteria are not met, automatic sample re-injection is performed.

3.2.2.2 Procedure

Due to the narrow capillary tubes in the equipment, the equipment can only be used to measure dissolved organic carbon (DOC). Any suspended solids in the sample have to be removed prior to injection into the system. In this work sample filtration through 0.22 µm pore size PTFE syringe-driven filters (Millipore Millex® GN) was applied. After filtration the sample was injected and automatically analysed for DOC by the Shimadzu TOC-5050A analyser as described above. Each measurement was based on two injections with a maximum coefficient of variance of less than 2% (otherwise automatic sample re-injection takes place). The measurement should be performed as soon as possible after sampling because samples containing dissolved iron and hydrogen peroxide (Fenton's reagent) are not stable over a long time.

3.2.2.3 Quality control parameters

Standard solutions are injected periodically to check the correct operation of the equipment. Additionally, in degradation experiments with model contaminants the composition and the theoretical concentration of DOC of the model waste water are

known. The DOC measurement of the initial sample must be in agreement with this theoretical value. Finally, in this case DOC and HPLC-UV (High Performance Liquid Chromatography with UV detection) measurement of the initial sample have to be congruent.

3.2.3 Contaminant concentration by HPLC-UV

3.2.3.1 Equipment description and measurement theory

To follow the degradation of the studied model pollutants in High Performance Liquid Chromatography with UV detection (HPLC-UV) was used, whenever the pollutant allowed it, i.e. the molecule absorbs light with a wavelength greater than 200 nm sufficiently and can be separated by the chromatographic system.

The chromatographic system employed in this system consisted of a chromatograph of the Agilent 1100 series containing a vacuum solvent degassing system, a quaternary solvent pump, an autosampler, thermostatic column oven and a UV/Vis diodearray detection system. The chromatographic column used for separation was a C18 reversed-phase column (LUNA® 5 micron, 3 x 150 mm from Phenomenex), which was protected by a guard-column (Phenomenex Security Guard®). The whole system control and the data evaluation are conducted via a PC interface with Agilent ChemStation® software.

In HPLC a mobile phase is pumped through the system under laminar conditions, so that vertical mixing is negligible. The pressure drop along the chromatographic column is high due to the small pore size of the chromatographic column (usually in the range of 50-200 bars depending on the mobile phase's viscosity and the column properties). The equilibrium solution in stationary and mobile phase dependent on the analyte properties constitutes the separation principle of the method. Organic substances are dissolved into the stationary phase and re-dissolved again into the mobile phase as a function of their affinity to the stationary phase. In reversed-phase chromatography hydrophobic substances are retained stronger than hydrophilic substances, i.e. they move slower through the chromatographic column and hence are detected later. The ultrapure mobile phase is usually a mixture of an organic solvent (normally acetonitrile (ACN) or methanol) and water. As the percentage of the organic solvent in the mobile phase increases, the analytes become increasingly dissolved in the mobile phase and they migrate faster through the chromatographic system. To provide good separation

results the contaminants to be detected should be uncharged inside the chromatographic system. Consequently, in the case of weak acids or bases, the pH of the mobile phase is adjusted accordingly (e.g. acidic to detect weak acids). Depending on the difficulty of the separation problem, there are two different elution methods; isocratic elution (no change of mobile phase during the analysis) is preferred for simple separation problems, whereas gradient elution (change of mobile phase composition during the analysis) is applied to more complex problems, e.g. if several contaminants have to be analysed simultaneously.

After passing the chromatographic column the contaminant generates a signal at the UV/Vis detector passing the flow-through cell in relation with the contaminants absorptive properties and its concentration. The analogue signal is digitized and recorded against time by the software generating peaks with Gaussian form. For quantification there exists a linear relationship between the peak area and the contaminant concentration in the sample, which is obtained by calibration with standard solutions of the analyte.

3.2.3.2 Procedure

An appropriate volume of homogenised sample is drawn, if necessary diluted with ultrapure water and complemented with the organic solvent applied in the mobile phase to yield a final share of organic solvent similar to the percentage in the mobile phase at the time of injection. The whole procedure is effectuated in a graduated flask to obtain an accurate dilution factor. Any suspended solids in the sample have to be removed prior to injection into the system. In this work sample filtration through 0.22 μm pore size PTFE syringe-driven filters (Millipore Millex$^®$ GN) was applied. The filtered sample is then injected into the HPLC-UV system and analysed.

Several aspects concerning the sample preparation procedure applied should be noted. First, by addition of organic solvent prior to filtration adsorption of the contaminant on the filter disk is avoided and any organic compound present as a solid in suspended form is likely to be dissolved before the filtration. Second, because of the preparation procedure the sample matrix is similar to the mobile phase at the time of injection, which optimises the chromatographic performance and avoids so-called peak fronting. Finally, by the addition of comparably large amounts of organic solvent any further reaction of the analytes due to the presence of Fenton's reagent is quenched.

Consequently, the samples can be regarded as stable, once the sample preparation procedure is completed.

As indicated the appropriate elution and detection conditions depend on the analyte's characteristics. **Table 3.2** shows the corresponding conditions for the model substances applied in this work. The flow of the mobile phase was 0.5 mL min^{-1} in all elution programmes. Detection limits depend on the analyte's properties but are usually below 100 µg L^{-1}.

Table 3.2: HPLC-UV elution and detection conditions of target compounds.

Target compounds	Mobile phase (ratio)	Wavelength	Detection limit
4-nonylphenol	H$_2$O/ACN (90/10), 0 - 1 min; H$_2$O/ACN (90/10-5/95), 1 - 4 min; H$_2$O/ACN (5/95), 4 - 15 min	225 nm	30 µg L^{-1}
alachlor	H$_2$O/ACN (40/60)	225 nm	20 µg L^{-1}
atrazine	H$_2$O/ACN (55/45)	254 nm	60 µg L^{-1}
chlorfenvinphos	H$_2$O/ACN (40/60)	240 nm	40 µg L^{-1}
diuron	H$_2$O/ACN (40/60)	254 nm	10 µg L^{-1}
isoproturon	H$_2$O/ACN (55/45)	240 nm	10 µg L^{-1}
pentachlorophenol	H$_2$O(pH 3)/ methanol (10/90)	220 nm	7 µg L^{-1}
pesticide mixture (ALC, ATZ, CFVP, DIU, IPR)	H$_2$O/ACN (65/35), 0 - 12 min; H$_2$O/ACN (35/65), 12.1 - 25 min	as with single substances	as with single substances

3.2.3.3 Quality control parameters

Standard solutions were injected daily to check the correct operation of the equipment. Additionally, in degradation experiments with model contaminants the initial theoretical concentration is known and must be in agreement with the measurement of the initial sample. Also, in model waste water of known composition concentrations determined in HPLC-UV should contribute accordingly to the measured DOC value, provided that the analyte is dissolved and no adsorption on the filter disk takes place in the sample preparation for DOC measurement.

3.2.4 Ion Chromatography (IC)

3.2.4.1   Equipment description and measurement theory

Ion chromatography (IC) is another type of HPLC, but with a different separation principle. With IC compounds present in ionic form in aqueous solution can be detected, i.e. the counter ions of weak and strong acids and bases. In IC the stationary phase inside the chromatographic column in IC contains synthetic ion exchange resin with charged anchor groups as active sites. There are two types of resins depending on the nature of the ion to be retained. Cationic ion exchange resins contain negatively charged anchor groups such as sulphonic or carboxylic acids (strong or weak acid). Anionic ion exchange resins usually contain positively charged quaternary or primary amines (strong or weak base). Consequently, two types of IC systems exist; those designed to separate anions and those for cations. The general set-up is common to both types of IC and generally an IC equipment prepared to separate anions can easily be re-equipped by changing some components to measure cations and vice versa. The mobile phase usually consists of an aqueous solution containing ions that compete with the analytes for the active sites on the stationary phase. In the case of anion IC the most common mobile phases contain hydrogen carbonate/ carbonate, hydroxide or boric acid/ tetraborate. Cation IC mobile phase usually contains sulphuric acid, methanesulphonic acid or hydrochloric acid.

The most common detection system is an electric conductivity detector, which registrates the increase of electric conductivity of the mobile phase as the analyte passes the detector. The problem in the initial development stages of IC was that the signal had a large background due to the mobile phase. Consequently, the sensitivity of the method was very bad. This changed when in the seventies of the past century eluent suppression was developed. The principle of modern membrane suppression is that the eluent is neutralised by supplying hydronium or hydroxyl ions generated by electrolysis via ion exchange membranes to the eluent. Therefore, the background at the detector is greatly reduced and the sensitivity enhanced, so that the detection limits of modern standard IC systems are in the range of several µg L^{-1}. Like in other chromatographic systems the detector signal is recorded and generates peaks of Gaussian shape, the area of which is evaluated. The response of the electric conductivity detector does not have a linear

response over a wide dynamic range (cf. Kohlrausch square root law). Therefore, the calibration applied in this work consisted of three partial linear calibration curves (0.1 – 1, 1 – 10, 10 – 50 mg L^{-1}). In the case of ammonium these partial calibration curves were second degree polynomial regression curves, because the dissociation degree at neutral pH (after suppression) of weak acids/ bases is affected by their concentration. The standard deviation of both systems is around 3%. Operation and data evaluation of both IC systems at PSA were done by a PC interface with Chromeleon$^{®}$ software from Dionex.

The anion IC system at PSA is used to quantify fluoride, chloride, nitrite, nitrate, bromide, sulphate and phosphate with a fast gradient elution programme and acetic acid, formic acid, propionic acid, pyruvic acid, oxalic acid and maleic acid with a slower gradient elution programme. The anion IC system is a Dionex DX-600 system consisting of an autosampler (Dionex AS40 Automated Sampler), quaternary pump (Dionex GP50 Gradient Pump), thermostatic column oven (Dionex LC30 Chromatography Oven) and an electric conductivity detector (Dionex ED50). The mobile phase passes an anion trap column (Dionex Ionpac ATC-3) before the injection valve to guarantee the purity of the mobile phase. Then the eluent flows through a guard column (Dionex Ionpac AG11-HC 4x50mm), the chromatographic column (Dionex Ionpac AS11-HC 4x250 mm), the suppression module (Dionex ASRS-Ultra II 4 mm) and the electric conductivity cell. Then the flow is directed into a full, closed, pressure-resistant 250 mL bottle, where the eluent is mixed to yield a composition changing only very slowly. From the full vessel at the same time the liquid displaced is supplied to the regeneration port of the suppression module. This tailor-made set-up permits working in "AutoSuppression Recycle Mode", while using gradient elution programmes, because it provides the suppression module with a regeneration solution of stable composition.

The cation IC system at PSA is used to determine ammonium, sodium, potassium, magnesium and calcium. It is a Dionex DX-120 system consisting of an autosampler (Dionex AS40 Automated Sampler), a quaternary pump, a guard column (Dionex Ionpac CG12A 4x50 mm), the chromatographic column (Dionex Ionpac CS12A 4x250mm), the suppression module (Dionex CSRS-Ultra 4 mm) and the electric conductivity cell. After passing the conductivity cell the eluent is fed to the regeneration port of the suppression module. So, this IC system is working in the standard configuration for "AutoSuppression Recycle Mode", which is possible, because only isocratic elution is applied.

3.2.4.2   Procedure

The homogenised sample is directly filtered into the sample vials provided for the Dionex autosampler. Sample filtration through 0.22 μm pore size PTFE syringe-driven filters (Millipore Millex® GN) was applied. It has to be noted that samples are not very stable due to the presence of Fenton's reagent and should be measured immediately.

The flow rates were 1.5 and 1.3 mL min^{-1} for the anion and the cation IC system, respectively. The eluent conditions are listed in Table 3.3.

Table 3.3: Eluent composition for IC systems

Equipment	Ions	Mobile phase	Gradient	
			Start (ratio)	End (ratio)
Dionex DX-120	Na^+, NH_4^+, K^+ Mg^{2+}, Ca^{2+}	H_2SO_4, 20 mN	Isocratic	
Dionex DX-600	Cl^-, NO_3^-, NO_2^-, SO_4^{2-}, PO_4^{3-}	H_2O / NaOH 100mM	0 min (80/20) 10 min (65/35)	10 min (80/20) 15 min (65/35)

3.2.4.3   Quality control parameters

Standard solutions were injected daily to check the correct operation of the equipment. Besides, the theoretical final concentration after total mineralisation is known in experiments containing only model compounds and can be used as additional control parameter.

3.2.5 Dissolved iron concentration (Fe^{2+}, Fe^{3+} and total iron)

3.2.5.1   Measurement principle

Dissolved ferrous iron forms a chelate complex with three molecules of 1,10-phenantroline, which has a orange-red colour. The coloured solution follows Beer's law and its absorbance does not change from pH = 3 to 9. In this work the molar extinction coefficient of the complex was determined to be 11720 ± 60 L mol^{-1} cm^{-1} at $\lambda = 510$ nm (95% confidence interval). A pH from 3 to 3.5 ensures rapid and quantitative development of the colour. Consequently, the measurement should be conducted in a buffered solution. Oxidising agents (such as hydrogen peroxide) interfere with the test, because they oxidise ferrous iron to ferric iron, which does not form complexes with the

reagent. Other strong complexing agents such as cyanides, nitrites and polyphosphonates compete with phenantroline for the ferrous iron. Several heavy metals can also form complexes (Cr^{3+}, Zn^{2+}, Co^{2+}, Cu^{2+}, Ni^{2+}) with phenantroline or precipitate it (Ag^{2+}, Bi^{3+}, Hg^{2+}, Cd^{2+}, MoO_4^{2-}). Colour in the sample interferes as well. Several procedures exist to avoid these interferences [135]. In the case of photo-Fenton experiments the usual interferences are mainly colour and of course the presence of hydrogen peroxide.

3.2.5.2 Procedure

For dissolved ferrous iron measurement the sample is filtered through 0.22 μm pore size PTFE syringe-driven filters (Millipore Millex® GN). Then, if necessary, the sample is diluted with distilled water. 4 mL of the filtered and eventually diluted sample are mixed with 1 mL of 1,10-phenantroline solution (0.1% w/v in distilled water) and 1 mL buffer solution (250 g L^{-1} ammonium acetate and 700 mL L^{-1} acetic acid in distilled water). After 1 minute the assay's absorbance at 510 nm is measured in a spectrophotometer (Unicam-II spectrophotometer) against a blank prepared the same way, but replacing the 1,10-phenantroline solution with the same volume of distilled water. This way any colour interference is cancelled.

For total dissolved iron measurement a spatula tip of ascorbic acid is added to the assay readily prepared for ferrous iron measurement. Ascorbic acid reduces ferric iron, hydrogen peroxide and any other oxidant in the solution. Then, the assay is homogenised and suspended ascorbic acid is left to settle. The same procedure is applied to the blank. The absorbance of the sample is measured at 510 nm against the blank after 1 minute.

3.2.5.3 Quality control parameters

The proper state of spectrophotometer and the solutions necessary for the test is verified by the measurement of ferrous iron standard solutions. A further control measure is the measurement of the first samples after iron addition of the degradation experiment, whose value should correspond itself to the theoretical value calculated from the iron addition.

Several things should be noted. First, the sample must be measured immediately due to the presence of hydrogen peroxide, if the objective is to measure the equilibrium ratio of ferrous and ferric iron inside the (photo)reactor. Otherwise, only measurement of total

dissolved iron is meaningful, but also this measurement should be performed quickly to avoid false values due to slow precipitation processes. Second, colour should develop practically immediately corresponding to dissolved ferrous iron. Consequently, the absorbance value of the solution should be constant in the absence of ferric iron, which might be reduced slowly augmenting the colour. Absorbance, which increases slowly, might be due to polymeric ferric iron present in the assay, which is re-dissolved gradually in the presence of complexing agents (ascorbic acid, acetate) and subsequently reduced (ascorbic acid). The problem is solved by the filtration step.

3.2.6 Hydrogen Peroxide concentration by iodometric titration

3.2.6.1 Measurement principle

Iodometry can be applied to measure many oxidising agents. The principle is that an excess of iodide is added to the sample in acidic solution. Then, the oxidising agent reacts quantitatively with the iodide to form a stoichiometrically equivalent amount of triiodide anion, Eq. (3.20). By titration the amount of triiodide anion formed is determined by addition of thiosulphate, which reacts quantitatively to tetrathionate, Eq. (3.21). Starch forms a blue-grey complex with the triiodide ion. Consequently, in the presence of starch as an indicator the complete disappearance of the triiodide ion can be visually observed, because the assay's colour changes from dark blue-grey to transparent.

$$H_2O_2 + 3\,I^- + 2\,H^+ \leftrightarrow I_3^- + 2\,H_2O \tag{3.20}$$

$$I_3^- + 2\,S_2O_3^{2-} \leftrightarrow 3\,I^- + S_4O_6^{2-} \tag{3.21}$$

3.2.6.2 Procedure

20 mL 1 M H_2SO_4 and 25 mL 0.2 M KI (33.2 g L^{-1}) solution are added to the sample (typically 1 – 50 mL). Upon addition of iodide solution in the presence of an oxidant the solution becomes dark yellow. The solution is left standing for 30 - 45 min at room temperature in a closed bottle protected from light. Then, 5 – 10 drops of zinc iodide-starch solution ready for use (Merck Ref. 5445) are added as an indicator. The solution becomes even darker upon the addition of the starch solution. Subsequently, titration is

performed with 0.05 M $Na_2S_2O_3$ (24.82 g L^{-1}) solution. The hydrogen peroxide concentration can be calculated with Eq. (3.22) assuming that all oxidation of iodide to triiodide ion is due to its presence.

$$c_{H_2O_2} = \frac{V_{Na_2S_2O_3}}{V_{sample}} \ 1700 \ \text{mg L}^{-1} \tag{3.22}$$

3.2.6.3 Quality control parameters

To check the proper conditions of the reagents and the burette standard solutions of hydrogen peroxide are evaluated periodically. In degradation experiments with slow hydrogen peroxide consumption the first sample after addition of hydrogen peroxide should have a value close to the theoretical value calculated for the initial concentration. If hydrogen peroxide concentrations below 50 - 100 mg L^{-1} shall be quantified, interferences from dissolved ferric iron and especially dissolved oxygen (both can oxidise iodide) can be considerable and the method is not recommended in this range.

3.2.7 On-line hydrogen peroxide measurement

3.2.7.1 Measurement principle and sensor description

Only few on-line hydrogen peroxide sensors are commercially available (Prominent, Alldos). The sensor applied in this work in the CADOX plant was an Alldos 314-800 sensor specifically developed for hydrogen peroxide measurement. The sensor is connected to an Alldos Conex 350-2200 controller. The signal can then be re-transmitted by the controller to any data acquisition (DAQ) system via an analogue 4 – 20 mA signal. The sensor measures the hydrogen peroxide concentration by an amperometric measurement on a gold electrode (see **Figure 3.3**). The electrode is separated from the sample by a H_2O_2-selective membrane disk. According to the manufacturer the amperometric signal is directly proportional to the hydrogen peroxide concentration in the sample between 20 and 2000 mg L^{-1} and the slope of the current is around 0.8 mA (mg L^{-1} H_2O_2)$^{-1}$. To complete the electric circuit an oxidant enclosed inside the membrane cap is sacrificed at the counter electrode. Consequently, occasionally the electrolyte filling of the membrane cap has to be replaced with

electrolyte provided by the manufacturer (Alldos Ref. 48.1121). The sensor includes internal temperature compensation.

1... 4 pole connection socket

2... electrode shaft with integrated electronics

3... counter and reference electrode

4... measuring electrode

5... O-ring 14 x 1.8 mm

6... membrane cap

7... valve opening

8... hose ring

9... membrane disk holder

10. membrane disk
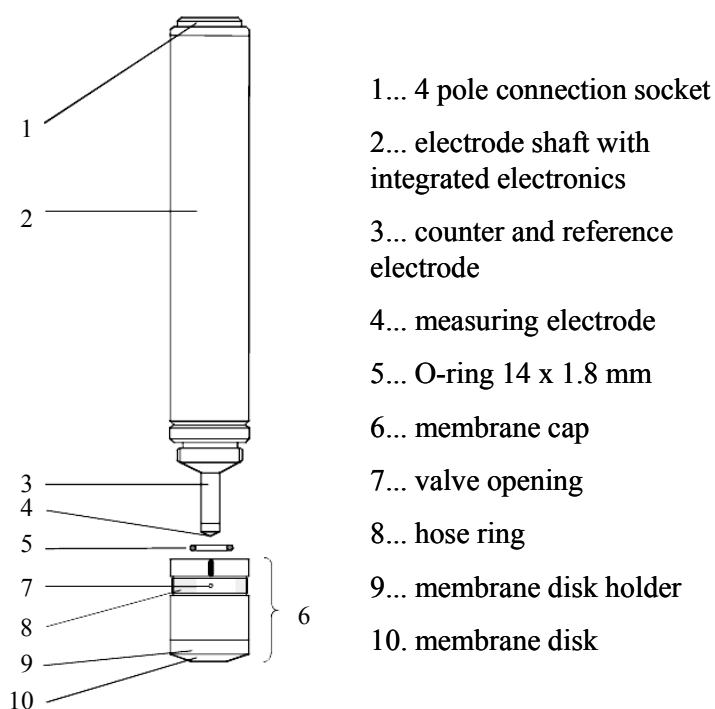
Figure 3.3: Schematic drawing of the Alldos 314-800 sensor.

3.2.7.2   Operation and quality control parameters

The sensor is inserted vertically in the tailor-made mounting provided by the manufacturer. A minimum flow of the sample through the flow-through mounting of 30 L min^{-1} has to be provided. Basically, the sensor is then ready for measurement, but there are several crucial aspects in the operation of the sensor.

- According to the manufacturer no offset of the measurement exists. In this work a variable offset of 30 – 60 mA was detected, which has to be determined daily. The slope was equal to 0.90 mA (mg L^{-1} H$_2$O$_2$)$^{-1}$. In this context field indication of the physical electrode signal (mA) and manual concentration calculation is preferable compared to the direct field concentration indication based on the controller's own calibration function (linear one point calibration without offset). Several daily off-line hydrogen peroxide determinations should be performed by iodometric titration (see chapter 3.2.6) to verify the correct operation of the sensor.

- In the start-up phase the sensor needs around 30 minutes to equilibrate.

- The manufacturer states that within 5 minutes 90% of a concentration change is recorded by the sensor. In this work this response time was measured to be 10 minutes.

- Although the sensor has internal temperature compensation, the compensation mechanism is slow and temperature changes should not be higher than 10 ºC hour^{-1}. Especially, fast temperature fluctuations will be reflected by variation of 2 – 3% of the indicated value per ºC of variation. Related to this, deep insertion of the sensor in the mounting is important to provide fast temperature adaptation of the sensor to changes in the sample.

- The selective membrane is very sensitive to elevated hydrogen peroxide concentration in the water under stopped-flow conditions. If such a state continues for more than approximately 15 minutes, afterwards the sensor indicates far too high values and it takes hours until the sensor recovers its correct behaviour. Consequently, after stopping the flow the sensor mounting has to be flushed with distilled water.

3.2.8 On-line dissolved oxygen (DO) concentration

3.2.8.1 Measurement principle and sensor description

According to Henry's law the concentration of a dissolved gas in distilled water is a function of the Henry constant, the gas' partial pressure in the gaseous phase over the liquid phase and the temperature of the solution [136]. Changes to the aqueous phase, e.g. change of ionic strength, also affect the gas' solubility. Under equilibrium and atmospheric conditions (O_2 partial pressure approximately 200 mbar) about 8 and 6 mg L^{-1} oxygen are dissolved in distilled water at 20 and 40 ºC, respectively [137].

Under dynamic conditions, i.e. O_2 is generated or scavenged inside the solution, the deviation of the concentration from the equilibrium depends largely on the experimental system. Parameters such as if and how O_2 is interchanged with the atmosphere are important as well as how quick O_2 is generated or consumed inside the solution. Consequently, both, DO concentrations below and above the equilibrium concentration are possible depending on the system. E.g., Malato and co-workers [45] state that in wastewater treatment by solar TiO_2 photocatalysis, in plants similar to those used in this

work, to prevent excessive DO depletion a mixed tank open to the atmosphere feeds sufficient oxygen to the solution.

The measurement system employed in this work was a WTW Trioximatic® 700IQ sensor. The sensor employed uses a three-electrode potentiostatic principle to make polarographic measurements. The electrochemical measuring system consists of a gold cathode (working electrode) and two silver electrodes. One silver electrode functions as the current-carrying anode; the other is an independent reference electrode with no current flow. The three electrodes are separated from the media by a membrane cap similar as in the hydrogen peroxide electrode described above (see **Figure 3.3**). The sensor is equipped with internal temperature compensation. The analysis of the signal is performed by the controller pertaining to the WTW IQ Sensornet® system, which subsequently can transform the value in an analogue current signal. According to the manufacturer the sensor has a response time of 180 s at 25 ºC and the measurement range is from 0 to 60 mg L^{-1} DO.

3.2.8.2 Operation and quality control parameters

For operation the sensor is simply inserted in the flowpath of the hydraulic circuit by a proper mounting supplied by the manufacturer (WTW EBST 700-DU flow-thru adapter). The minimum flow velocity is 0.005 m s^{-1}.

During correct operation and in the absence of DO sources and sinks the sensor should mark a value close to the theoretical equilibrium concentration in distilled water. An offset of the measurement can be detected by submersing the DO sensor in a Mn^{2+} solution, where the DO concentration should be close to zero. Calibration at air should be performed every 3 - 6 months. The calibration history gives evidence of abnormal drift phenomena.

3.2.9 Laboratory and on-line pH measurement

3.2.9.1 Definition, measurement principle and sensor description

The pH value is by definition the negative common logarithm of the activity of the positively charged hydrogen ions in aqueous solution. Theory and measurement are not as trivial as usually considered, which is demonstrated by the edition of whole books on the topic [138]. Whenever the pH value of a solution is reported this data should be accompanied by the temperature at which it was measured. Alternatively, the pH value

can be corrected by convention to a fixed temperature, which is the usual approach. In this work all pH values measured are corrected to a value at 25 ℃. The correction was either done manually in the case of laboratory measurements performed without temperature compensation and automatically in the case of on-line measurement in the pilot-plant. Eq. (3.23) used for manual temperature correction can be derived from the Nernst equation.

$$pH_{25\,°C} = 7 - \frac{413 - 59\,pH_{T_m\,°C}}{54 + 0.2\,T_m} \tag{3.23}$$

In Eq. (3.23) $pH_{T_m\,°C}$ is the value of the pH measurement at T_m ℃. Correction becomes more important as the temperature difference from 25 ℃ and the deviation from neutral pH increase.

The measurement principle of the most common devices and those applied in this work is based on potentiometric measurement of the potential generated by a concentration difference on a membrane or a diaphragm. In the laboratory pH measurements were performed with a pH-meter from Crison, model micro pH 2002, equipped with a standard glass electrode from Crison. This measurement was performed without automatic temperature compensation. In the CADOX plant the pH was measured with a WTW® Sensolyt SEA electrode inserted in a WTW Sensolyt® 700IQ sensor having integrated internal temperature compensation. The WTW sensor was connected to the WTW IQ sensornet® controller for signal processing and re-transmission. In both electrodes the reference electrode system is a conventional Ag/AgCl/Cl electrode system, which in the case of the WTW electrode is embedded in a solid gel-polymer electrolyte. In this case the polymer matrix/ process fluid interphase consists of a pinhole diaphragm; i.e. an electrical flux is established through two fine holes in the glass wall of the electrode.

3.2.9.2 Operation and quality control parameters

Measurement in the laboratory was as simple as submersing the electrode and waiting until the instrument reached equilibrium, while the sample was stirred magnetically. The on-line WTW sensor was simply inserted in the flowpath of the hydraulic circuit by a proper mounting supplied by the manufacturer (WTW EBST 700-DU flow-thru adapter). The flow velocity during measurement was usually 0.08 m s^{-1}.

A correct calibration of the system is fundamental for correct measurement. To this end both systems were calibrated with two point calibration with two standard buffer solutions at pH 4.01 and pH 7.00 (obtained from Panreac). Flow and mixing conditions were adjusted to be as similar as possible during calibration and measurement. In the laboratory the calibration was performed weekly, and in the on-line sensor every three months. The calibration history can be used to detect malfunctioning and deterioration of the pH electrode.

3.2.10   On-line ORP measurement

3.2.10.1 Definition, measurement principle and sensor description

The Oxidation-Reduction potential (ORP) is a measure of the reducing or oxidizing strength of a solution. A negative potential value means that the solution has a reducing action when compared with a reference electrode. The classic reference electrode is the standard hydrogen electrode, but nowadays, most measurements refer to an Ag/AgCl/Cl electrode system, because it is easily implemented in commercial electrodes. Whenever the ORP value of a solution is reported this data should be accompanied by the temperature at which it was measured, because high temperature dependence exists. Alternatively, the ORP value can be corrected by convention to a fixed temperature, which is the usual approach. In this work all ORP values measured are corrected to a value at 25 ºC. The formula for temperature correction can be derived from the Nernst equation, like in Eq. (3.23).

In an ideal measurement system the ORP value would be sensitive to all present species, but under real conditions this is not the case due to electrode inhibition and irreversible electrode reactions. Consequently, the ORP value is most sensitive towards ionic redox couples, such as H^+/H_2, or Fe^{2+}/Fe^{3+}, but not towards H_2O_2. Therefore, the ORP value should not be regarded as a thermodynamic measurement, but a kinetic one largely influenced by electrode kinetics.

The measurement principle of the most common devices and the one employed in this work is based on potentiometric measurement of the potential generated by the sample on a platinum working electrode. In the CADOX plant the ORP was measured with a WTW Sensolyt® PtA electrode inserted in a WTW Sensolyt® 700IQ sensor having

integrated internal temperature compensation. The sensor was connected to the WTW IQ sensornet® controller for signal processing and re-transmission.

The reference electrode system is a conventional Ag/AgCl/Cl electrode system, which is embedded in a solid gel-polymer electrolyte. The polymer matrix/ process fluid interphase consists of a pinhole diaphragm; i.e. an electrical flux is established through a fine hole in the glass wall of the electrode.

3.2.10.2 Operation and quality control parameters

The operation of the on-line WTW sensor is as simple as insertion in the flowpath of the hydraulic circuit by a proper mounting supplied by the manufacturer (WTW EBST 700-DU flow-thru adapter). The flow rate during measurement was usually 0.08 m s^{-1}.

ORP measurement does not require calibration, because the electrode gives an absolute value. Nevertheless, the correct operation of the measurement system is checked periodically by measurement of standard solutions of 220 and 468 mV redox potential (obtained from Crison). Flow and mixing conditions were adjusted to be as similar as possible during measurement of standards and process fluid. The history of these periodical checks can be used to detect malfunctioning and deterioration of the ORP electrode.

3.3 Pilot-Plants

3.3.1 BRITE plant

Two identical reactors of this type are installed at PSA (see **Figure 3.4**). The hydraulic circuit of the reactor consists of a continuously stirred tank, a centrifugal re-circulation pump, a solar collector and connecting tubing and valves. The plant is designed for operation in batch mode. The total volume in the experiments was 35 L (the maximum volume of the whole system with a completely full tank is 39 L), the volume irradiated in the solar collector was 22.4 L.

Each solar collector consists of three CPC modules in series (total irradiated surface: 3.08 m^2) placed on fixed supports inclined 37° (latitude of PSA) with respect to the horizontal plane and facing south. The CPC reflector has a concentration factor of 1 and the radiation acceptance angle is 90º, meaning that all radiation (direct and diffuse) incident on the collector plane is being collected. The reflectors consist of electro-

polished aluminium. The plug flow photoreactor is made of borosilicate glass tubes (inner diameter 29.2 mm, outer diameter 32.0 mm, length 1.37 m, 24 tubes). All the tubes and the collectors are connected in series. A detailed description of the properties of the materials used in the set-up of the CPC was given by Blanco and co-workers [32]. The 10 L round-bottom borosilicate glass tank provides aeration and samples for analyses. The connected tubing is made of inert high-density polyethylene tubing with a ¾" inner diameter. The reaction solution is continuously fed to the plug flow photoreactor from the tank by means of a centrifugal pump (PAN WORLD, Model: NH-100 PX, 100 W). The flow rate, constant in all experiments, was 1.2 m^3 h^{-1}. The Reynolds number was about 17000, indicating a turbulent regime of the flow inside the tubes. Temperature is measured by a thermocouple inside the tubing and indicated in the field.
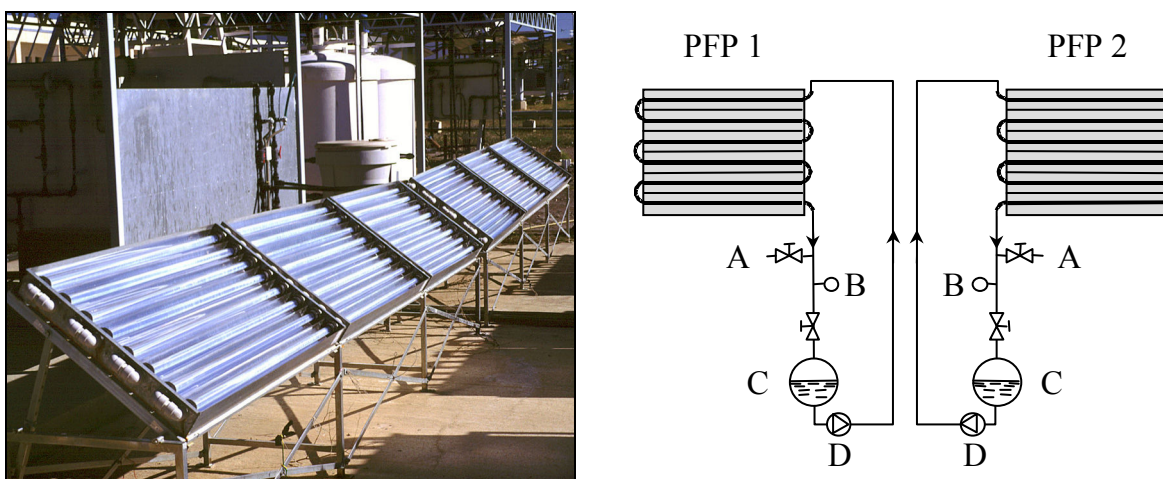
Figure 3.4: Photo and flow diagram of the two BRITE plants at PSA: (A) sampling valve; (B) thermocouple; (C) tank; (D) pump; (PFP) plug flow photoreactor.

3.3.2 CADOX plant

The hydraulic circuit of the reactor consists of a continuously stirred tank, a centrifugal re-circulation pump, a solar collector and connecting tubing and valves. In the connecting tubing several on-line sensors and devices for heating and cooling of the process fluid are incorporated. Furthermore, 3 dosing pumps are installed, which can automatically dose reagents directly to the tank. The system is completed by an instrument panel in the field containing all the electric and electronic installations and a

PC in the office for on-line data acquisition and making of process control decisions. **Figure 3.5** shows a flow diagram of the CADOX plant and a photo of its solar collector.
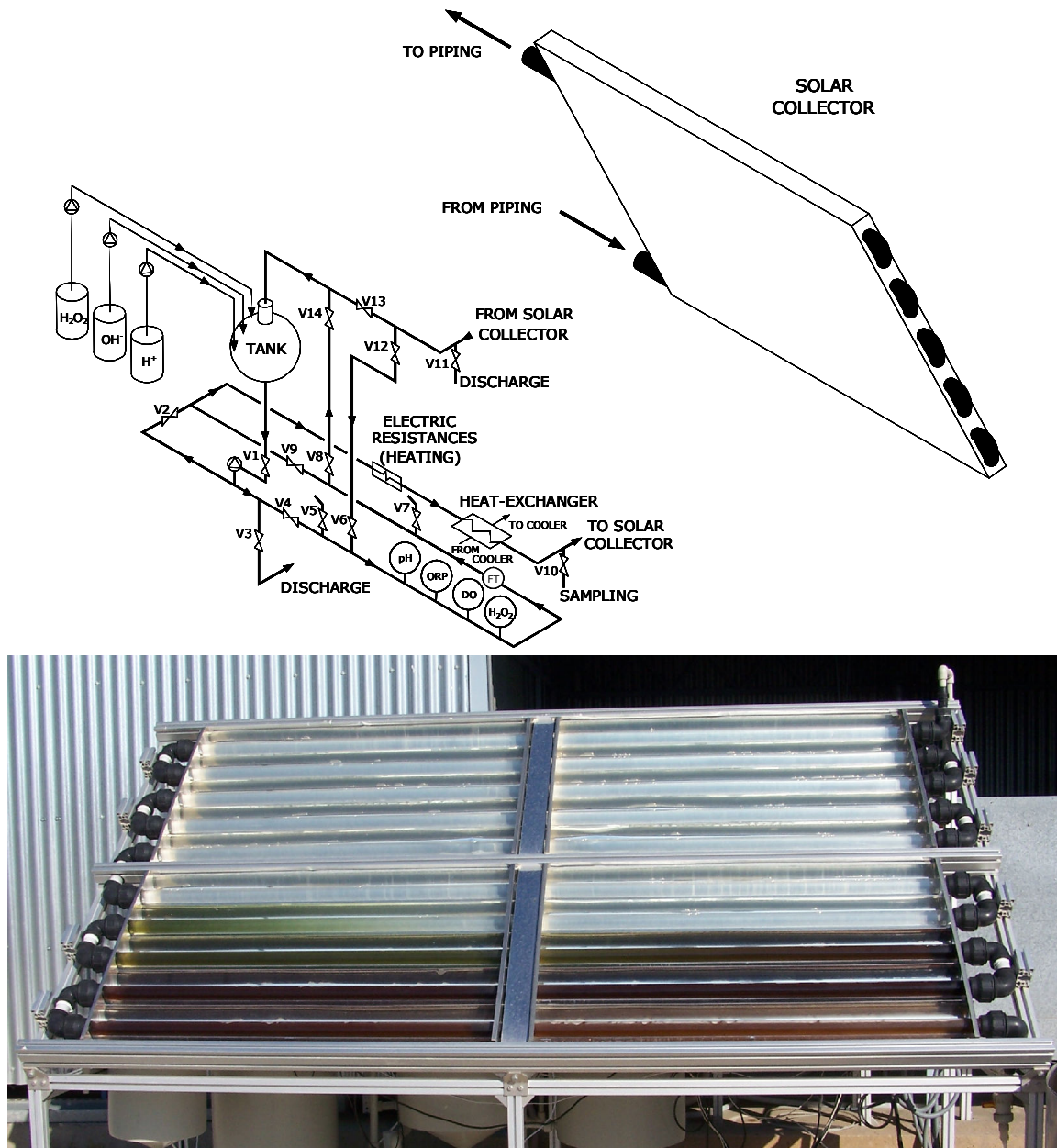
Figure 3.5: Photo and isometric drawing of the CADOX plant at PSA

The plant is designed for operation in batch mode. The total volume in the experiments was 75 L (the maximum volume of the whole system with a completely full tank is 82 L), the volume irradiated in the solar collector could be varied between 8.9 L and 44.6 L, which corresponds to uncovering 20% and 100% of the collector surface, respectively. This was done by covering the corresponding part of the collector with tailor-made aluminium sheets.

The solar collector consists of four CPC modules (total irradiated surface: 0.83 - 4.16 m^2, see above) placed on fixed supports inclined 37° with respect to the horizontal plane and facing south. The plug flow photoreactor is made of borosilicate glass tubes (inner diameter 46.4 mm, outer diameter 50.0 mm, length 1.32 m, 20 tubes). The CPC reflector has a concentration factor of 1 and the radiation acceptance angle is 90º (confer section 2.1.4). The reflectors consist of electro-polished aluminium. All the tubes and the collectors are connected in series. [32] describes the properties of the materials used in the set-up of the CPC.

The tank is a 20 L round bottom borosilicate glass flask. Piping and valves are made of inert polypropylene with a ¾" inner diameter. To be able to manipulate the flow rate an abnormal shaft driven pump was chosen (Bominox SIM-1051, 370 W, 400V AC), which can be regulated by a three-phase frequency regulator. Nevertheless, flow was constant in all experiments (1.5 m^3 h^{-1}), which corresponds to turbulent flow inside the photoreactor with a Reynolds number of 13000.

The on-line measurement system consists of:

- flow meter: Electromagnetic flow meter $0.3 - 3$ m^3 h^{-1} tailor-made by Comaquinsa S.A.
- pH: WTW Sensolyt® IQ 700 sensor with WTW Sensolyt® SEA electrode for WTW IQ Sensornet® system
- ORP: WTW Sensolyt® IQ 700 sensor with WTW Sensolyt® PtA electrode for WTW IQ Sensornet® system
- DO: WTW Trioximatic® 700 for WTW IQ Sensornet® system
- H$_2$O$_2$: Alldos 314-850 H$_2$O$_2$ selective amperometric electrode connected to a Alldos Conex 350-2200 controller

Temperature could be obtained from each of the WTW sensors from the temperature probe integrated for internal temperature correction.

Piping and the valves of the plant have been designed in such a way, that two configurations were possible (see **Figure 3.5**). In the first configuration the sequence of the re-circulation loop was "tank – re-circulation pump – sensors – temperature adjustment – solar collectors – tank" (open valves: V1, V4, V9, V13). In the second, the sequence is "tank – re-circulation pump –temperature adjustment – solar collectors – sensors – tank" (open valves in the order as the fluid passes them: V1, V2, V12, V6, V8, V14). Thereby, on-line measurements can be performed at the inlet or the outlet of

the solar collector depending on the configuration chosen. In the experiments the first configuration was chosen if not stated differently.

All on-line data acquisition instruments transmit their information via an analogue output of their respective controllers to a series of FieldPoint I/O modules (Advantech ADAM® 4000 series). These modules transmit data based on an RS485 protocol and can be connected to the serial interface of a personal computer by applying an intermediate RS485/RS232 converter module from the same manufacturer.

Custom SCADA (Supervisory Control And Data Acquisition) software for this was programmed in National Instruments LabVIEW® 7.0 at Plataforma Solar de Almería. This software performs data acquisition and supervisory control of the plant at the same time.

Several types of control actions are available. First, temperature can be controlled by turning on and off thermal resistances that warm the fluid by heating up part of the pipes containing the fluid and by opening and closing electrovalves that turn the secondary cooling-fluid flow through the connected heat exchanger on and off (see **Figure 3.5**). Second, pH can be controlled by addition of acid or base to the system batch re-circulation tank. Finally, control of hydrogen peroxide concentration is performed in a similar way by addition of 30% w/v hydrogen peroxide solution to the batch re-circulation tank. Acid, base, and hydrogen peroxide are all added by diaphragm dosing pumps provided by Alldos (Alldos Primus® 208 Etron Profi E26-0.8). The pump flow can be controlled by varying stroke frequency, which is done by an analogue current signal. This signal is calculated and transmitted to the dosing pumps by the above-mentioned SCADA software and the Advantech ADAM® I/O modules.

3.3.3 Fenton reactor

A few dark Fenton experiments were performed in the laboratory in a single-necked 5 L borosilicate glass bottle. The solution was protected from light but open to the atmosphere to permit gas exchange between atmosphere and solution. A conventional magnetic stirrer equipped with a heating plate and a temperature probe was used to homogenise the reaction solution and to control the solution temperature. All sampling and reagent dosing was done manually through the bottleneck.

3.4 Experimental Set-up – Degradation experiments

3.4.1 Photo-Fenton degradation experiment – General procedure

The preparation of the photo-Fenton experiments followed a strict protocol:

- The solar collectors were covered to prevent any photochemical reactions and filled with distilled water.

- The pollutant was introduced into the pilot-plant. All pollutants treated have only low-to-medium solubility (4-nonylphenol, pesticides) or are volatile (NBCS). Consequently, special procedures were applied to ensure that the whole amount of pollutant was dissolved inside the pilot-plant (see below).

- The pilot-plant was re-circulated until perfect homogenisation and pollutant dissolution was attained. In thermostatic experiments in this phase also the temperature of the process fluid was adjusted. The duration of this phase was 15 – 60 min.

- The initial sample (sample 1) was taken and the pH was adjusted immediately afterwards to the desired value with sulphuric acid. The plant was re-circulated 15 min to ensure perfect homogenisation. This step was omitted in pentachlorophenol degradation experiments (see Results and Discussion for details).

- Sample 2 was drawn and immediately afterwards the calculated amount of ferrous sulphate heptahydrate was added pre-dissolved in 30 – 50 mL aqueous solution at pH 2. The plant was re-circulated 15 minutes to ensure perfect homogenisation.

- Sample 3 was drawn and immediately afterwards the calculated amount of initial H_2O_2 (30% w/v solution) was added. The plant was re-circulated 15 minutes to ensure perfect homogenisation. Dark Fenton reaction occured during these 15 minutes.

- Sample 4 was drawn and immediately afterwards the light protection was removed from the solar collectors. This is the moment, in which the photo-Fenton degradation experiment begins (zero time and accumulated UV radiation energy)

- Once the photo-Fenton phase had begun the concentration of peroxide in the pilot-plant was frequently determined and controlled by addition of small

portions of hydrogen peroxide to be in the concentration range of 200 – 500 mg L^{-1}. Lower dosing (~50 mg L^{-1} maintained) was applied in PCP and lindane experiments because of the low initial chemical oxygen demand of the model wastewater. 4-Nonylphenol experiments received only an initial H$_2$O$_2$ dosing because of the same reason. After the beginning of the photo-Fenton degradation experiment neither further pH adjustments nor iron additions were done.

3.4.2 Pollutant dissolution procedures

As stated above different procedures were applied to introduce the pollutant into the pilot-plant. The reasons were mainly due to low-to-medium water solubility or high volatility of the model compounds. Consequently, direct addition of the pollutant into distilled water inside the pilot-plant is not a reliable procedure due to the design of the photoreactors including its necessary dead ends and knees.

- Method A (NBCS in BRITE plant): The solubility of these compounds is rather high, but they can be very easily volatilised due to their low boiling point. Furthermore, due to their high density they can settle in dead ends in the piping. So, the necessary quantity was dissolved in distilled water in a closed 2.5 L glass bottle. When the compound was completely dissolved, the solution was added to the pilot plant.

- Method B (4-nonylphenol, atrazine, diuron, pentachlorophenol and lindane in BRITE plant): An auxiliary 100 L-tank, connected to a centrifugal pump for water re-circulation was filled and saturated solutions were prepared by adding 50 g of the pure compound and mixing overnight. In the morning, the re-circulation was stopped to enable gravity phase separation of the residual, not dissolved pollutant. After 15 minutes a sample was taken from the centre of the solution and analysed by HPLC-UV to determine the exact dissolved concentration. Afterwards, the necessary quantity of solution was withdrawn from the centre of the tank and transferred to the pilot plant to achieve the desired initial concentration inside the pilot-plant. Only in the case of lindane only 5.5 g of the commercial product (90% w/w) were added to the 100 L-tank and after mixing overnight 35 L were directly transferred to the pilot-plant

because no analytical method was available to measure the lindane concentration.

- Method C (alachlor, chlorfenvinphos and isoproturon in BRITE plant): An auxiliary 100 L-tank, connected to a centrifugal pump for water re-circulation was filled and 100 mg L^{-1} solutions were prepared by adding 10 g of the pure compound and mixing overnight. Determination and transfer of the necessary amount of solution to achieve the desired initial concentration were performed like in Method B.

- Method D (all experiments in CADOX plant): Due to the increased volume of the CADOX plant and the possibility of heating inside the pilot-plant the procedure was changed. A concentrated solution was prepared by adding the pure compound and mixing overnight in the laboratory in two light-protected five-litre flasks (i.e. 10 L) at 60 ºC. Afterwards, the water was transferred to the CADOX plant pre-heated to 50 ºC. The solution was re-circulated during 1 hour and finally, the water temperature was set to the desired temperature before the experiment continued.

3.4.3 4-Nonylphenol in the BRITE plant

All experiments were performed in the BRITE plant with 35 L total volume. 4-Nonylphenol (4-NP) has a low solubility (7 mg L^{-1}). Consequently, it might adhere to the polymer and glass walls of the pilot-plant. Experiment NP1 was performed as blank experiment to be able to distinguish adsorption inside the system from degradation.

Table 3.4: Experimental set-up of 4-NP experiments in the BRITE plant.

Exp.	A/ V_{ill}	c_{Fe}	T	pH	$H_2O_2^o$	substance	c^i	Prep.
	[m^2]/ [L]	[mg L^{-1}]	[ºC]		[mg L^{-1}]		[mg L^{-1}]	
NP1	0/ 0	0	27-43	2.8	0	4-NP	1.8	B
NP2	1.03/ 7.5	5	33-39	2.8	100	4-NP	2.2	B
NP3	1.03/ 7.5	1	25-33	2.8	100	4-NP	1.9	B

"Prep." refers to the dissolution procedures described in chapter 3.4.2.

Due to the expected high reaction rate only one CPC module was exposed to the sun in the degradation experiments. The initial hydrogen peroxide dosing was the only

addition along the experiment and was approximately 8 times the theoretical stoichiometric H_2O_2 amount (6.3 times higher than the pollutant concentration) necessary for mineralisation. Further details on the experimental set-up are listed in **Table 3.4**.

Analytical determinations included 4-NP concentration by HPLC-UV, on-line UV measurement, on-line temperature inside solution, off-line pH, off-line H_2O_2 concentration and dissolved iron concentration.

3.4.4 Non-biodegradable chlorinated solvents in the BRITE plant

All NBCS experiments were performed in the BRITE plant with 35 L total volume. To check for possible volatilisation blank experiments were. All degradation experiments were performed at two different iron concentrations. Further details on the experimental set-up are listed in **Table 3.5**.

Table 3.5: Experimental set-up of NBCS experiments in the BRITE plant.

Exp.	A/V_{ill}	c_{Fe}	T	pH	$H_2O_2{}^o$	substance	c^i	Prep.
	$[m^2]/[L]$	$[mg\,L^{-1}]$	[ºC]		$[mg\,L^{-1}]$		$[mg\,L^{-1}]$	
DCM1	0/ 0	0	20-30	2.8	0	DCM	50	A
DCM2	3.08/ 22.4	2	16-32	2.8	600	DCM	50	A
DCM3	3.08/ 22.4	55.8	19-24	2.8	600	DCM	50	A
TCM1	0/ 0	0	14-30	2.8	0	TCM	50	A
TCM2	3.08/ 22.4	2	17-36	2.8	600	TCM	50	A
TCM3	3.08/ 22.4	55.8	29-40	2.8	600	TCM	50	A
DCE1	0/ 0	0	20-28	2.8	0	DCE	50	A
DCE2	3.08/ 22.4	2	23-40	2.8	600	DCE	50	A
DCE3	3.08/ 22.4	55.8	18-26	2.8	600	DCE	50	A

"Prep." refers to the dissolution procedures described in chapter 3.4.2.

Analytical determinations in the blank experiments without irradiation included the measurement of DOC, temperature inside solution on-line and pH off-line.

In the NBCS photo-Fenton degradation experiments the analytical determinations were on-line UV irradiance, DOC, chloride concentration by IC, temperature inside solution on-line, pH off-line, H_2O_2 off-line and dissolved iron measurement.

3.4.5 Pesticides in the BRITE plant

Photo-Fenton degradation experiments were performed in the Brite plant with a total volume of 35 L. All substances were degraded at two different iron concentrations (2 and 55.8 mg L^{-1}), except alachlor, which was degraded also in a third experiment at 10 mg L^{-1}. Initial hydrogen peroxide concentrations were selected as a function of the chemical oxygen demand of the model wastewater. Further details on the experiments can be found in **Table 3.6**.

Table 3.6: Experimental set-up of pesticide experiments in the BRITE plant.

Exp.	A/ V_{ill}	c_{Fe}	T	pH	$H_2O_2^o$	substance	c^i	Prep.
	$[m^2]/[L]$	$[mg\ L^{-1}]$	$[^oC]$		$[mg\ L^{-1}]$		$[mg\ L^{-1}]$	
ALC1	3.08/ 22.4	2	23-30	2.8	530	ALC	50	C
ALC2	3.08/ 22.4	55.8	24-31	2.8	530	ALC	50	C
ALC3	3.08/ 22.4	10	30-39	2.8	530	ALC	50	C
ATZ1	3.08/ 22.4	2	26-38	2.8	360	ATZ	30	B
ATZ2	3.08/ 22.4	55.8	24-30	2.8	360	ATZ	30	B
CFVP1	3.08/ 22.4	2	33-40	2.8	320	CFVP	50	C
CFVP2	3.08/ 22.4	55.8	37-40	2.8	320	CFVP	50	C
DIU1	3.08/ 22.4	2	13-27	2.8	260	DIU	30	B
DIU2	3.08/ 22.4	55.8	32-39	2.8	260	DIU	30	B
IPR1	3.08/ 22.4	2	24-32	2.8	660	IPR	50	C
IPR2	3.08/ 22.4	55.8	27-38	2.8	660	IPR	50	C
LIN1	3.08/ 22.4	2	32-33	2.8	160	LIN	30	B
LIN2	3.08/ 22.4	55.8	32-34	2.8	160	LIN	30	B
PCP1	3.08/ 22.4	2	19-23	6.4	96	PCP	20	B
PCP2	3.08/ 22.4	55.8	28-31	6.4	96	PCP	20	B

"Prep." refers to the dissolution procedures described in chapter 3.4.2.

The analytical determinations performed included on-line UV irradiance, the pollutant concentration (by HPLC-UV), DOC, evolution of inorganic ions (NH_4^+, NO_2^-, NO_3^-, Cl^-, PO_4^{3-}) by IC, on-line temperature measurement inside the plant, off-line hydrogen peroxide concentration, dissolved iron concentration and off-line pH. Only, in the case of lindane the pollutant concentration was not determined due to the absence of an HPLC-UV analysis method (the lindane molecule does not absorb photons with a wavelength higher than 200 nm).

3.4.6 Single pesticides and mixtures of pesticides in the CADOX plant

Photo-Fenton degradation experiments were performed in the CADOX plant with a total volume of 75 L. Temperature was controlled by the temperature control system of the CADOX plant. To simulate more complex wastewater, mixtures of five low-medium soluble pesticides were prepared. Thereby, also mixtures of higher total concentrations were obtained (Experiments MIX3 and MIX4 had a total initial pesticide concentration of 150 mg L^{-1}). To check for reproducibility the mixture experiments were performed in duplicate. Details can be found in **Table 3.7**.

Table 3.7: Experimental set-up of experiments with single substances and mixtures of pesticides in the CADOX plant.

Exp.	A/ V_{ill}	c_{Fe}	T	pH	$H_2O_2^o$	substance	c^i	Prep.
	[m^2]/ [L]	[mg L^{-1}]	[°C]		[mg L^{-1}]		[mg L^{-1}]	
ALC4	4.16/ 44.6	20	30	2.8	400	ALC	50	D
ALC5	4.16/ 44.6	55.8	20	2.8	400	ALC	100	D
ATZ3	4.16/ 44.6	20	30	2.8	400	ATZ	30	D
CFVP3	4.16/ 44.6	20	30	2.8	400	CFVP	50	D
DIU3	4.16/ 44.6	20	30	2.8	400	DIU	30	D
IPR3	4.16/ 44.6	20	30	2.8	400	IPR	50	D
MIX1	4.16/ 44.6	10	30	2.8	460	ALC, ATZ, CFVP, DIU, IPR	10 each	D
MIX2	4.16/ 44.6	10	30	2.8	460	ALC, ATZ, CFVP, DIU, IPR	10 each	D
MIX3	4.16/ 44.6	10	30	2.8	460	ALC, ATZ, CFVP, DIU, IPR	30 each	D
MIX4	4.16/ 44.6	10	30	2.8	460	ALC, ATZ, CFVP, DIU, IPR	30 each	D

"Prep." refers to the dissolution procedures described in chapter 3.4.2.

The analytical determinations performed were the same as with these substances in the BRITE plant, namely, on-line UV irradiance, the pollutant concentration (by HPLC-UV), DOC, evolution of inorganic ions (NH_4^+, NO_2^-, NO_3^-, Cl^-, PO_4^{3-}) by IC, on-line temperature measurement inside the plant, off-line hydrogen peroxide concentration, dissolved iron concentration and off-line pH. Additionally, on-line DO, ORP and pH value were measured.

3.4.7 Factorial design - alachlor experiments in the CADOX plant

To assess three process input variables (factors) an experimental design based on a three factor central composite design without star points was performed with alachlor as a model pollutant. The varied factors were the iron concentration, the solution temperature and the collector area (which is at the same time a variation of V_{ill}/ V_{tot}). The most significant constant process variables were the total volume, the pH value, the initial pollutant concentration and the H_2O_2 concentration (maintained between 200-500 mg L^{-1}). The experimental design is described in detail in **Table 3.8**. The experiment ALC5 does not belong to the factorial design. Experiment ALC6 was performed in the Fenton reactor in the dark with conditions otherwise identical to CUBE5 and CUBE7.

Table 3.8: Three factor central composite design of alachlor experiments in the CADOX plant.

Exp.	A/ V_{ill}	c_{Fe}	T	pH	$H_2O_2^o$	substance	c^i	prep.
	$[m^2]$/ [L]	[mg L^{-1}]	[ºC]		[mg L^{-1}]		[mg L^{-1}]	
CENTRE1	2.49/ 26.8	11	35	2.6	400	ALC	100	D
CENTRE2	2.49/ 26.8	11	35	2.6	400	ALC	100	D
CENTRE3	2.49/ 26.8	11	35	2.6	400	ALC	100	D
CUBE1	0.83/ 8.9	2	50	2.6	400	ALC	100	D
CUBE2	0.83/ 8.9	2	20	2.6	400	ALC	100	D
CUBE3	4.16/ 44.6	2	50	2.6	400	ALC	100	D
CUBE4	4.16/ 44.6	2	20	2.6	400	ALC	100	D
CUBE5	0.83/ 8.9	20	50	2.6	400	ALC	100	D
CUBE6	0.83/ 8.9	20	20	2.6	400	ALC	100	D
CUBE7	4.16/ 44.6	20	50	2.6	400	ALC	100	D
CUBE8	4.16/ 44.6	20	20	2.6	400	ALC	100	D
ALC5	4.16/ 44.6	55.8	20	2.6	400	ALC	100	D

Prep." refers to the dissolution procedures described in chapter 3.4.2.

The analytical determinations performed were the same as for the experiments described above (see section 3.4.6).

3.5 Automatic H_2O_2 control experiments

The tests of the automatic H_2O_2 control were performed without any pollutant, because the only objective was to provoke consumption of hydrogen peroxide at consumption rates similar to those to be expected to occur in real wastewater treatment (approximately $0 - 3\ g\ L^{-1}\ h^{-1}$). To this end, iron salts ($c_{Fe} = 0.5 - 4\ mg\ L^{-1}$) were dissolved at pH 2.5 inside the CADOX reactor. Covering part of the reactor was used to control the H_2O_2 consumption rate. Covering or uncovering collector area served also to simulate rapid changes in consumption rate to test the response of the control system to such changes. Hydrogen peroxide addition was performed through the utilisation of a dosing pump controlled by the tailor-made SCADA software (see chapter 3.3.2), where the control system acted directly via an analogue signal upon the frequency of the dosing pump's piston movement.

The following experiments were performed at different H_2O_2 consumption rates:

- Simulating the start-up phase, i.e. reaching a set-point starting from zero initial concentration, with and without H_2O_2 consumption.
- Simulating reaching a set-point lower than the actual concentration after a set-point change to a lower set-point.
- Maintaining a set-point, while an abrupt change of the H_2O_2 consumption rate is caused (positive and negative).

All types of experiments were performed with two different controllers.

- Conventional PI controller (feedback control)
- PI controller with antireset windup (feedback control)

3.6 Solar irradiance evaluation and figures-of-merit

In solar photo-Fenton experiments the intensity of solar irradiance is obviously an important input process variable. At the same time it is never constant due to its multiple influences (see chapter 2.1) and cannot be controlled, either. It is therefore logical that to compare experiments performed under different solar irradiance conditions (i.e. any experiment not performed at the same time) some methodology has to be developed taking into account the actually measured solar irradiance values. A simple way is to introduce a standardised illumination time. As stated before (see chapter 3.2.1) the measurement of broadband UV radiation can be considered the most

appropriate spectral range to standardise photo-Fenton experiments. 30 W m^{-2} can be considered a standard global UV irradiance ($I^o_{G,UV}$) under clear skies at PSA [97]. Consequently, under constant global UV irradiance Eq. (3.24) yields an expression for the normalised irradiation time t_{30W}. Yet, Eq. (3.25) has to be used under real conditions, because, as stated, solar irradiance is never constant. In the description of the degradation experiments in the Results and Discussion section also negative times are used. These correspond to the real time before illumination was started in the degradation experiment. $t_{30W} = 0$ corresponds to the moment, when illumination was started.

$$t_{30W} = t \frac{I_{G,UV}}{I^o_{G,UV}}$$

(3.24)

$$t_{30W} = \frac{1}{I^o_{G,UV}} \int_0^t I_{G,UV}(t)dt$$

(3.25)

One step beyond follows the suggestion to incorporate the specifications of the solar hardware as well. This makes comparison of the experimental performance of different solar collectors possible. The best concept to compare different technical solutions would be, naturally, the treatment cost [139] in the absence of other compelling criteria (e.g. compliance with legal discharge limits). Yet, assessment of treatment costs is difficult and in most cases not very accurate. Hence, IUPAC recommended comparing solar systems based on the collector area necessary to achieve a certain goal in a unit time [140]. One problem of the application of the IUPAC recommendations for the photo-Fenton process is that both proposed methods require defined reaction kinetics; either zero order or first order kinetics. Unfortunately, such clear kinetic laws usually cannot be deduced for photo-Fenton treatment due to the complexity of the system. Nevertheless, the approach results useful and will be employed in this work. To this end Q, the accumulated UV energy incident on the collector surface per litre waste water, is calculated by Eq. (3.26) [45]. The degradation experiment example shown in **Figure 3.6** clearly demonstrates the usefulness of applying Q (or t_{30W}), when discussing experimental results. The degradation curve depicted vs. the experiment time t has a shape including three inflection points difficult to interpret, whereas the degradation curve depicted vs. Q probably could be described well by first order reaction kinetics.

Finally, with Eq. (3.27) the collector area per mass as defined by IUPAC [140] can be calculated, where Δc is the concentration difference regarding the analytical target parameter between start and end of the treatment.

$$Q = \frac{A}{V_{tot}} \int_0^t I_{G,UV}(t)dt \qquad (3.26)$$

$$A_{CM} = \frac{Q}{I^o_{G,UV} \, \Delta c} \qquad (3.27)$$
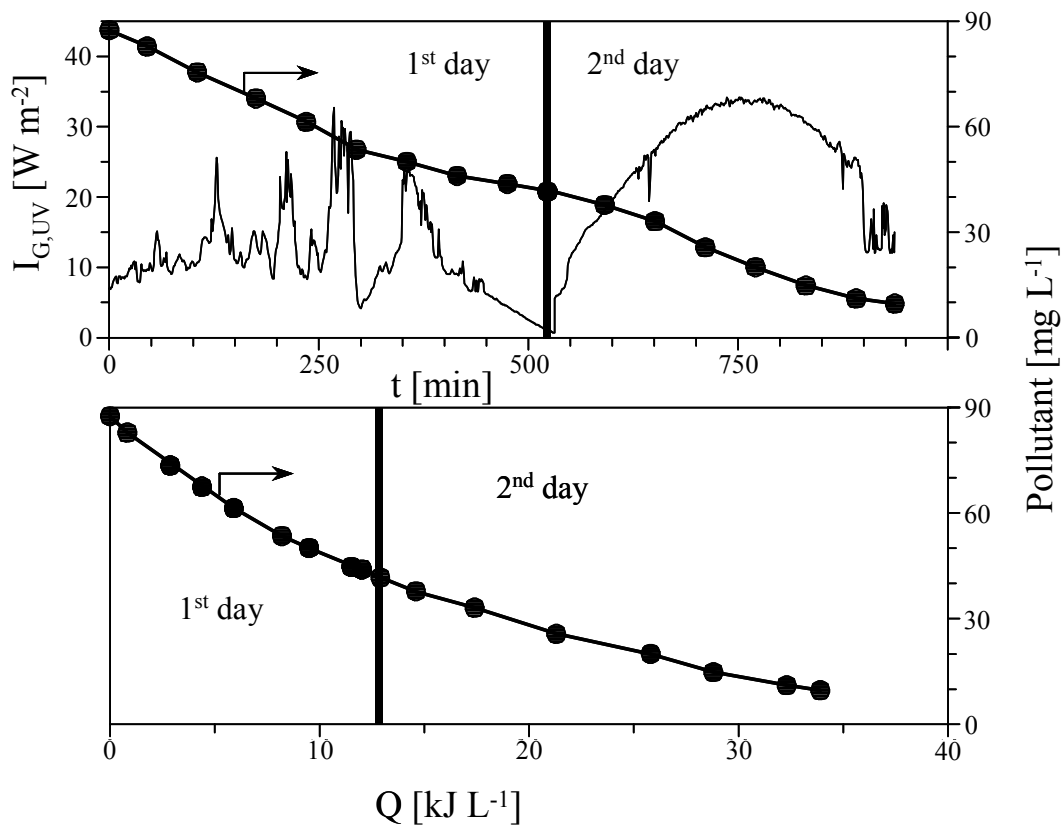
Figure 3.6: Example of solar degradation experiments. Depicted first vs. t, then vs. Q.

To ensure effective detoxification, wastewater detoxification must intrinsically involve process assessment. Measurements of biodegradability enhancement, decrease in toxicity, chemical oxygen demand or dissolved organic carbon are among the most frequently applied figures-of-merit. In this work, DOC degradation was chosen for most aspects of process evaluation, because other figures-of-merit can be estimated based upon this measure, if empirically determined values are available for the given waste water and oxidation process [96, 97].

During this work some more different qualitative aspects of the experiments will be compared (see Results and Discussion section). However, kinetic comparison of experiments will be based exclusively on DOC data. To this end the following parameters were deduced from the degradation curves:

$t_{30W}^{50\%DOC}$ t_{30W} needed to degrade 50% of the initial DOC

$t_{30W}^{80\%DOC}$ t_{30W} needed to degrade 80% of the initial DOC

$Q^{50\%DOC}$ Q needed to degrade 50% of the initial DOC

$Q^{80\%DOC}$ Q needed to degrade 50% of the initial DOC

$A_{CM}^{50\%DOC}$ Collector area per mass at 50% of the initial DOC

$A_{CM}^{80\%DOC}$ Collector area per mass at 80% of the initial DOC

Finally, the hydrogen peroxide consumption is a crucial aspect regarding the reagent costs of a photo-Fenton treatment. Therefore, the following figures-of-merit have been defined:

$H_2O_2^{50\%DOC}$ H_2O_2 needed to degrade 50% of the initial DOC

$H_2O_2^{80\%DOC}$ H_2O_2 needed to degrade 80% of the initial DOC

$X_{H_2O_2}^{50\%DOC}$ H_2O_2 consumption mass ratio to degrade 50% of the initial DOC

$X_{H_2O_2}^{80\%DOC}$ H_2O_2 consumption mass ratio to degrade 80% of the initial DOC

$\eta_{H_2O_2}^{80\%DOC}$ stoichiometric efficiency of H_2O_2 consumption to degrade 80% of the initial DOC

$X_{H_2O_2}^{50\%DOC}$, $X_{H_2O_2}^{80\%DOC}$ and $\eta_{H_2O_2}^{80\%DOC}$ are calculated by Eq. (3.28), (3.30) and (3.30)

$$X_{H_2O_2}^{50\%DOC} = \frac{H_2O_2^{50\%DOC}}{0.5 \, DOC^i} \tag{3.28}$$

$$X_{H_2O_2}^{80\%DOC} = \frac{H_2O_2^{80\%DOC}}{0.8 \, DOC^i} \tag{3.29}$$

$$\eta_{H_2O_2}^{80\%DOC} = \frac{H_2O_2^{theor}}{H_2O_2^{80\%DOC}} \tag{3.30}$$

3.7 Tools for model building and simulations

For Response Surface Methodology (RSM) calculations any multiple linear regression (MLR) and variable selection procedures in MLR (forward selection) were done with a

programme called Datalab$^®$, which is a tool included in [123]. Non-linear curve fitting was done by the corresponding tool integrated in Origin$^®$ v7.03 software applying Levenberg-Marquardt algorithm.

For the model simulations of the H_2O_2 consumption and the control system's response MathWorks MATLAB$^®$ and Simulink$^®$ were used.

4 Results and Discussion

4.1 Degradation of Model Compounds in BRITE plant

4.1.1 Non-Biodegradable Chlorinated Solvents

4.1.1.1 Dichloromethane (DCM)

All the main parameters of the DCM degradation experiments are depicted in Figure 4.1. Dichloromethane is very soluble in water (13 g L^{-1}), but highly volatile (Boiling point = 40 ºC). Therefore, a blank experiment in the dark (DCM1) at pH 2.8 without Fenton's reagent was done to determine the loss of DCM due to volatilisation in the pilot plant (the re-circulation tank is at atmospheric pressure and open, see chapter 3.3.1). The temperature of the blank experiment was almost constant around 25 ºC, very similar to the average temperature during the degradation tests (between 15 ºC and 33 ºC, DCM2 and DCM3). As shown in **Figure 4.1**, near 50% of DCM is lost in 4 hours due to volatilisation in the blank experiment. In DCM2 only 20% of the initial compound is lost during the treatment with 2 mg L^{-1} Fe (DCM2) and none with 1 mM Fe (DCM3), as stated by chloride analysis. Cl$_{theor.max.}$ is the maximum expected concentration of chloride when all the DCM has been decomposed. Cl$_{theor.max.}$ has been calculated from the total quantity of DCM added to the pilot plant (1.75 g per 35 L $\Leftrightarrow$ 50 mg L^{-1}).

Dichloromethane was successfully degraded by photo-Fenton at both iron concentrations. The "dark" Fenton (from "2" until t = 0) reaction produced a significant degradation of the compound at the highest iron concentration (DCM3, 55 mg L^{-1} Fe) but not at the lowest iron concentration applied (DCM2, 2 mg L^{-1} Fe). Total mineralisation (i.e., disappearance of DOC) can be attained at either concentration only after irradiation. Chloride evolves very quickly with Fe = 1 mM and slowlier with Fe = 2 mg L^{-1}. Total dechlorination and DOC disappearance is confirmed in both cases, but as mentioned previously, with about 20% losses in the case of Fe = 2 mg L^{-1}.

The evolution of chloride and DOC concentration shows that chloride is formed approximately at the same rate than DOC is reduced (see **Figure 4.2**). This suggests that intermediates after the removal of the first chlorine continue to react quickly releasing further chloride.
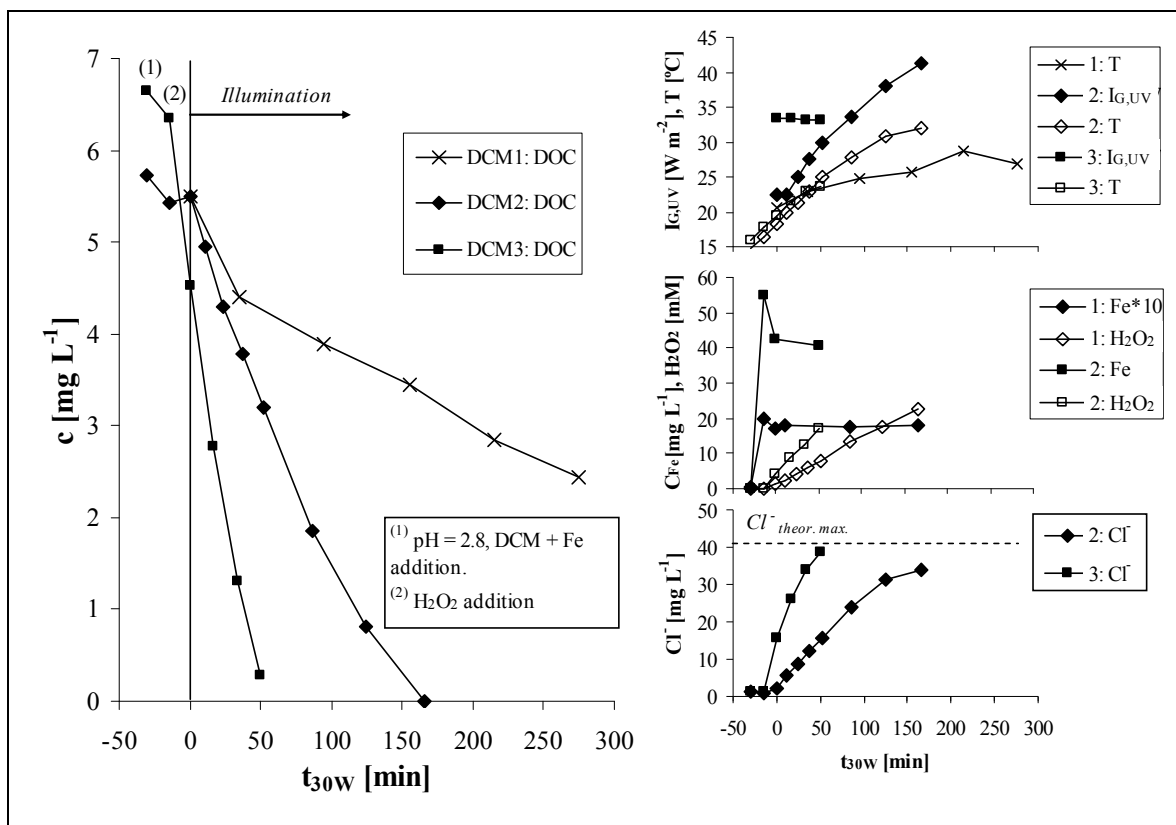
Figure 4.1: DCM degradation. Main degradation parameters. DCM1 was performed in the dark and was depicted against the real time t (t = 0 min ⇔ 10 min after DCM addition), DCM2 and DCM3 are depicted against t_{30W}.

After the complete dechlorination of the molecule, also the DOC disappears fast. The reason could be either fast degradation or very high volatility of the intermediate compound. However, the only highly volatile compound containing one carbon atom would be methane, which is harmless if released to the atmosphere. Methane could be generated if reductive attack on the chlorinated solvent prevails as suggested for the reaction of Fenton's reagent with chlorinated solvents [141]. **Figure 4.2** suggests that actually the losses due to volatilisation were close to zero, once Fenton's reagent was added. This indicates that the difference of 20% between the final chloride concentration in DCM2 and the theoretical maximum chloride concentration released corresponding to an initial DCM concentration of 50 mg L^{-1} is only caused by losses in the experiment preparation phase, which is of no importance in the treatment of real wastewater. This assumption is also supported by the fact that the measured initial DOC concentrations in experiments DCM2 and DCM3 are different (see **Figure 4.1** and **Figure 4.2**). Consequently, the complete release of organic chlorine as inorganic

chloride is confirmed by IC measurements according to the stoichiometry proposed in equation (3.1). Whereas in the blank experiment DCM1 substantial volatilisation takes place, it does not happen on a similar time scale in DCM2. The reason could be the fast formation of a non-volatile intermediate, which still contains both chlorine atoms. Another possibility would be that the presence of hydrogen peroxide affects the evaporation of DCM from the solution.

Around 10% and 25% of the dissolved iron were lost in DCM2 and DCM3.
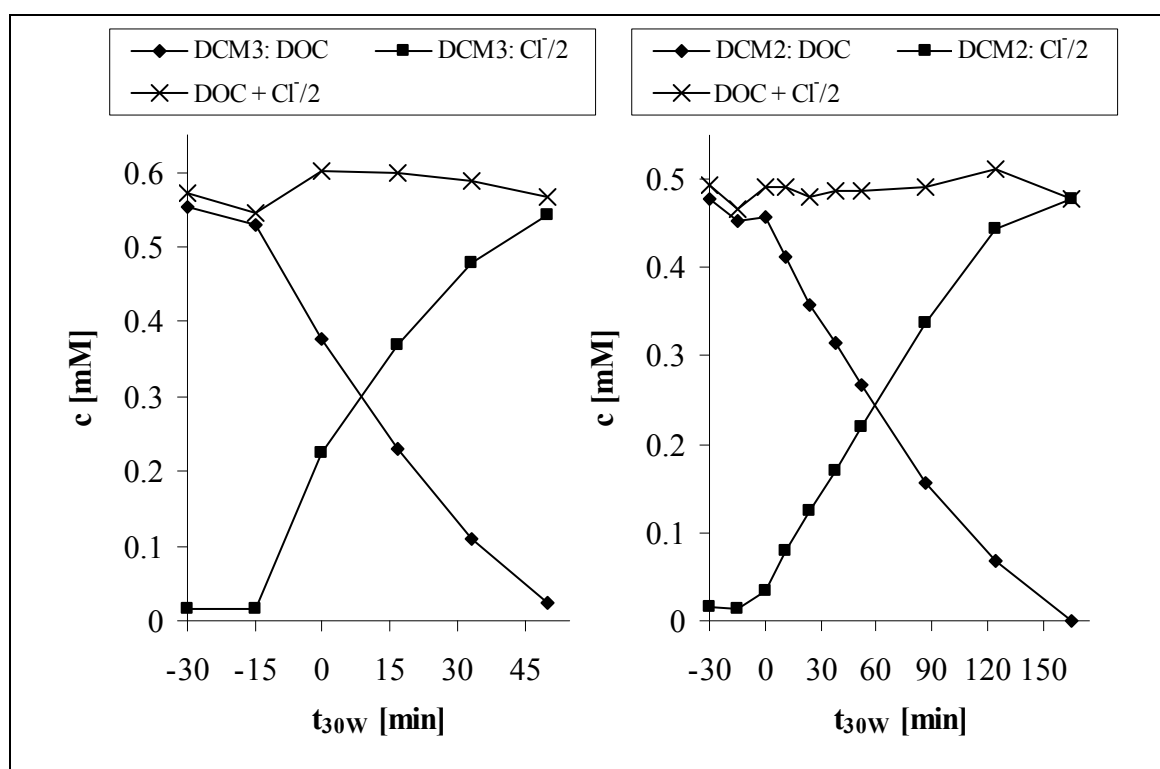
Figure 4.2: DCM mineralisation. Molar concentrations of DOC and chloride released into the solution. Left: DCM3 (55 mg L^{-1} Fe); right: DCM2 (2 mg L^{-1} Fe).

4.1.1.2   Trichloromethane (TCM)

All the main parameters of the TCM degradation experiments are depicted in **Figure 4.3**. TCM is very soluble in water (7.6 g L^{-1}), but highly volatile (Boiling point = 61.7 °C). Therfore, like for the other non-biodegradable chlorinated solvents (NBCS) a blank experiment in the dark (TCM1) at pH 2.8 without Fenton's reagent was done to determine the loss of TCM due to volatilisation. The temperature of the blank experiment was between 15 °C and 30 °C, a bit lower than in the degradation experiments, where the temperature rose to 35 – 40 °C (TCM2 and TCM3). As shown

in **Figure 4.3**, near 40% of TCM is lost in 4 hours due to volatilisation in TCM1. Similar to the DCM study, neither for TCM2 nor for TCM3 100% of the theoretical maximum chloride concentration was achieved (approximately 90% in TCM2, 80% in TCM3), which would indicate some volatilisation.
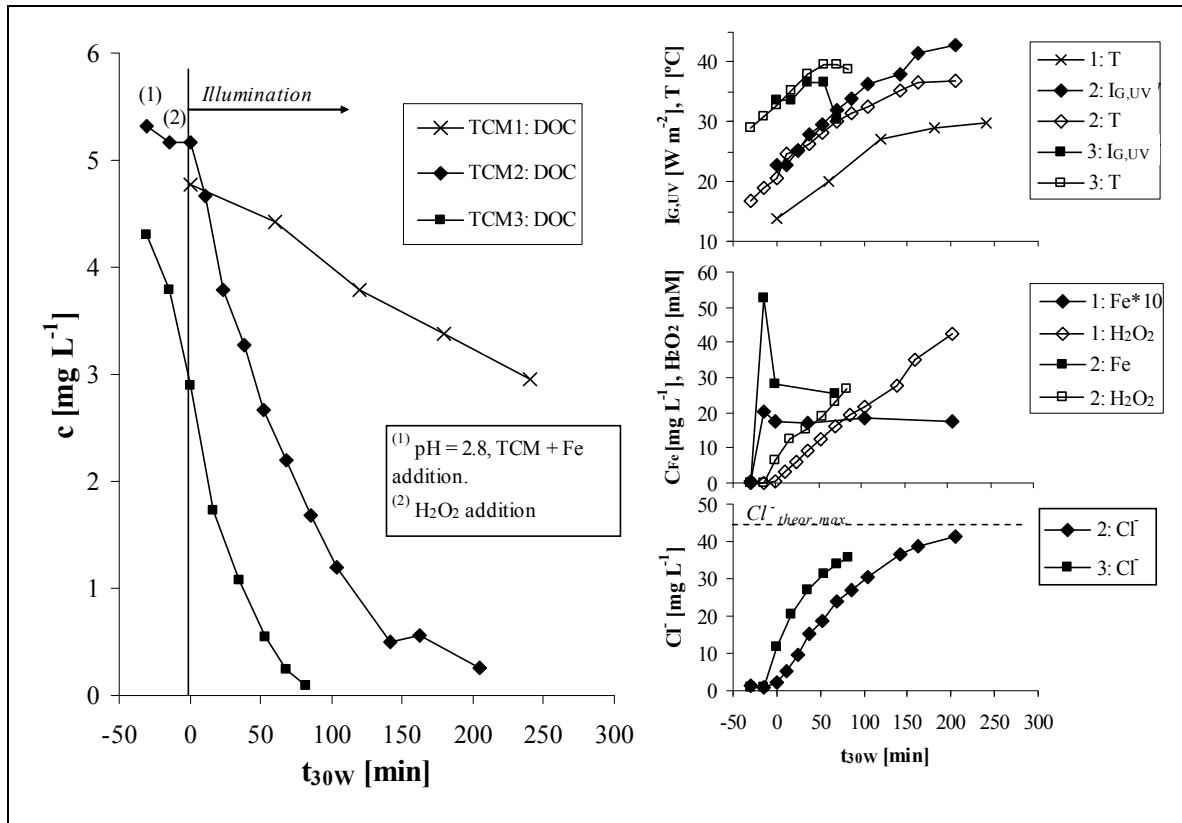
Figure 4.3: TCM degradation. Main degradation parameters. TCM1 was performed in the dark and was depicted against the real time t (t = 0 min ⇔ 10 min after TCM addition), TCM2 and TCM3 are depicted against t_{30w}.

Again, as in the DCM experiments, the representation of molar concentrations of the DOC and the evolved chloride shows that 100% of the theoretical maximum chloride concentration are not obtained because of a lower initial concentration in the model wastewater due to losses suffered in the experiment preparation procedure, mainly in TCM3 (see **Figure 4.4**). The high losses in the experiment preparation phase of TCM3 are probably due to the high initial temperature. As opposite to DCM degradation, in the case of TCM degradation at the lower iron concentration fewer losses due to evaporation were observed (around 10%, see **Figure 4.4**). The reason might be the higher temperature in TCM2 compared to DCM2 (compare **Figure 4.1** and **Figure 4.3**).

Complete TCM removal from the solution was confirmed at both iron concentrations. Substantial removal during the dark reaction was observed only at the higher iron concentration (TCM3: 1 mM Fe). The results presented in **Figure 4.4** indicate that subsequent removal of the remaining two chlorine atoms from the molecule and disappearance of the DOC must happen quicker than the removal of the first chlorine atom. Otherwise, in the case of the presence of significant amounts of intermediates with 0, 1 or 2 chlorine atoms an intermediate rise of the sum of DOC and chloride concentration divided by three should be observed in **Figure 4.4**. The mentioned total dechlorination confirms that the TCM removal was due to degradation processes, but not due to volatilisation.

Around 10% and respectively 50% of the dissolved iron were lost by precipitation in TCM2 and TCM3, respectively.
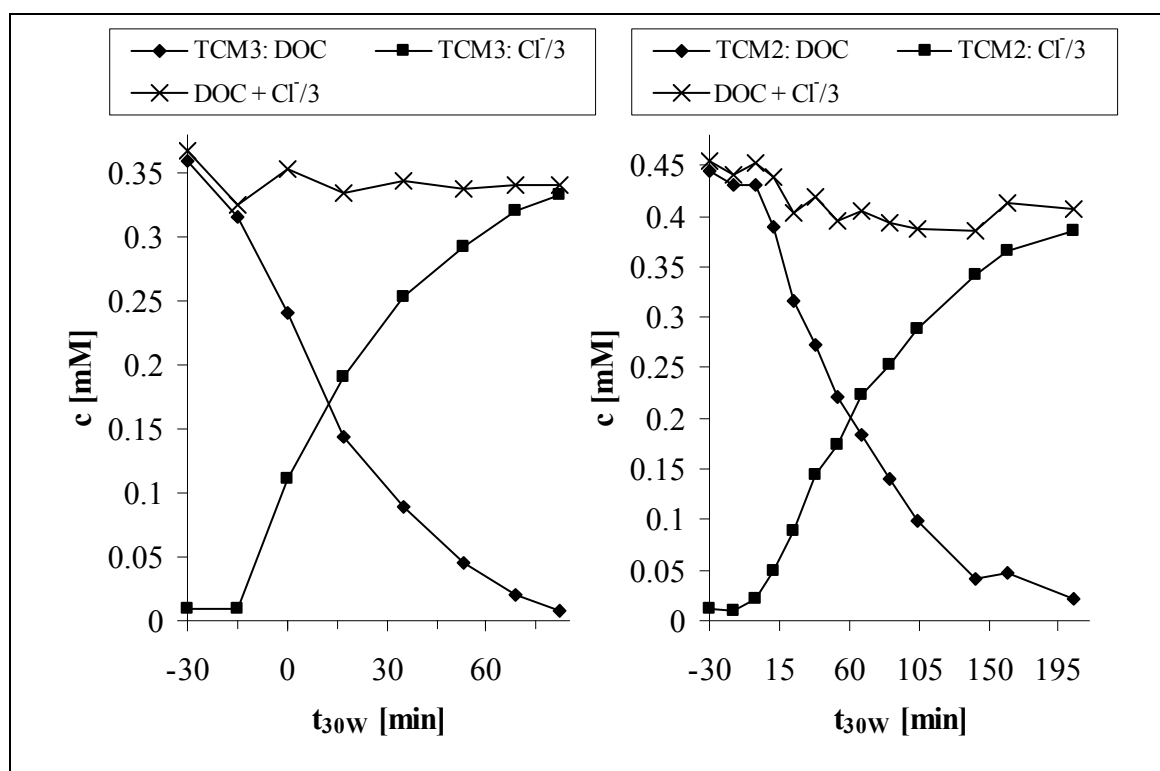
Figure 4.4: TCM mineralisation. Molar concentrations of DOC and chloride released into the solution. Left: TCM3 (55 mg L^{-1} Fe); right: TCM2 (2 mg L^{-1} Fe).

4.1.1.3 1,2-Dichloroethane (DCE)

All the main parameters of the DCE experiments are depicted in **Figure 4.5**. Like the other NBCS, DCE is very soluble in water (5.1 g L^{-1}), but highly volatile (Boiling

point = 80.4 ºC). Consequently, again a blank experiment in the dark (DCE1) at pH 2.8 without Fenton's reagent was done to determine losses due to volatilisation in the BRITE plant. The temperature of the blank experiment was between 20 ºC and 30 ºC, a bit lower than in the corresponding degradation experiment at $2 \, mg \, L^{-1}$ Fe concentration, in which the temperature rose until 40 ºC (DCE2). **Figure 4.5** shows that although the boiling point of DCE is higher than those of DCM and TCM nearly 60% of TCM is lost in 4.5 hours due to volatilisation in the blank experiment.
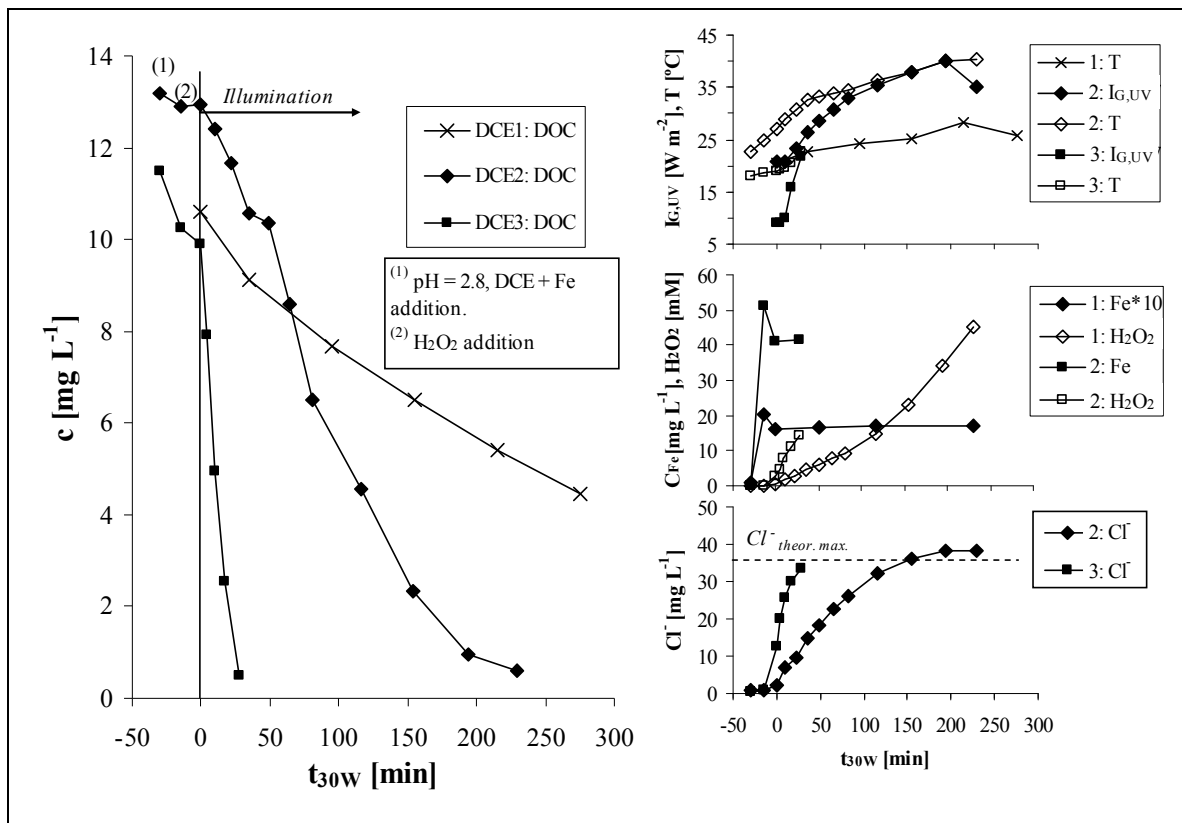
Figure 4.5: DCE degradation. Main degradation parameters. DCE1 was performed in the dark and was depicted against the real time t (t = 0 min ⇔ 10 min after DCE addition), DCE2 and DCE3 are depicted against t_{30W}.

Similar to the other NBCS degradation experiments complete DOC removal was observed at both iron concentrations. In the case of DCE fewer losses occurred in the experiment preparation procedure compared to the more volatile NBCS. In consequence, at both iron concentrations total dechlorination of DCE according to the stoichiometry proposed in Eq. (3.3) was confirmed and no losses due to volatilisation took place. This is also shown by depicting molar concentrations of the DOC and the

evolved chloride (see **Figure 4.6**). Contrary to the other NBCS significant amounts of intermediates after the removal of the first chlorine atom have been detected as indicated by the intermediate rise of the sum of DOC and chloride concentration in **Figure 4.6**. Again, significant degradation before illumination took place only at the higher iron concentration (DCE3). Dissolved iron losses during the degradation experiments were around 15% and respectively 25% in DCE2 and DCE3.
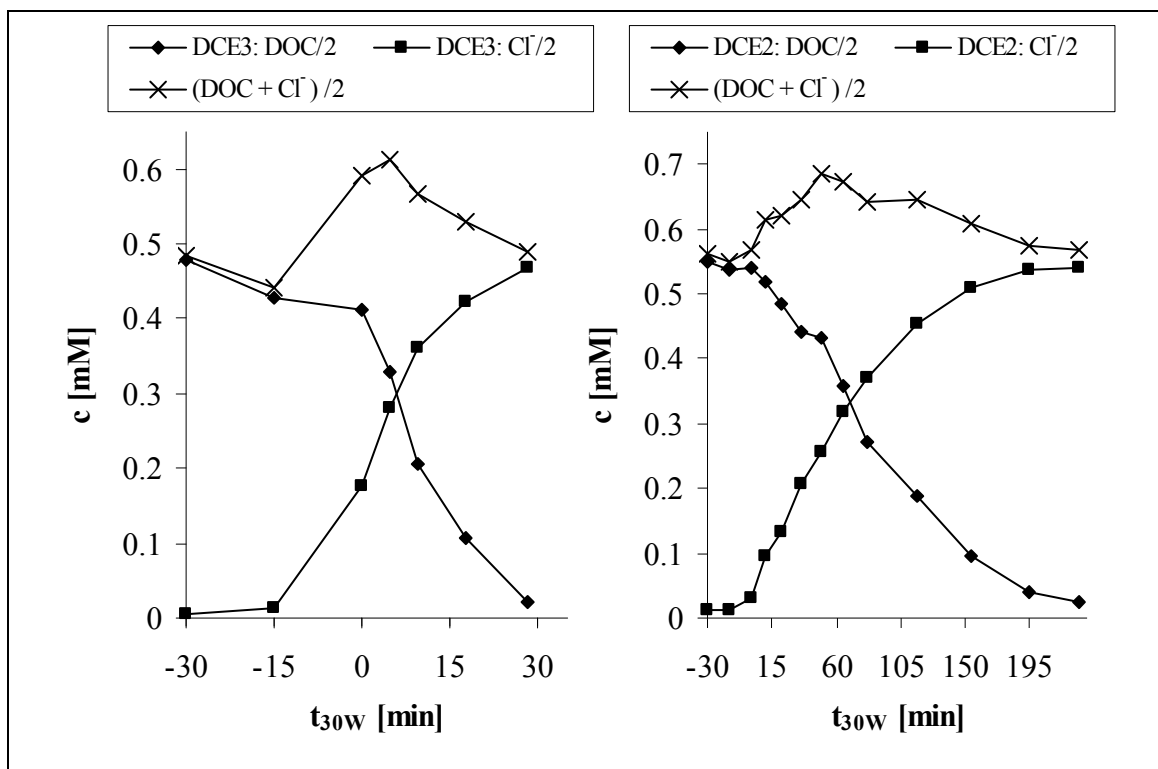
Figure 4.6: DCE mineralisation. Molar concentrations of DOC and chloride released into the solution. Left: DCE3 (55 mg L^{-1} Fe); right: DCE2 (2 mg L^{-1} Fe).

4.1.1.4   Comparison of degradation of different NBCS

Table 4.1 shows the figures-of-merit of the NBCS degradation experiments as defined in section 3.6. DOC^i refers to the measured DOC concentration at $t_{30W} = -15$ min, i.e. before hydrogen peroxide was added. From DOC^i the corresponding initial pollutant concentration c^i was calculated, assuming that the pollutant is the only substance present containing organic carbon. $t_{30W}^{50\%DOC}$, $t_{30W}^{80\%DOC}$, $H_2O_2^{50\%DOC}$ and $H_2O_2^{80\%DOC}$ refer to 50% and 80% degradation of DOC^i respectively, and were determined by linear interpolation between the two adjacent measured samples.

t_{30W}, defined in Eq. (3.25), takes into account the actual irradiance to compensate variations of the non-constant solar irradiation power. Q, Eq. (3.26), furthermore incorporates parameters describing the plant (volume and collector area). As long as the experiments are performed with the same plant configuration (here 35 L and 3.08 m^2), conclusions drawn from both parameters, t_{30W} and Q, regarding a comparison of experiments, will be the same. In general, it can be observed that DCM and TCM degradation rates are very similar, whereas DCE2 was slower than DCM2 and TCM2, while DCE3 was faster than DCM3 and TCM3. The reason is probably the two carbon atom structure of DCE. This means that more reaction steps are necessary to achieve mineralisation. Furthermore, the formation of more intermediates is possible (compare **Figure 4.6**), which can interact directly with dissolved iron forming photoactive complexes. Consequently, the increase of iron concentration from 2 mg L^{-1} to 1 mM (55.8 mg L^{-1}) has a stronger beneficial effect in the DCE degradation, i.e. treatment time is reduced by a factor 7 – 9, while it is reduced by a factor 2.5 – 5 for DCM and TCM. Note also that the increase in reaction rate is not as high as the increase in iron concentration (55.8 mg L^{-1} : 2 mg L^{-1} = 27.9).

$A_{CM}^{50\%DOC}$ and $A_{CM}^{80\%DOC}$ take into account the DOC degraded, Eq. (3.27). Similar values of $A_{CM}^{50\%DOC}$ and $A_{CM}^{80\%DOC}$ in the experiments at lower iron concentration (DCM2, TCM2 and DCE2) are due to the absence of a significant lag phase or slowing down, and degradation behaviour similar to zero order kinetics until 80% of DOC degradation is reached. In the case of 1 mM iron the difference of A_{CM} at the two degradation levels is significant, because a considerable part of the DOC (especially in DCM3 and TCM3) is degraded in the dark Fenton reaction already. This means that subsequently less illumination is required to achieve the degradation (measured from the moment of addition of H_2O_2) of a unit mass of DOC per hour of operation, resulting in less $A_{CM}^{50\%DOC}$ than $A_{CM}^{80\%DOC}$. The large differences between DCM, TCM and DCE in A_{CM} are partly due to the different weight share of organic carbon in the molecule, which results also in different DOC^i, although c^i is roughly the same mass.

Concerning H_2O_2 consumption, TCM seems to be the substance, which requires the highest amount of oxidant to achieve degradation. Tendentiously, it seems also that at a higher iron concentration, less hydrogen peroxide is needed to achieve DOC degradation, especially until 80% of the initial DOC is degraded. Nevertheless, this is probably due to slightly lower H_2O_2 concentration in the experiments at high iron concentration. It was difficult to maintain the H_2O_2 concentration constant, because of

its high rate of consumption. Consequently, more decomposition of H_2O_2 yielding oxygen and water would take place by oxidation of H_2O_2 by hydroxyl radicals.

Table 4.1: Figures-of-merit for NBCS degradation experiments in BRITE plant.

		DCM2	DCM3	TCM2	TCM3	DCE2	DCE3
DOC^i	[mg L^{-1}]	5.4	6.4	5.2	3.8	12.9	10.3
c^i	[mg L^{-1}]	38.3	45.3	51.8	37.8	53.2	42.5
c^i	[mM]	0.45	0.53	0.43	0.32	0.54	0.43
$H_2O_2^{theor}$	[mM]	0.90	1.07	0.43	0.32	2.69	2.35
$t_{30W}^{50\%DOC}$	[min]	64	13	55	14	82	9
$t_{30W}^{80\%DOC}$	[min]	114	34	107	45	150	20
$Q^{50\%DOC}$	[kJ L^{-1}]	10.1	2.1	8.7	2.2	13.0	1.4
$Q^{80\%DOC}$	[kJ L^{-1}]	18.1	5.4	16.9	7.1	23.8	3.2
$A_{CM}^{50\%DOC}$	[m^2 h kg^{-1}]	34800	5960	31000	10800	18600	2560
$A_{CM}^{80\%DOC}$	[m^2 h kg^{-1}]	38700	9740	37700	21700	21300	3560
$H_2O_2^{50\%DOC}$	[mM]	9.7	7.9	12.9	11.4	9.3	7.3
$H_2O_2^{80\%DOC}$	[mM]	16.2	12.9	22.4	17.4	22.2	11.7
$X_{H_2O_2}^{50\%DOC}$	[-]	122	84	169	204	49	44
$X_{H_2O_2}^{80\%DOC}$	[-]	128	86	183	195	73	44
$\eta_{H_2O_2}^{80\%DOC}$	[%]	5.6%	8.3%	1.9%	1.8%	12.1%	20.1%

DOC^i is the DOC at $t_{30W} = -15$ min. c^i is calculated by converting DOC^i in the theoretical equivalent amount of pollutant. 50% and 80% degradation refer to DOC^i. $X_{H_2O_2}^{50\%DOC}$, $X_{H_2O_2}^{80\%DOC}$ and $\eta_{H_2O_2}^{80\%DOC}$ take into account $H_2O_2^{50\%DOC}$, $H_2O_2^{80\%DOC}$, DOC^i and $H_2O_2^{theor}$ (see Eq. (3.28) - (3.30)).

Furthermore, the data in **Table 4.1** shows that depending on the substance the relation between hydrogen peroxide needed in the experiments and the theoretical amount (being directly calculated from the chemical oxygen demand of the solution) strongly varies (compare values for $\eta_{H_2O_2}^{80\%DOC}$, $H_2O_2^{theor}$, $H_2O_2^{50\%DOC}$ and $H_2O_2^{80\%DOC}$). This indicates that a rather low percentage of the hydrogen peroxide is effectively used to degrade the pollutant. The rest is decomposed in oxygen and water without producing pollutant oxidation, which obviously is undesirable. The same can be observed for the hydrogen peroxide consumption mass ratios calculated, $X_{H_2O_2}^{50\%DOC}$ and $X_{H_2O_2}^{80\%DOC}$. Therefore, estimations of the hydrogen peroxide needed for the degradation based on

measurements of chemical oxygen demand or DOC, but without taking into account the chemical nature of the pollutants in the wastewater, have to be regarded with care for NBCS.

4.1.2 Low to medium soluble pesticides

4.1.2.1 Alachlor (ALC)

The main degradation parameters are shown in **Figure 4.7**. Alachlor was successfully degraded by photo-Fenton at both iron concentrations, in the case of the highest iron concentration, ALC was completely converted already during the "dark" Fenton (from "3" until $t_{30W} = 0$) reaction. The "dark" Fenton reaction produced little mineralisation of the pesticide before illumination at Fe = 2 mg L^{-1}. At Fe = 1 mM the mineralisation was 40%. Nevertheless, total mineralisation (i.e., disappearance of DOC) can be attained only after irradiation at both concentrations.
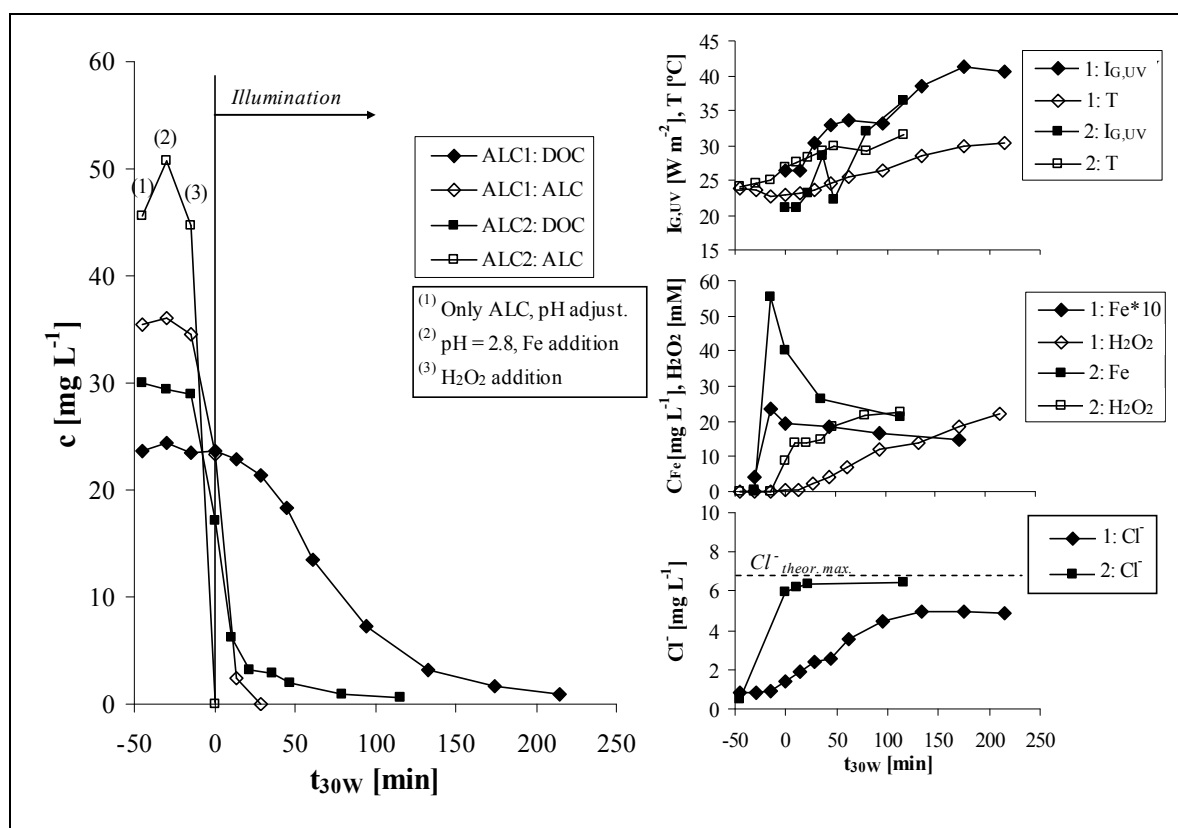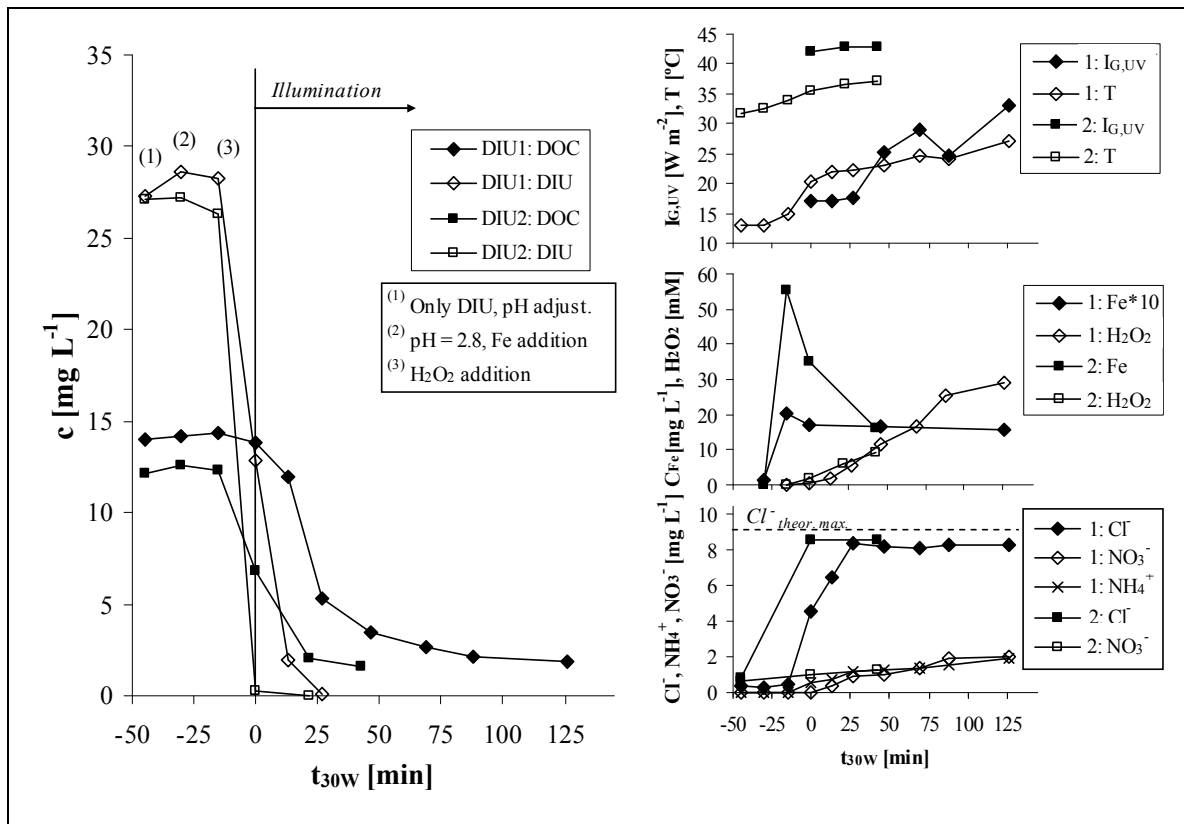

Figure 4.7: ALC main degradation parameters at two different initial iron concentrations (ALC1: 2 mg L^{-1} Fe; ALC2: 55 mg L^{-1} Fe).

The release of heteroatoms as inorganics is confirmed by IC analysis according to the stoichiometry proposed in reactions (3.5) and (3.6). Chloride evolves very quickly with Fe = 1 mM and slowlier with Fe = 2 mg L^{-1}. The nitrogen mass balance was not investigated in these experiments, but in other ALC experiments (see section 4.2.3). Total dechlorination is confirmed in both cases suggesting a very fast degradation/dechlorination step compared to DOC disappearance. The "missing" chloride concentration in ALC2 (see **Figure 4.7**) results from a difference in the initial concentration obtained after the experiment preparation (35 mg L^{-1}) and the theoretical initial concentration (50 mg L^{-1}). Although the difference is considerable the general considerations are still valid and also the quantitative parameters take into account the measured initial concentration. DOC has been completely mineralised at both Fe = 1mM and Fe = 2 mg L^{-1}.

20% in ALC2 and 60% in ALC3 of the initial iron concentration were lost by precipitation.

4.1.2.2 Atrazine (ATZ)

The main ATZ degradation parameters are shown in **Figure 4.8**. Initial measured DOC was about 20% higher than the DOC calculated for a 30 mg L^{-1} ATZ solution, which is 13.4 mg L^{-1}. This is due to the experiment preparation procedure in which saturated solutions of ATZ are prepared with an excess of ATZ. The ATZ used in this study is 95% pure, which implies that it contains 5% of impurities of unknown composition. These impurities are more soluble than ATZ and contain organic carbon. Then, an amount higher than 5% of ATZ was dissolved in the preparation of the saturated ATZ solution. Furthermore, DOC always increased during the initial stage of the experiment. This can be attributed to undissolved ATZ, eliminated by filtration prior to DOC measurement, but subsequently being dissolved when part of the ATZ was decomposed at the beginning of the test. Longer mixing time and increasing solution temperature (compare samples 1, 2, 3 of ATZ1 and ATZ2 in **Figure 4.8**) contribute also to a better dissolution of ATZ, because ATZ was employed close to the solubility limit.

ATZ was quickly converted into intermediate degradation products by photo-Fenton at both iron concentrations as confirmed by HPLC measurements. The "dark" Fenton (from "3" until t = 0) reaction did not produce any mineralisation of the pesticide before illumination, but it cannot be completely guaranteed because of the commented effect of "solubilization due to degradation". Nevertheless, mineralisation (i.e., disappearance of

DOC) can be attained only after irradiation. The measured release of heteroatoms as inorganic ions leaves incomplete mass balances with regard to the stoichiometry proposed in Eq. (3.7) – (3.10). Chloride evolves very quickly with Fe = 1 mM and slowlier with Fe = 2 mg L^{-1}. In both cases this chloride is released substantially faster than DOC mineralisation takes place. Yet, only little more than 50% of the theoretical maximum chloride concentration was obtained in both cases. This means that the residual DOC contains also chlorinated compounds. The nitrogen balance was not investigated.
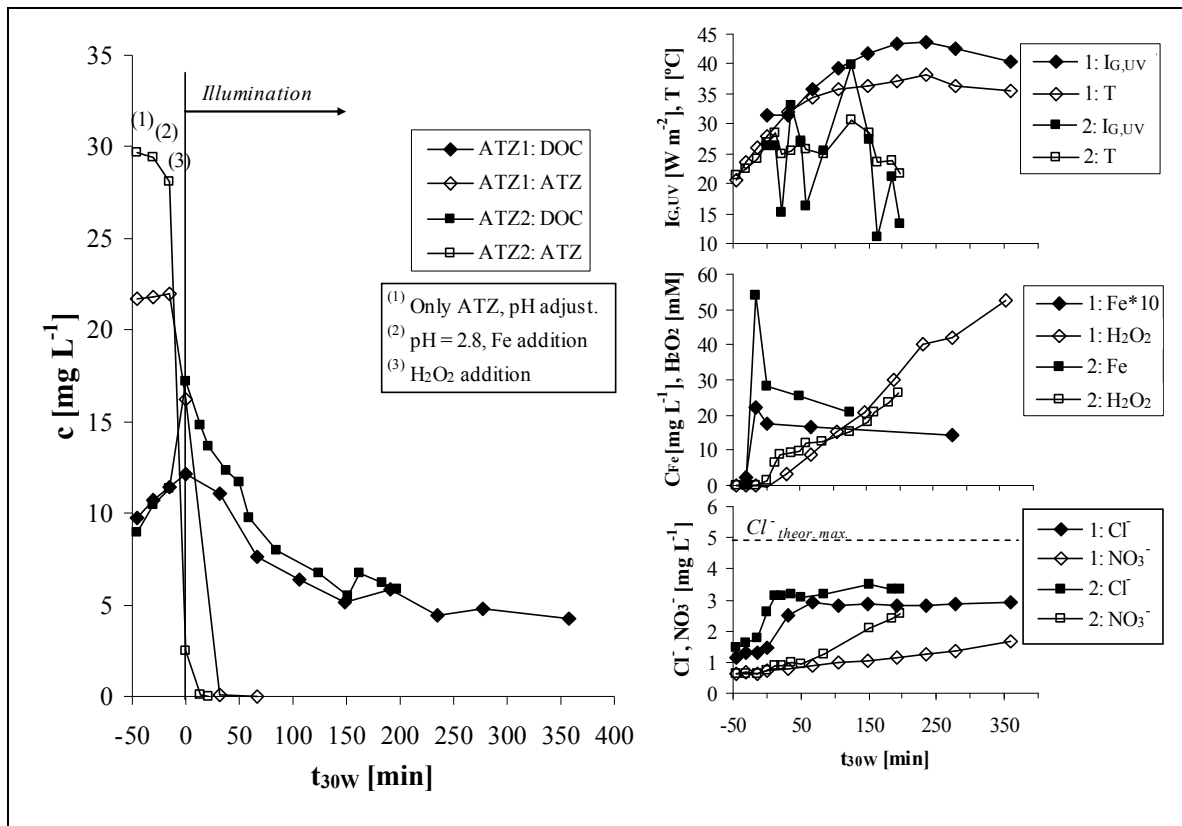
Figure 4.8: ATZ main degradation parameters at two different initial iron concentrations (ATZ1: 2 mg L^{-1} Fe; ATZ2: 55 mg L^{-1} Fe).

Total mineralisation of DOC did not occur, which needs of further comment. It has been demonstrated by different authors that triazines cannot be mineralised by AOPs, because the triazine ring is very resistant to hydroxyl radical attack [95, 132, 142, 143]. But it has also been demonstrated that it is possible to prolong the oxidation until cyanuric acid, a non-toxic compound, is obtained as final product [132]. The DOC

content of cyanuric acid is 3/8 of the equimolar amount of ATZ. During the tests the residual DOC was almost exactly 3/8 of the initial atrazine DOC:

- 22 mg L^{-1} of ATZ (ATZ2) correspond to 9.8 mg L^{-1} of DOC and the residual value was 4.2 mg L^{-1}
- 30 mg L^{-1} of ATZ (ATZ1) correspond to 13.4 mg L^{-1} of DOC and the residual value was 5.9 mg L^{-1}

In this study the intermediates of the ATZ degradation were not studied, but Hincapié et al. [143] state that in the case of photo-Fenton degradation after 20 hours irradiation the final products are mostly ammelide and ammeline and only a few percent of cyanuric acid. On the other hand, ATZ is transformed into cyanuric acid in around 2 hours by TiO_2 photocatalysis enhanced with $Na_2S_2O_8$ as electron acceptor.

Similar to ALC degradation around 25% of iron was precipitated at 2 mg L^{-1} initial iron concentration and 60% at 1 mM initial iron concentration.

4.1.2.3 Chlorfenvinphos (CFVP)

The main degradation parameters of CFVP degradation are shown in **Figure 4.9**. Chlorfenvinphos was successfully degraded by photo-Fenton at both iron concentrations. The "dark" Fenton reaction (from "3" until $t_{30W} = 0$) did convert 60% of CFVP but did not produce any mineralisation of the pesticide before illumination at Fe = 2 mg L^{-1}. At Fe = 1 mM CFVP conversion was complete and the mineralisation was more pronounced before illumination started. Yet, total mineralisation (i.e., disappearance of DOC) can be attained only after irradiation. The release of heteroatoms as inorganic ions is confirmed by the stoichiometry proposed in reaction (3.11). Chloride evolves very quickly at both iron concentrations and total dechlorination is confirmed in both cases suggesting a very fast dechlorination compared to DOC disappearance. This means that the residual DOC at the end of experiment CFVP1 did not correspond to any chlorinated compound. Phosphate seems to evolve quickly as well, but it is being precipitated with the dissolved iron. This is the reason why the measured phosphate amounts do not correspond to the theoretical maximum concentrations (13.8 mg L^{-1} PO_4^{3-} for 50 mg L^{-1} CFVP). In the case of a lower iron concentration, this precipitation seriously affects the degradation performance by precipitation of substantial parts of the catalyst (dissolved iron is diminished by 80% during CFVP1). At the highest iron concentration the precipitation is less severe (55% of initially dissolved iron disappears).
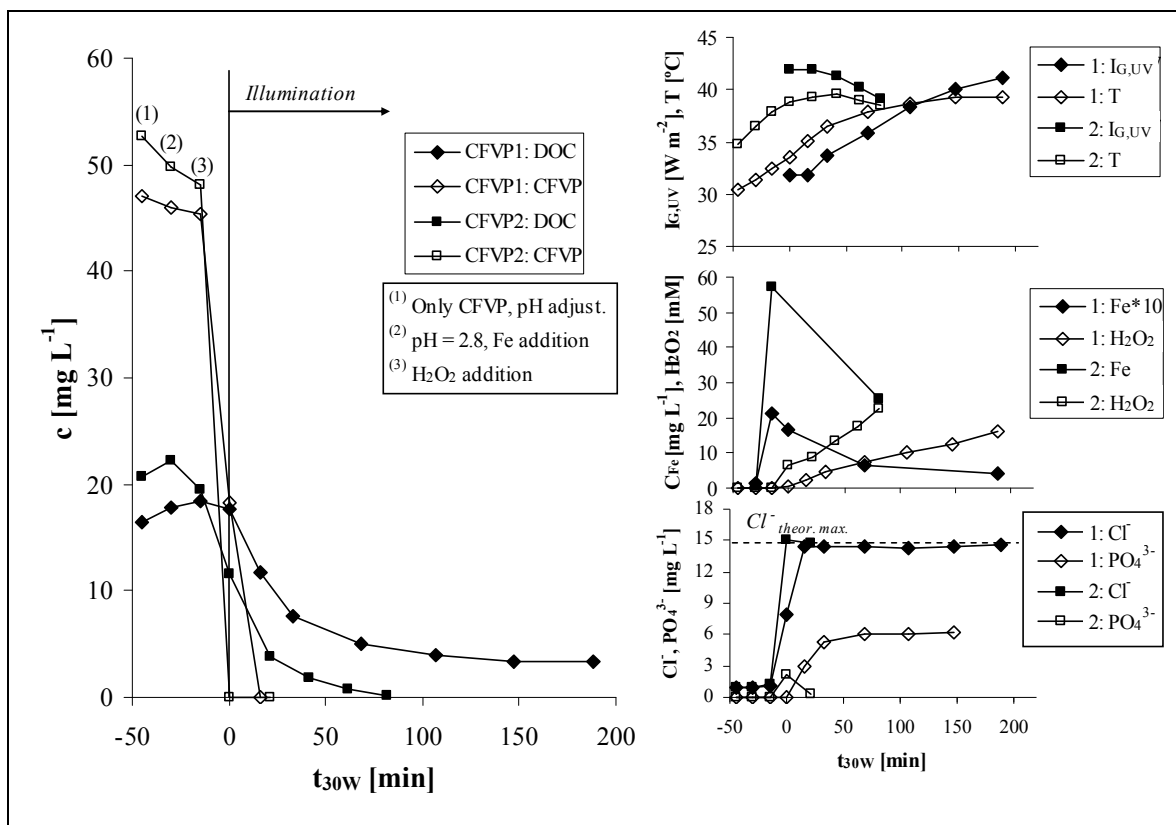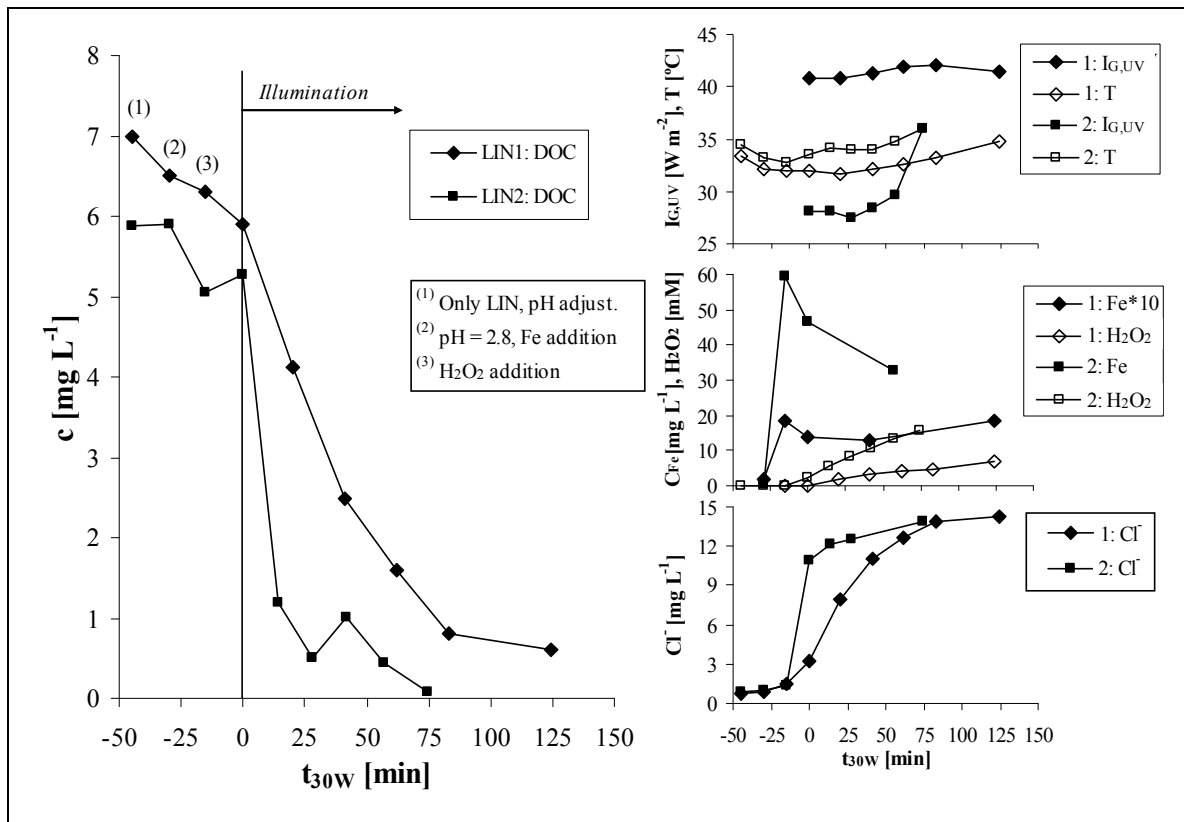
Figure 4.9: CFVP main degradation parameters at two different initial iron concentrations (CFVP1: 2 mg L^{-1} Fe; CFVP2: 55 mg L^{-1} Fe).

4.1.2.4 Diuron (DIU)

The main degradation parameters of DIU degradation are shown in **Figure 4.10**. Diuron was successfully degraded by photo-Fenton at both iron concentrations, in the case of the higher iron concentration already by the dark Fenton reaction (from (3) until $t_{30W} = 0$). The dark Fenton reaction did not produce any mineralisation of the pesticide before illumination at Fe = 2 mg L^{-1}. At Fe = 1 mM the mineralisation was more pronounced. Nevertheless, a high degree of mineralisation (i.e., disappearance of DOC) can be attained only after irradiation. Chloride evolves according to the stoichiometry proposed in reactions (3.12) and (3.13) at both iron concentrations. Total dechlorination is confirmed in both cases suggesting a very fast degradation/dechlorination stage compared to DOC disappearance. This means that the residual DOC at the end of the experiment did not correspond to any chlorinated compound. Less than 10 % of the initial DOC seems to be difficult to degrade. Nitrogen mass balance made up of measured ammonium and nitrate is incomplete in DIU1. Only around 60% of the theoretical nitrogen amount was found to be mineralised. Maletzky and Bauer [144]

reported that urea could hardly be mineralised by the photo-Fenton reaction. It is likely that diuron, a phenylurea herbicide, will generate urea as stable intermediate. This urea could account for the remaining DOC as well as for the incomplete nitrogen mass balance. Urea is non-toxic and it can be easily metabolised by microorganisms. It must be mentioned that this is a hypothesis that was not verified experimentally.

Part of the initially added iron was precipitated as seen in previous experiments. At the higher initial iron dosage precipitation was 70% and at the lower one 20% of the added iron.

Figure 4.10: DIU main degradation parameters at two different initial iron concentrations (DIU1: 2 mg L^{-1} Fe; DIU2: 55 mg L^{-1} Fe).

4.1.2.5 Isoproturon (IPR)

The main degradation parameters of IPR degradation are shown in **Figure 4.11**. Isoproturon was degraded at both iron concentrations quickly. At the higher iron concentration IPR degradation was almost complete before illumination in the dark Fenton phase (from (3) until $t_{30W} = 0$), while at the lower iron concentration degradation lasted approximately 50 minutes after the start of illumination. In the case of IPR

surprisingly little mineralisation occurred before illumination even at Fe = 1 mM. Consequently, illumination was necessary in both cases to reach high degrees of mineralisation. Approximately 90% of the initial DOC was smoothly degraded, whereas the last 10% proved to be very difficult to degrade, even if the treatment was prolonged considerably at high iron concentrations (IPR2) and consuming high amounts of hydrogen peroxide. Nitrogen mass balance made up of measured ammonium and nitrate is incomplete in IPR1. After 190 minutes, only around 30% of the theoretical nitrogen amount was found to be mineralised. Similar as diuron, isoproturon, another phenylurea herbicide, could generate urea as an intermediate degradation product, which could account for the residual DOC and close the incomplete nitrogen mass balance.

As in the other experiments iron precipitation occurred also in IPR1 and IPR2, being 10% and 80% respectively, of the initially added iron.
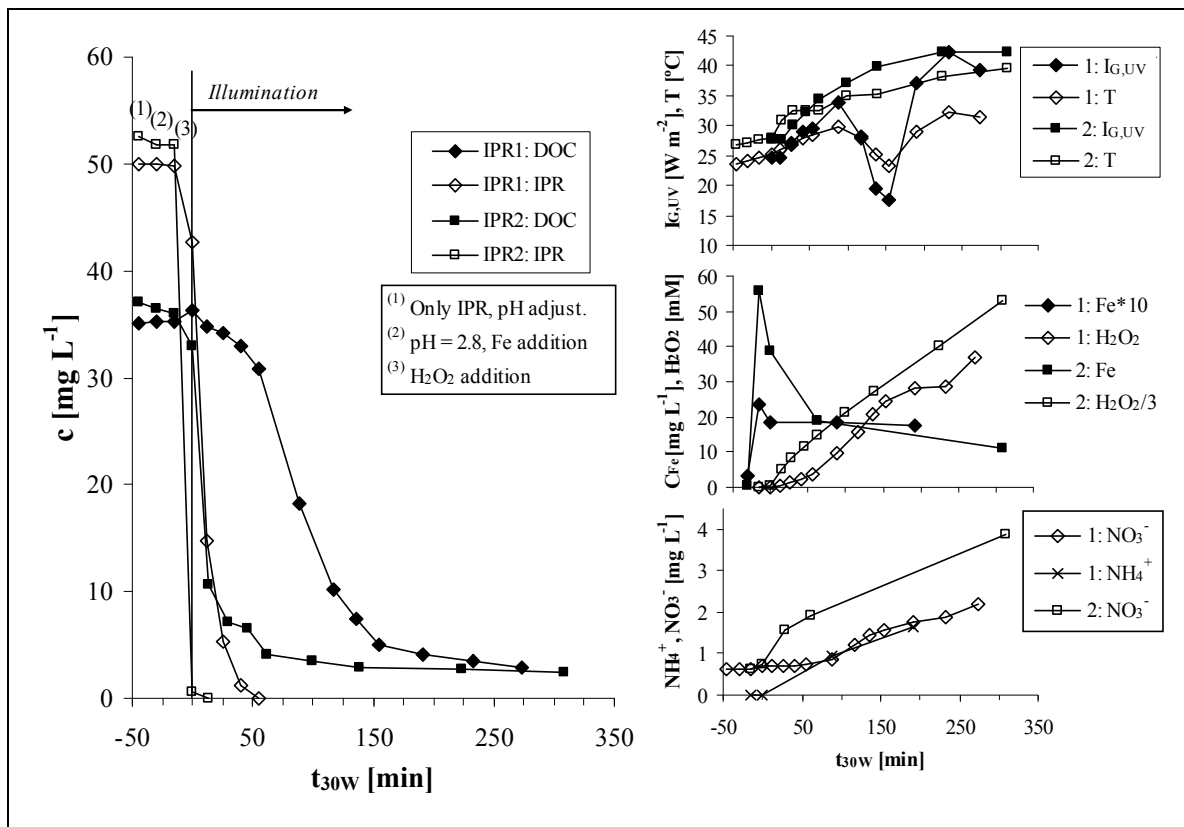
Figure 4.11: IPR main degradation parameters at two different initial iron concentrations (IPR1: 2 mg L^{-1} Fe; IPR2: 55 mg L^{-1} Fe).

4.1.2.6 Pentachlorophenol (PCP)

The most relevant parameters of PCP degradation can be found in **Figure 4.12**. PCP has a low solubility (14 mg L^{-1} at 25 ºC, neutral pH) and it is weakly acidic (pK$_a$ = 4.7). Due to its acidity it becomes even less soluble at low pH. Therefore, in the case of PCP no sulphuric acid was added to the solution. This implies that iron is added at a pH around 6, which induces iron precipitation. Yet, iron precipitation is not an instantaneous process, but it is governed by kinetics [50, 51]. Furthermore, ferrous iron is more soluble than ferric iron and is only slowly oxidised to ferric iron by dissolved oxygen. Therefore, after the homogenisation phase of 15 minutes at pH 6 still 85% (Fe = 2 mg L^{-1}) and 80% (Fe = 1 mM) of the initially added ferrous iron remained in solution. In PCP2 (Fe = 1 mM) the addition of iron caused a decrease of pH until 4.8, which by itself caused a decrease of the dissolved PCP (see DOC and PCP decrease in **Figure 4.12**). Subsequently, hydrogen peroxide was added and the dark Fenton reaction was started. In PCP2 at the higher iron concentration most of the PCP disappeared during the dark Fenton reaction. A process of re-dissolution of previously precipitated PCP due to degradation of the dissolved PCP can be assumed to be similar to the ATZ experiments and is indicated by the increase of DOC during the dark Fenton reaction in PCP2 (-15 < t$_{30W}$ < 0). At the same time the pH decreases due to the release of chloride by mineralisation of PCP. The complete dechlorination in PCP at the start of illumination most probably is not true. The presumed error might be due to slow analysis times inherent to the ion chromatograph. This means that dark Fenton reaction continued some more time producing complete dechlorination until injection was done and the analysis started. On the other hand, in the sample preparation for PCP analysis in HPLC the sample is mixed with organic solvent, which quenches further reaction, and this makes this analysis result more reliable (compare sections 3.2.3 and 3.2.4). No attempt was done to repeat the experiment, because the error is inherent to the type of sample (presence of Fenton's reagent) and the experiments aim was to demonstrate possible complete dechlorination and mineralisation. This error is increased by the nature of the contaminant (phenolic substance), which is especially prone to oxidation by Fenton's reagent.

The degradation at the lower iron concentration is similar but slower. For the same reason, the notable decrease and increase due to precipitation and re-dissolution occurs also around 15 minutes later. Furthermore, complete dechlorination was proved in the case of the lower iron concentration. The difference with respect to the theoretical

chloride concentration is due to a lower initial PCP concentration (18 mg L^{-1}) compared to the targeted initial concentration of 20 mg L^{-1}.

Due to the release of chloride, the final pH in PCP1 is 3.4 and in PCP2 2.7 respectively. This causes, that in the end the degrees of iron precipitation are not very different from other substances, being 30% in PCP1 and 70% in PCP2.
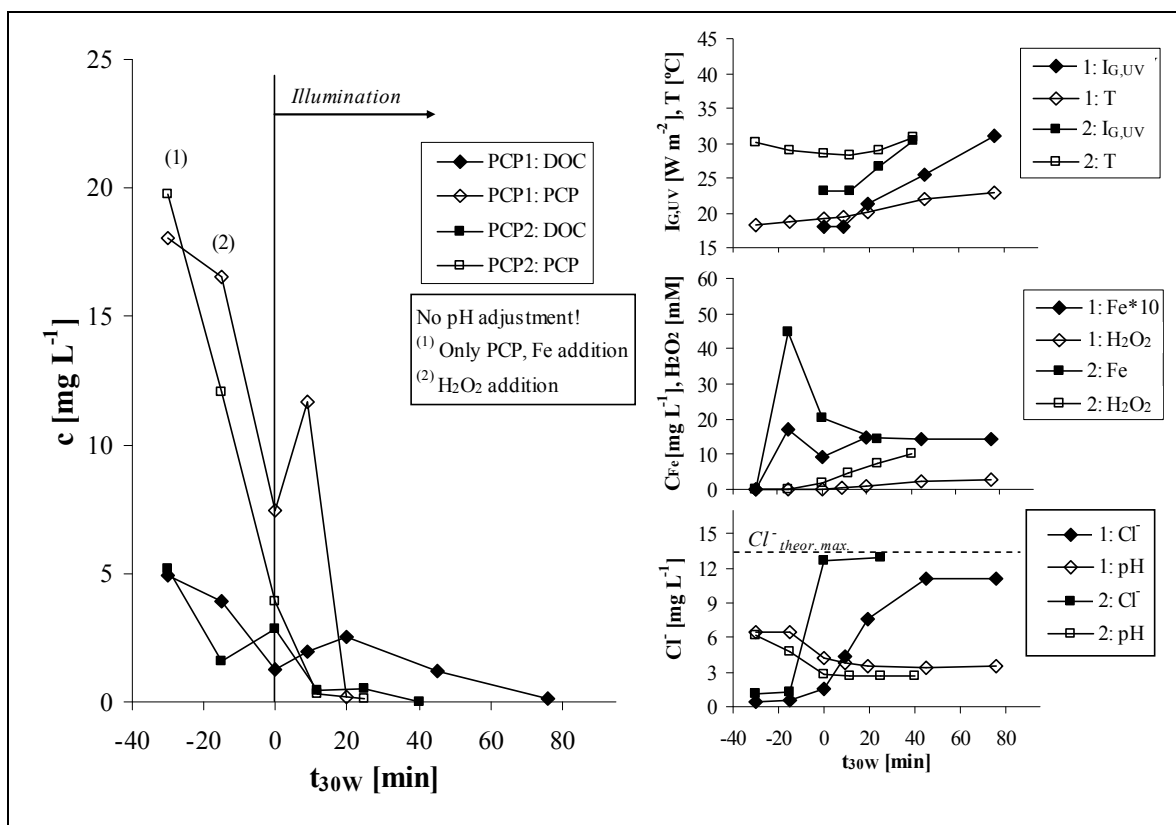
Figure 4.12: PCP main degradation parameters at two different initial iron concentrations (PCP1: 2 mg L^{-1} Fe; PCP2: 55 mg L^{-1} Fe).

4.1.2.7 Lindane (LIN)

The development of the most important degradation parameters of the lindane experiments is shown in **Figure 4.13**. In the case of lindane no analytical method was available to directly determine lindane. The measured DOC concentration neither presents a reliable measure for the lindane concentration, because a commercial formulation of lindane (90% w/w) was applied and the contribution of the unknown compounds to the DOC is uncertain. Furthermore, lindane is applied as a saturated solution, which means that part of the lindane could precipitate inside the reactor due to a lower temperature and could be eliminated by filtration. In any case, the aim of the

experiments is to prove the feasibility of a photo-Fenton treatment. For that reason, total mineralisation (disappearance of DOC) as occurring at both iron concentrations can be regarded as the achievement of the goal. In both treatments, around 13.5 mg L^{-1} of chloride are released into the solution. In terms of stoichiometry this corresponds to about 19 mg L^{-1} of lindane or 5 mg L^{-1} of DOC. It can be observed that the initial DOC is slightly higher in both experiments. Due to the pollutant dissolution procedure (5.5 g commercial product 90% w/w in 100 L) a theoretical maximum of 5.5 mg L^{-1} of unknown compounds could have been added. This seems to have happened accounting for the additional DOC.

Iron precipitation was somewhat less than in the other pesticide experiments, being only 10% and 40% at low and high iron concentration, respectively. This could be caused by a slightly lower pH towards the end of the degradation (2.4 – 2.5) due to more generation of inorganic acid (HCl) by the pollutant mineralisation, as compared to the other pesticides.

Figure 4.13: LIN main degradation parameters at two different initial iron concentrations (LIN1: 2 mg L^{-1} Fe; LIN2: 55 mg L^{-1} Fe).

4.1.2.8 Comparison of degradation of different pesticides

Table 4.2 and **Table 4.3** show the figures-of-merit of the PS pesticide degradation experiments as defined in section 3.6. DOC^i and c^i refer to the measured concentration at $t_{30W} = -15$ min, i.e. before hydrogen peroxide was added. $H_2O_2^{theor}$ is calculated taking into account c^i and the stoichiometries of Eq. (3.6), (3.10), (3.11), (3.13), (3.15), (3.16) and (3.17). $t_{30W}^{50\%DOC}$, $t_{30W}^{80\%DOC}$, $H_2O_2^{50\%DOC}$ and $H_2O_2^{80\%DOC}$ refer to 50% and 80% degradation of DOC^i, respectively, and were determined by linear interpolation between the two adjacent measured samples.

Table 4.2: Figures-of-merit for pesticide degradation experiments in BRITE plant (ALC, ATZ, CFVP).

		ALC1	ALC2	ATZ1	ATZ2	CFVP1	CFVP2
DOC^i	[mg L^{-1}]	23.5	28.9	9.8	12.5	18.4	19.5
c^i	[mg L^{-1}]	34.6	44.6	22.0	28.1	45.4	48.2
c^i	[mM]	0.13	0.17	0.10	0.13	0.13	0.13
$H_2O_2^{theor}$	[mM]	4.37	5.63	1.53	1.96	3.54	3.75
$t_{30W}^{50\%DOC}$	[min]	72	3	96	76	26	6
$t_{30W}^{80\%DOC}$	[min]	118	12	220	135	127	21
$Q^{50\%DOC}$	[kJ L^{-1}]	11.4	0.5	15.2	12.0	4.1	1.0
$Q^{80\%DOC}$	[kJ L^{-1}]	18.7	1.9	34.8	21.4	20.1	3.3
$A_{CM}^{50\%DOC}$	[m^2 h kg^{-1}]	8987	304	45973	28495	4145	903
$A_{CM}^{80\%DOC}$	[m^2 h kg^{-1}]	9206	761	65847	31635	12654	1974
$H_2O_2^{50\%DOC}$	[mM]	8.4	10.3	13.7	12.4	3.7	7.1
$H_2O_2^{80\%DOC}$	[mM]	13	13.9	36.7	16.5	11.3	8.6
$X_{H_2O_2}^{50\%DOC}$	[-]	24	24	152	108	14	25
$X_{H_2O_2}^{80\%DOC}$	[-]	24	20	255	90	26	19
$\eta_{H_2O_2}^{80\%DOC}$	[%]	33.6%	40.5%	4.2%	11.9%	31.3%	43.7%

DOC^i is the DOC at $t_{30W} = -15$ min, except ATZ, which is calculated from c^i. c^i is measured by HPLC at $t_{30W} = -15$ min. 50% and 80% degradation refer to DOC^i, except for ATZ, where it means 50% and 80% degradation of 5/8 of DOC^i. Also for calculation of A_{CM}, $X_{H_2O_2}^{50\%DOC}$, $X_{H_2O_2}^{80\%DOC}$ and $\eta_{H_2O_2}^{80\%DOC}$ for ATZ only 5/8 of DOC^i are regarded (see section 4.1.2.2). $X_{H_2O_2}^{50\%DOC}$, $X_{H_2O_2}^{80\%DOC}$ and $\eta_{H_2O_2}^{80\%DOC}$ take into account $H_2O_2^{50\%DOC}$, $H_2O_2^{80\%DOC}$, DOC^i and $H_2O_2^{theor}$ (see Eq. (3.28) - (3.30)).

First, regarding DOC^i and c^i it is obvious that the concentrations in the different experiments vary considerably, which is mainly due to the different solubilities of the substances but also to their different molecular structure. Especially, the low DOC^i of PCP and LIN experiments should be mentioned, which is due in part to the low mass share of carbon in the molecule (around 25%). Also the stoichiometric need of oxidant ($H_2O_2^{theor}$) for these two pesticides is lower than for the others.

Table 4.3: Figures-of-merit for pesticide degradation experiments in BRITE plant (DIU, IPR, PCP, LIN).

		DIU1	DIU2	IPR1	IPR2	PCP1	PCP2	LIN1	LIN2
DOC^i	[mg L^{-1}]	14.4	12.4	35.2	36.1	4.9	5.1	4.7	4.7
c^i	[mg L^{-1}]	28.2	26.3	49.9	51.7	18.1	19.8	19.0	19.0
c^i	[mM]	0.12	0.11	0.24	0.25	0.07	0.07	0.07	0.07
$H_2O_2^{theor}$	[mM]	2.18	2.03	7.02	7.28	0.61	0.67	0.78	0.78
$t_{30W}^{50\%DOC}$	[min]	23	3	93	9	21	2	44	10
$t_{30W}^{80\%DOC}$	[min]	63	19	139	29	52	10	78	18
$Q^{50\%DOC}$	[kJ L^{-1}]	3.6	0.5	14.7	1.4	3.3	0.3	7.0	1.6
$Q^{80\%DOC}$	[kJ L^{-1}]	10.0	3.0	22.0	4.6	8.2	1.6	12.4	2.9
$A_{CM}^{50\%DOC}$	[m^2 h kg^{-1}]	4685	710	7750	731	12571	1150	27455	6240
$A_{CM}^{80\%DOC}$	[m^2 h kg^{-1}]	8021	2809	7240	1473	19456	3595	30419	7020
$H_2O_2^{50\%DOC}$	[mM]	4.4	2.3	10.6	10.6	1.1	2.4	2.4	4.6
$H_2O_2^{80\%DOC}$	[mM]	15.2	5.3	21.2	25	2.5	4.3	4.2	6.3
$X_{H_2O_2}^{50\%DOC}$	[-]	21	13	20	20	15	32	35	67
$X_{H_2O_2}^{80\%DOC}$	[-]	45	18	26	29	22	36	38	57
$\eta_{H_2O_2}^{80\%DOC}$	[%]	14.3%	38.3%	33.1%	29.1%	24.5%	15.6%	18.7%	12.4%

DOC^i is the DOC at $t_{30W} = -15$ min, except LIN, which is calculated from c^i. c^i is measured by HPLC at $t_{30W} = -15$ min, except LIN (estimated, see section 4.1.2.7). 50% and 80% degradation refer to DOC^i. $X_{H_2O_2}^{50\%DOC}$, $X_{H_2O_2}^{80\%DOC}$ and $\eta_{H_2O_2}^{80\%DOC}$ take into account $H_2O_2^{50\%DOC}$, $H_2O_2^{80\%DOC}$, DOC^i and $H_2O_2^{theor}$ (see Eq. (3.28) - (3.30)).

Regarding kinetic interpretation, conclusions drawn from both parameters, t_{30W} and Q, will be the same as long as all the experiments are performed in the same plant (compare Eq. (3.25) and (3.26) for calculation of t_{30W} and Q, respectively). At the highest iron concentration, degradation of 50% and 80% of DOC^i is very quick (2 – 10

and 10 – 29 minutes), except for ATZ (76 and 135 minutes). Also, at the lower iron concentration ATZ needs the longest illumination times to achieve the degradation goals and is obviously the substance most difficult to degrade. The quickest degradation occurs with PCP, DIU and LIN, which are also the experiments with the lowest theoretical hydrogen peroxide demand. CFVP degradation is fast until 50% DOC degradation, but it slows down in continuation due to the precipitation of iron with the released phosphate (see **Figure 4.9**).

A_{CM} takes also into account the amount of mass (with respect to DOC) degraded, and not only the percentage of DOC degradation (see Eq. (3.27)). Regarding the experiments at higher iron concentration (Fe = 1 mM), in most experiments $A_{CM}^{50\%DOC}$ is significantly lower than $A_{CM}^{80\%DOC}$. This is due to the strong influence of the dark Fenton reaction at such a high iron concentration in relation to the pollutant concentration. Thereby, after the mineralisation of DOC^i occurring before the start of illumination only little radiation is needed to proceed the degradation until the disappearance of 50% of DOC^i (cf. also the low values for $t_{30W}^{50\%DOC}$ in these experiments). This effect cannot be observed at the lower iron concentration (Fe = 2 mg L^{-1}), because the dark Fenton reaction before illumination does not play an important role for mineralisation. So large differences between $A_{CM}^{50\%DOC}$ and $A_{CM}^{80\%DOC}$ can only be observed, if the mineralisation slows down in the later stages of the experiments. This occurred in CFVP1 and to a lesser extent in DIU1 and PCP1. In the case of CFVP it is due to precipitation of the iron catalyst as mentioned above. DIU has a considerable amount of DOC difficult to degrade and in the case of PCP it is probably due to the fact that very low DOC values have to be achieved to reach 80% mineralisation (below 1 mg L^{-1}).

Comparing the different substances, differences between them are remarkable. E.g. $A_{CM}^{80\%DOC}$ at low iron concentration varies from 7200 (IPR1) to 65800 (ATZ1) m^2 h kg^{-1}, and at high concentration even from 760 (ALC2) to 31600 (ATZ2) m^2 h kg^{-1}. As for the degradation times ATZ is the substance, which requires the longest treatment times. Due to their low carbon content, PCP and LIN show considerably higher values than IPR, DIU, ALC and CFVP.

The ratio between high and low iron concentration is around 28 (55.8 mg L^{-1}/ 2 mg L^{-1}). It is interesting to observe that at $A_{CM}^{50\%DOC}$ the ratio between the values for low and high iron concentration varies between 30 (ALC) and 1.6 (ATZ). For the other pesticides this ratio is from 4.4 to 11. This indicates that raising the iron concentration

has the greatest impact in the case of ALC due to an efficient dark Fenton reaction and especially little influence on ATZ degradation. For $A_{CM}^{80\%DOC}$ the ratio varies less due to the reduced influence of the initial dark Fenton reaction as discussed above, i.e. from 12 (ALC) to 2.1 (ATZ). For the other contaminants this ratio is remarkably similar (2.9 – 6.4). This data indicates that for degradation of 50% of the initial DOC the necessary collector area decreases by a factor of 9.7 (average of the seven substances) when the iron concentration was raised from 2 mg L^{-1} to 1 mM. The factor is 6.6, if the median of the values for the different experiments is considered "the average pollutant". For 80% degradation of initial DOC the factors are 5.4 or 4.9, depending whether average or median of the seven ratios is considered.

Concerning the absolute hydrogen peroxide consumption ($H_2O_2^{50\%DOC}$ and $H_2O_2^{80\%DOC}$), the hydrogen peroxide consumption mass ratio ($X_{H_2O_2}^{50\%DOC}$ and $X_{H_2O_2}^{80\%DOC}$) and the stoichiometric hydrogen peroxide consumption efficiency ($\eta_{H_2O_2}^{80\%DOC}$) few generally valid comments can be made. First, the actual hydrogen peroxide consumption is considerably higher than $H_2O_2^{theor}$ (i.e. $\eta_{H_2O_2}^{80\%DOC}$ is low). This is especially true for ATZ, but also for PCP and LIN, probably due to their low initial concentrations (which favour side reactions leading to H_2O_2 destruction without oxidation of the contaminant). In case of ATZ there is the additional effect of its refractory behaviour towards photo-Fenton treatment already discussed. Second, a decrease of the hydrogen peroxide consumption mass ratio can be distinguished, if higher mineralisation degrees are required (marked by a higher value of $X_{H_2O_2}^{80\%DOC}$ compared to $X_{H_2O_2}^{50\%DOC}$). This tendency can be especially observed when looking at the experiments with low iron concentrations. The effect is most pronounced, when the reaction is slowed down or remaining refractory DOC is present (ATZ1, CFVP1, DIU1). At the higher iron concentration this was not observed. The different behaviour of the experiments at low and high iron concentration cannot be explained logically.

ATZ1, ATZ2 and LIN2 are the three experiments with the lowest hydrogen peroxide consumption mass ratio. If these experiments are omitted, the rest of the experiments have a rather homogeneous hydrogen peroxide consumption mass ratio. The average for $X_{H_2O_2}^{50\%DOC}$ is then 22.1 with a standard deviation of 7.0. For $X_{H_2O_2}^{80\%DOC}$ the average is 27.5 with a standard deviation of 8.7, and if values for $X_{H_2O_2}^{50\%DOC}$ and $X_{H_2O_2}^{80\%DOC}$ are regarded together the average is 24.8 with a standard deviation of 8.0. This means that under

similar conditions a rough estimation of the hydrogen peroxide demand can be established, based on the measurement of DOC, as long as no "special" contaminants are present such as ATZ.

A similar approach can be applied for $\eta_{H_2O_2}^{80\%DOC}$. In this case the average stoichiometric hydrogen peroxide consumption efficiency is 25.1%, if calculated for all experiments. This means that as an average four times the theoretical stoichiometric hydrogen peroxide amount has to be added to achieve 80% DOC reduction.

4.1.3 Photo-Fenton method at low contaminant concentration

4.1.3.1 4-Nonylphenol (4-NP)

4-NP is neither a pesticide nor a chlorinated solvent, but a moiety of many surfactants, particularly nonylphenol ethoxylates. It is also classified as priority substance by the Water Framework Directive. 4-NP is in fact the part of the surfactant molecule, which is not biodegradable and remains unchanged after metabolisation of the ethoxylate chain in a biological treatment plant.

Apart from its importance as a contaminant in this study 4-NP was also selected because of its low solubility. Although its solubility limit (7 mg L^{-1} at 25 ºC) is similar to that of lindane, it is more difficult to obtain a highly concentrated solution, because 4-NP very easily adheres to surfaces. Consequently, in this study some degradation experiments were performed with initial contaminant concentrations around 2 mg L^{-1}. The results of these experiments are shown in **Figure 4.14**. A blank experiment (NP1) without illumination and catalyst was performed inside the pilot-plant to ensure that an eventual decrease of 4-NP is actually due to degradation but not to adsorption on the reactor's surfaces. The blank experiment clearly showed that 4-NP slowly disappeared from the solution at a rate of approximately 0.2 mg L^{-1} h^{-1} during 4 hours (only first 2.5 h shown in **Figure 4.14**).

Due to the expected fast reaction rate in relation to the low initial concentrations only one of three collector modules (each 1.03 m^2) of the BRITE plant was exposed to sunlight. Due to the low concentrations only the contaminant concentration was measured but not the DOC. The results showed that the dark Fenton reaction was considerable at both iron concentrations (40% and 80% 4-NP degradation at 1 and 5

mg L^{-1} Fe, respectively), which indicated that at such low contaminant concentration mere dark Fenton treatment might be possible without the need of large iron amounts.

In these experiments the hydrogen peroxide concentration was not maintained, but only one initial dosage of 100 mg L^{-1} was added at the beginning of the experiments. This corresponds to about eight times the theoretical stoichiometric need for total mineralisation of 2 mg L^{-1} 4-NP according to Eq. (3.4). As shown in **Figure 4.14** degradation of 4-NP only occurs after consumption of this amount of hydrogen peroxide. This means that approximately 1.5 mM of hydrogen peroxide is needed to degrade 1 mg L^{-1} of contaminant, which is far more compared to the pesticide experiments described in section 4.1.2 (compare **Figure 4.7** to **Figure 4.12**).

As a concluding remark it can be said that photo-Fenton and also dark Fenton treatment may be applied to waste water with such low contaminant concentrations, but it invokes higher costs per mass of pollutant degraded as compared to waste water treated at higher concentrations. It may be added that this cost issue at low concentrations is not specific to photo-Fenton, it is indeed applicable to any environmental remediation.
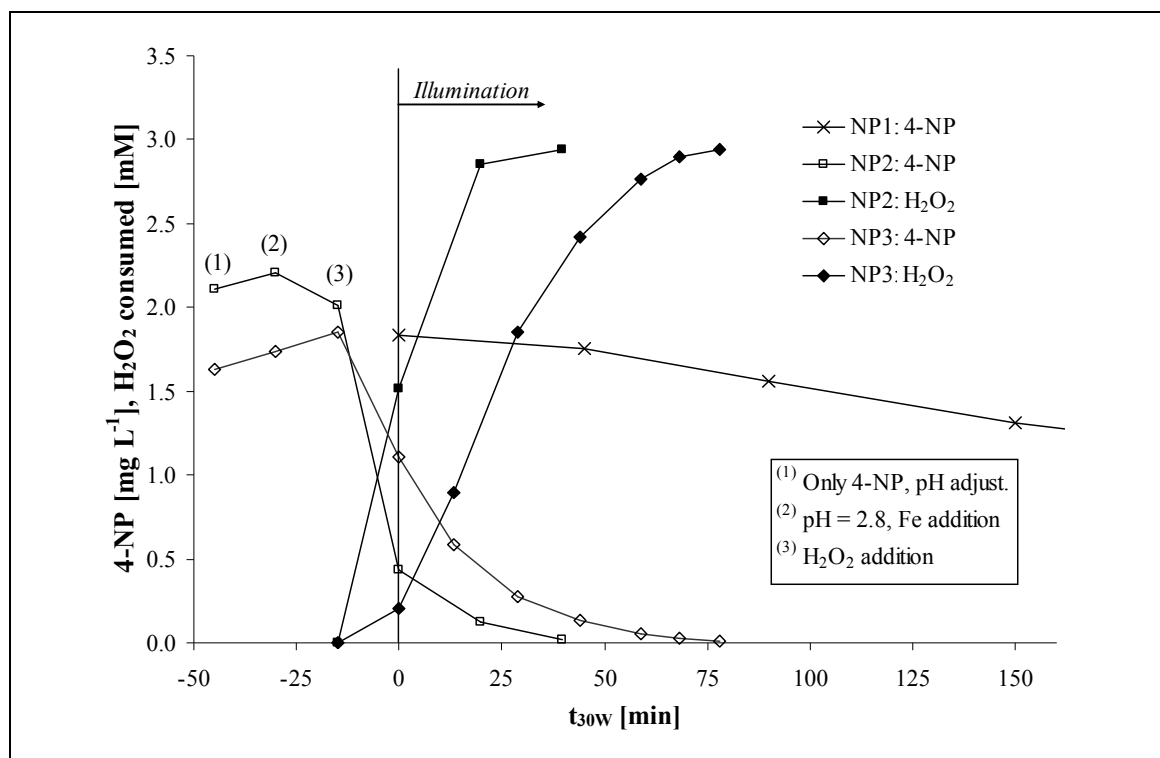
Figure 4.14: 4-NP main degradation parameters at two different initial iron concentrations (NP2: 5 mg L^{-1} Fe; NP3: 1 mg L^{-1} Fe). NP1 is a blank experiment in the dark.

4.1.4 Degradation of mixtures of ALC, ATZ, CFVP, DIU and IPR in CADOX plant

Real waste water usually contains a series of different substances. Consequently, after confirming the feasibility of the treatment of each contaminant by its own, mixtures of five pesticides (ALC, ATZ, CFVP, DIU and IPR) were treated. In the pesticide experiments with single contaminants also an influence of the initial pesticide concentration was found, especially concerning the efficient use of hydrogen peroxide (see section 4.1.2 and section 4.1.3). To appreciate this influence more clearly without the uncertainty of varying contaminants, experiments with the same composition (pesticide mixture) but at different initial concentrations were performed. These experiments were done inside the CADOX plant to cancel the effect of varying temperature of the waste water. The experiments were repeated to confirm the reproducibility of the experiments.
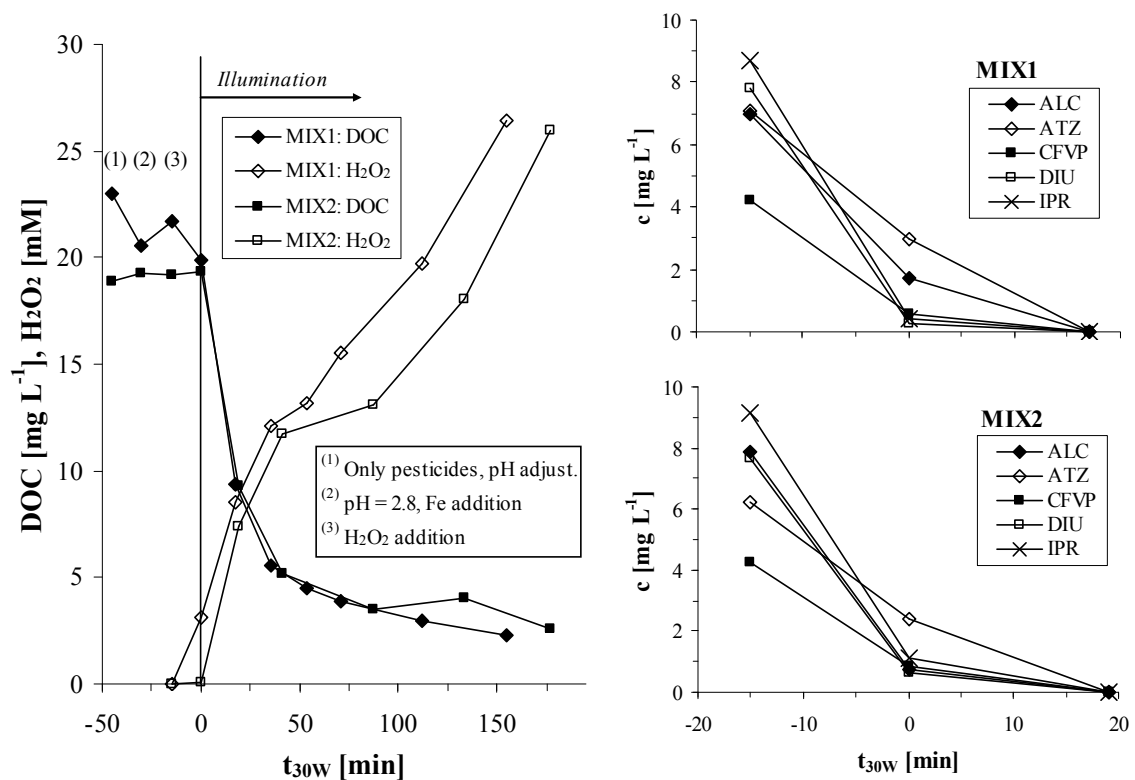
Figure 4.15: Degradation of mixtures of pesticides in CADOX plant (Experiments: MIX1, MIX2).

Figure 4.15 shows the degradation of the experiments MIX1 and MIX2 (identical set-up), which have an initial concentration of 10 mg L^{-1} adding up to a total amount of 50 mg L^{-1} of pesticides inside the model waste water. **Figure 4.16** shows the degradation of MIX3 and MIX4, each of which contains 30 mg L^{-1} adding up to a total amount of 150 mg L^{-1} of pesticides.

The HPLC measurements show three things. First, the initial concentration of CFVP is considerably lower than the other pesticides' concentration. This indicates some difficulty with the dissolution procedure applied, although it is uncertain, whether CFVP is lost by adsorption to the walls of the dissolution vessel or the photoreactor, or if it is partly converted by the high temperature (stirring overnight at 60 ºC, see section 3.4.2), e.g. by hydrolysis of the ester groups. Second, ATZ is most recalcitrant to the Fenton reaction, which is in concordance with the observed behaviour of ATZ as a single substance. Finally, the measurements show that also in a mixture all contaminants are converted very quickly into degradation intermediates.
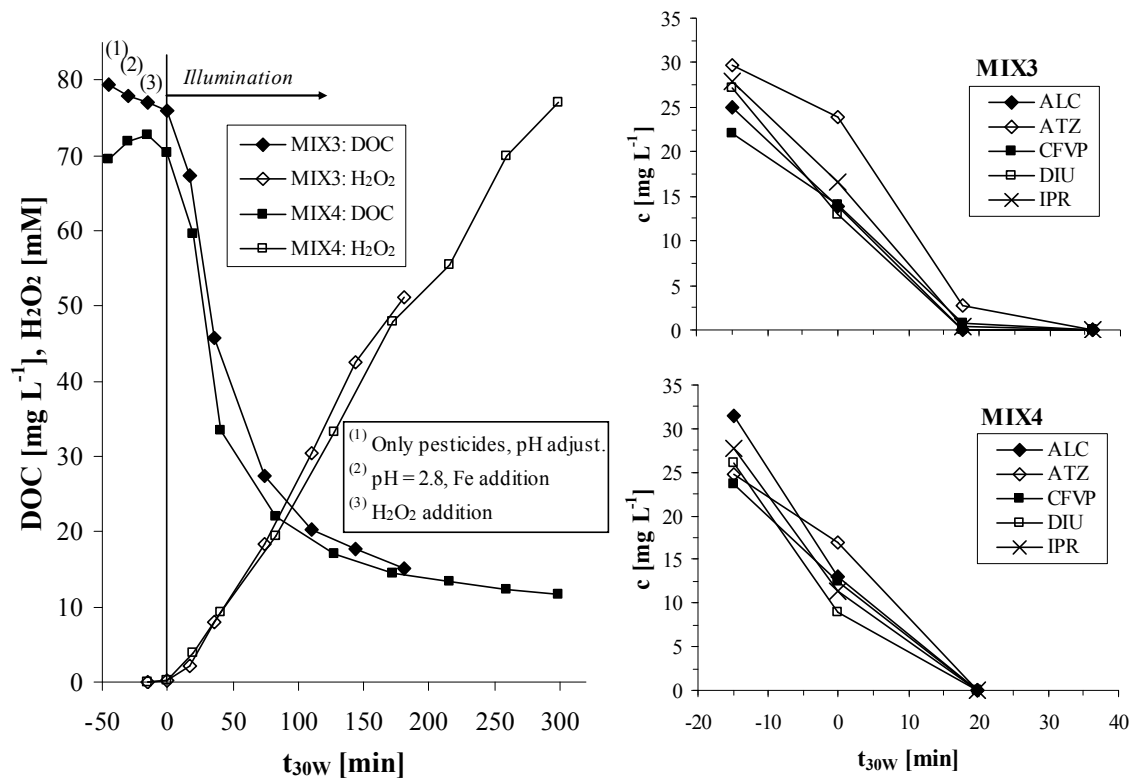
Figure 4.16: Degradation of mixtures of pesticides in CADOX plant (Experiments: MIX3, MIX4)

The mineralisation of the pesticides proceeds without any problems. Only after the mineralisation of around 80% of the initial DOC, the further decrease of DOC slows down. This might presumably be attributed to the same recalcitrant degradation intermediates as in the previous single substance experiments.

Furthermore, at the higher initial contaminant concentration the individual contaminants are all quickly converted into other degradation intermediates. Again, ATZ is shown to be the most recalcitrant pollutant, whereas the other pollutants react similarly. At this higher concentration CFVP has the lowest initial concentration, but the total amount disappearing during the experiment preparation procedure is similar as in the experiment at lower initial concentration. Consequently, conversion during the dissolution can be ruled out. What is more, the DOC degradation takes place in a similar way like at lower initial concentration, except for that it is slightly slower and shows a short lag phase at the beginning of the experiment. The reproducibility of the experiments can be regarded satisfying taking into account that the experiments are pilot-plant experiments and are carried out with varying solar irradiance.

The average values of $t_{30W}^{50\%DOC}$ and $t_{30W}^{80\%DOC}$ are 17 and 67 min at low initial pesticide concentration and 45 and 174 min at high initial concentration. For $A_{CM}^{50\%DOC}$ and $A_{CM}^{80\%DOC}$ the values are 1510 and 3750 m^2 h kg^{-1} and 1110 and 2690 m^2 h kg^{-1} at low and high initial concentration, respectively. This data shows that the degradation per collector area and time unit is higher at higher initial contaminant concentration.

The average hydrogen peroxide consumption to achieve 50% decrease of DOC ($H_2O_2^{50\%DOC}$) is 1.5 times its theoretical stoichiometric demand in the case of the lower initial pesticide concentration, and 0.7 times its stoichiometric demand for total mineralisation at higher concentration. The $X_{H_2O_2}^{50\%DOC}$ values are 9.4 and 24.8 mg H_2O_2 consumed for each mg DOC degraded at low and high initial pesticide concentration. The value for the lower concentration is quite similar to the corresponding values in **Table 4.2** and **Table 4.3**, whereas the value at the higher concentration is lower than the lowest value in the single contaminant experiments. It can be concluded that in the presence of higher amounts of organic matter the use of the oxidant is more efficient, because at higher concentration the organic matter better competes with hydrogen peroxide for the hydroxyl radicals generated.

4.1.5 Comparison of pesticides, NBCS and 4-NP experiments

All contaminants studied have been easily converted into intermediates when they were applied as single substances as well as in mixtures. In the single contaminant experiments at low iron concentration (2 mg L^{-1}) conversion was completed within few minutes of illumination. At higher iron concentration (1 mM) in most cases this happened via the dark Fenton reaction even without illumination. The pesticide mixtures (at 50 and 150 mg L^{-1} initial total pesticide concentration) were degraded applying a medium iron concentration (10 mg L^{-1}) and conversion occurred within few minutes after illumination. Subsequently, the degradation intermediates continued being oxidised until mineralisation to carbon dioxide and inorganic ions took place.

Complete mineralisation could not be achieved for all contaminants due to the formation of intermediates refractory to the applied treatment. This happened in the cases of atrazine and the phenylurea herbicides diuron and isoproturon. In the case of the phenylurea herbicides the incomplete contaminant mineralisation is likely due to the formation of urea refractory to oxidative treatment, which on the other hand is non-toxic and biodegradable. In the case of atrazine intermediates are formed, which still contain the triazine ring system. Cyanuric acid is the final stable degradation product, but with photo-Fenton treatment it could only be obtained after very long treatment times and high oxidant consumption (just like with TiO_2/UV).

As a consequence, the feasibility of a photo-Fenton treatment for the contaminants studied can be granted, because each contaminant (except atrazine) could be mineralised to inorganic substances or non-toxic organic substances in economically feasible treatment times (e.g. 50% of mineralisation took 3 – 14 minutes at Fe = 1 mM and 21 – 93 minutes at Fe = 2 mg L^{-1}). It was confirmed that the performance of the treatment did not change significantly upon applying it to mixtures.

Blank experiments without degradation showed, furthermore, that possible volatilisation of contaminants has to be taken into account, at least in the case of the NBCS studied (DCM, TCM and DCE). Nevertheless, the mass balances established in the degradation experiments indicated that under the conditions of the photo-Fenton treatment practically no volatilisation occurred and the whole amount of contaminant was mineralised. To prevent volatilisation a quick treatment is recommendable, i.e. by maximising the degradation rate. Also changes in the plant set-up are recommendable to prevent volatilisation in the tank, which is in contact with the atmosphere.

Concerning the degradation rates, the effect of the elevated iron concentrations is strong in all the single contaminant experiments, especially during the initial stages of the degradation, where the larger amount of ferrous iron present provokes considerable oxidation through the dark Fenton reaction already before illumination. Nevertheless, the apparent effect in the corresponding figures-of-merit ($t_{30W}^{50\%DOC}$, $t_{30W}^{80\%DOC}$, $Q^{50\%DOC}$, $Q^{80\%DOC}$, $A_{CM}^{50\%DOC}$, $A_{CM}^{80\%DOC}$, see **Table 4.1**, **Table 4.2** and **Table 4.3**) is not as pronounced as the increase in iron concentration (55.85 / 2 mg L^{-1} Fe $\approx$ 28).

The amount of DOC degraded per time unit and collector area also strongly depends on the contaminant nature. E.g. the collector area per mass to degrade 80% of DOC° ($A_{CM}^{80\%DOC}$) at 2 mg L^{-1} iron ranges from 7200 to 12700 m^2 h kg^{-1} for the group of ALC, CFVP, DIU and IPR, 19500 and 30400 for the less soluble PCP and LIN (performed at lower initial concentrations), 65800 for ATZ and 21300 to 38700 for the NBCS. Several conclusions may be drawn. First, the data show that more contaminant is degraded per collector area and time at higher initial concentrations (ALC, CFVP, DIU and IPR compared to PCP and LIN). This is confirmed also in the experiments with pesticide mixtures, where $A_{CM}^{80\%DOC}$ is 2690 m^2 h kg^{-1} at a total initial pesticide concentration of 150 mg L^{-1}, and 3750 m^2 h kg^{-1} at lower pesticide concentration (50 mg L^{-1}). Second, in the NBCS degradation experiments less DOC is degraded per collector area compared to the pesticides. Finally, the particularly refractory behaviour of ATZ is reflected as well.

Hydrogen peroxide consumption was always higher than the theoretical amount of reagent required by mineralisation according to stoichiometry. E.g. for the degradation of 50% of DOC^i the consumption of hydrogen peroxide ($H_2O_2^{50\%DOC}$) was 1 – 2 times the theoretical amount needed for the group of ALC, CFVP, DIU and IPR, 2 – 6 times for PCP and LIN, 6 – 9 times for ATZ, 3 for DCE, 7 – 36 times for DCM and TCM and 1.5 and 0.7 times the stoichiometric demand at low and high initial concentration in the pesticide mixture experiments (compare also $\eta_{H_2O_2}^{80\%DOC}$ in **Table 4.1**, **Table 4.2** and **Table 4.3**). For the pesticides it is shown again that the degradation at lower initial pollutant concentration is less efficient and use of hydrogen peroxide is more efficient in the presence of higher amounts of contaminant. DCM and TCM need very high amounts of hydrogen peroxide compared to their theoretical demand. Also, the exceptional behaviour of ATZ in comparison with the other pesticides is confirmed.

The successful degradation of 4-nonylphenol (4-NP) confirmed that treatment of very low concentrated solutions is theoretically possible. But as already confirmed in the experiments with the other contaminants, a multiple of the theoretical hydrogen peroxide demand for complete mineralisation is needed even to convert more than 99% of the 4-NP into intermediates (approximately 8 times the stoichiometric demand for mineralisation).

As already mentioned an obviously positive influence on the degradation rates was observed by increasing the iron concentration from 2 mg L^{-1} to 1 mM, though the detected effect was not as strong as the increase in iron concentration. This might be due to the increased precipitation found at the higher iron concentration. Precipitated iron causes turbidity, which decreases the photoreactor's light scavenging efficiency, because part of the incident light does not enter the photoreactor but is lost due to scattering.

The final iron concentration measured in the experiments at the higher initial iron concentration ranged from 11 to 25 mg L^{-1} in the group of experiments of ALC, ATZ, CFVP, DIU and IPR, where the pH stayed more or less constant at 2.8. In the experiments with DCM, TCM, DCE and LIN larger amounts of chloride are released, which lower the pH to values of 2.4 – 2.6. In these experiments the final iron concentrations observed range from 25 to 41 mg L^{-1}, i.e. less precipitation occurs. At the lower iron concentration less precipitation occurred, generally being 10 to 30% of the initial amount. It may be concluded that conducting the experiment at a slightly lower pH (e.g. 2.5 – 2.6) will be advantageous concerning inhibition of iron precipitation. This is contrary to most literature, which states 2.8 as the optimal pH (see section 2.2.2). Yet, the work in these references is usually performed at 20 ºC and often at iron concentrations similar to the lower iron concentration in this work. The influence of the iron concentration and also the solution temperature (often 30 – 40º in a solar plant) is usually neglected.

4.2 Comparison of BRITE and CADOX pilot-plants

4.2.1 Absorber tube diameter and length of optical path

An important design parameter for tubular photoreactors is the diameter, since in photocatalytic processes all incident efficient photons must be kept inside the reactor

and not allowed to pass through without absorption. The dispersion and absorption of light causes photon density to diminish over the length of the optical path, as described by Lambert-Beer. Depending on the absorption properties of the solution and the catalyst/ sensitizer different shares of radiation are harvested inside the photoreactor. The goal is to adjust the catalyst/ sensitizer concentration, so that no photons are lost. **Figure 4.17** shows the absorption properties of ferric iron solutions (the catalyst in photo-Fenton treatment) at pH 2.8 at 350 nm as a function of the length of optical path. It can be appreciated that at higher length of optical path, less catalyst concentration is needed to absorb a given share (e.g. 95%) of all photons entering the photoreactor [145]. The determination of the optimal catalyst loading always has to be confirmed experimentally, because the absorption properties in real waste water are strongly affected by complexes formed between ferric iron and organic substances. Another influencing parameter can be the absorption properties of the wastewater itself, because in case of light absorption by the wastewater there is a competition with the catalyst for the incident photons. In such case usually an increased catalyst concentration is necessary.
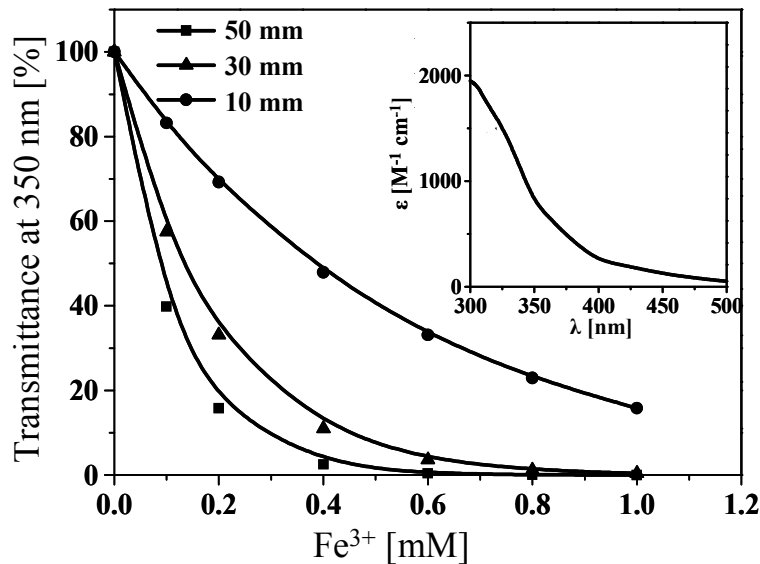
Figure 4.17: Transmittance at 350 nm of Fe^{3+} dissolved in water at pH 2.8 at different optical pathlengths, the inset shows the absorption spectra of Fe^{3+} at the same pH.

Larger absorber tube diameters have several more advantages that should be mentioned. Larger tube diameter implies larger collector aperture and fewer absorber tubes per

collector. This will make the production of the aluminium mirrors easier and more accurate. The assembly of the collectors will also be easier and faster. Besides, fewer elbows are needed for the collector manufacture. As a consequence the price of the production process and the pieces will be reduced. Moreover, fewer problems with breakage and leaking can be expected by reducing the tube number, which will decrease the maintenance costs.

Additionally, the illuminated volume per collector area will increase, because the collector aperture is proportional to the tube diameter, whereas the cross-section area is proportional to its square. Furthermore, the pressure drop inside the tubes for a given flow is lower in tubes with a bigger diameter. A reduction of elbows in the piping of the installation reduces the pressure drop. Therefore, the pump energy needed during operation will decrease.

4.2.2 Alachlor degradation at different iron concentrations

According to Lambert-Beer's law at higher lengths of optical path the same solution has a lower light transmittance. **Figure 4.17** shows this relationship for ferric iron solutions at an average wavelength of solar UV light (350 nm). According to this figure at 50 mm length of optical path (CADOX plant 46.4 mm) above a ferric iron concentration of 0.3 mM more than 90% of incoming photons at this wavelength are absorbed, whereas at 30 mm length (BRITE plant 29.2 mm) of optical path, about 0.45 mM of ferric iron are needed. Consequently, lower iron concentrations can be used in the CADOX plant to make use of nearly all incoming photons for the reduction of ferric to ferrous iron by Eq. (2.54). This is important because under common photo-Fenton conditions this reduction step of the catalyst is the rate-limiting step. As a consequence, no substantial increase of reaction rate can be expected from a further increase of iron concentration, because no additional photochemical reduction takes place, and only thermal reactions are slightly enhanced.

Figure 4.18 and **Figure 4.19** show DOC degradation results of alachlor solutions at different iron concentrations from 2 to 55.8 mg L^{-1} in both pilot plants. It can be seen that in the BRITE plant there is still a considerable increase in the maximum degradation rate of the DOC when passing from the medium to the highest iron concentrations.

Two aspects have to be taken into account when trying to assess the influence of the iron concentration on the efficiency of the photochemical reaction. First, the different initial concentrations of ferrous iron cause a different degree of degradation progress during the dark Fenton reaction. As a consequence, the photochemical reaction (after the commencement of illumination) starts from different points. Second, in the BRITE plant temperature control was impossible. Consequently, the wastewater temperatures are different, which influences the degradation rate substantially. E.g. the temperature difference between the experiment at medium concentration and highest iron concentration is around 5 ℃ on average. Therefore, it can be assumed that under equal conditions the difference in degradation rate would be greater between both experiments.
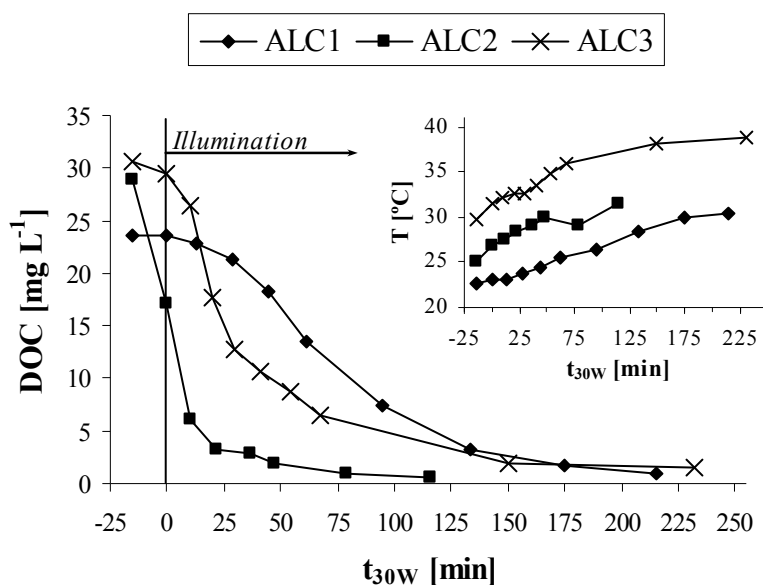
Figure 4.18: Alachlor degradation in BRITE plant at different iron concentrations. ALC1 = 2 mg L^{-1} Fe, ALC2 = 55.8 mg L^{-1} Fe, ALC3 = 10 mg L^{-1} Fe. Initial ALC concentration is 50 mg L^{-1}.

In the CADOX plant the latter difficulty is cancelled as the temperature was controlled and kept constant at 20 ℃. Only the different extents of the dark Fenton reaction affect the interpretation. Nevertheless, **Figure 4.19** shows that the degradation rate is practically the same in the experiments at medium and high iron concentration after illumination. Therefore, 20 mg L^{-1} iron (or less) can be regarded as a good choice for a maximum catalyst concentration in the CADOX plant for ALC degradation.

Furthermore, 20 mg L^{-1} iron is also the legal limit in many countries for disposal of waste water into natural water bodies.
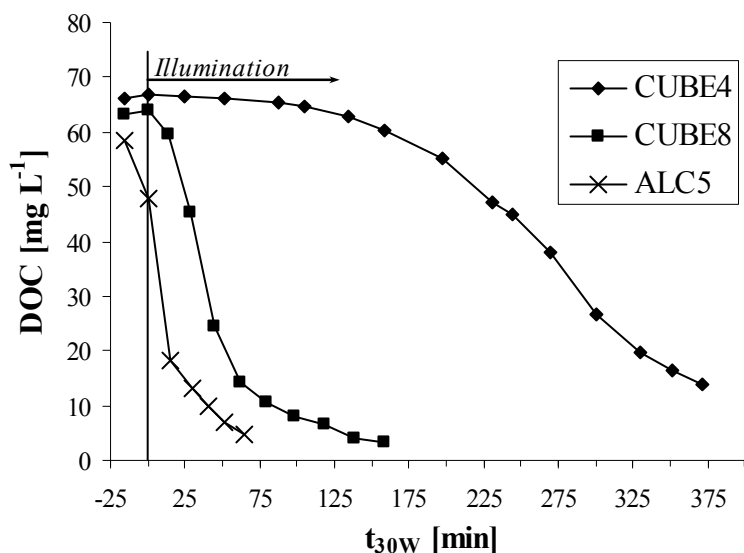
Figure 4.19: Alachlor degradation in CADOX plant at different iron concentrations. CUBE4 = 2 mg L^{-1} Fe, CUBE8 = 20 mg L^{-1} Fe, ALC5 = 55.8 mg L^{-1} Fe. Initial ALC concentration is 100 mg L^{-1} and temperature maintained constant at 20 ºC in all experiments.

4.2.3 ALC, ATZ, CFVP, DIU and IPR degradation in CADOX plant

Figure 4.20 to **Figure 4.24** show the degradation of ALC, ATZ, CFVP, DIU and IPR in the CADOX plant. The qualitative observations are the same as in the experiments in the BRITE plant (see section 4.1.2). Complete mineralisation is possible for ALC and CFVP, some DOC remains in the case of DIU and IPR and only the carbon in the side groups of the triazine ring can be mineralised in the case of ATZ. Chloride release was complete in ALC, CFVP and DIU (small differences in the case of CFVP are due to the difference to the calculated initial concentration of 50 mg L^{-1}), whereas in ATZ only little more than 50% of the theoretical chloride amount was released. In contrast, the nitrogen balance was only complete for ALC, where all the nitrogen was mainly released as ammonium. In the case of DIU and IPR only 40% and 30%, of the nitrogen were found as ammonium or nitrate, respectively. As discussed in section 4.1.2 this is probably due to the formation of urea, which is difficult to degrade by an oxidative treatment such as photo-Fenton. It is probably also the reason for the recalcitrant

residual DOC in these experiments. In the ATZ molecule there are 3 nitrogen atoms in the triazine ring and 2 outside, located on side chains. As mentioned in section 4.1.2 the triazine ring cannot be broken up by photo-Fenton treatment. The total amount of nitrogen found as ammonium or nitrate equals only 10% of the nitrogen amount contained in the side chains, while the DOC contained in these side chains has already been mineralised. This means that at this stage of the process the majority of the intermediates formed have already lost the carbon but still contain all nitrogen atoms. Hincapié et al. [143] discuss the formation of intermediates during solar photo-Fenton treatment of ATZ.

In difference to the experiments described previously the irradiance conditions were really bad in two of these experiments (ALC4 and DIU3). Especially, the DIU experiment was performed under not only cloudy but even partly rainy conditions. Nevertheless, degradation proceeded also at a sufficient rate ($t_{30W} = 30.2$ min corresponds to 90 min real illumination time in experiment DIU3).
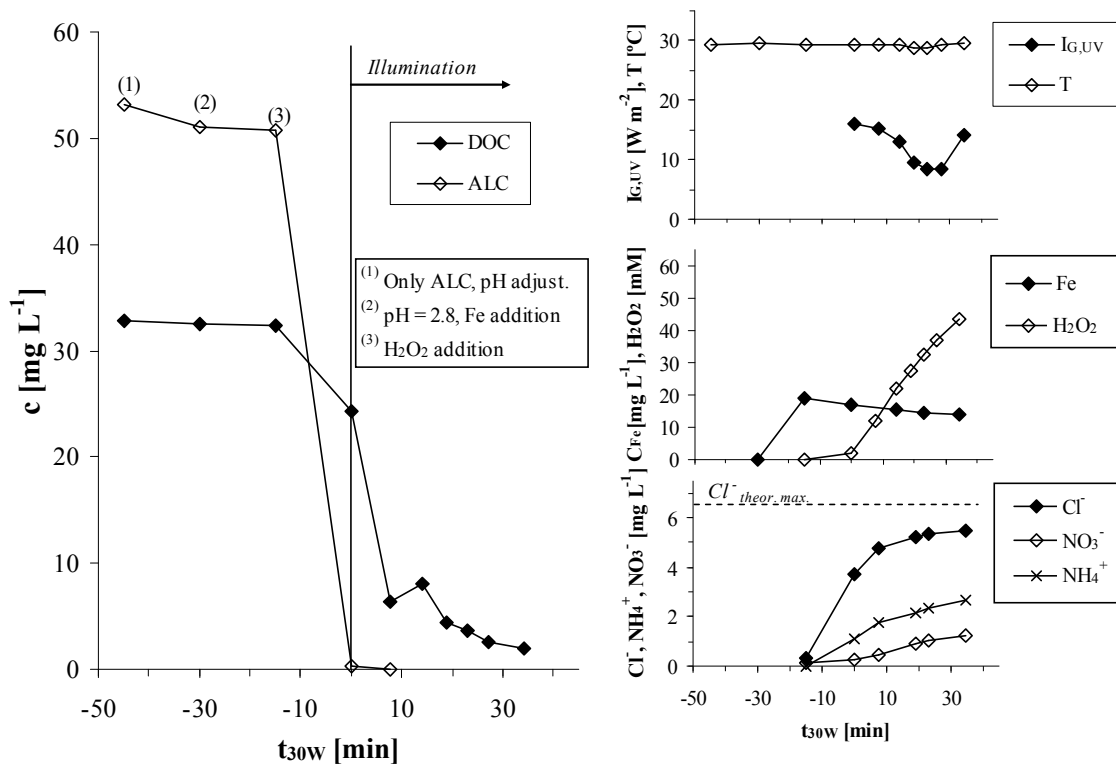
Figure 4.20: ALC degradation in CADOX plant (Experiment: ALC4)
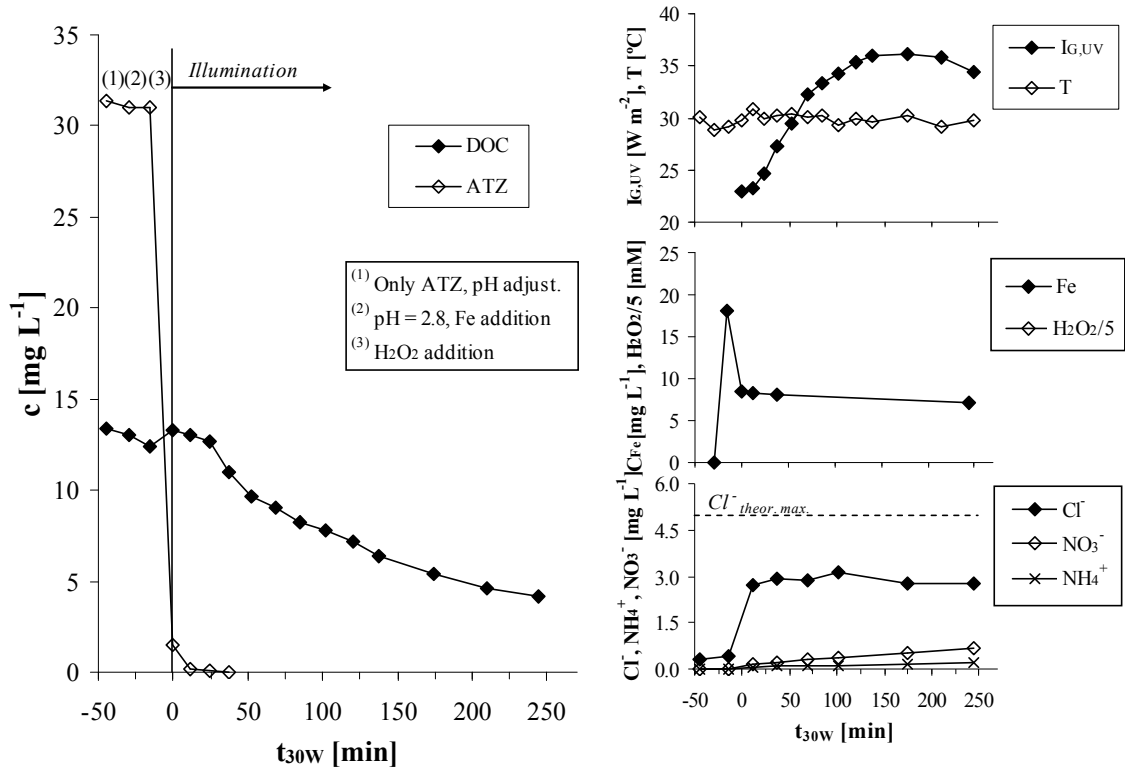
Figure 4.21: ATZ degradation in CADOX plant (Experiment: ATZ3)
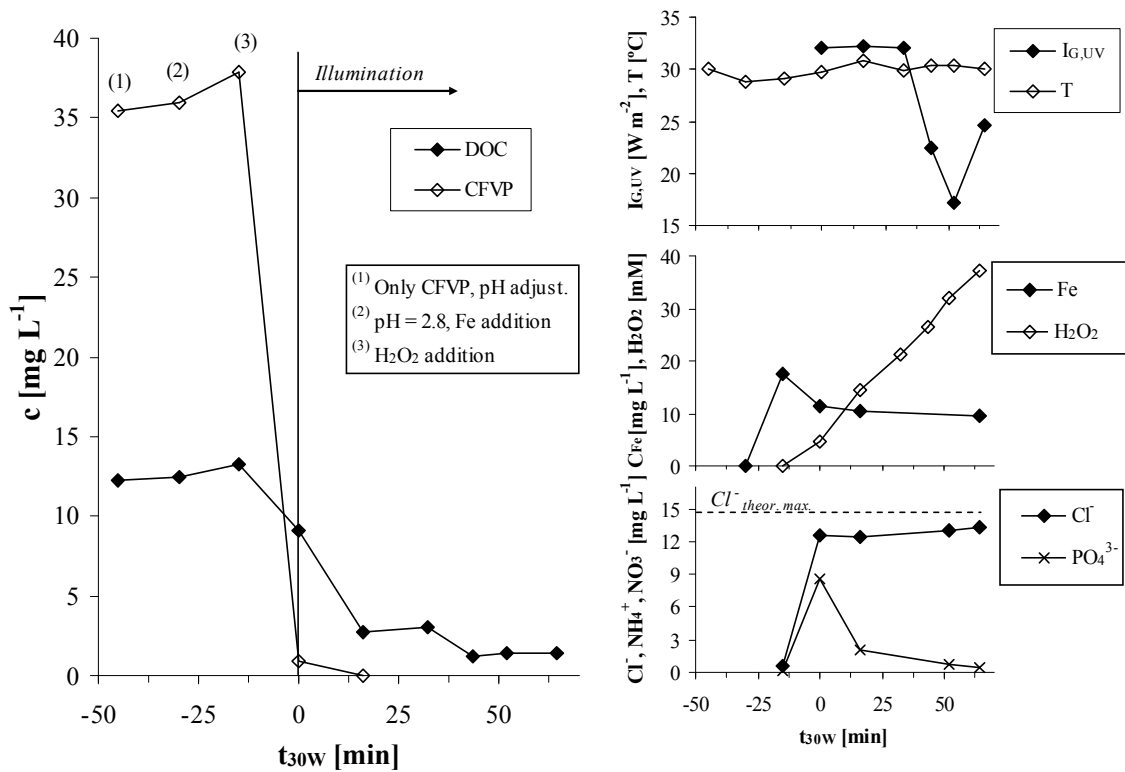
Figure 4.22: CFVP degradation in CADOX plant (Experiment: CFVP3)
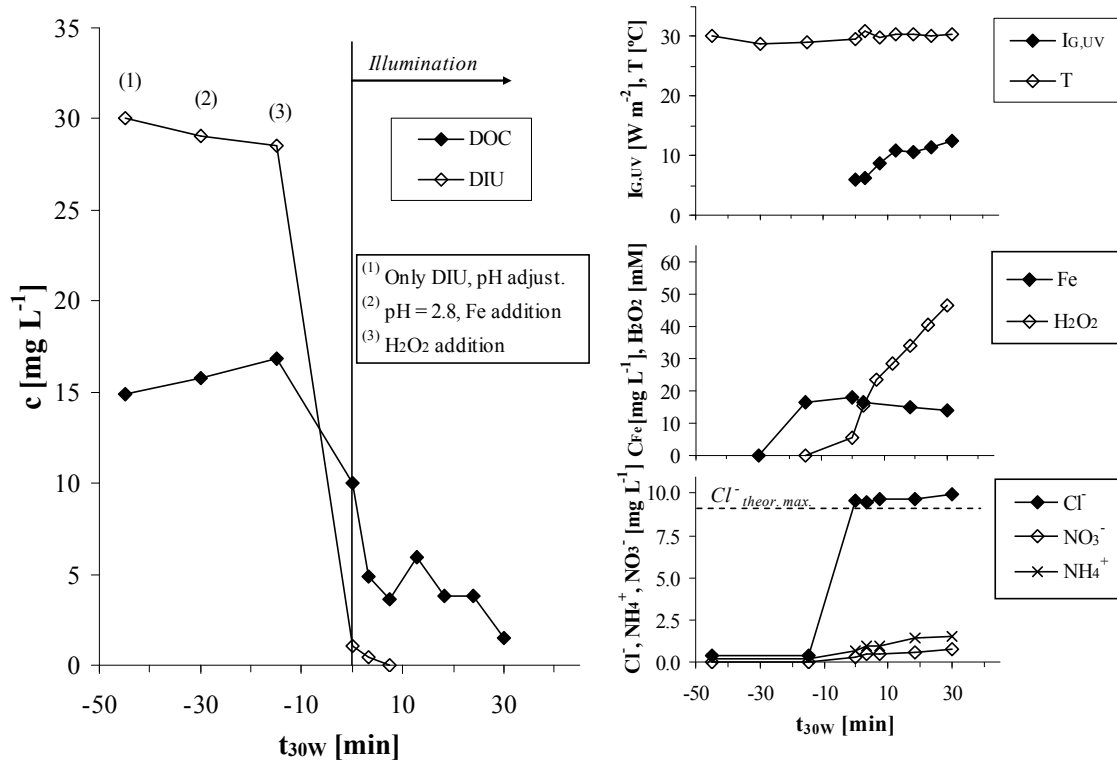
Figure 4.23: DIU degradation in CADOX plant (Experiment: DIU3)
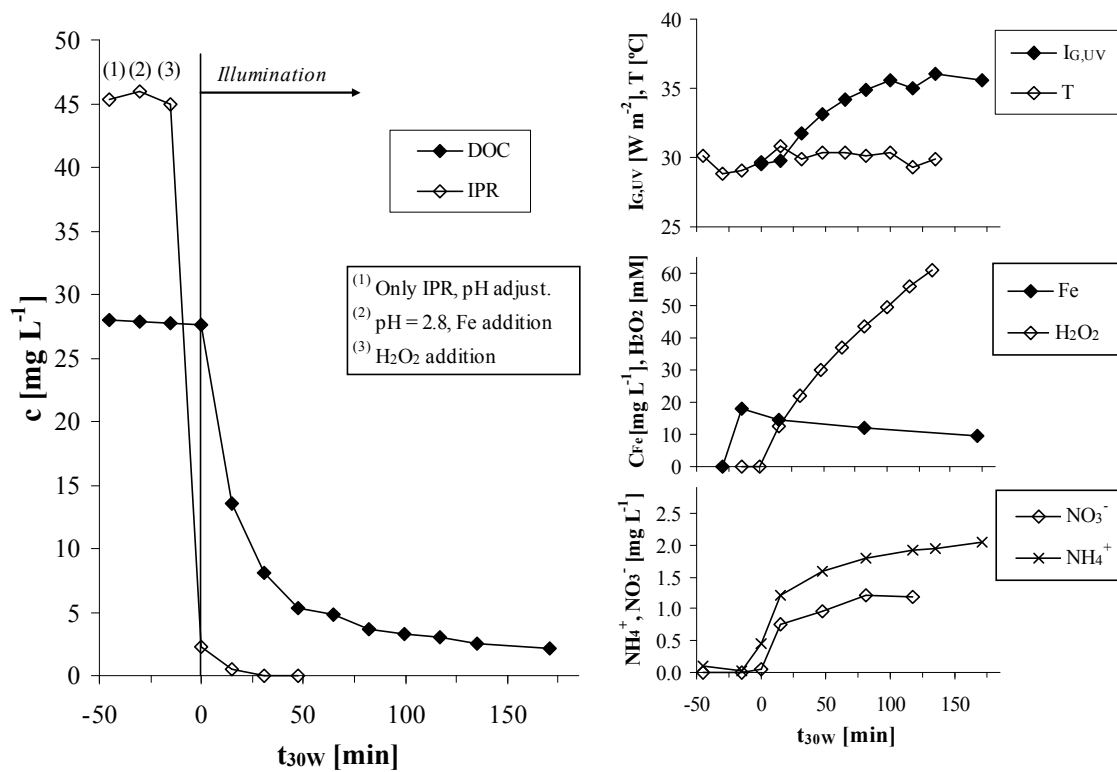
Figure 4.24: IPR degradation in CADOX plant (Experiment: IPR3)

Table 4.4: Figures-of-merit for pesticide degradation experiments in CADOX plant (ALC, ATZ, CFVP, DIU, IPR).

		ALC4	ATZ3	CFVP3	DIU3	IPR3
DOC^i	[mg L^{-1}]	32.3	13.8	13.3	16.8	27.8
c^i	[mg L^{-1}]	50.7	31.0	37.9	28.5	45.0
c^i	[mM]	0.19	0.14	0.11	0.12	0.22
$H_2O_2^{theor}$	[mM]	6.40	2.16	2.95	2.20	6.33
$t_{30W}^{50\%DOC}$	[min]	3.5	56	7	1	14
$t_{30W}^{80\%DOC}$	[min]	16	126	33	25	45
$Q^{50\%DOC}$	[kJ L^{-1}]	0.3	5.6	0.7	0.1	1.4
$Q^{80\%DOC}$	[kJ L^{-1}]	1.6	12.6	3.3	2.5	4.5
$A_{CM}^{50\%DOC}$	[m^2 h kg^{-1}]	200	11996	973	110	931
$A_{CM}^{80\%DOC}$	[m^2 h kg^{-1}]	572	16869	2867	1720	1871
$H_2O_2^{50\%DOC}$	[mM]	6.7	33.1	8.9	8.9	11.5
$H_2O_2^{80\%DOC}$	[mM]	24.2	61.5	21.6	41.7	28.9
$X_{H_2O_2}^{50\%DOC}$	[-]	14	261	46	36	28
$X_{H_2O_2}^{80\%DOC}$	[-]	32	303	69	105	44
$\eta_{H_2O_2}^{80\%DOC}$	[%]	26.4%	3.5%	13.7%	5.3%	21.9%

DOC^i is the DOC at t_{30W} = -15 min, except ATZ, which is calculated from c^i. c^i is measured by HPLC at t_{30W} = -15 min. 50% and 80% degradation refer to DOC^i, except for ATZ, where it means 50% and 80% degradation of 5/8 of DOC^i. Also for calculation of A_{CM}, $X_{H_2O_2}^{50\%DOC}$, $X_{H_2O_2}^{80\%DOC}$ and $\eta_{H_2O_2}^{80\%DOC}$ for ATZ only 5/8 of DOC^i are regarded (see section 4.1.2.2). $X_{H_2O_2}^{50\%DOC}$, $X_{H_2O_2}^{80\%DOC}$ and $\eta_{H_2O_2}^{80\%DOC}$ take into account $H_2O_2^{50\%DOC}$, $H_2O_2^{80\%DOC}$, DOC^i and $H_2O_2^{theor}$ (see Eq. (3.28) - (3.30)).

Two values are suitable for comparison of the reaction rate between the experiments in the BRITE plant and the CADOX plant, t_{30W} and Q. t_{30W} is a simple measurement of how long the experiment took to reach a certain degradation level (50% or 80% of disappearance of DOC). To compare the performance it seems most appropriate to compare the values of the experiments in the CADOX plant (at 20 mg L^{-1} Fe) to their respective equivalent experiments in the BRITE plant (at 1 mM Fe) for a degree of DOC degradation of 80%, because at the lower percentage the different yields of the dark Fenton reaction will have a stronger influence. The complete array of values describing the results of these experiments can be found in **Table 4.2**, **Table 4.3** and

Table 4.4. The values of these experiments concerning the reaction rate ($t_{30W}^{80\%DOC}$, $Q^{80\%DOC}$, $A_{CM}^{80\%DOC}$ and T) have been summarised in **Table 4.5**.

Due to the differences in the design of the two plants (mainly in the collector) the volume per collector area is different for each of them. Volume per area is 11.4 L m^{-2} in the BRITE plant and 18.0 L m^{-2} in the CADOX plant. Hence, in the same amount of time under identical irradiance conditions less photons (or less UV energy) per litre of waste water enter the absorber tubes in the CADOX plant. This means that in the BRITE plant during 6.2 min of UV irradiance at 30 W m^{-2} 1 kJ L^{-1} UV energy is collected at the CPC area, while it takes 10.0 min of irradiance under the same conditions to collect the same amount of UV energy per volume in the CADOX plant (see section 3.6 for the corresponding equations).

Table 4.5: Comparison of kinetic parameters between BRITE and CADOX plant for several pesticides.

		ALC	**ATZ**	**CFVP**	**DIU**	**IPR**
$t_{30W}^{80\%DOC}$	BRITE:	12	135	21	19	29
[min]	CADOX:	16	126	33	25	45
$Q^{80\%DOC}$	BRITE:	1.9	21.4	3.3	3	4.6
[kJ L^{-1}]	CADOX:	1.6	12.6	3.3	2.5	4.5
$A_{CM}^{80\%DOC}$	BRITE:	761	31600	1970	2810	1470
[m^2 h kg^{-1}]	CADOX:	572	16900	3870	1720	1870
T	BRITE:	24-31	24-30	37-40	32-39	27-38
[ºC]	CADOX:	30	30	30	30	30

Experiments: ALC2, ALC4, ATZ2, ATZ3, CFVP2, CFVP3, DIU2, DIU3, IPR2, IPR3. For further details see also Table 4.2, Table 4.3 and Table 4.4.

A comparison between the values of t_{30W}^{80DOC} and then between those of $Q^{80\%DOC}$ in **Table 4.5** for both plants shows that the treatment times are slightly longer in the CADOX plant, but at the same time less UV energy is needed to achieve the degradation goal. In this context it is also necessary to take into account the reaction temperature. The balance is especially favourable for the BRITE plant in the experiments of CFVP and IPR, which have the highest temperature in the BRITE plant. But knowing that higher temperature accelerates the reaction rate it can be assumed that under similar temperature conditions these numbers would be less favourable. The

conclusions concerning $A_{CM}^{80\%DOC}$ are similar, showing that the performance of the CADOX plant was at least equal to the BRITE plant. This has been achieved although in the BRITE plant the effect of the dark Fenton reaction is stronger due to the higher concentration of ferrous iron (1 mM). Also during the photochemical reaction a higher catalyst concentration is present in solution.

4.3 Influence of iron concentration, temperature and collector area per volume

4.3.1 Degradation results

Alachlor is classified by the United States Environmental Protection Agency as Type III, that is, toxic and slightly hazardous, and as a priority substance (PS) by the European Commission (EC) within the scope of the Water Framework Directive (WFD). Furthermore, alachlor's molecular structure (see **Figure 3.1**) can be regarded as that of a rather typical non-biodegradable contaminant, having an aromatic ring structure, aliphatic carbon and organically bound chlorine and nitrogen. Therefore, in addition to its importance as a contaminant, its use as a model compound in a generic study on the influence of process parameters is fully justified.

A three factor central composite design without star points was applied to assess the influence of iron concentration, temperature and the collector area per volume of waste water treated in a batch. The latter factor can also be understood as the ratio of time under illumination and time in darkness of the waste water. As described above (see section 3.4) the same initial pollutant concentration of 100 mg L^{-1} was used throughout all factorial design experiments. Hydrogen peroxide concentration was also maintained constant at around 200 – 400 mg L^{-1} by manual additions during the degradation and initial pH was adjusted to 2.6.

The initial DOC values were 65.1 mg L^{-1} (standard deviation of 2.1 mg L^{-1}), which corresponds almost perfectly to the theoretical DOC of 62.3 mg L^{-1} of 100 mg L^{-1} ALC. The small difference is due to the application of technical grade ALC with a purity of 95%. Consequently, there is a small contribution from unknown organic impurities of the technical grade pesticide.
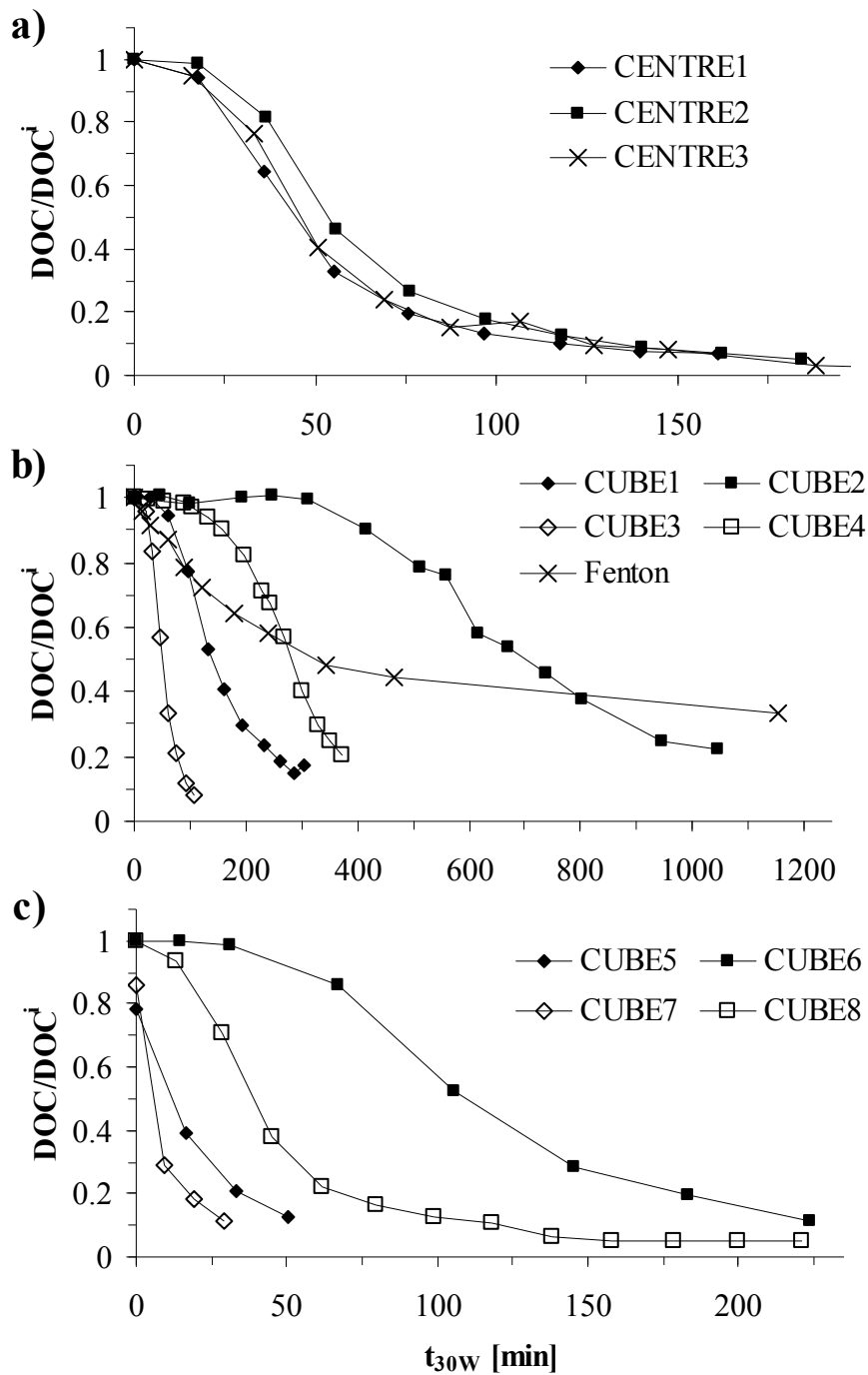
Figure 4.25: ALC factorial design – DOC degradation curves. Cube points with even numbers are performed at 20ºC, with odd numbers at 50ºC. Cube 1, 2, 5, 6 with 0.83 m^2, cube 3, 4, 7, 8 with 4.16 m^2 collector; a) centre points, b) cube points with 2 mg L^{-1} iron & Fenton experiment at 50ºC and 20 mg L^{-1} iron c) cube points with 20 mg L^{-1} iron.
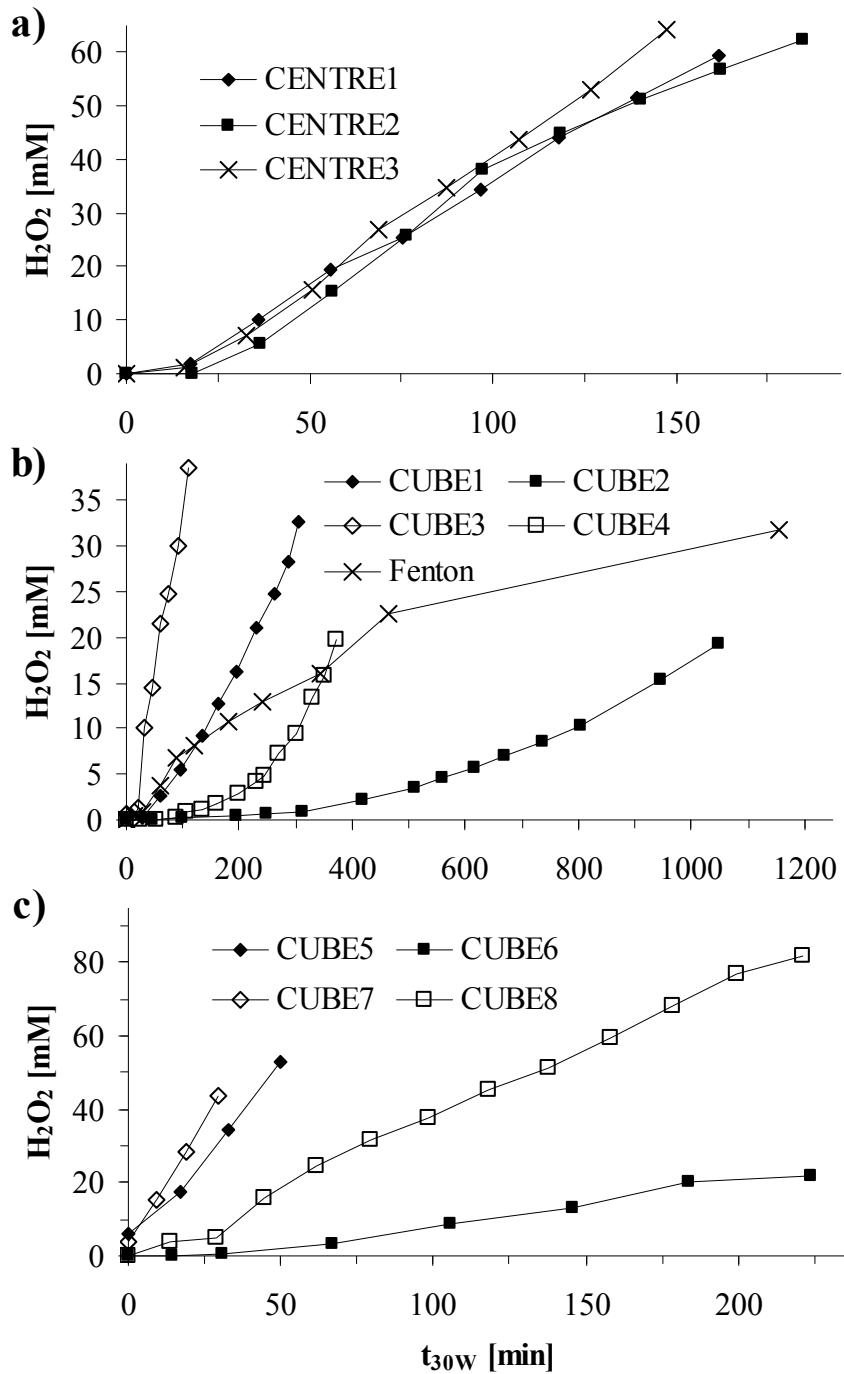
Figure 4.26: ALC factorial design – H_2O_2 consumption curves. Cube points with even numbers are performed at 20ºC, with odd numbers at 50ºC. Cube 1, 2, 5, 6 with 0.83 m^2, cube points 3, 4, 7, 8 with 4.16 m^2 collector; a) centre points, b) cube points with 2 mg L^{-1} iron & Fenton experiment at 50ºC and 20 mg L^{-1} iron c) cube points with 20 mg L^{-1} iron.

Figure 4.25 shows the DOC degradation curves, while **Figure 4.26** shows the hydrogen peroxide consumption during the eleven experiments of the factorial design. The kinetic parameters describing these experiments are summed up in Table 4.6. $t_{30W}^{DOC50\%}$ and $t_{30W}^{DOC80\%}$ values were obtained by linear interpolation between the two points adjacent to the limit value. For CUBE2 and CUBE4 experiments, $t_{30W}^{DOC80\%}$ was obtained by linear extrapolation from the last three measured points. This method provides accuracy (relative error 3-5%) enough compared to the overall reproducibility of the experiments as detected by the repetition of the centre points of the factorial design (relative error 10-11%, compare **Figure 4.25** and Table 4.6).

First of all, DOC degradation was confirmed under all the experimental conditions tested in the photo-Fenton experiments, even at the rather low iron concentration of $2\,mg\,L^{-1}$ (see Figure 4.25b). The stoichiometric release of the organically bound nitrogen and chlorine to ammonium, nitrate and chloride, was also confirmed (data not shown). Reproducibility of the results is confirmed (see Figure 4.25a). Referring to the values for $t_{30W}^{50\%DOC}$ and $t_{30W}^{80\%DOC}$ of the centre experiments in Table 4.6, the standard deviations are 4.9 and 9.3 minutes respectively, what corresponds to 10 and 11% of their mean values. In the case of $A_{CM}^{50\%DOC}$ and $A_{CM}^{80\%DOC}$ the standard deviations are only 7 and 8% of their mean value, respectively.

A dark Fenton control experiment was performed at $20\,mg\,L^{-1}$ iron and $50\,^{\circ}C$, because these are the most favourable conditions in the experimental region investigated. Figure 4.25b) shows that although degradation was confirmed, the reaction was considerably slower than the corresponding experiments under illumination (CUBE5 and CUBE7, see Figure 4.25c). Furthermore, it seems that DOC degradation cannot be achieved to the same extent as under illumination, and intermediates produced in the degradation process further slowed the reaction. Therefore, it may be concluded that illumination is necessary to achieve high DOC degradation grades.

The factorial design clearly shows that the variation of each of the three chosen process variables has a strong influence on the process performance across the whole range of the values of the other two. E.g. raising the iron concentration from 2 to $20\,mg\,L^{-1}$ shortens the treatment time ($t_{30W}^{80\%DOC}$) by a factor of 7.2 (CUBE1 and CUBE5), 5.9 (CUBE2 and CUBE6), 4.3 (CUBE3 and CUBE7) and 5.4 (CUBE4 and CUBE8) (each pair was performed with the same collector area and temperature, see **Table 3.8** and **Table 4.6**). Similar observations can be made for a temperature increase from 20 to

50ºC (treatment shortens by factors from 3.8 to 5.2) and a collector area increase from 0.83 to 4.16 m^2 (treatment shortens by factors from 1.9 to 3.3).

It is important to note that increasing the iron concentration by a factor of ten causes a treatment time decrease by a factor of only 4.3 – 7.2 (see above). This is in perfect agreement with the considerations stated in section 4.2.1 (compare **Figure 4.17**) and the Lambert-Beer law, which ascertains a non-proportional correlation between the share of radiation absorbed and the concentration of the absorbing substance in solution. The increase is still high, probably due the effect of thermal reactions, which are not affected by the availability of photons in the solution. This is supported by the fact that the increase of the iron concentration was most effective in the experiments at low collector area, in which the thermal reactions should be of higher importance.

By reducing the illuminated area from 4.16 to 0.83 m^2 (uncovering only part of the CPC) the reaction rate decreases with respect to t_{30W}. But while the illuminated area is reduced by a factor of five, the real treatment time increases only by a factor ranging from 1.9 to 3.3 instead of 5, as it would be expected if all the reactions were to be induced by photochemical processes (at least as a rate-limiting step involved in the recycling of ferrous iron). This means that only about 39 to 65% of the number of photons are necessary with less illuminated area and implies that an important part of the reactions are thermally induced in the dark. Several possibilities could explain the difference in the number of photons needed for degradation depending on the relationship between dark and illuminated reactor volume. Either intermediates are formed under illumination, and they boost the reaction further after leaving the illuminated reactor zones (e.g. hydroquinones/quinones maintaining the catalytic iron cycle [71]), or intermediates are formed in the dark, and then react quickly under illumination (e.g. organic acids forming photo-active complexes with ferric iron). A combination of both explanations is also possible.

This behaviour of the degradation performance as a function of the collector area is reflected in the other two kinetic parameters given in **Table 4.6**, accumulated UV energy, Q, and collector area per mass, A_{CM}. While the treatment time increases as the collector area is decreased, Q and A_{CM} decrease as well. This is an observation of the utmost importance, because it means that the potential savings of the capital costs by reducing installed collector surface are considerable. The issue is to optimise the time under illumination and in the dark. In this context, not only this ratio but also the duration of the continuous residence time under illumination has to be optimised

considering the reasons and mechanisms causing the observed phenomena proposed above.

The $A_{CM}^{50\%DOC}$ and $A_{CM}^{80\%DOC}$ values are very similar for most of the experiments, with the exception of the two fastest and the slowest experiments. In the fastest experiments (CUBE5 and CUBE7, both high iron concentration and high temperature) considerable degradation already occurs before illumination begins (see Figure 4.25c). Hence, 50% DOC degradation is reached after very short period of illumination. In the case of the slowest experiment, the $A_{CM}^{80\%DOC}$ value is lower than the $A_{CM}^{50\%DOC}$ value, because there is a rather long lag phase at the beginning of the experiment, which results in a quite long time necessary to reach 50% DOC degradation, whereas further on degradation proceeds rather smoothly until 80% degradation.

Table 4.6: ALC factorial design – kinetic degradation parameters.

	ALC [min]	$t_{30W}^{DOC50\%}$ [min]	$t_{30W}^{DOC80\%}$ [min]	$Q^{DOC50\%}$ [kJ L^{-1}]	$Q^{DOC80\%}$ [kJ L^{-1}]	$A_{CM}^{DOC50\%}$ [m^2 h kg^{-1}]	$A_{CM}^{DOC80\%}$ [m^2 h kg^{-1}]
CENTRE1	35	45	75	2.7	4.5	758	790
CENTRE2	35	54	92	3.2	5.5	857	913
CENTRE3	32	46	77	2.8	4.6	782	818
CUBE1	60	141	252	2.8	5.0	824	921
CUBE2	416	703	1060	14	21	4023	3791
CUBE3	33	50	77	5.0	7.7	1380	1328
CUBE4	159	308	375	31	37	8609	6544
CUBE5	0[*]	12	35	0.25	0.70	71	127
CUBE6	67	110	181	2.2	3.6	643	661
CUBE7	0[*]	5.9	18	0.59	1.8	170	324
CUBE8	29	39	69	3.9	6.9	1139	1260

[*] ALC was already converted during the dark Fenton reaction before illumination started.

ALC column refers to the complete conversion of ALC into intermediates.

The mentioned lag time can be more clearly appreciated in the slower experiments. CUBE4 and CUBE6 are shown as paradigmatic examples in **Figure 4.27**. At the beginning of the experiments the hydrogen peroxide consumption rate is very low. Only after an initial lag phase is overcome, the reaction rate increases and mineralisation of DOC begins.
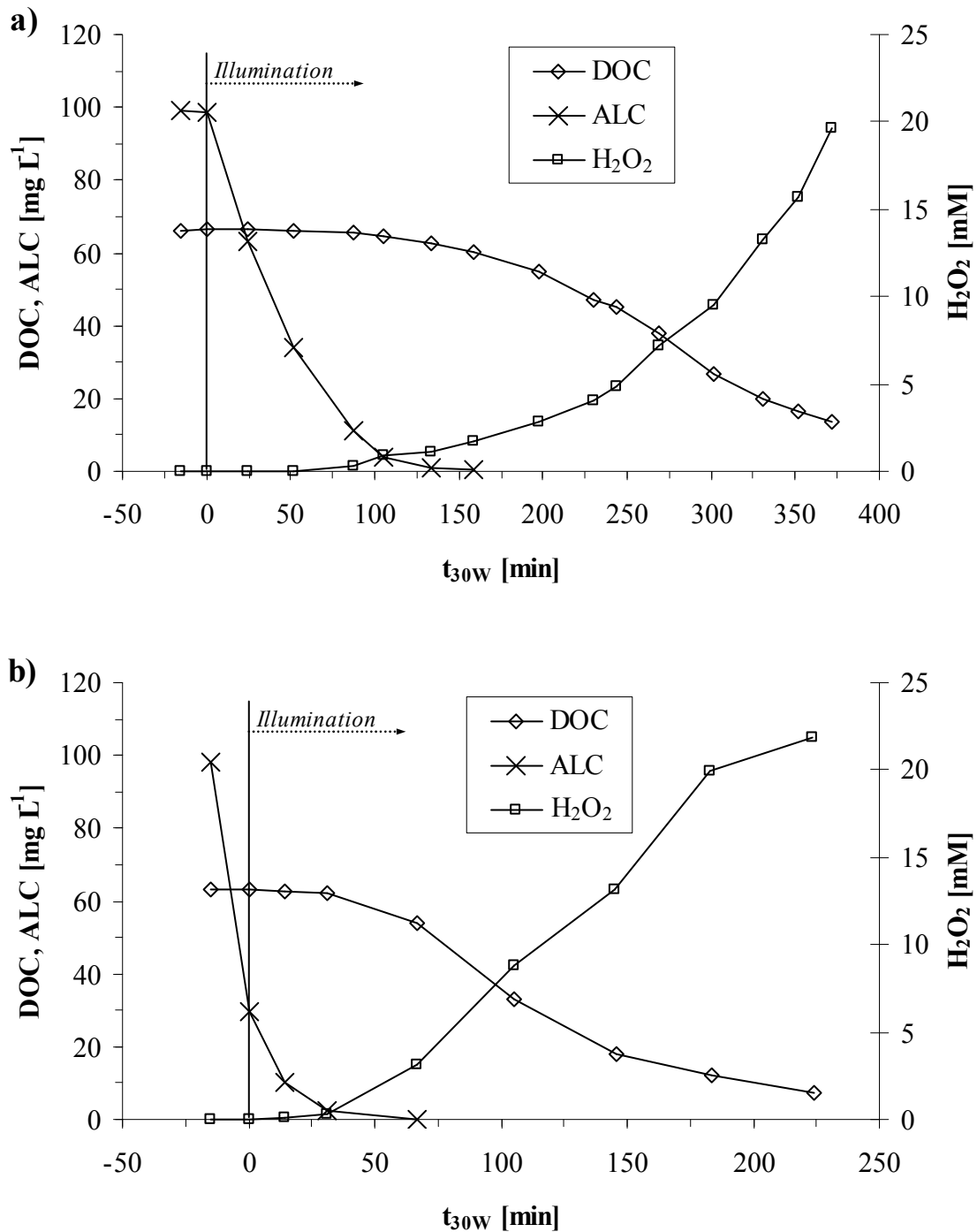
Figure 4.27: DOC vs. ALC degradation for CUBE4 and CUBE6.

Figure 4.27 also shows that mineralisation starts once of the initial ALC has been converted into intermediates. **Figure 4.28** shows HPLC chromatograms recorded at 225 nm wavelength of experiment CUBE6. At least 12-15 peaks can be distinguished as intermediates. However, neither identifying these compounds nor investigating the degradation pathway was within the scope of this study as this had been done before by

Peñuela and Barceló [146]. The disappearance of the peaks in the chromatograms at 225 nm during degradation also confirms the disappearance of aromatic compounds, which are at least slightly absorbing at this wavelength.
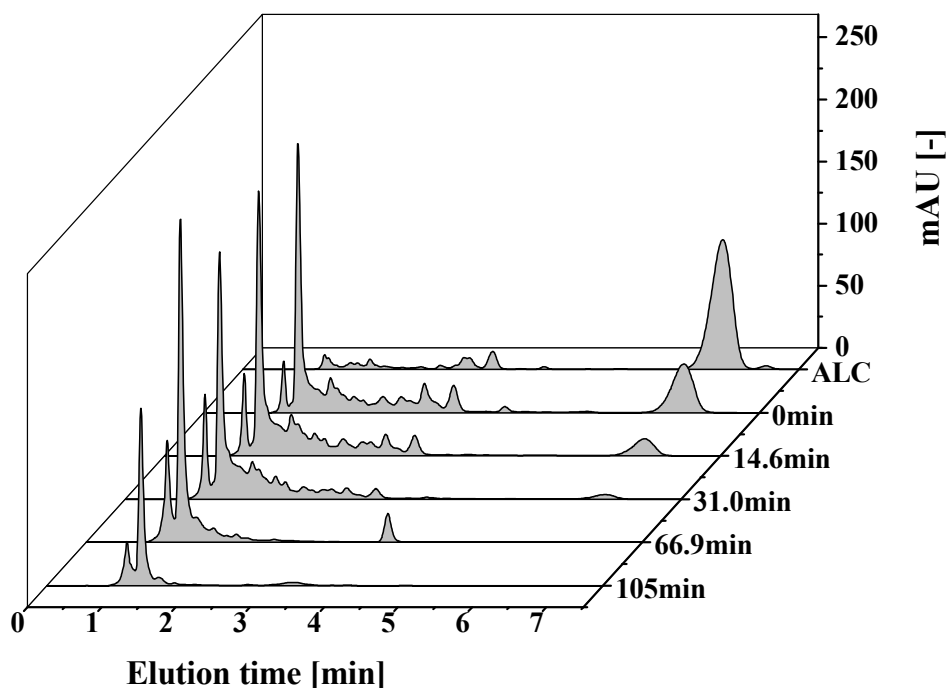
Figure 4.28: HPLC chromatograms of a typical degradation experiment (CUBE6) at 225 nm wavelength of detection showing the formation and degradation of intermediates. ALC is the chromatogram before H_2O_2 addition and 0 min refers to the chromatogram after the Fenton reaction in the dark.

Figure 4.29 shows DOC degradation as a function of hydrogen peroxide consumption. It can clearly be seen that the amount of degradation is correlated to the amount of hydrogen peroxide consumed. Within the range of the parameters investigated, no influence of any of the selected process variables (iron concentration, temperature and collector area) on the amount of hydrogen peroxide consumption needed for degradation could be detected. This is shown in **Figure 4.29** by the rather homogeneous distribution of the points around the curve fits regardless of their temperature or iron concentration. On the contrary, **Figure 4.29** shows that Fenton degradation needed more hydrogen peroxide to reach the same degradation level compared to photo-Fenton.

This is in accordance with the fact that, contrary to the dark Fenton reaction, Eq. (2.19), in photo-Fenton, transformation of ferric to ferrous iron takes place mainly without hydrogen peroxide consumption, Eq. (2.54). The consumption of hydrogen peroxide (mM) as a function of DOC degradation (between 0 and 1) can be estimated with a polynomial function (Eq. (4.1), coefficient of determination (square of Pearson's coefficient) of 0.94, standard deviation of error 5.1 mM), where H_2O_2 represents the hydrogen peroxide consumption (mM) and %DOC the share of initial DOC degraded (between 0 and 1).
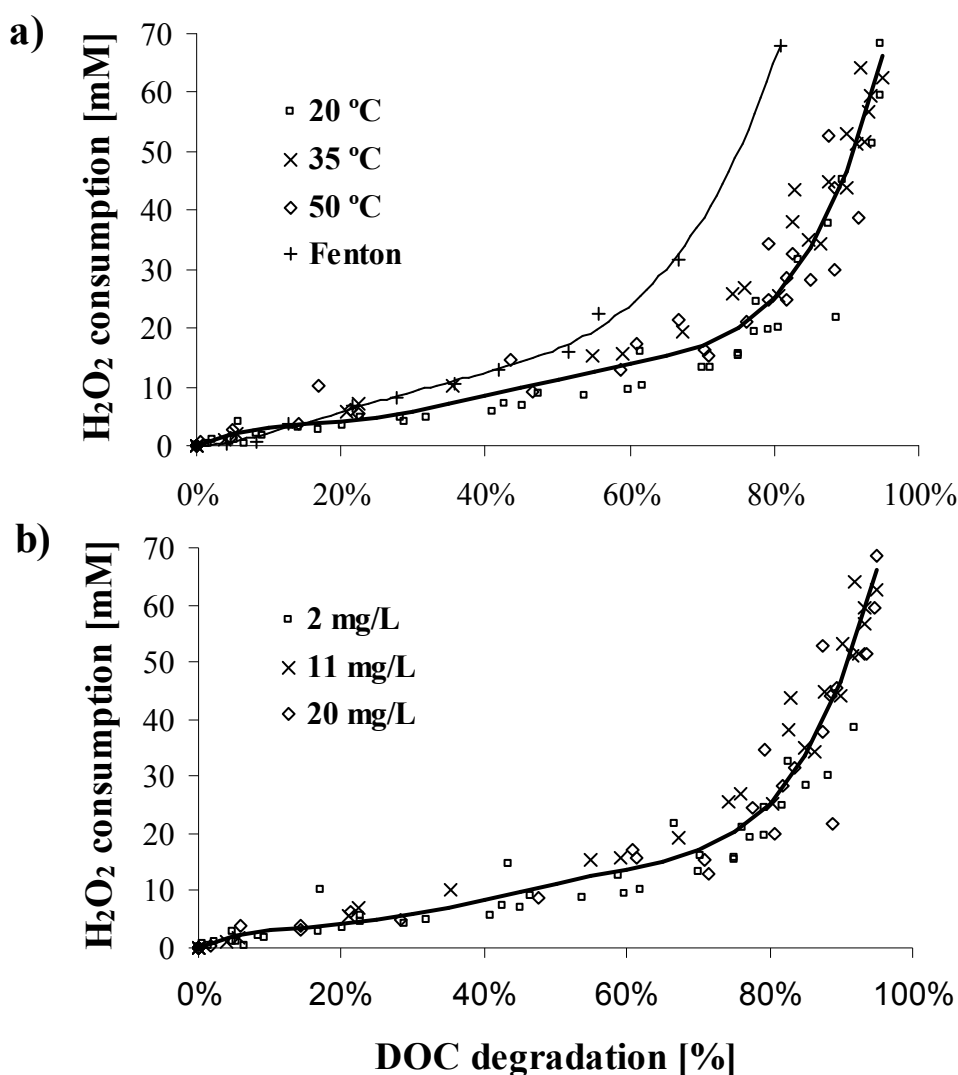
Figure 4.29: H_2O_2 consumption versus the measured DOC/DOC^i values of all experiments performed, including the Fenton experiment. The polynomic curve fits show the H_2O_2 consumption for photo-Fenton and Fenton a) points are marked according to temperature; b) points are marked according to iron concentration.

$$H_2O_2 = 1110 \cdot \%DOC^5 - 2100 \cdot \%DOC^4 + 1430 \cdot \%DOC^3 - \\ - 400 \cdot \%DOC^2 + 58.9 \cdot \%DOC - 0.0325 \qquad (4.1)$$

The theoretical stoichiometric hydrogen peroxide consumption for complete mineralisation of 100 mg L^{-1} ALC is 12.6 mM calculated with Eq. (3.6). According to Eq. (4.1), 55% of DOC mineralisation takes place before this amount is consumed. The correlation established in Eq. (4.1) could be used for process control. Data and correlation shown are only valid for the case in hand, because hydrogen peroxide consumption depends on many parameters, mainly the type and amount of wastewater contamination. So similar empirical data will have to be obtained for different cases before such a correlation can be established.

Figure 4.29 shows, furthermore, that extensive DOC degradation needs considerably higher amounts of hydrogen peroxide than moderate DOC degradation (e.g., 11.3, 25.2, 46.5 and 66.2 mM for 50%, 80%, 90% and 95% DOC degradation, calculated with Eq. (4.1)). Thus, apart from merely extending treatment time (and associated costs), increased reagent consumption has to be included in the economic considerations to decide when to stop treatment and/or with a view to possible combination of photo-Fenton with subsequent biological treatment.

4.3.2 Static modelling of the degradation progress

DOC degradation curves are usually sigmoidal, because in the initial degradation stages, the pollutant is transformed into oxygenised intermediates but without a loss of carbon dioxide resulting in initially stable DOC. When degradation proceeds, DOC decrease accelerates until it slows down again in the final stages. This particular behaviour impedes calculating rate constants based on simple rate equations. Alternatively, process efficiency can be compared on the basis of a given DOC decrease [94, 97]. According to Hincapié et al. [96], detoxification of an Alachlor solution can be confirmed once DOC degradation reaches 50% to 80% of the initial value. It was therefore an objective to develop a model that could predict the time ($t_{30w}^{50\%DOC}$; $t_{30w}^{80\%DOC}$) required for these levels of degradation.

Response Surface Methodology (RSM) has recently been applied by several authors to modelling tasks related to photo-Fenton [109, 111, 112]. These works applied polynomic models of second order like Eq. (2.62). The same mathematical approach

was attempted in this work, but fitting $t_{30W}^{50\%DOC}$ and $t_{30W}^{80\%DOC}$ with second order polynomial equations was unsuccessful. When all parameters were included, the resulting models were over-fitted and the response surfaces folded, and gave local minima and maxima where their occurrence was not logical from a physical-chemical perspective. When the number of parameters was limited by forward selection of parameters, the models simply were not able to predict the target variables satisfactorily. A disadvantage of the model is that the target values have very high relative deviations for fast experiments. This is due to least square minimisation, which also takes into account absolute differences. To account for this effect, the model calculation was directly weighted with the target value ($t_{30W}^{50\%DOC}$; $t_{30W}^{80\%DOC}$) in order to put additional weight on the fast experiments, but the approach yielded poor results nevertheless.

The main reason for the failure of this methodological approach is probably the wide range of results that the model must cover. For the fastest experiment $t_{30W}^{50\%DOC}$ and $t_{30W}^{80\%DOC}$ were 6 and 18 minutes, respectively; for the slowest one 703 and 1060 minutes. Therefore, the polynomial function approach to the problem proved to be invalid.

Next it was tried to search for functions which seemed appropriate to describe the problem in a mechanistic approach, given the pre-existing knowledge about the photo-Fenton process and the expected influence of T, Fe and the relationship of collector surface (or illuminated volume) to total volume.

After carefully examining the data and testing several types of functions, it was decided that the target function should be a product of functions of the process parameter. To be able to model the curvature in the n-dimensional space the potential function was selected. The resulting equation was Eq. (4.2), where C, p_{Fe}, p_T and p_A are the four parameters that have to be optimised, while c_{Fe}, T and A are the iron concentration, the temperature and the collector surface. This equation was then used to model $t_{30W}^{50\%DOC}$ and $t_{30W}^{80\%DOC}$.

$$t_{30W}^{50\%DOC} \text{ or } t_{30W}^{80\%DOC} = C \cdot c_{Fe}^{p_{Fe}} \cdot T^{p_T} \cdot A^{p_A} \qquad (4.2)$$

A second degree polynomial for three factors, including linear, quadratic, cross-product terms and offset, has ten parameters that have to be adjusted. The advantage of Eq. (4.2)

in this aspect is obvious, as for a given data set for n observations it leaves more degrees of freedom, which for a given Pearson's coefficient results in a higher Fisher's value in ANOVA analyses, i.e., a more plausible model. Furthermore, polynomial functions tend to have poor extrapolation qualities, which is another reason for searching for alternative functions more closely related to the physical-chemical behaviour of the system.

The results of parameter optimisation are given in Eq. (4.3) and (4.4). The results of the model applied to the experimental results are given in **Table 4.7**. The model results are accurate, except for very fast experiments, where the relative error is considerable.

$$t_{30W}^{50\%DOC} = 220200 \cdot c_{Fe}^{-0.800} \cdot T^{-1.765} \cdot A^{-0.515} \tag{4.3}$$

$$t_{30W}^{80\%DOC} = 167000 \cdot c_{Fe}^{-0.740} \cdot T^{-1.558} \cdot A^{-0.638} \tag{4.4}$$

Table 4.7: ALC factorial design – Prediction of $t_{30W}^{50\%DOC}$ and $t_{30W}^{80\%DOC}$ with static model.

	Measured values		Prediction with static model		Absolute error	
	$t_{30W}^{50\%DOC}$	$t_{30W}^{80\%DOC}$	$t_{30W}^{50\%DOC}$	$t_{30W}^{80\%DOC}$	$t_{30W}^{50\%DOC}$	$t_{30W}^{80\%DOC}$
	[min]	[min]	[min]	[min]	[min]	[min]
CENTRE1	45	75	38	62	-7	-13
CENTRE2	54	92	38	62	-16	-30
CENTRE3	46	77	38	62	-8	-15
CUBE1	141	252	140	254	-1	2
CUBE2	703	1060	703	1058	0	-2
CUBE3	50	77	61	91	11	14
CUBE4	308	375	307	378	-1	3
CUBE5	12	35	22	46	10	11
CUBE6	110	181	111	192	1	11
CUBE7	5.9	18	10	17	4	-1
CUBE8	39	69	49	69	10	0

Note that the effect of changing a process factor can be estimated directly when the value of the exponent is known according to Eq. (4.3) and (4.4). The influence of changes of each of the parameters is illustrated in **Figure 4.30**.
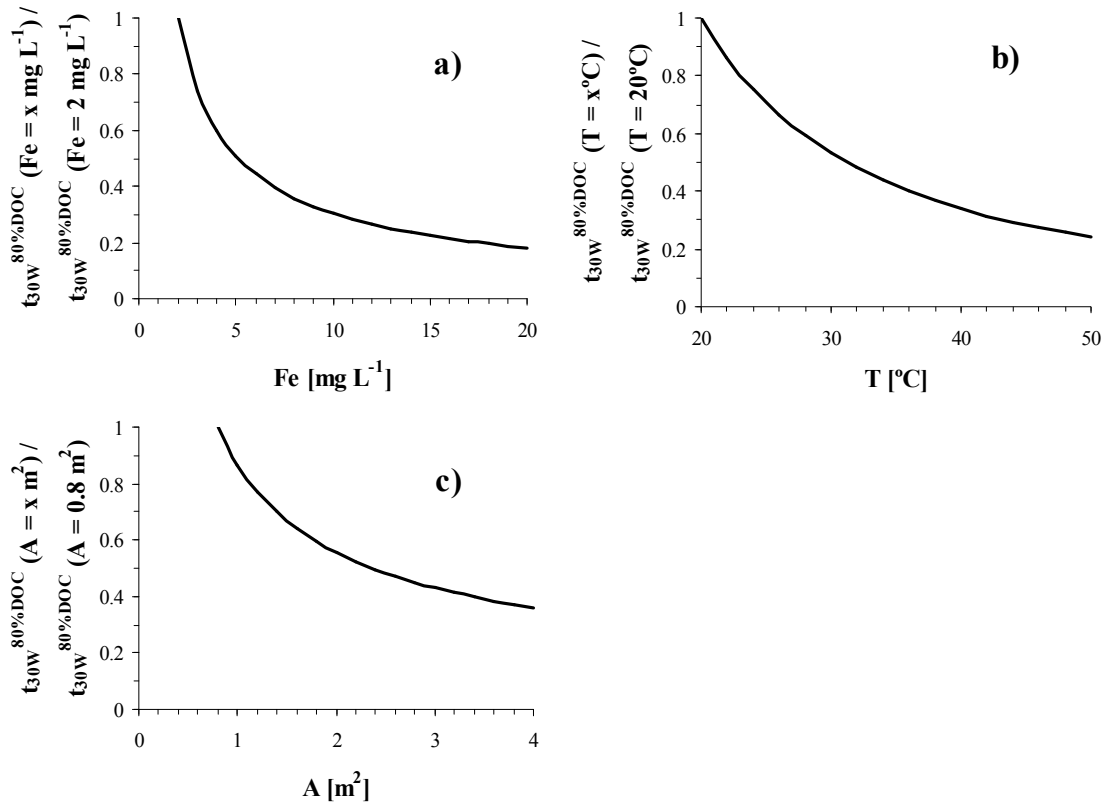
Figure 4.30: Dependences of $t_{30W}^{80\%DOC}$ on each of the process factors (c_{Fe}, A, T). The values shown are in relation to the highest $t_{30W}^{80\%DOC}$ in the experimental region investigated.

As the initial DOC concentration and all data with respect to the pilot-plant are known for these experiments, the static model also can be used to predict the collector area per mass. If one of the three variables is fixed the dependence of the collector area per mass on the other two process factors can be depicted in a two-dimensional contour plot like in **Figure 4.31**. By doing so, the observations made above are confirmed (see section 4.3.1), showing that less collector area per volume (or a lower ratio of illuminated to total volume) conveys a higher throughput per collector area and time unit.
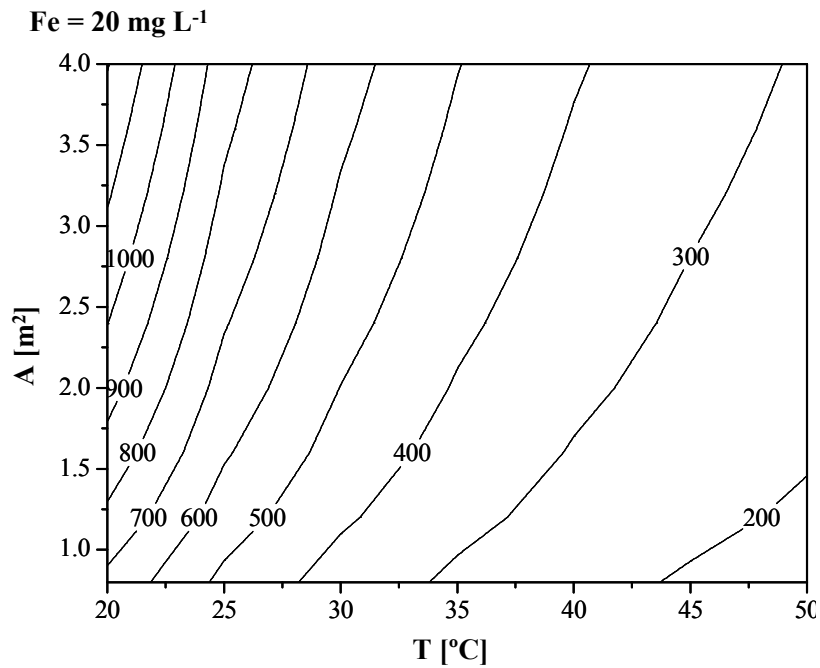
Fe = 20 mg L^{-1}

Figure 4.31: $A_{CM}^{80\%DOC}$ (m^2 h kg^{-1}) as a function of temperature and collector area. Predicted with the static model for degradation of ALC solutions (c^i = 100 mg L^{-1}) at an iron concentration of 20 mg L^{-1}.

The results of these models are only valid for constant process factors, i.e., those which do not change, such as temperature, iron concentration and collector area. The latter would not change in a real case plant either, of course, while temperature obviously changes in a solar collector, if no external temperature control is applied. The same is possible for the iron concentration, if there were precipitation due to high pH or the presence of phosphate, for example.

4.3.3 Dynamic modelling of the degradation progress

The static model described has two basic drawbacks. First, it is intrinsic to the type of model that it is only valid for constant process factors. Second, it only predicts the necessary illumination time until a determined level of degradation (50% or 80% of DOC, respectively). It would be desirable to have a dynamic model which is capable of predicting the reaction rate and progress at every moment of the degradation process.

As mentioned, DOC degradation curves have a sigmoidal form. Of the common curves fitting sigmoidal tendencies, the Boltzmann function and the Logistic Dose Response (LDR) curve are outstanding for their simplicity. Both have only four parameters to adjust. The problem with the Boltzmann function is that its curvature is symmetrical at

both sides of the point of inflection, which is not necessarily the case in a DOC degradation curve. So this function must be discarded in favour of the Logistic Dose Response curve, which is commonly used to describe Dose Response curves in pharmacology. The four parameters of Eq. (4.6) are A_1 and A_2, the normalised initial and final DOC values ($DOC^i/ DOC^i = 1$; DOC^f/ DOC^i), $t^{1/2}$, the time when degradation is half-way between DOC^i and DOC^f and p, an exponent largely determining the curvature and the slope of the curve. DOC in Eq. (4.6) refers to the measured DOC value at any time during degradation.

$$\frac{DOC}{DOC^i} = \frac{A_1 - A_2}{1 + (t_{30W}/t^{1/2})^p} + A_2 \qquad (4.5)$$

$$\frac{DOC}{DOC^i} = \frac{0.95}{1 + (t_{30W}/t^{1/2})^p} + 0.05 \qquad (4.6)$$
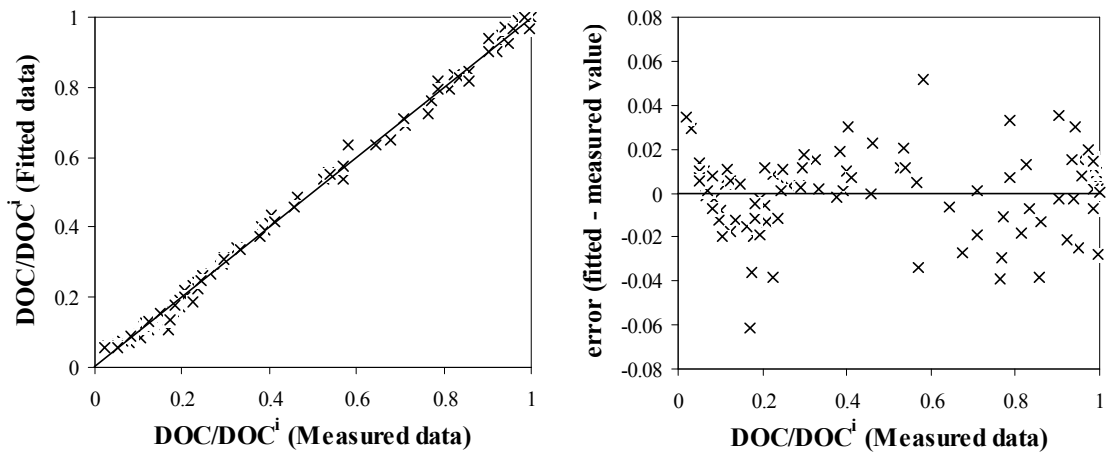
Figure 4.32: DOC/DOC^i values calculated by LDR curve modelling of the real data for each experiment against measured DOC/DOC^i from all experiments (see text). The right graph shows the homogeneous error distribution of the fitted values.

As normalised values (DOC/DOC^i) were used, A_1 was always one, except for the experiments in which 20 mg L^{-1} iron was used at 50ºC, because these were the only ones in which DOC degradation during the Fenton reaction before illumination was remarkable. Consequently, A_1 was set at 0.82, the average value of both experiments at zero illumination time (see **Figure 4.25**c). At the same time, it was assumed that the DOC^f is always 5% of DOC^i. Hence A_2 is 0.05, thus yielding a non-linear fitting

problem with only two parameters, Eq. (4.6). This last assumption was made to optimise modelling between 20 and 80% DOC degradation, which can be considered the most relevant region because detoxification takes place somewhere in this phase of the degradation process [96, 97]. It has to be noted that $t^{1/2}$ consequently equals t_{30w} after 52.5% DOC degradation ($A_1/2 - A_2/2$) and is therefore slightly higher than $t_{30w}^{50\%DOC}$.

Then, each experiment was fitted, which gave an excellent coefficient of determination (square of Pearson's coefficient) higher than 0.99 for each experiment and also when all measured samples were plotted against their calculated value (see **Figure 4.32**). This confirms the adequacy of the LDR curve to this problem. The fitted parameters are given in **Table 4.8**.

Table 4.8. LDR curve parameters modelled from single experiments, Dynamic Model parameters and fitted values for $t_{30w}^{50\%DOC}$ and $t_{30w}^{80\%DOC}$ calculated with the Dynamic Model.

	Fitted values of LDR modelling of single experiments [*]		Dynamic Model parameters [**]		Fitted values with Dynamic Model [***]	
	$t^{1/2}$	p	$t^{1/2}$	p	$t_{30w}^{50\%DOC}$	$t_{30w}^{80\%DOC}$
	[min]		[min]		[min]	[min]
CENTRE1	42	3.02	36	3.17	38	62
CENTRE2	53	3.39	36	3.17	38	62
CENTRE3	45	3.13	36	3.17	38	62
CUBE1	139	2.93	140	2.95	145	247
CUBE2	689	4.27	688	4.24	706	1022
CUBE3	48	3.86	55	3.86	57	85
CUBE4	272	4.91	272	4.92	278	383
CUBE5	15	1.77	22	1.76	24	58
CUBE6	107	3.51	110	3.55	114	177
CUBE7	5.1	1.26	8.9	1.27	9.6	33
CUBE8	37	2.82	44	2.82	45	79

[*] refer to text for details on calculation.

[**] calculated with Eq. (4.7) and Eq. (4.8).

[***] calculated with Eq. (4.9) and Eq. (4.10).

Then $t^{1/2}$ was fitted the same way as described in section 4.3.2 for $t_{30W}^{50\%DOC}$ and $t_{30W}^{80\%DOC}$ (see Eq. (4.2)) by non-linear curve fitting and the result was Eq. (4.7). No logical reason for any correlation between p and the influencing process variables could be found. In response a second degree polynomial including cross-products of the variables was applied. This time the results of the multivariate linear regression were logical and consistent. Forward selection was applied to find the optimum selection of parameters in the multivariate linear regression process [122, 123] based on the criteria of maximising not only coefficient of determination (square of Pearson's coefficient), but also the Fisher's value. Eq. (4.8) was the result (Fisher's value of 135). Values for the single experiments fitted with Eq. (4.7) and Eq. (4.8) are given in **Table 4.8**. It also lists the values calculated with the Dynamic Model for $t_{30W}^{50\%DOC}$ and $t_{30W}^{80\%DOC}$ reckoned with Eq. (4.9) and Eq. (4.10) (both derived from Eq. (4.6)), respectively.

$$t^{1/2} = 197000 \cdot c_{Fe}^{-0.795} \cdot T^{-1.740} \cdot A^{-0.576} \qquad (4.7)$$

$$p = -0.0431 \cdot T + 0.203 \cdot A - 0.000929 \cdot c_{Fe} \cdot T \\ -0.0235 \cdot c_{Fe} \cdot A + 0.00237 \cdot T \cdot A + 4.97 \qquad (4.8)$$

$$t_{30W}^{50\%DOC} = t^{1/2} \cdot \left(\frac{10}{9}\right)^{p^{-1}} \qquad (4.9)$$

$$t_{30W}^{80\%DOC} = t^{1/2} \cdot \left(\frac{16}{3}\right)^{p^{-1}} \qquad (4.10)$$

The final equation for the DOC degradation curve as a function of illumination time, temperature, iron concentration, collector surface and irradiation intensity implicitly included in the illumination time (see Eq. (3.24) and (3.25)), results from inserting Eq. (4.7) and Eq. (4.8) into Eq. (4.6). The results calculated for all samples measured are plotted against the measured values in **Figure 4.33**. The fit is very good for most experiments, except for, similar to the above modelling problems, fitting very fast experiments, probably due to the extremely wide intervals of the reaction rates observed.
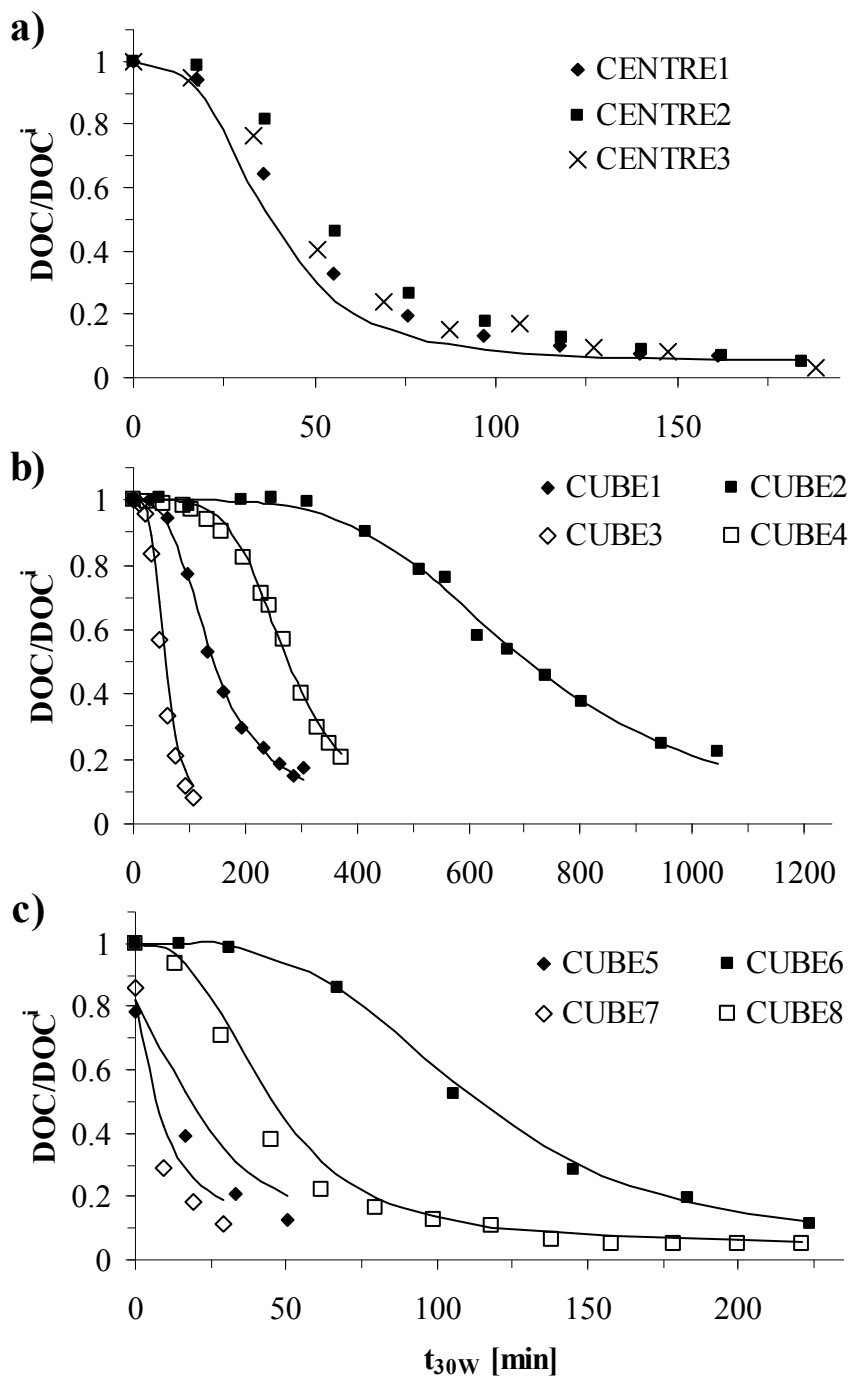
Figure 4.33: ALC factorial design – DOC degradation curves measured and predicted with the Dynamic Model. Cube points with even numbers are performed at 20ºC, with odd numbers at 50ºC. Cube 1, 2, 5, 6 with 0.83 m², cube 3, 4, 7, 8 with 4.16 m² collector; a) centre points, b) cube points with 2 mg L^{-1} iron c) cube points with 20 mg L^{-1} iron.

The partial derivative with respect to illumination time of the resulting equation (after inserting Eq. (4.7) and Eq. (4.8) into Eq. (4.6)) represents the DOC degradation rate

when the other parameters are constant (except changes in irradiation intensity, which are taken into account). If the other parameters are not constant, the degradation curve can be calculated in parts. A complete degradation curve can thus be reconstructed for varying process parameters. This would not be a problem should online prediction of the degradation curve be necessary, as long as temperature and radiation intensity are measured on-line and information about changes in iron concentration is made available to the control system. Therefore, this is a possibility for on-line prediction of process progress and for taking decisions about when to end the process and whether to transfer or discharge the treated effluent. Nevertheless, it has to be mentioned that these correlations and coefficients are only valid for the present case. Yet, the described procedure (factorial design + modelling) might be proposed as a methodology to obtain these correlations for different waste water.

4.4 Economic on-line measurement for process assessment and control

4.4.1 UV/Vis absorbance

UV/Vis absorbance is a parameter that can easily be measured on-line and the measurement of which is not very expensive, especially if the measurement can be limited to a certain wavelength or wavelength range, i.e. no spectral resolution is needed. According to Lambert-Beer's law the absorbance of a solution is a function of the substances contained in a solution (i.e. their absorption properties), their respective concentrations and the optical length of path. Thereby, from a solution's absorbance properties conclusions may be drawn about its chemical composition, although the fact that UV/Vis absorbance is a function of all substances limits its application.

In fact light absorbance by the solution at 254 nm can be used in wastewater treatment to estimate the content of aromatic substances (DIN 38404-C3). However, this approximation only is applicable to waste water with a rather constant composition such as urban waste water, as it depends largely on the molecular extinction coefficient of the present organic substances at the chosen wavelength.

In the photo-Fenton reaction system, as described previously in this work (see section 2.2.2), ferric iron complexes with water, hydroxyl ions and organic substances as ligands absorb light, which can induce the photochemical reduction to ferrous iron.

Ferrous iron species have lower molar extinction coefficients and their concentrations are low in the presence of hydrogen peroxide. Consequently, compared to ferric iron they absorb less photons. Hydrogen peroxide has very low extinction coefficients above 300 nm (which is the reason why direct photolysis does not happen under solar illumination), but shows considerable absorbance between 200 and 300 nm. Some extinction coefficients and their respective absorbance up to 300 nm are given in **Table 4.9**.

Table 4.9: Molar extinction coefficients (ε) of H_2O_2 and resulting absorbance and transmittance values for a 10 mM (340 mg L^{-1}) solution at 1 cm length of optical path (source of molar extinction coefficients: www.H2O2.com. November 2005).

		220 nm	240 nm	254 nm	260 nm	280 nm	300 nm
ε	[L mol^{-1} cm^{-1}]	76	35	19.6	13	4.2	1
A	[-]	0.76	0.35	0.196	0.13	0.042	0.01
T	[%]	17.4	44.7	63.7	74.1	90.8	97.7

In the experiments of the factorial design with alachlor as model compound UV/Vis absorbance spectra were recorded. These spectra are depicted in **Figure 4.34** and **Figure 4.35** for the experiments CUBE6 (A = 0.83 m^2, T = 20 °C, c_{Fe} = 20 mg L^{-1}) and CUBE2 (A = 0.83 m^2, T = 20 °C, c_{Fe} = 2 mg L^{-1}), respectively. Alachlor itself only absorbs only slightly below 280 nm (see left margin of the area in the 3D representation in **Figure 4.34**). Iron addition increases the absorbance over the whole UV region (the sample at t_{30W} = -15 min contains ALC and Fe^{2+}). Finally, H_2O_2 addition oxidises ferrous iron to ferric iron and the absorbance rises even more. Yet, **Figure 4.34** shows that after some time the absorbance of the solution decreases until it reaches a steady-state after the degradation of about 50% of the DOC. This observation suggests that the increased absorbance in the first stages of the degradation is not only due to the oxidation of ferrous to ferric iron. The presence of H_2O_2 can be excluded as well because as shown in **Table 4.9** the absorbance of H_2O_2 in the concentration range applied is at maximum around 0.2 at 254 nm and negligible at 300 nm or above. Nevertheless, the increase of absorbance can be detected along the whole UV region. Typical intermediate degradation products of aromatic substances include phenols, quinones and hydroquinones. These intermediates usually absorb at higher wavelengths

than their parent compound, because their structure favours delocalisation of electrons in the ring system. **Figure 4.28** shows the disappearance of intermediate degradation products in the HPLC chromatograms obtained (at 225 nm) in experiment CUBE6, which roughly coincides also with the observed decrease in UV/Vis absorbance. At the same time a monitoring of the presence of these types of compounds is especially desirable, because due to their reactivity they have a considerable acute toxicity, often higher than that of the parent compound. The increase of acute toxicity after the start of an AOP treatment was observed by other authors for alachlor [96] and other pesticides [96, 97, 147, 148], whereas towards the end of the treatment acute toxicity fell below the initial value, just similar to the evolution of absorbance in these experiments.
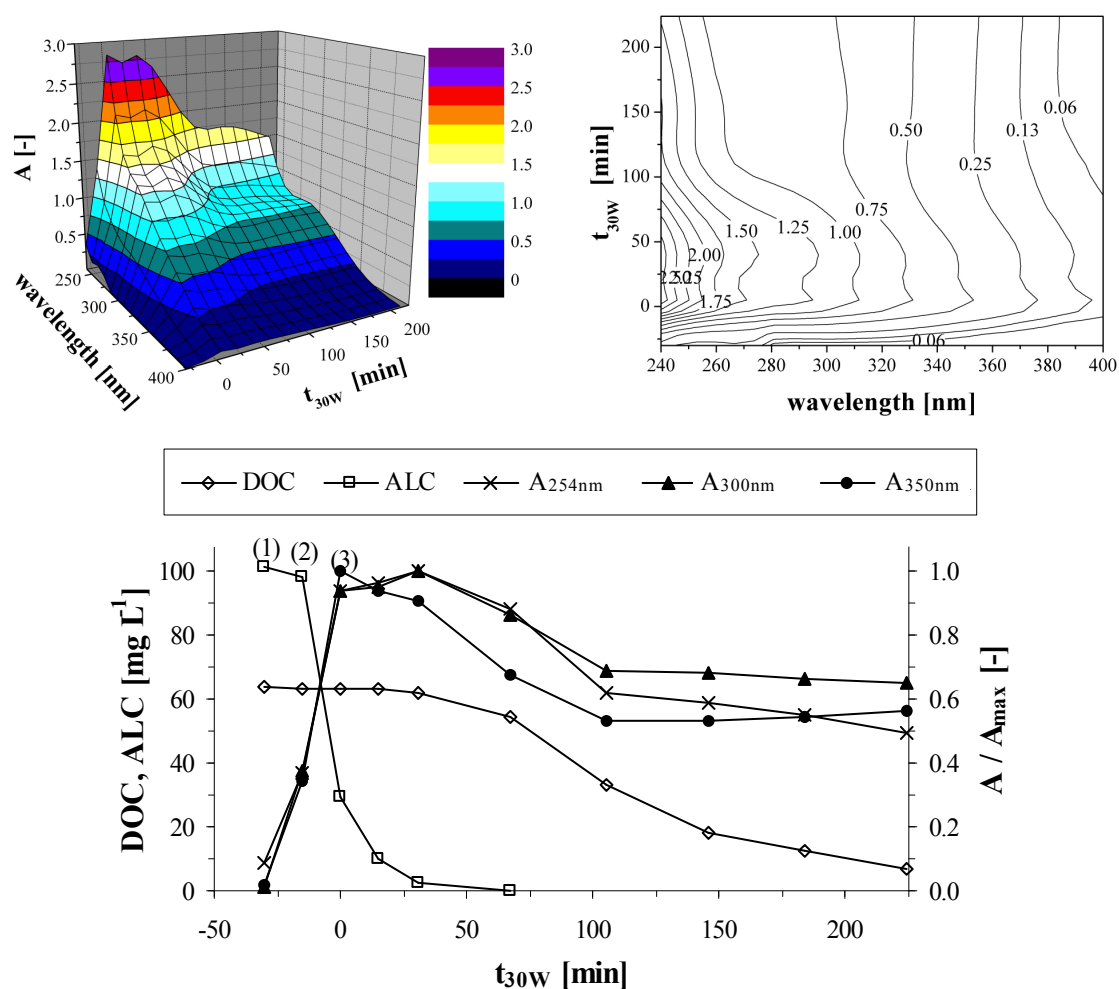
Figure 4.34: Experiment CUBE6 (see **Table 3.8**). Absorbance (1 cm length of optical path) as a function of wavelength and degradation time. (1) ALC = 100 mg L^{-1}, t_{30W} = -30 min, pH = 2.5, addition of Fe^{2+}; (2) t_{30W} = -15 min, addition of H$_2$O$_2$; (3) t_{30W} = 0 min, start of illumination.

Another reason for variation of the absorbance could be found in changes of the iron species itself. As described in section 2.2.2.1 the aquatic iron chemistry of dissolved iron is rather complex and temperature and concentration dependent formation of iron oligomers with absorptive properties different from monomeric dissolved iron can take place [50 - 52]. Furthermore, organic acids can form complexes with iron, which absorb light far into the visible light region. **Figure 4.35** shows absorbance data of an experiment with a lower iron concentration (2 mg L^{-1}), which should enable to better distinguish the effect of the changes in the organic matter content.

In fact in this case the absorbance rises also upon the addition of first ferrous iron and then H_2O_2, but to a much lesser extent. On continuation, the absorbance keeps rising until reaching its maximum (depending on wavelength) after about 250 to 300 min coinciding with the conversion of most of the parent compound but before mineralisation begins. The maximum absorbance value is about twice as high as the value at zero illumination time.

The steep decrease at 415 minutes corresponds to the necessary break caused by the fall of evening in this experiment, which was the experiment lasting longest and thereby the only one performed on two consecutive days. Nevertheless, although illumination stopped for 16 hours, some hydrogen peroxide present in the solution was consumed (approx. 50 mg L^{-1}, corresponding to 8% of total consumption) and produced this decrease. On the second day the absorbance continued to fall until reaching 15 to 25% of its maximum value, depending on the wavelength. The steady-state of the absorbance was again reached at around 50% degradation of the initial DOC.

The comparison of both experiments confirms that the iron concentration is an important interfering factor in this parameter. E.g. final absorbance at 350 nm is 0.5 and 0.15 of maximum absorbance at 20 and 2 mg L^{-1} dissolved iron, respectively (corresponding to an absorbance of 0.27 and 0.024 at 1 cm of length of optical path). Yet, having a closer look in both experiments the absorbance at 350 nm begins to decrease earlier than that at lower wavelengths. Also the ratio of final to maximum absorbance seems to be lower at higher wavelengths. Near UV absorbance is more adequate to monitor the development of the organic matter, because iron species and especially hydrogen peroxide in solution interfere less with the measurement at those wavelengths. Finally, the development of the absorbance is clearly related to the process progress, because qualitative behaviour (relating ALC, DOC and absorbance) is the

same not only in the two experiments shown in **Figure 4.34** and **Figure 4.35**, but also in the rest of the experiments pertaining to the ALC factorial design.
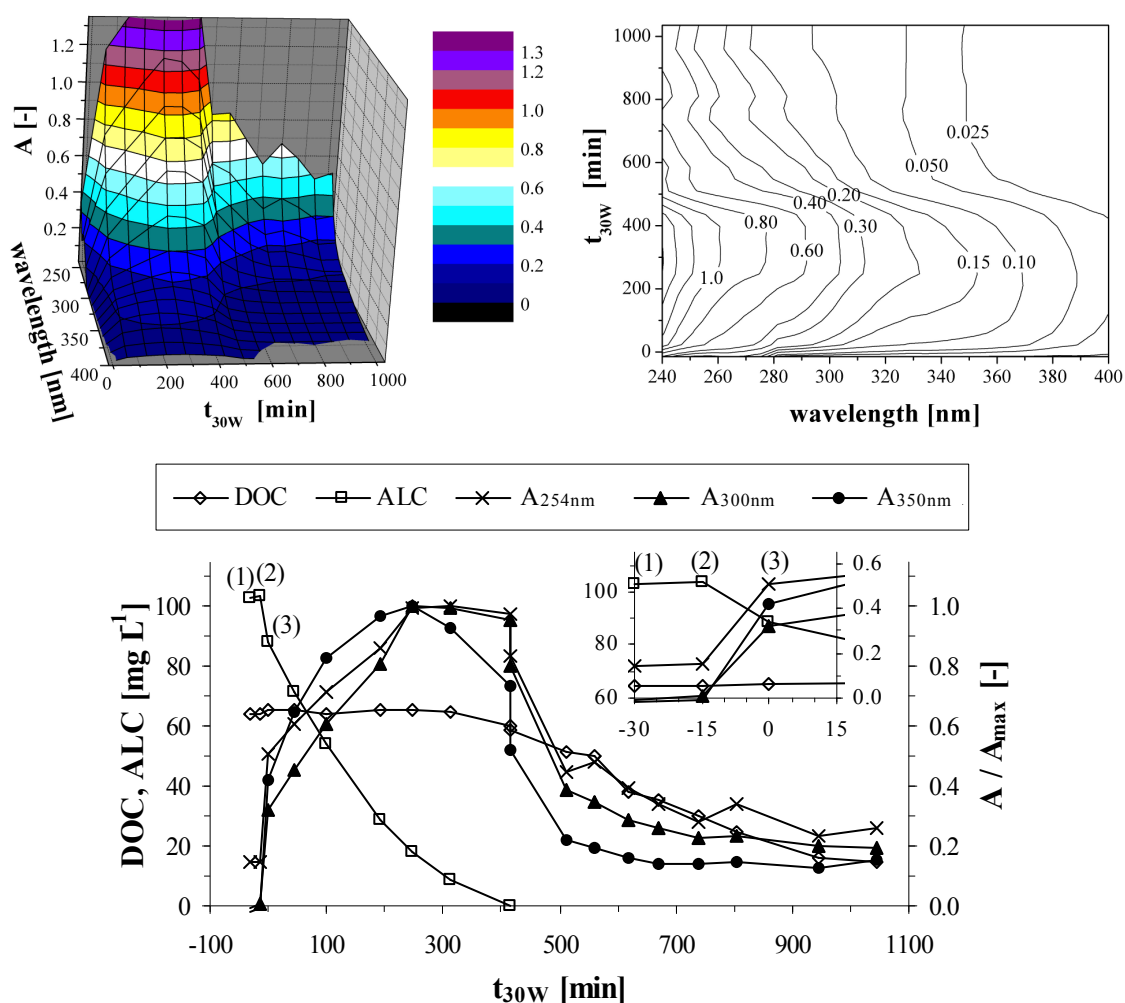
Figure 4.35: Experiment CUBE2 (see **Table 3.8**). Absorbance (1 cm length of optical path) as a function of wavelength and degradation time. (1) ALC = 100 mg L^{-1}, t_{30W} = -30 min, pH = 2.5, addition of Fe^{2+}; (2) t_{30W} = -15 min, addition of H$_2$O$_2$; (3) t_{30W} = 0 min, illumination begins.

Absorbance spectra were also recorded in the experiments of the pesticide mixture to check if the results obtained with a single pesticide can be confirmed with a different model wastewater. Also, in these experiments the pollutant concentration varied from a total amount of 50 to 150 mg L^{-1} (Experiments MIX2 and MIX3, see **Table 3.7**).
The results for both experiments are depicted in **Figure 4.36**. It can be seen that in both experiments the maximum absorbance at 254 nm is practically reached at the very

beginning of the experiment due to the absorbance of the different model pollutants (ATZ, CFVP, DIU and IPR absorb up to higher wavelengths compared with ALC). Yet, these substances absorb only little above 300 nm. So, the generation of degradation intermediates and ferric iron upon the addition of hydrogen peroxide provokes a steep increase of absorbance at 300 and 350 nm during the 15 min dark Fenton stage immediately before illumination starts. Then, at the lower contaminant concentration (see **Figure 4.36**a) a moderate decrease of the absorbance occurs, which is more pronounced at 254 nm. Again, a steady-state of the absorbance is reached at 50 to 75% of the mineralisation of initial DOC (depending on the wavelength). In the case of the higher pesticide concentration (i.e. ratio of pollutant to iron concentration is higher) the decrease of the absorbance is stronger, especially at the higher wavelengths. Steady-state absorbance is reached after approximately 50% of DOC mineralisation. The different behaviour between both contaminant concentrations has two reasons. First, the ratio of pollutant to iron is higher at higher pollutant concentration, which diminishes the relative effect of the iron interference. Second, at the lower contaminant concentration the pollutants were degraded very quickly, whereas samples were taken only every 15 min, and thereby probably the real maximum value could even have occurred at a value different from that at zero illumination time. The other experiment at low pollutant concentration (MIX1) had a slightly higher reaction rate at the beginning and the difference between steady-state and maximum absorbance were even less. This suggests that probably the maximum absorbance occurs during the dark Fenton reaction. Of course this behaviour could be observed and interpreted better by an on-line measurement with a sampling frequency in the range of seconds.

In principle the experiments with the pesticide mixture confirmed the results of the ALC experiments. UV/Vis absorbance in the range of 300 to 350 nm, and to a lesser extent, at 254 nm, can be a valuable tool to assess the process progress on-line quickly. Yet, this tool has several restrictions. First, the nature of the pollutant to be treated is crucial as it seems mostly appropriate for waste water containing aromatic pollutants in considerable amounts as the main problematic contaminant. In the case of aliphatic contaminants such as the NBCS tested as another group of model compounds (see section 4.1.1) the parameter is not useful. Second, the measurement is seriously interfered by the presence of iron and at wavelengths around 250 nm (and below) also by hydrogen peroxide. Consequently, the ratio of pollutant to photo-Fenton reactants is crucial to obtain clear results.
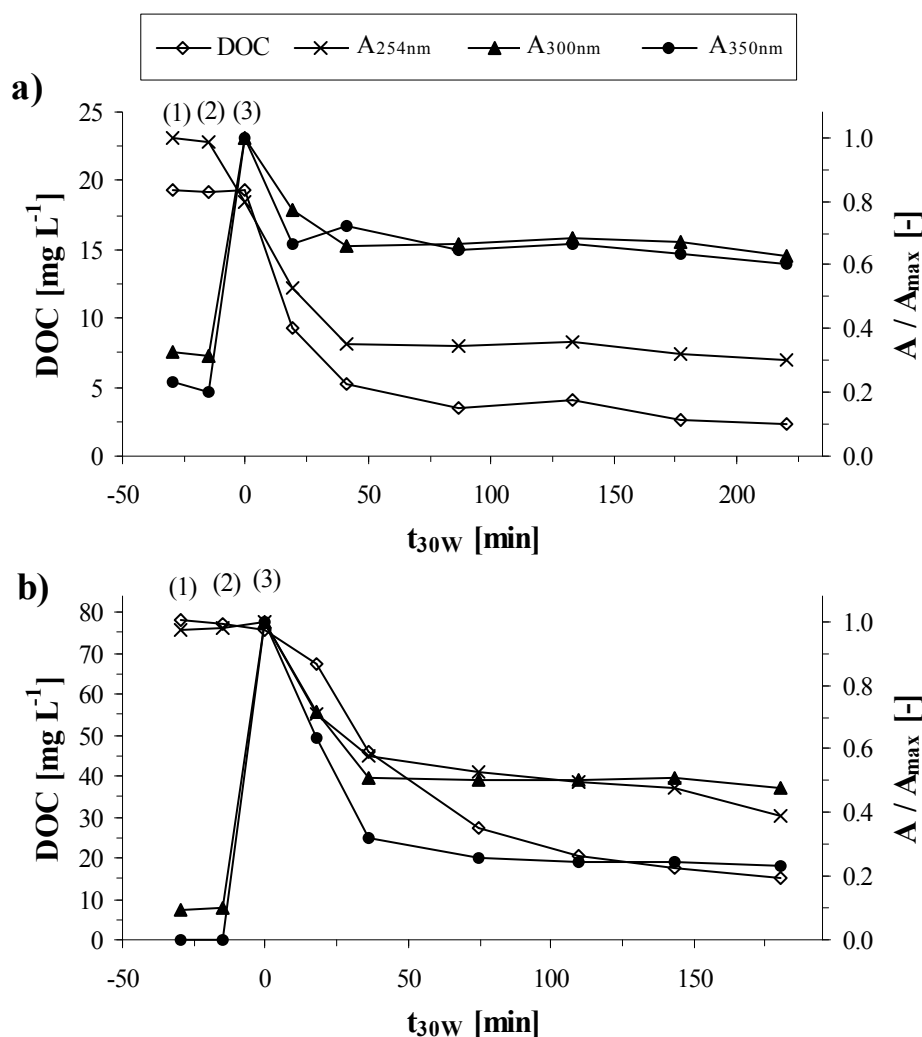
Figure 4.36: Absorbance (1 cm length of optical path) as a function of wavelength and degradation time. a) experiment MIX2; b) experiment MIX3 (for set-up see **Table 3.7**). (1) t_{30W} = -30 min, pH = 2.8, addition of Fe^{2+}; (2) t_{30W} = -15 min, addition of H_2O_2; (3) t_{30W} = 0 min, illumination begins.

4.4.2 Dissolved oxygen (DO)

DO is a parameter frequently measured in wastewater treatment, especially in aerobic biological wastewater treatment as commonly done for urban areas. Consequently, due to the large number of equipments sold the sensor technology is especially well developed, robust and cheap in comparison with many other analytical on-line sensors. Characteristic DO profiles were reported before for Fenton treatment [149] and photo-Fenton treatment [72, 150]. These authors stated an initial decrease of DO in the solution. This behaviour is due to scavenging of the DO by organic radicals generated

according to the Dorfman-mechanism, Eq. (2.40) and (2.41) [69, 70]. **Figure 4.37** shows the DO profiles obtained in the experiments pertaining to the ALC factorial design. It can be seen that the same initial decrease was observed in these experiments. Yet, even more obvious is the big increase occurring in all experiments leading to considerable supersaturation inside the reactor compared to the oxygen solubility under atmospheric pressure conditions (partial pressure of oxygen around 2000 Pa). [149] and [72] did not observe this supersaturation, whereas [150] did. Wether supersaturation occurs is largely determined by the kinetics of oxygen production inside the solution and the degassing of the DO to the atmosphere. Reactor geometry obviously plays a crucial role. In this sense the CPC reactor favours the formation of supersaturation, because it is nearly a closed system with a very small surface available for gas exchange with the atmosphere in the tank. Also due to the tubing and the collector a considerable pressure drop is suffered along the system, which increases the partial pressure of the oxygen in the high pressure zones and hence the solubility inside the reactor. The systems used by the other authors were laboratory-scale reactors and did not show these particular characteristics. Nevertheless, [150] observed this behaviour associated with a very fast hydrogen peroxide decomposition.

The change in the reacting system provoking the DO increase is related to a change of the relation of readily oxidisable organic compounds to hydrogen peroxide concentration. When hydrogen peroxide is very abundant it competes successfully with organic compounds for the hydroxyl radicals present in solution and the formation of peroxyl radicals by Eq. (2.22) takes place. This radical can further react with ferric iron by Eq. (2.20) and (2.21) to ferrous iron and oxygen. As a consequence the decomposition of hydrogen peroxide is accelerated (because the catalytic iron cycle is boosted), yet without involving the oxidation of organic substances. The effect is therefore not desirable and leads to exhaustive consumption of hydrogen peroxide for the final stages of mineralisation of DOC (compare **Figure 4.29**, page 121). As a consequence, hydrogen peroxide concentration should be controlled carefully along the treatment and an optimal concentration at the start of an experiment might not be the optimal concentration towards its end. On the other hand injection of oxygen could be beneficial towards reduction of hydrogen peroxide consumption during the initial stages of the treatment, because the participation of oxygen in the reaction mechanism could replace part of the hydrogen peroxide needed to oxidise the solution (see section 2.2.2.2).
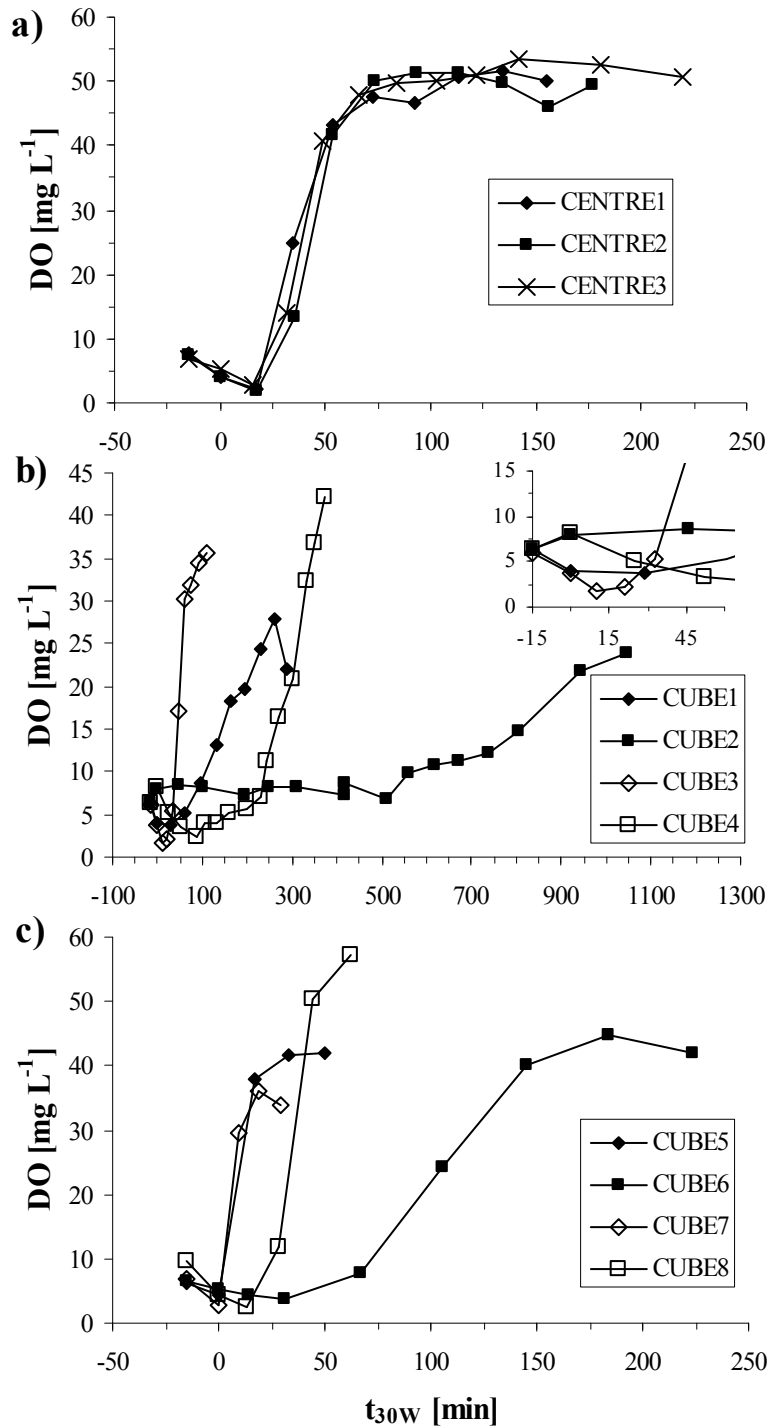
Figure 4.37: ALC factorial design – dissolved oxygen (DO) evolution. Cube points with even numbers are performed at 20ºC, with odd numbers at 50ºC. Cube 1, 2, 5, 6 with 0.83 m^2, cube 3, 4, 7, 8 with 4.16 m^2 collector; a) centre points, b) cube points with 2 mg L^{-1} iron c) cube points with 20 mg L^{-1} iron.
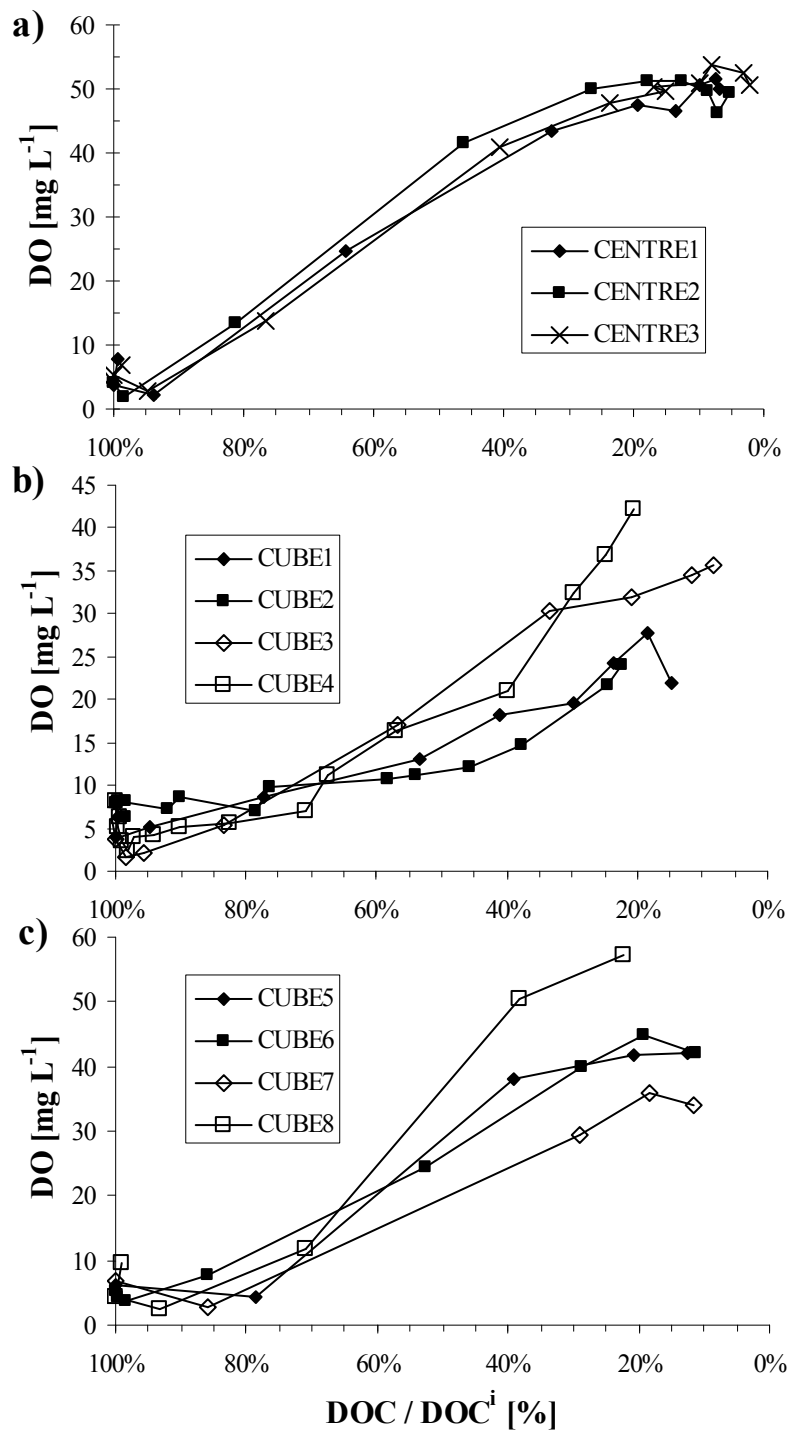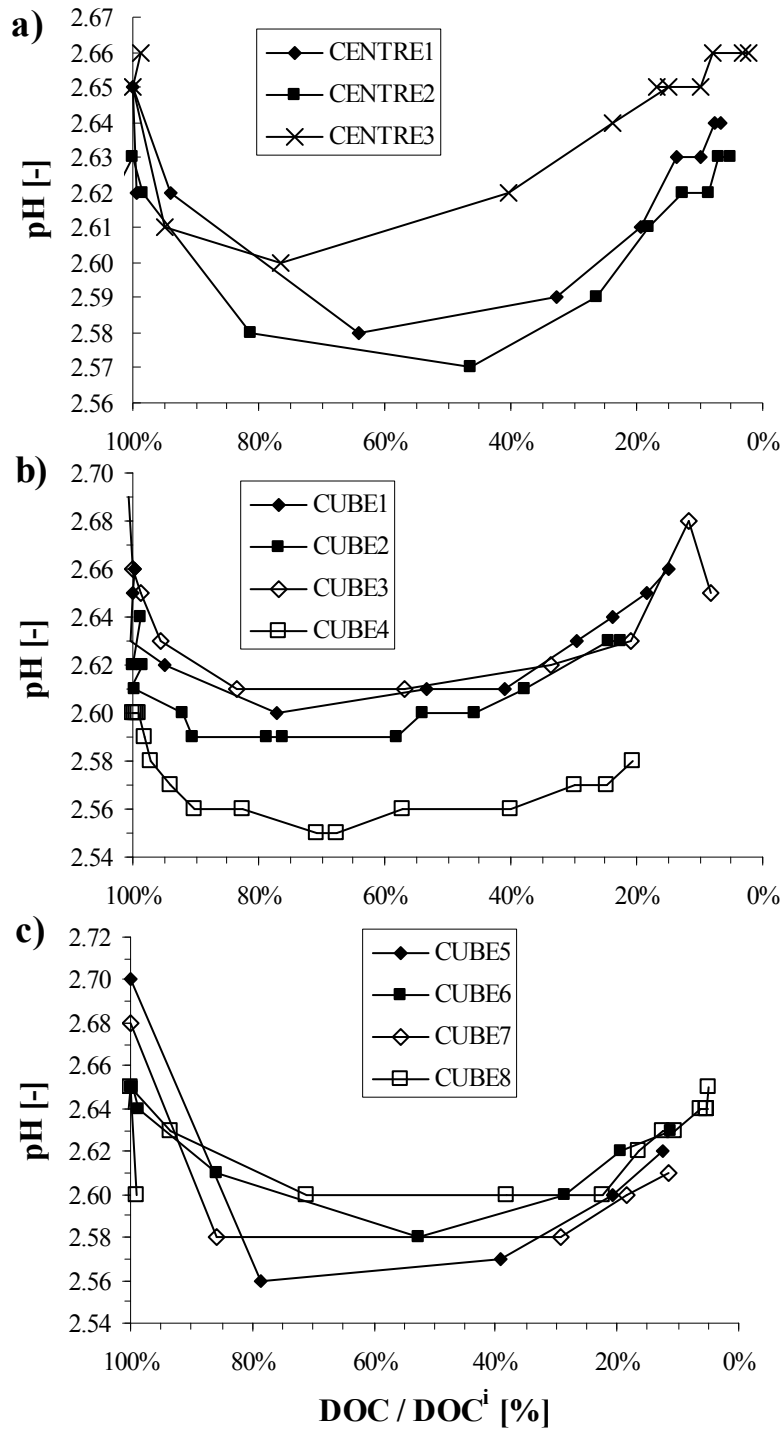
Figure 4.38: ALC factorial design – dissolved oxygen (DO) evolution vs. DOC degradation. Cube points with even numbers are performed at 20ºC, with odd numbers at 50ºC. Cube 1, 2, 5, 6 with 0.83 m^2, cube 3, 4, 7, 8 with 4.16 m^2 collector; a) centre points, b) cube points with 2 mg L^{-1} iron c) cube points with 20 mg L^{-1} iron.

Figure 4.38 shows also the DO values of the ALC factorial design, but here represented against the remaining DOC inside the solution. First, **Figure 4.38**a shows that reproducibility is also confirmed for the evolution of the DO value. Second, it can be observed that the DO concentration always begins to increase between 10 and 25% of DOC mineralisation depending mainly on the reaction rate. This roughly coincides with the moment when UV/Vis absorbance is decreasing strongly (see **Figure 4.34**, **Figure 4.35** and **Figure 4.36**) and DOC mineralisation accelerates (see **Figure 4.25**, page 114). Finally, the DO concentration for the employed reactor is not only a function of the reaction rate (and thereby the kinetics of oxygen generation) but also of the temperature inside the solution. When comparing the experiments at different temperatures (20 vs. 50 ºC) in **Figure 4.38** the experiment at 20 ºC usually reaches a higher final DO concentration due to the enhanced solubility although their reaction rate is several times lower.

Another application of monitoring the DO concentration could be the detection of hydrogen peroxide depletion in the supersaturation phase. An experiment was performed to simulate the decomposition of hydrogen peroxide to oxygen during photo-Fenton treatment applying only hydrogen peroxide and iron but without any radical scavenging organic substance. Hydrogen peroxide was maintained constant by the control system described in section 4.4.5, until a constant DO concentration was obtained. Then the hydrogen peroxide addition was stopped to observe the correlation between hydrogen peroxide and DO concentration. To confirm the effect of temperature this experiment was performed at 20 and 35 ºC. The results are presented in **Figure 4.39**. It can be seen that the hydrogen peroxide concentration fluctuated more strongly at 35 ºC. This is due to the higher H_2O_2 consumption rate at this temperature which increases the tendency to fluctuation unmanageable by the PI controller applied. The fluctuation in H_2O_2 concentration causes also variations in the oxygen generation rate, which are reflected in the DO concentration profile. After stopping the H_2O_2 addition both, H_2O_2 and DO concentration begin to decrease, with a little lag (5 to 10 minutes) in the DO concentration compared to H_2O_2. The observations are very similar at both temperatures confirming the observations made previously. The influence of temperature could be observed as well; although the hydrogen peroxide consumption rate was higher at 35 ºC, a higher constant DO concentration was reached at 20 ºC.
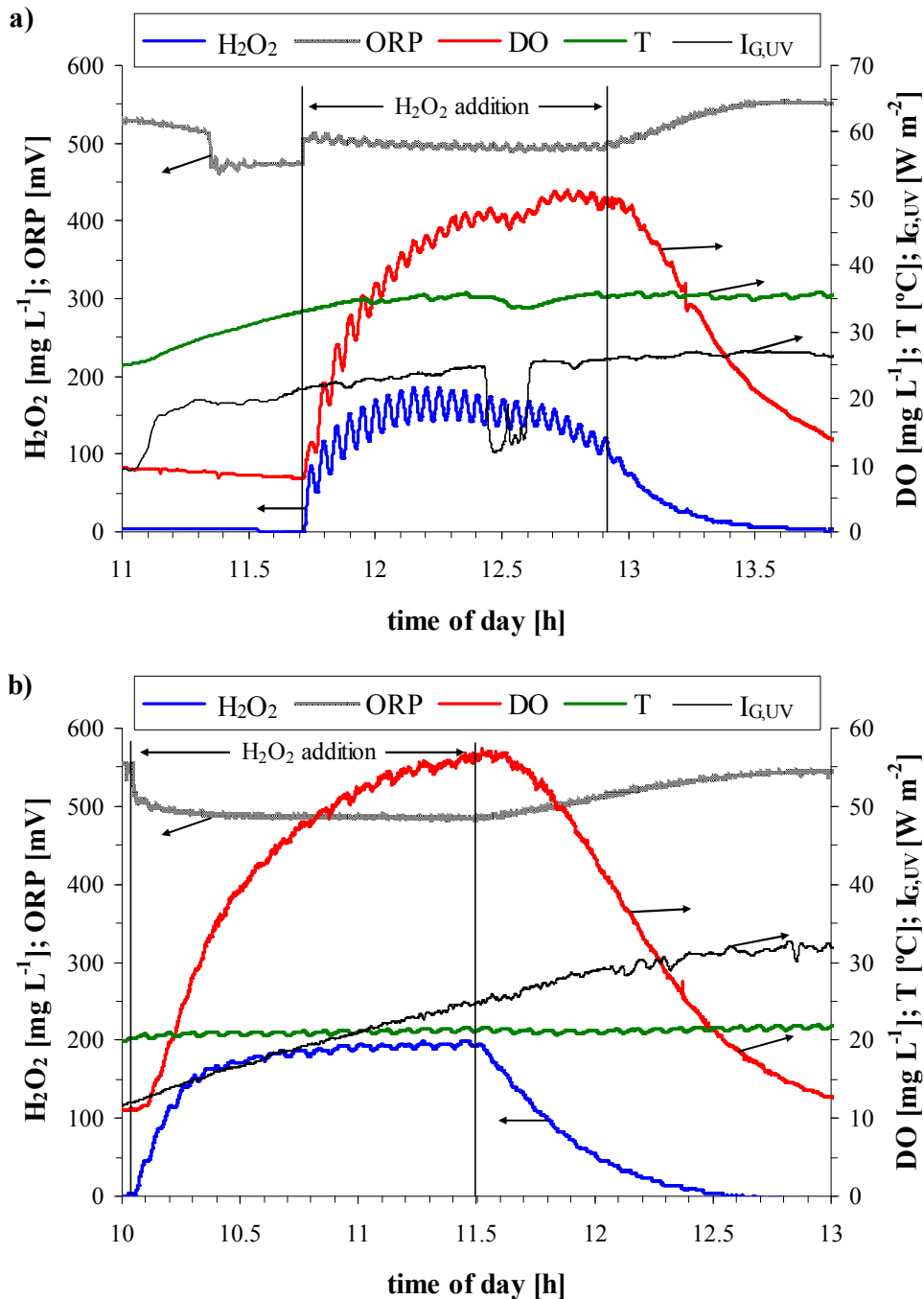
Figure 4.39: DO and ORP evolution during lack of H_2O_2 in solution. $c_{Fe} = 3$ mg L^{-1}. a) $T = 35°C$; b) $T = 20°C$.

Besides, it should be mentioned that although **Figure 4.39** could suggest that H_2O_2 is merely an interference in the DO measurement the results presented in **Figure 4.37** contradict this suspicion, because in the slow experiments DO was low during considerable time in the presence of 200 – 400 mg L^{-1} H_2O_2. Furthermore, an eventual effect of high pressure in the tubing (due to pressure drop) during the measurement was

excluded, because the point of measurement inside the system could be changed by switching several valves (see section 3.3.2 for description). Therefore, DO was measured also at the outlet of the solar collector just before the fluid returned to the tank, i.e. under atmospheric pressure conditions, and no change in the DO concentration was observed.

All these observations together suggest that it may be possible to design a hydrogen peroxide control based on the data of DO and temperature inside the solution. E.g. a fixed DO concentration could be the set-point governing the addition of hydrogen peroxide. This system would avoid excessive hydrogen peroxide dosage at any stage of the process, because it automatically adapts to the changing conditions in the reaction system inside the wastewater, i.e. it limits the hydrogen peroxide concentration towards the end of the process to avoid the undesirable reagent decomposition without oxidation of contaminants. Yet, it has to be taken into account that at the beginning of the degradation process, when DO is scavenged by organic radicals from the solution, the DO concentration does not provide any correlation with the hydrogen peroxide concentration. Consequently, the control system must be designed in such a way that overshooting the desired hydrogen peroxide concentration values at the beginning by uncontrolled H_2O_2 addition is avoided. Otherwise, remnant high H_2O_2 concentration from the initial phase could be decomposed unefficiently after the described phase change in the reacting system.

4.4.3 Oxidation-Reduction Potential (ORP)

Like DO measurement ORP measurement is a standard parameter in wastewater treatment being inexpensive and technically well-developed. ORP measurements from the ALC factorial design are shown in **Figure 4.40**. It can be observed that the largest variations occur during the experiment preparation phase, because the ORP value is largely affected by the pH value and the dissolved iron concentration. The ORP value changed strongly, when the pH was adjusted between -45 and -30 min. Ferrous iron was added affecting again the ORP value between -30 and -15 min and finally hydrogen peroxide was added oxidising ferrous to ferric iron. After illumination starts no clear tendency can be established concerning the evolution of ORP. Similar observations were made in the pesticide mixture experiments (data not shown).

Similar to DO, it might be suggested that the ORP value could be used to detect a depletion of H_2O_2, because, theoretically under illumination this should cause a change in the ratio of ferrous and ferric iron concentration by slowing down the oxidation of ferrous iron by the Fenton reaction, Eq. (2.16). **Figure 4.39** shows the evolution of the ORP value during a simulated photo-Fenton experiment (presence of dissolved iron and hydrogen peroxide at acidic pH under illumination in the reactor). In **Figure 4.39**a the initial conditions (11:00 – 11:20 h) are acidified distilled water at pH = 2.6 and under illumination. It can be seen that the ORP value is around 520 mV. The observed drift is probably due to the slow dissolution of traces of iron oxide remnant from former experiments. The steep decrease to approximately 475 mV at 11:20 h is caused by the addition of pre-dissolved ferrous iron to the reactor. The reason of the subsequent oscillation of the ORP is the incomplete mixing inside the reactor during the first 15 minutes after the addition. Then, at 11:45 hydrogen peroxide addition started and the ORP value changed immediately to a value from 490 to 500 mV. During this phase oscillations occur with the same frequency as those of H_2O_2 and DO concentration, i.e. one peak every 3 min, which equals the time necessary to re-circulate the whole batch volume once. However, the ORP peaks occur with a lag of about 45 seconds.

The physical reason for the oscillation of the ORP is unclear, but it could be e.g. due to a change of ferrous/ ferric iron ratio or even a change in the free radical concentration caused by the changing rate of hydrogen peroxide concentration.

After stopping the hydrogen peroxide addition the ORP value rises again until reaching a final value of approximately 550 mV. The response time to the decrease of the hydrogen peroxide concentration is rather quick (3 – 5 min), yet, it is surprising that the ORP is not returning to its initial value before the initial hydrogen peroxide addition, as it might be assumed if all ferric iron was reduced to ferrous iron again. The reason could be the formation of stable oligomers, which are only slowly reduced. The quick formation of iron oligomers was reported by Krýsová et al [52] and Měšťánková et al [151, 152]. Measurements of dissolved ferrous and ferric iron confirmed that most of the iron was present as ferric iron, when the steady state was reached at 13:30. The experiment was repeated the following day at 20 ºC without changing the solution inside the reactor and all the observations from the previous day were confirmed (see **Figure 4.39**b).

The last observations are highly interesting from a mechanistic point of view. Concerning the usefulness of the ORP value for control, it seems that its only practical

use can be the detection of a lack of H_2O_2. Yet, care must be taken on possible interferences from the wastewater matrix.
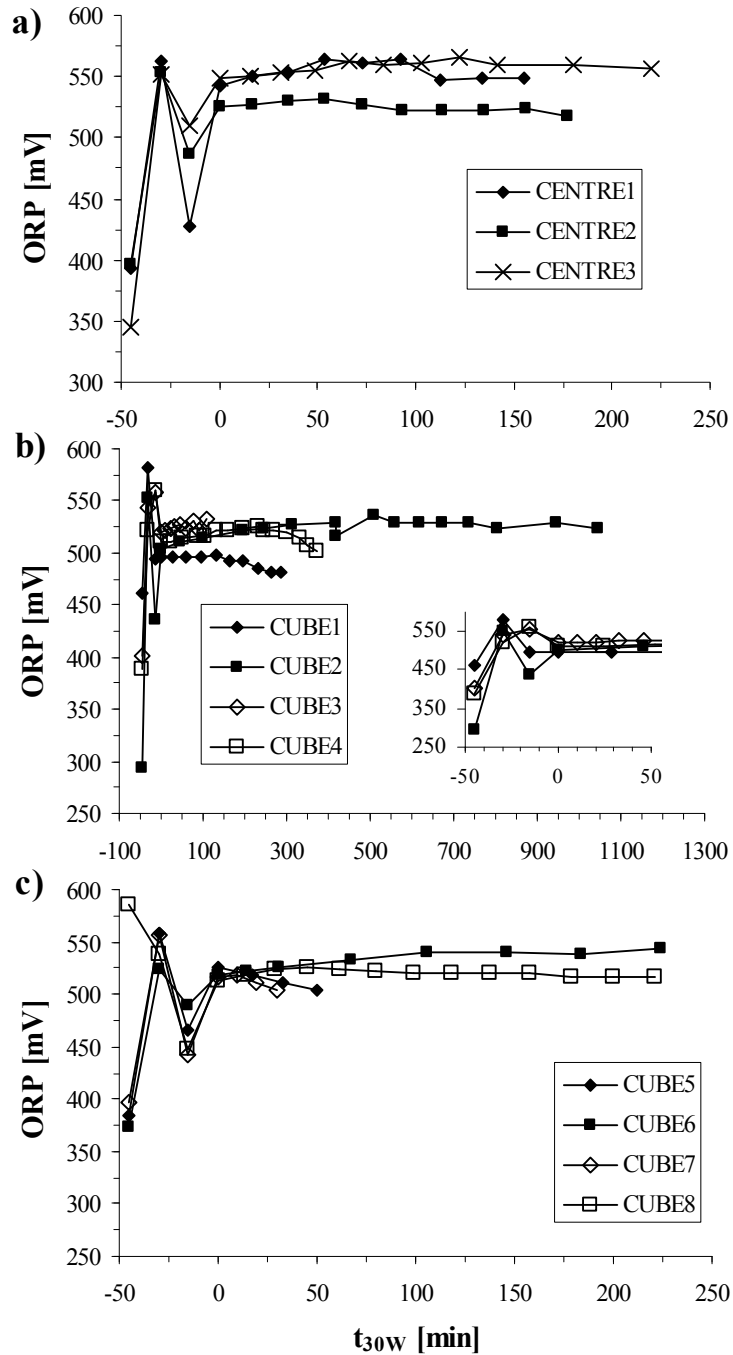
Figure 4.40: ALC factorial design – ORP evolution. Cube points with even numbers are performed at 20ºC, with odd numbers at 50ºC. Cube 1, 2, 5, 6 with 0.83 m^2, cube 3, 4, 7, 8 with 4.16 m^2 collector; a) centre points, b) cube points with 2 mg L^{-1} iron c) cube points with 20 mg L^{-1} iron.

4.4.4 pH value

pH measurement is a standard application not only in wastewater treatment but in many industrial processes. Consequently, reliable sensor technology is easily available at low prices in the market. In photo-Fenton treatment the pH value is a parameter of crucial importance because, in the absence of iron precipitating anions, it is the main influencing factor concerning the precipitation of iron oxides. At the same time it is determining the ligands of dissolved iron aquocomplexes affecting the light absorbance properties of iron containing solutions (refer to section 2.2.2 for detailed discussion of photo-Fenton chemistry).

During photo-Fenton treatment of waste water the pH value varies depending on the intermediates and inorganic ions generated. E.g. organic chlorine is mineralised to hydrochloric acid, organic sulphur to sulphuric acid etc. Also bases can be formed, e.g. ammonia out of organic nitrogen. Depending on the amount of these inorganic ions formed they affect the pH value to a greater or a lesser extent.

Detection of the release of the organically bound inorganics (i.e. the heteroatoms in the molecules) into the solution as inorganic ions is especially desirable, because their presence is very often the cause for non-biodegradability or acute toxicity of an organic compound. The second influence on the pH values is the formation of oxidised organic intermediates containing acidic moieties, most typically short-chain organic acids such as formic, acetic or oxalic acid.

Figure 4.41 and **Figure 4.42** show the development of the pH value during the treatment of the ALC factorial design experiments depicted against the remaining DOC concentration and the degradation time, respectively. In the case of the ALC molecule in the course of mineralisation according to the stoichiometry proposed in Eq. (3.5) and (3.6) and confirmed by the experimental results described in section 4.2.3 ammonium, nitrate and chloride will be formed. Ammonium formation outweighs that of nitrate approximately by a factor 10, which makes the complete mineralisation practically pH neutral. Nevertheless, **Figure 4.41** shows that although the absolute values vary slightly from experiment to experiment a broad minimum phase of the pH value can be observed from 20 to 60% DOC degradation as a general trend.

Figure 4.41: ALC factorial design – pH evolution vs. DOC degradation. Cube points with even numbers are performed at 20ºC, with odd numbers at 50ºC. Cube 1, 2, 5, 6 with 0.83 m^2, cube 3, 4, 7, 8 with 4.16 m^2 collector; a) centre points, b) cube points with 2 mg L^{-1} iron c) cube points with 20 mg L^{-1} iron.
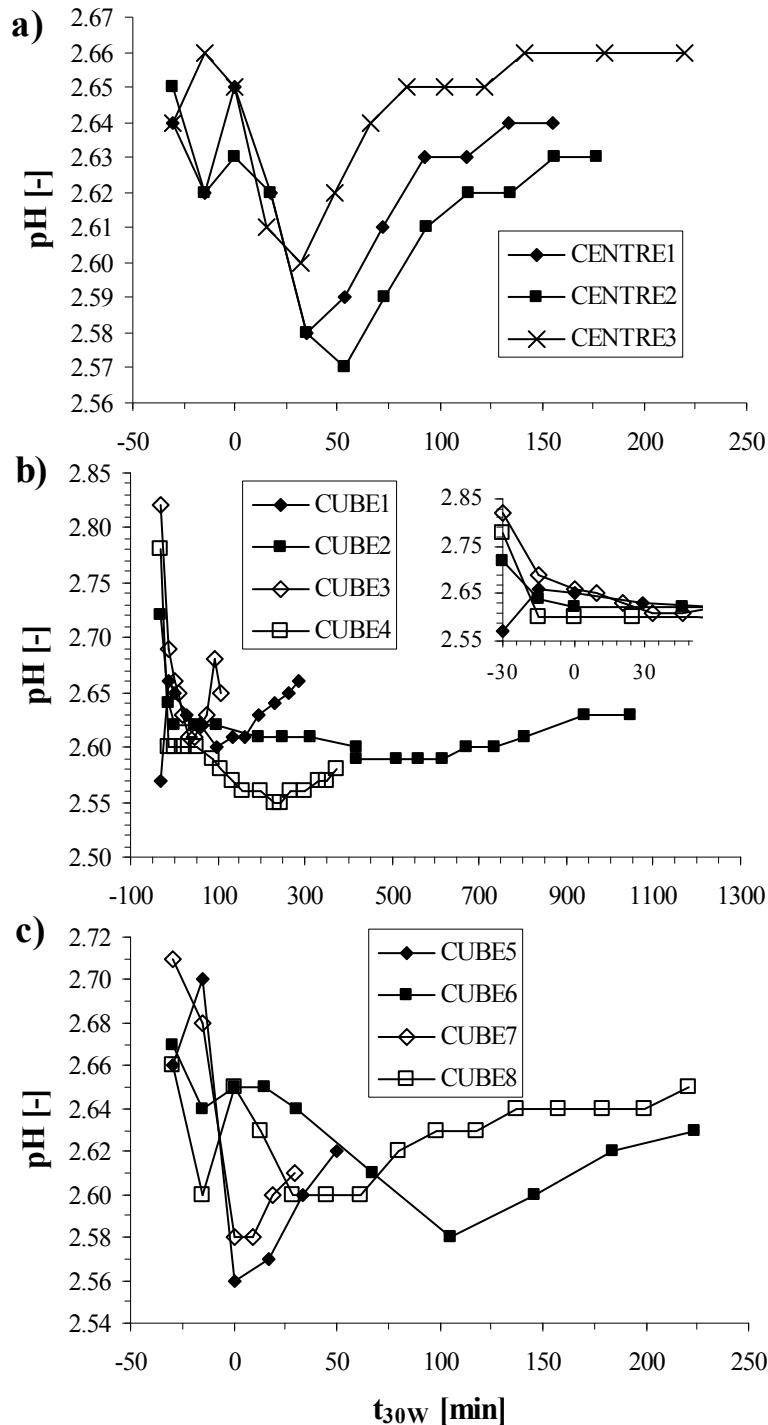
Figure 4.42: ALC factorial design – pH evolution vs. DOC degradation. Cube points with even numbers are performed at 20ºC, with odd numbers at 50ºC. Cube 1, 2, 5, 6 with 0.83 m², cube 3, 4, 7, 8 with 4.16 m² collector; a) centre points, b) cube points with 2 mg L^{-1} iron c) cube points with 20 mg L^{-1} iron.

The decrease of pH is due to the formation of organic acids. Then, probably a sort of temporary steady-state occurs, during which formation and mineralisation rates of these

acids are roughly the same. In the final degradation phase their mineralisation still continues, but due to the absence of larger molecule fragments, no further formation takes place, pH rises again and total mineralisation is achieved. Similar observations have been described in literature [148, 153].

It is remarkable that, although the minimum seems to be rather broad in **Figure 4.41**, in fact, this decreased pH lasts only during a short time interval, as shown in **Figure 4.42**, because it coincides with the phase of the maximum degradation rate. The reduction of ferric iron is usually the rate-limiting step in the photo-Fenton reaction system and ferric iron/ organic acid complexes need less energy (i.e. more photons are available) to undergo the LMCT photo-reduction of the ferric iron compared to ferric iron/ aquo complexes. Furthermore, the quantum yield is higher as well. Consequently, the presence of the organic acids should boost the catalytic iron cycle. Nevertheless, the increase of the reaction rate could also be due to the accelerated reduction of ferric iron due to reaction mechanisms involving quinones and hydroquinones as described in Eqs. (2.42) – (2.46) and (2.60), or most probably due to a combination of both effects.

From the point of view of process control, the observations described suggest that the on-line measurement of the pH value is a highly valuable parameter in photo-Fenton treatment. First, it is a basic operating value because maintaining the solution in a certain pH range is crucial to prevent precipitation of the catalyst. At the same time it is neither desirable to lower the pH too much because the ferric iron complexes formed change their composition and become less photo-active. This can be of importance in waste water releasing large amounts of inorganic ions affecting the pH value. Second, the reported data shows that, intrinsic to the intermediate degradation products formed and the inorganic ions released, the evolution of the pH value can give direct information on the progress of the treatment. Yet, it should be remarked, that such relations have to be established on a case-by-case basis for each type of waste water considered for treatment.

4.4.5 Hydrogen peroxide concentration control

Hydrogen peroxide is the primary reagent needed for the oxidation of the pollutants present in the waste water. Several aspects have already been mentioned in former sections of this work. First, it has been shown (see section 4.3.1) that correlations can be established between the amount of hydrogen peroxide consumed and the degradation

progress. Furthermore, it has been shown and explained that hydrogen peroxide is being decomposed without oxidising pollutants, if its concentration is high compared to the organic matter present (see sections 2.2.2, 4.3.1 and 4.4.2).

In this respect, the optimal range of hydrogen peroxide concentration during photo-Fenton treatment depends on the type and degree of wastewater pollution. Within this optimal range, there is neither rate limitation due to a lack of hydrogen peroxide, nor useless hydrogen peroxide consumption due to a concentration too high. An automatically controlled hydrogen peroxide dosing system to keep the hydrogen peroxide concentration optimised throughout the photo-Fenton treatment would therefore be a very valuable tool to minimise the reagent consumption.

H_2O_2 sensors for on-line measurement exist (Alldos Eichler GmbH, Prominent Dosiertechnik GmbH), although they are not very commonly employed. In this work the sensor from Alldos Eichler GmbH was installed and used for the development of a H_2O_2 feedback control system. The sensor works well although it is less robust than more common sensors such as DO, pH or ORP and has several drawbacks listed in section 3.2.7.

One of the basic components of the feedback control system is the hydrogen peroxide sensor (gauge), which transmits the measured H_2O_2 value via analogue signals and signal converters to a SCADA software running on a PC (see also section 3.3.2 and 3.7). Then, the SCADA software records and processes the data on-line with a sampling frequency of 0.5 s^{-1}. A PI controller algorithm is included in the software. The software allows selecting a H_2O_2 set-point, the controller proportional gain and the controller integral time. Subsequently, the controller output is again converted to an analogue signal sent to a dosage pump. The dosage pump adds H_2O_2, which works within a frequency range of 0 to 100% of its physical capacity ($0 - 120$ s^{-1}), according to the analogue signal received by the controller.

The first step is to characterise the system dynamics. Figure 4.43a shows the system response to an addition of five minutes, operating the pump at maximum frequency. Figure 4.43b shows the same variables for the addition of five minutes, operating the pump at 20 % of its frequency range. In this plot, it can be appreciated how the use of the same model parameters as in the previous case produces modelling errors, for, in fact, the model parameters should have been adjusted to the new operating conditions.

From a theoretical point of view, the system behaviour is nonlinear, but a linear approximation seems appropriate for the task and increases the simplicity of the model.

When analysing the physical structure of the system and the response to input excitations as those shown in Figure 4.43, it is reasonable to think that the output of the system acts as an integrator when H_2O_2 is added (the response to a pulse has the shape of a first order system with a delay and superposed oscillations). This type of behaviour has been observed when controlling pH in photobioreactors [154]. Notice that the pump can only add H_2O_2, but it does not provide any possibility of removing it. Therefore, if the pump is operated at a constant frequency, the H_2O_2 concentration increases continuously, if there is no simultaneous H_2O_2 consumption. The oscillatory behaviour shown in Figure 4.43 is due to mixing effects and the re-circulation of the injected H_2O_2 through the closed hydraulic circuit. The re-circulation time of approximately 180 seconds is imposed by the constant flow rate (0.42 L s^{-1} ≈ 1.5 m^3 h^{-1}) of the fluid and the volume inside the reactor (75 L). Once the H_2O_2 has been added to the mixed tank, the whole system only becomes homogenous after the fluid has been re-circulated several times, because homogenisation mostly takes place in the re-circulation tank, whereas longitudinal mixing scarcely occurs in the tubular reactor zone. This oscillatory behaviour can be represented by a second order term (with natural frequency $\omega_n = 0.034$ rad s^{-1} and damping factor $\delta = 0.1$ for the selected operating conditions). Finally, a delay of the system output (i.e. the H_2O_2 concentration as measured by the sensor) with respect to the addition of H_2O_2 of approximately $t_r = 40$ s is estimated. Then, the transfer function in the Laplace variable s, which relates the output of H_2O_2 concentration in the dissolution to the input frequency of the pump, expressed in percentage with respect to its maximum value, can be described by Eqs. (4.11) and (4.12):

$$c_{H_2O_2} = G_u(s) \cdot u \qquad (4.11)$$

$$G_u(s) = \frac{K}{s} \frac{\omega_n^2}{s^2 + 2\delta\delta_n s + \omega_n^2} e^{-t_r s} \qquad (4.12)$$

Where,

- c_{H2O2}: H_2O_2 concentration in the dissolution [mg L^{-1}]
- u: percentage of H_2O_2 pump frequency range, dimensionless [%]
- K: static gain of the system [mg L^{-1}]

- ω_n: the natural oscillation frequency in the absence of damping, thus determining the speed of response [rad s^{-1}]

- δ: the damping coefficient, which modulates the amplitude of the oscillations, dimensionless [-]

- t_r: system delay [s].

The parameters of the previous transfer functions can be reckoned by empirical observation of temporal responses or by using the identification toolbox of MATLAB$^{®}$. This toolbox allows for building mathematical models for a dynamic system based on measured data. This toolbox was used to model K, ω_n and δ to the measured data depicted in **Figure 4.43**a. The resulting model output was calculated and shown for the operating conditions applied in both experiments depicted in **Figure 4.43**.
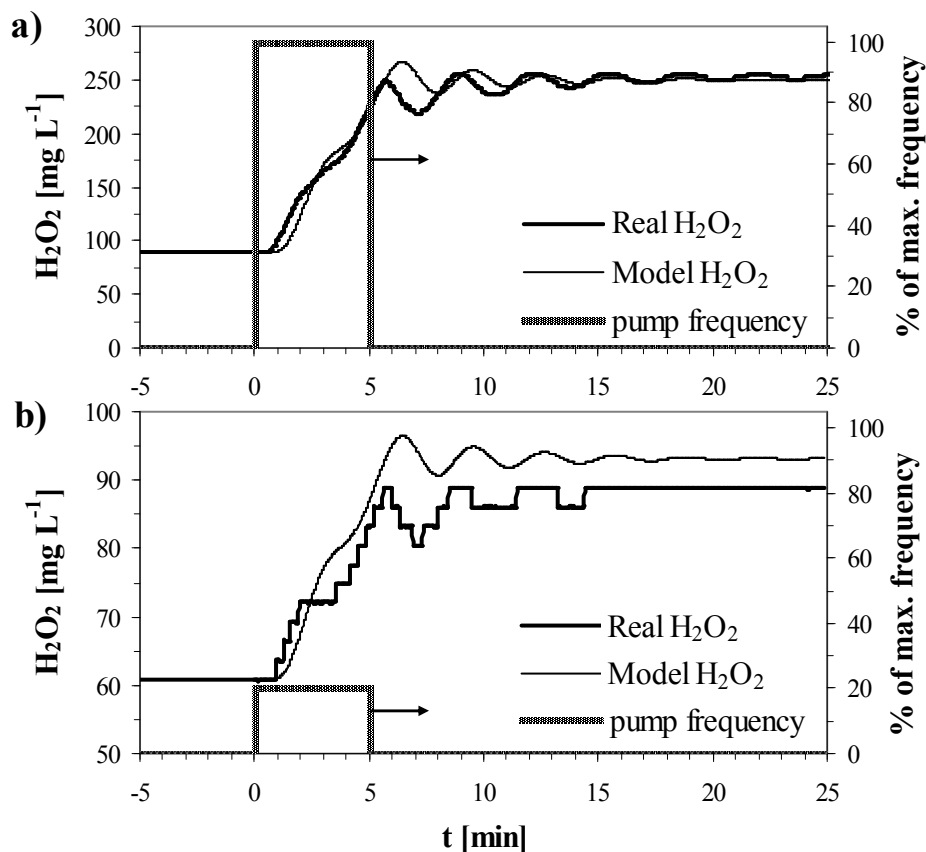
Figure 4.43: H_2O_2 concentration response (model and real system) on a pulse of constant H_2O_2 addition without H_2O_2 consumption. a) 5 min addition at max. pump frequency; b) 5 min addition at 20% pump frequency.

Based on this experimental data and the values of K, ω_n and δ a PI controller was modelled using MathWorks Simulink® and the proportional gain K_c and the integral time τ_I were determined. Then a second controller model was designed, which entailed also an antireset windup module with the basic structure of the controller shown in **Figure 2.11** (page 34). The antireset windup function prevents the calculated frequency from drifting out of the range of the physical possibilities of the pump (0% - 100%) due to the effect of the integral action of the controller (this action changes the integral term when saturation occurs). Without the anti-windup function the controller output could be out of this range, producing a mismatch between the output of the controller and the real output injected in the system (saturated). Moreover, such out-of-range controller output would slow the answer of the controller due to its posterior influence in the integral term (see **Figure 4.44**).

In **Figure 4.44** the results of a simulation of the two constant gain PI controllers with and without antireset windup are shown. The simulation consists of reaching a first H_2O_2 concentration set-point of 200 mg L^{-1}, without any H_2O_2 consumption taking place. Then at t = 2000 s ($\approx$ 33 min) instantaneous start of very strong constant H_2O_2 consumption happens (100 mg L^{-1} min^{-1}). In the real case this could happen after addition of catalyst or start of illumination. As observed in **Figure 4.44**, the PI controller with antireset windup module performs better than the controller of type PI, because the latter surpasses the set-point. In addition, the PI controller with antireset windup responds better to the disturbances due to the start of H_2O_2 consumption. As shown in **Figure 4.44**b, the output of the PI with antireset windup never exceeds the range of the pump, whereas the output of the PI controller reaches values over the range, which produces a slower answer to changes in the set-point because of the windup effect of the integral term of the controller.
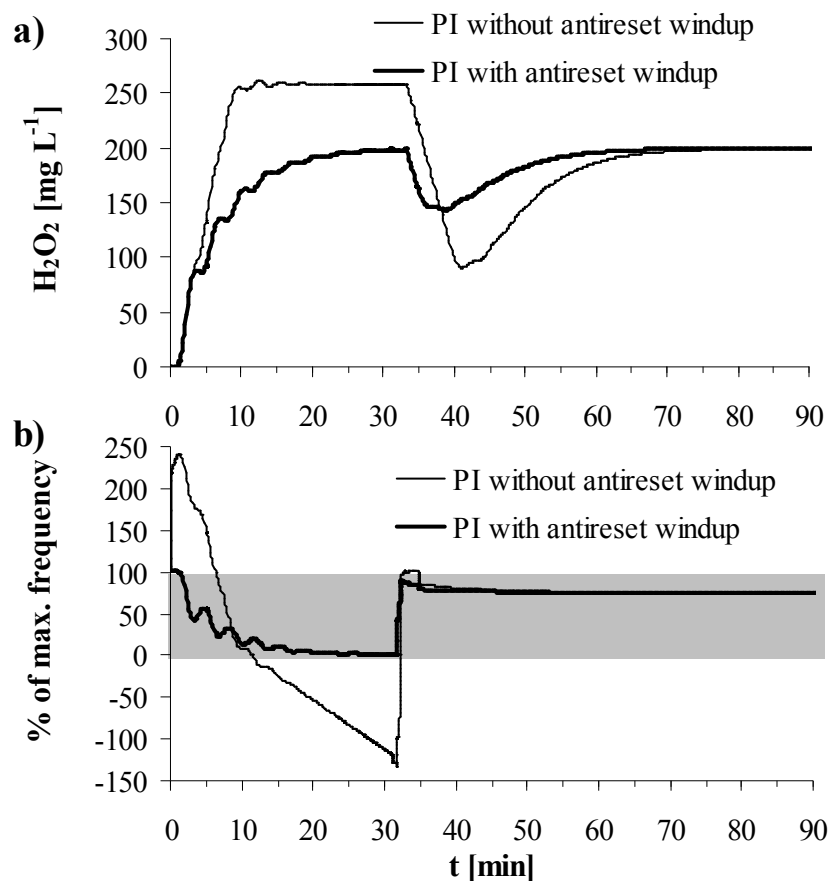
Figure 4.44: Effect of antireset windup of performance of PI controller (modelling results, set-point = 200 mg L^{-1}, H$_2$O$_2$ consumption = 100 mg L^{-1} min^{-1} starting at 33 min). a) H$_2$O$_2$ concentration; b) output of the controller to the dosage pump. The grey zone is the physically possible operation range of the pump. If the controller output signal is out of range the pump operates at zero or max. frequency, respectively.

Finally, real tests of the developed PI controller including an antireset windup module were performed to test its performance. A special objective was to test the stability and response time of the controller to sudden condition changes. The experiment was designed in analogy to the simulation depicted in **Figure 4.44** and its results are shown in **Figure 4.45**. First, a set-point of 500 mg L^{-1} H$_2$O$_2$ was fixed and during the first phase (55 min) of the experiment this set-point was achieved with a slight tendency of staying approximately 20 mg L^{-1} below the targeted set-point. During this phase the hydrogen peroxide consumption rate was practically zero because dissolved iron catalyst was only present in traces due to impurities present in the pilot-plant from previous experiments. Then, at 55 minutes a first lower iron dose was added to the reactor provoking reagent consumption. The addition of iron happens pointwise, i.e.

during the first 15 min after the addition, the iron is not homogeneously distributed inside the reactor. Thereby, also the reagent consumption is inhomogeneous along the system. Accordingly, this is somewhat the worst-case scenario of operation from the point of view of the control system. Yet, due to the solar nature of the process it is something that can very easily happen under real conditions, because whenever the radiation intensity changes due to a cloud passing the sun's path, sudden changes to the hydrogen peroxide decomposition rate can be expected and a robust controller is required.
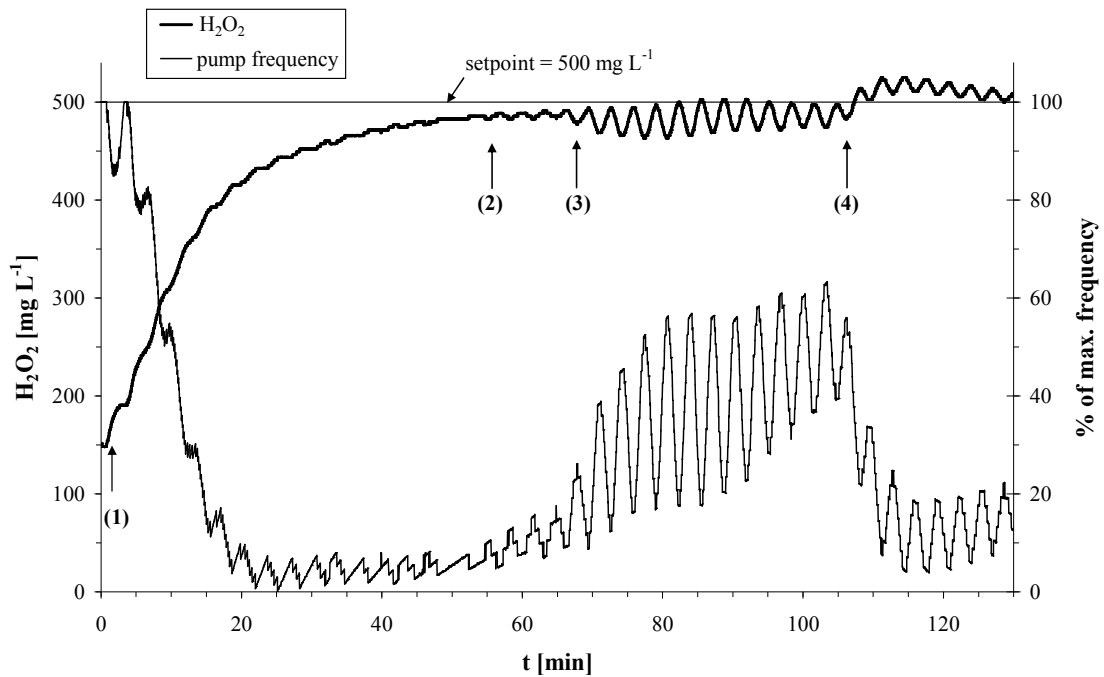
Figure 4.45: Real test of PI controller with antireset windup – H_2O_2 concentration and dosage pump frequency. (1) only traces of iron, pH 2.5, collector illuminated, H_2O_2 dosage start; (2) addition of 1 mg L^{-1} Fe, H_2O_2 consumption rate approx. 10 mg L^{-1} min^{-1}; (3) addition of 3 mg L^{-1} Fe, H_2O_2 consumption rate approx. 50 mg L^{-1} min^{-1}; (4) covering of CPC, H_2O_2 consumption rate approx. 15 mg L^{-1} min^{-1}.

Then at about 70 minutes another addition of iron takes place leading to a rather high hydrogen peroxide consumption rate. While after the first addition the oscillations induced to the system response were practically negligible, this time their amplitude was considerable (approximately 40 mg L^{-1}). Furthermore, it is noticeable that the system needs very long time to level these oscillations. In fact, after 40 minutes the amplitude of the oscillation had decreased only by about 30%. Then, at 110 minutes

another sudden condition change was induced to the system by covering the solar collectors. Thereby, the hydrogen peroxide consumption rate was lowered by about 70%. As a consequence, the system response slightly overshoots the set-point but soon returns to its previous value.

These observations suggest that the applied controller is able to adjust the system output to a fixed set-point. It has a rather quick response time to disturbances but shows also some tendency to enter in oscillation without possessing the ability to eliminate it quickly.

Yet, some more system particularities should be considered when assessing the efficiency and usefulness of the controller. The system consists of a re-circulation tank (10 L) in which perfect mixing can be assumed. From an engineering point of view, the rest of the volume is a tubular plug-flow reactor with negligible longitudinal mixing consisting of around 50 L of volume inside the solar collector (different from the illuminated volume of 44.6 L, because it includes knees etc., see also section 3.3.2) and 15 L volume of connecting tubing. Around 14 L of this tubing are located before the fluid enters the collector and the last litre represents the tubing connecting the collector outlet with the tank. Under the given flow conditions (1.5 m^3 h^{-1}) the residence time of a differential volume inside the reactor is 180 s. The hydrogen peroxide measurement is situated practically immediately before the fluid enters the solar collector. The following assumptions were made:

- Case 1: Perfect steady-state control at 500 mg L^{-1} H_2O_2, no H_2O_2 decomposition in the dark zones of the reactor, pseudo-zero order H_2O_2 decomposition in the illuminated part of the reactor.

- Case 2: Perfect steady-state control at 500 mg L^{-1} H_2O_2, pseudo-zero order H_2O_2 decomposition in the illuminated part and in the dark part of the reactor, but with different reaction rates.

The H_2O_2 decomposition rate data obtained in the real test of the PI controller (10 – 50 mg L^{-1} min^{-1}, see **Figure 4.45**) was applied to calculate the H_2O_2 concentration in the different zones of the reactor and the results are shown in **Figure 4.46**. For case 1 (only light reaction) and 50 mg L^{-1} min^{-1} H_2O_2 peroxide decomposition, the difference between maximum and minimum concentration is 150 mg L^{-1}. For case 2 the reaction rate in the dark was calculated to be around 22% of the reaction rate in the light (estimated from data with and without illumination under otherwise identical conditions

in **Figure 4.45**). The resulting concentration difference between calculated maximum and minimum concentration is then 140 mg L^{-1}.
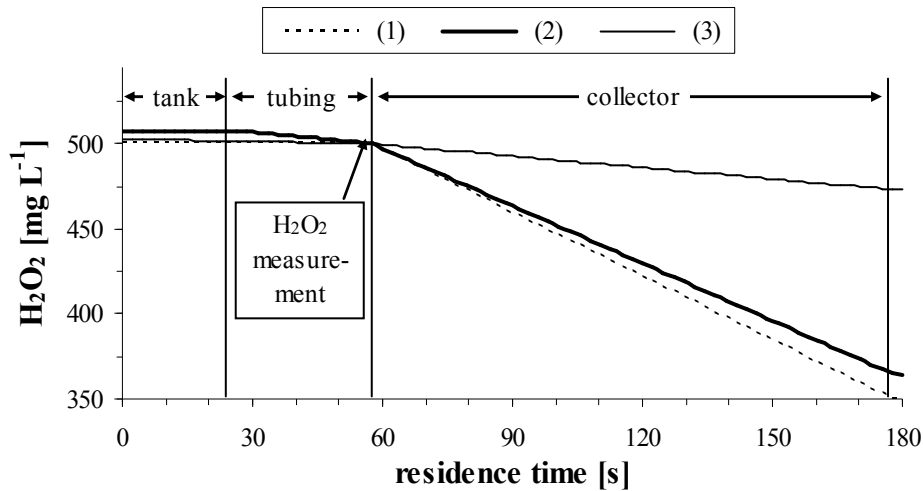
Figure 4.46: Calculated H_2O_2 concentration in the different sections of the illuminated reactor with perfect steady-state control (set-point 500 mg L^{-1}). (1) Case 1, H_2O_2 consumption = 50 mg L^{-1} min^{-1}; (2) Case 2, H_2O_2 consumption = 50 mg L^{-1} min^{-1}; (3) Case 2, H_2O_2 consumption = 10 mg L^{-1} min^{-1}.

If we now compare the amplitude of the oscillations observed in the real test with these estimated differences inside the reactor, they are in fact rather small compared to other factors causing concentration gradients occurring in the system. Such considerations are crucial when designing a real-scale plant, where the residence times inside the collectors might be much higher compared to the present pilot-plant. Injection of hydrogen peroxide at various points of the system would be necessary, if large concentration gradients of hydrogen peroxide should be avoided. At the same time the system probably becomes more difficult to control with a single gauge, because the response time of the gauge to an addition in a point too far away could be strongly distorted by the system dynamics.

As a conclusion it may be said that hydrogen peroxide concentration measurement, control and mass balancing promise to be very valuable tools in the control of photo-Fenton treatment.

5 Conclusions and Summary

5.1 Feasibility of solar photo-Fenton treatment

One of the goals of this work was to prove the feasibility and identify eventual problems of the treatment of a variety of model waste waters containing Priority Substances (PS) by solar photo-Fenton treatment. To this end, 11 substances from the list of Priority Substances were selected. The solar photo-Fenton treatment was performed in pilot-plants based on Compound Parabolic Collector technology. The experiments were assessed based on measurements of the proper contaminant by HPLC, the Dissolved Organic Carbon, analysis of the inorganic ions released by the contaminants by Ion Chromatography, temperature, pH value, UV radiation measurement, dissolved iron concentration by colorimetric measurement and hydrogen peroxide consumption and concentration by iodometric titration.

The pollutants can be grouped into three non-biodegradable chlorinated solvents (NBCS) (dichloromethane, trichloromethane and 1,2-dichloroethane), seven pesticides (alachlor, atrazine, chlorfenvinphos, diuron, isoproturon, lindane, pentachlorophenol) and one surfactant metabolite (4-nonylphenol). Pollutant concentrations successfully treated reached from 2 mg L^{-1} (4-nonylphenol) to 150 mg L^{-1} (mixture of pesticides).

All the model pollutants were treatable within the tested conditions, but some contaminants presented a particular behaviour. This must be taken into account, when the presence of these substances is to be expected in a wastewater stream. From the 11 model substances the following pecularities must be emphasized:

- Non-biodegradable chlorinated solvents: The treatment has to be fast to avoid volatilisation and to provide complete mass balance by chloride measurements.
- Atrazine: DOC mineralisation is not complete. Cyanuric acid is not the final product unless the applied treatment times are excessively long.
- Diuron/ isoproturon: Neither DOC mineralisation nor nitrogen balances were complete. The residual DOC is most probably urea, which presents no environmental concern.
- Chlorfenvinphos releases phosphate during the degradation, which precipitates the iron catalyst. As a consequence, depending on the amount of phosphate released higher amounts of catalyst have to be applied.

The collector area per mass strongly varied depending on the type of contaminant, its concentration and other process parameters such as iron concentration, solution temperature and reactor set-up:

- Iron concentration: Increasing the iron concentration from 2 to 55.8 mg L^{-1} (factor ≈28) lowered the collector area per mass by a factor of 6.8 (average of all substances).

- Pollutant concentration: Average collector area per mass was 4600 m^2 h kg^{-1} for alachlor, chlorfenvinphos and isoproturon (50 mg L^{-1} initial concentration) and 13500 m^2 h kg^{-1} for pentachlorophenol and lindane (20 mg L^{-1} initial concentration).

- Pollutant type: Average collector area per mass in the NBCS experiments was 19700 m^2 h kg^{-1}, which is substantially higher than in comparable pesticide experiments (see previous point). For atrazine it was 43000 m^2 h kg^{-1}.

Hydrogen peroxide consumption was always higher than the theoretical amount of reagent required for mineralisation according to stoichiometry. E.g. for the degradation of 50% of the initial DOC the consumption of hydrogen peroxide was 1 − 2 times the theoretical amount needed for the group of alachlor, chlorfenvinphos, diuron and isoproturon, 2 − 6 times for pentachlorophenol and lindane, 6 − 9 times for atrazine, 3 times for 1,2-dichloroethane and 7 − 36 times for dichloromethane and trichloromethane.

Iron precipitation was detected in these experiments, although the maximum pH value was 2.8. The reasons for detecting it to a greater extent than other authors proposing this pH as the optimal one, are the considerable treatment times and the solution temperatures clearly above room temperature, both favouring iron precipitation. Moreover, a clear dependence on the pH was observed, because in the NBCS experiments the pH was lowered during the treatment due to the liberation of hydrochloric acid by mineralisation of the pollutant (until 2.3 − 2.5) and iron precipitation was observed to a lesser extent in these experiments. As a consequence, working at pH 2.5 is recommended to avoid catalyst precipitation.

5.2 Solar collector optimisation

Another goal of this work was the installation of a pilot-plant with new solar collector technology. The main difference was an increased absorber tube diameter in this new

collector (from 29.2 to 46.4 mm inner diameter). This plant was compared with an already existing plant. The two different Compound Parabolic Collectors were assessed theoretically and experimentally. The increased tube diameter in the new plant proved to be beneficial, because a lower catalyst concentration can be applied while still providing the absorbtion of the full amount of radiation inside the photoreactor.

Higher irradiated volumes per square metre in the new collector lead to lower collector area per mass figures, which is of the utmost importance, because the capital investment due to the collector field is a major cost factor in wastewater treatment by solar photo-Fenton.

The lower collector area per mass found at higher reaction solution temperatures and lower ratios of illuminated to not illuminated volume (see next section) suggests that possible collector insulation and combinations of heat absorber and photochemical collectors or hybrid collectors should be taken into consideration in future work.

5.3 Influence of iron concentration, solution temperature and collector area per volume

Another goal of this work was the assessment of the influence of catalyst concentration, temperature and the ratio between illuminated and dark volume upon the process performance. With this aim, degradation experiments were performed in the newly built pilot-plant applying alachlor as a model compound, its initial concentration being 100 mg L^{-1}. Iron concentration (2 – 20 mg L^{-1}), solution temperature (20 – 50 ºC) and the ratio of illuminated to total volume (0.12 – 0.59) were varied according to a central composite factorial design without starpoints. Hydrogen peroxide (200 – 400 mg L^{-1}) was maintained constant.

The experiments were assessed based on measurements of the proper contaminant by HPLC, the Dissolved Organic Carbon, analysis of the inorganic ions released by the contaminants by Ion Chromatography, temperature, pH value, UV radiation measurement, dissolved iron concentration by colorimetric measurement and hydrogen peroxide consumption and concentration by iodometric titration. However, for the kinetic discussion and the model building the measurement of DOC as a function of degradation time was considered the crucial parameter.

Increase of temperature from 20 to 50 ºC and of iron concentration from 2 to 20 mg L^{-1} decreased the necessary time to achieve a desired DOC degradation level (50 – 80% of its initial value) by an approximate factor of 5 and 6 respectively.

Increasing the illuminated collector area from 0.83 to 4.16 m^2 decreased the degradation time by a factor of about 2.5. This means that at a lower ratio of illuminated to total volume (0.12), the collector area per mass was only about half its value at a ratio of 0.59. This is of the utmost importance to lower the capital costs of a photo-Fenton treatment plant.

Three models valid for the present model case were established from the data obtained:

- A static model predicting the influence of iron concentration, solution temperature and illuminated collector area (assuming constant values of these process parameters along the treatment) on the time necessary to reach 50 or 80% DOC degradation.

- A dynamic model based on the logistic dose response curve that models the whole DOC degradation curve as a function of varying process conditions (time, iron, temperature, collector area, UV irradiance).

- A simple polynomic model predicting DOC degradation as a function of the hydrogen peroxide amount consumed. It was shown that the extent of DOC degradation was only dependent on the amount of hydrogen peroxide consumed, but the hydrogen peroxide consumption was not affected by the process parameters varied (especially worth mentioning are the variation of temperature and iron concentration) within the experimental range investigated.

The followed methodology (experimental design and modelling) is proposed as a methodology for any other pilot-plant study aimed at obtaining similar correlations between process parameters and process progress.

5.4 Economic on-line measurement for process control

An additional aim of the present work was to perform a screening for parameters, which could be measured on-line and check their usefulness for application in automated process control strategies. Therefore, the newly installed pilot-plant was provided with an on-line measurement system consisting of sensors for the measurement of hydrogen peroxide concentration, dissolved oxygen, oxidation-reduction potential, pH value and temperature. The values transmitted by these sensors were acquired by a tailor-made

Supervisory Control and Data Acquisition (SCADA) system. UV/Vis absorbance measurement was not installed on-line, but measured off-line in the laboratory with a benchtop system.

Data available from different photo-Fenton degradation experimens in the new pilot-plant were used for this screening. Among those are the experiments of the factorial design employed for the assessement of the influence of process parameters with alachlor as a model compound and degradation experiments with mixtures of pesticides. Some more experiments were designed especially to test the control of hydrogen peroxide inside the plant by automatic dosage with a hydrogen peroxide pump and the behaviour of dissolved oxygen.

The following results were obtained:

- UV/Vis absorbance: In the case of aromatic pollutants a characteristic evolution of the UV/Vis absorbance along the degradation process can be distinguished and applied to assess the process progress. Dissolved iron interference depends on the ratio of iron to pollutant concentration. This interference can be partly overcome by measuring in the near UV range (e.g. at 350 nm).

- Dissolved oxygen concentration: Dissolved oxygen concentration was found to be dependent on the chemical composition of the wastewater matrix and the ratio of hydrogen peroxide to pollutant concentration. In advanced treatment stages H_2O_2 decomposition to oxygen was observed leading to supersaturation of dissolved oxygen. Dissolved oxygen concentration could therefore be utilised in three ways. First, to assess the process progress by recognising the start of supersaturation indicating the achieved degradation. Second, to limit automatised H_2O_2 addition, so that supersaturation is avoided, which indicates a waste of H_2O_2 due to its excess concentration in relation to the pollutant. Finally, a decrease of supersaturation during the treatment is a sign of H_2O_2 depletion.

- Oxidation-Reduction potential: The ORP value can mainly be used to assess H_2O_2 depletion inside the solution due to the changes in the iron composition inside the solution. However, possible interferences are unclear.

- pH value: A characteristic pH evolution during the photo-Fenton treatment of a waste water can be found usually, due to the release of inorganic ions from the organic pollutants and the formation of organic acids. The applicability of this indicator for the assessment of the degradation process progress depends mainly

on the wastewater matrix, i.e. the type and concentration of the pollutants contained. Furthermore, the usefulness of pH measurement for process control is intrinsic to the process, as working conditions out of the optimal pH range due the process can be recognised and corrected by a control system. This is an aspect of special importance for waste water that release high amounts of base (usually ammonia) and for systems working in continuous mode, where the influent conditions could vary.

- Hydrogen peroxide concentration: H_2O_2 concentration control under dynamic conditions proved to be feasible in the pilot-plant used, by applying a feedback control system utilising an on-line H_2O_2 sensor, which transmits its value to a PI controller acting upon the frequency controller of a H_2O_2 dosage pump. Model calculations showed that under the H_2O_2 consumption rates occurring in photo-Fenton the values of the H_2O_2 concentration at different positions inside the plant were considerable. This is a fact that has to be taken into account when designing real-size plants, with residence times inside the solar collector several times higher than at pilot-plant scale.

As a conclusion it may be said that several promising approaches for photo-Fenton process control have been found. However, any decision about a control approach has to be taken on a case-by-case basis as a function of the wastewater matrix to find the best possible tailor-made solution.

6 References

[1] UNEP (2002). Global environment outlook 3. Nairobi, Kenya.

[2] WHO and UNICEF Joint Monitoring Programme (2005). Water for Life: Making it happen. Geneva, Switzerland.

[3] European Commission (2003). Water for life. EU Water initiative. International cooperation from knowledge to action.

[4] European Commission (1976). Dangerous Substances Directive. EC Directive 76/464/EEC.

[5] Barceló D. (ed.) (2003). Emerging pollutants in water analysis. Special issue. *Trends Anal. Chem.*, **22 (10)**.

[6] European Commission (2000). The Water Framework Directive. EC Directive 2000/60/EC.

[7] European Commission (1999). COMMPS procedure. Study on the prioritisation of substances dangerous to the aquatic environment. Office for Official Publications of the European Communities (ISBN 92-828-7981-X), Luxembourg.

[8] European Commission (2000). List of 32 Priority Substances. Finally, the Commission adopted the Proposal for a European Parliament and Council Decision establishing the list of priority substances in the field of water policy on 07 February 2000. COM(2000) 47 final.

[9] European Commission (1996). Integrated Pollution Prevention and Control Directive. EC Directive 96/61/EEC.

[10] European Commission (1980). Drinking Water Directive. EC Directive 80/778/EEC.

[11] European Commission (1991). Urban Waste Water Treatment Directive. EC Directive 91/271/EEC.

[12] European Commission (1991). Nitrates Directive. EC Directive 91/676/EEC.

[13] European Commission (1976). Bathing Water Directive. EC Directive 76/160/EEC.

[14] EU union (2000). Presidency conclusions of the Lisbon European Council, 23 and 24 March 2000.

[15] European commission (2005). Common Actions for Growth and Employment: The Community Lisbon Programme. COM(2005) 330 final.

[16] European commission (2001). A Sustainable Europe for a BetterWorld: A European Union Strategy for Sustainable Development. COM(2001) 264 final.

[17] United Nations (2002). The Johannesburg Declaration on Sustainable Development. Document A/CONF.199/L.6/Rev.2.

[18] European commission (2002). Environmental technology for sustainable development. COM (2002) 122 final.

[19] European commission (2004). Stimulating Technologies for Sustainable Development: An Environmental Technologies Action Plan for the European Union. COM (2004) 38 final.

[20] European commission (2003). Environmental Technologies Action Plan - Discussion Paper. Report from the Water issue group as a contribution to the Environmental Technologies Action Plan. Brussels, August 2003.

[21] European commission (2005). Work Programme Sub-Priority 1.1.6.3 "Global Change and Ecosystems". 4th Call for Proposals. Call Identifier: FP6-2005-Global-4.

[22] Fröhlich C. and Brusa R.W. (1981). Solar Radiation and its variation in time. *Sol. Phys.*, **74**, 209-215.

[23] American Society for Testing and Materials (1987). Standard tables for terrestrial solar spectral irradiance at air mass 1.5 for a 37º tilted surface. Designation: E892-87.

[24] Iqbal M. (1983). An Introduction to Solar Radiation. Academic Press, Oxford.

[25] Minero C., Pelizzetti E., Malato S. and Blanco J. (1993). Large Solar Plant Photocatalytic Water Decontamination: Degradation of Pentachlorophenol. *Chemosphere*, **26**, 2103-2119.

[26] Wyness P., Klausner J.F. and Goswami D.Y. (1994). Performance of Nonconcentrating Solar Photocatalytic Oxidation Reactors, Part I: Flat-Plate Configuration. *J. Sol. Energ.-T ASME*, **116**, 2-7.

[27] Gernjak W., Krutzler T., Glaser A., Malato S., Cáceres J., Bauer R. and Fernández-Alba A.R. (2003). Photo-Fenton treatment of water containing natural phenolic pollutants. *Chemosphere*, **50**, 71-78.

[28] Well M., Dillert R.H.G., Bahnemann D.W., Benz V.W. and Mueller, M.A. (1997). A novel nonconcentrating reactor for solar water detoxification. *J. Sol. Energ.-T ASME*, **119**, 114-119.

[29] Wyness P., Klausner J.F. and Goswami D.Y. (1994). Performance of Nonconcentrating Solar Photocatalytic Oxidation Reactors, Part II: Shallow-Pond Configuration. *J. Sol. Energ.-T ASME*, **116**, 8-13.

[30] Muschaweck J., Spirkl W., Timinger A., Benz N., Dörfler M., Gut M. and Kose E. (2000). Optimized reflectors for non-tracking solar collectors with tubular absorbers. *Sol. Energy*, **68**, 151-159.

[31] Ajona J.I. and A. Vidal (2000). The use of CPC collectors for detoxification of contaminated water: design, construction and preliminary results. *Sol. Energy*, **68**, 109-120.

[32] Blanco J., Malato S., Fernández P., Vidal A., Morales A., Trincado P., de Oliveira J.C., Minero C., Musci M., Casalle C., Brunotte M., Tratzky S., Dischinger N., Funken K.-H., Sattler C., Vincent M., Collares-Pereira M., Mendes J.F. and Rangel C.M. (2000). Compound parabolic concentrator technology development to commercial solar detoxification applications. *Sol. Energy*, **67**, 317-330.

[33] Henze M., Harremoës P., La Cour Jansen J. and Arvin E. (2000). Wastewater Treatment: Biological and Chemical Processes. 3rd Ed. Springer-Verlag, Berlin.

[34] European Commission (2004). Implementation of Council Directive 91/271/EEC of 21 May 1991 concerning urban waste water treatment, as amended by Commission Directive 98/15/EC of 27 February 1998. COM(2004) 248 final.

[35] Chiron S., Fernandez-Alba A.R., Rodríguez A. and Garcia-Calvo E. (2000). Pesticide chemical oxidation: state-of-the-art. *Water Res.*, **34**, 366-377.

[36] American Water Works Association (1999). Water Quality and Treatment – A Handbook of Community Water Supplies. 5th Ed. Letterman R. D. (Ed.). McGraw-Hill, New York.

[37] Haag W.R. and Yao C.D. (1992). Rate Constant for Reaction of Hydroxyl Radicals with Several Drinking Water Contaminants. *Environ. Sci. Technol.*, **26**, 1005-1013.

[38] Buxton G.U., Greenstock C.L., Helman W.P. and Ross A.B. (1988). Critical review of rate constants for reactions of hydrated electrons, hydrogen atoms and hydroxyl radicals (OH$^\bullet$/O$^{\bullet-}$) in aqueous solution. *J. Phys. Chem. Ref. Data*, **17**, 513-886.

[39] Legrini O., Oliveros E. and Braun A. M. (1993). Photochemical Processes for Water Treatment. *Chem. Rev.*, **93**, 671-698.

[40] Gogate P.R. and Pandit A.B. (2004). A review of imperative technologies for wastewater treatment II: hybrid methods. *Adv. Environ. Res.*, **8**, 553-597.

[41] Gogate P.R. and Pandit A.B. (2004). A review of imperative technologies for wastewater treatment I: oxidation technologies at ambient conditions. *Adv. Environ. Res.*, **8**, 501-551.

[42] Herrmann J.M. (1999). Heterogeneous Photocatalysis: fundamentals and applications to the removal of various types of aqueous pollutants. *Catal. Today*, **53**, 115-129.

[43] Safarzadeh-Amiri A., Bolton J.R. and Cater S.R. (1996). The use of iron in Advanced Oxidation Processes. *J. Adv. Oxid. Techn.*, **1**, 18-26.

[44] Bauer R., Waldner G., Fallmann H., Hager S., Klare M., Krutzler T., Malato S. and Maletzky P. (1999). The photo-Fenton reaction and the TiO$_2$/UV process for wastewater treatment – novel developments. *Catal. Today*, **53**, 131-144.

[45] Malato S., Blanco J., Vidal A. and Richter C. (2002). Photocatalysis with solar energy at a pilot-plant scale: an overview. *Appl. Catal. B: Environ.*, **37**, 1-15.

[46] Oller I., Fernández-Ibáñez P., Maldonado M.I., Pérez-Estrada L., Gernjak W., Pulgarín C., Passarinho P.C., Malato S. (2006). Solar heterogeneous and homogeneous photocatalysis as a pre-treatment option for biotreatment. *Res. Chem. Interm.*, in press.

[47] Pulgarín C., Invernizzi M., Parra S., Sarria V., Polania R. and Péringer P. (1999). Strategy for the coupling of photochemical and biological flor reactions useful in mineralization of biocalcitrant industrial pollutants. *Catal. Today*, **54**, 341-352.

[48] Hawker P.N. and Twigg M.V. (1994). Iron: inorganic & coordination chemistry. In: King, P.B. (Ed.). Encyclopedia of Inorganic Chemistry. Wiley, Chichester, 1698-1725.

[49] Faust B. and Hoigné J. (1990). Photolysis of hydroxy-complexes as sources of OH• radicals in clouds, fog and rain. *Atmos. Environ.*, **24A**, 79-89.

[50] Flynn C.M. Jr. (1984). Hydrolysis of inorganic iron(III) salts. *Chem. Rev.*, **84**, 31-41.

[51] Blesa M. and Matijevic E. (1989). Phase transformation of iron oxides, oxohydroxides, and hydrous oxides in aqueous solution media. *Adv. Colloid Interface Sci.*, **29**, 173-221.

[52] Krýsová H., Jirkovský J., Krýsa J., Mailhot G. and Bolte M. (2003). Comparative kinetic study of atrazine photodegradation in aqueous $Fe(ClO_4)_3$ solutions and TiO_2 suspensions. *Appl. Catal. B: Environ.*, **40**, 1-12.

[53] Mazellier P. and Sulzberger B. (2001). Diuron degradation in irradiated, heterogeneous iron/oxalate systems: The rate-determining step. *Environ. Sci. Technol.*, **35**, 3314-3320.

[54] Sulzberger B., Laubscher H. and Karametaxas G. (1994). Photoredox reactions at the surface of iron(III)(hydr-)oxides. In: Helz G. R., Zepp R. G. and Crosby, D. G. (Eds.) Aquatic and surface photochemistry. Lewis Publishers, Boca Raton, 53-74.

[55] Sychev A.Y. and Isaak V.G. (1995). Iron compounds and the mechanisms of the homogeneous catalysis of the activation of O_2 and H_2O_2 and of the oxidation of organic substrates. *Russ. Chem. Rev.*, **64**, 1105-1129.

[56] Haber F. and Weiss J. (1934). The catalytic decomposition of hydrogen peroxide by iron salts. *Proc. Roy. Soc.*, **147**, 332-351.

[57] Barb W.G., Baxendale J.H., George P. and Hargrave K.R. (1951). Reactions of ferrous and ferric ions with hydrogen peroxide. *Trans. Faraday Soc.*, **47**, 462-500.

[58] Barb W.G., Baxendale J.H., George P. and Hargrave K.R. (1951). Reactions of ferrous and ferric ions with hydrogen peroxide. Part II. The ferric ion reaction. *Trans. Faraday Soc.*, **47**, 591-616.

[59] Walling C. (1975). Fenton's reagent revisited. *Acc. Chem. Res.*, **8**, 125-131.

[60] Kremer M.L. and Stein G. (1959). The catalytic decomposition of hydrogen peroxide by ferric perchlorate. *Trans. Faraday Soc.*, **55**, 959-973.

[61] Kremer M.L. (1962). Nature of intermediates in the catalytic decomposition of hydrogen peroxide by ferric ions. *Trans. Faraday Soc.*, **58**, 702-707.

[62] Kremer M.L. and Stein G. (1977). Kinetics of the Fe^{3+} ion - H_2O_2 reaction: steady state and terminal-state analysis. *Int. J. Chem. Kinet.*, **9**, 179-184.

[63] Bossmann S H., Oliveros E., Göb S., Siegwart S., Dahlen E.P., Payawan L. Jr., Straub M., Worner M. and Braun A.M. (1998). New evidence against hydroxyl radicals as reactive intermediates in the thermal and photochemically enhanced Fenton reactions", *J. Phys Chem.*, **102**, 5542-5550.

[64] Pignatello J.J., Liu D. and Huston P. (1999). Evidence for an additional oxidant in the Photoassisted Fenton reaction. *Env. Sci. Technol.*, **33**, 1832-1839.

[65] Fenton H.J.H. (1894). Oxidation of tartaric acid in presence of iron. *J. Chem Soc.*, **65**, 899-910.

[66] Gallard H., De Laat J. and Legube B. (1999). Spectrophotometric study of the formation of iron(III)–hydroperoxy complexes in homogeneous aqueous solution. *Water Res.*, **33**, 2929-2936.

[67] Bielski B.H., Cabelli D.E., Arudi R.L. and Ross A.B. (1985). Reactivity of HO_2/O_2 – radicals in aqueous solution. *J. Phys. Chem. Ref. Data*, **14**, 1041-1100.

[68] Huyser S. and Hawkins G.W. Ferrous ion catalyzed oxidations of 2-propanol with peroxyacetic acid. *J. Org. Chem.*, **48**, 1705-1708.

[69] Dorfman L.M., Taub I.A. and Bühler, R.E. (1962). Pulse radiolysis studies. I. Transient spectra and reaction-rate constants in irradiated aqueous solutions of benzene. *J. Chem. Phys.*, **36**, 3051-3061.

[70] von Sonntag C., Dowideit P., Fang X., Mertens R., Pan X., Schuchmann M. N. and Schuchmann H.-P. (1997). The fate of peroxyl radicals in aqueous solution. *Water Sci. Technol.*, **35(4)**, 9-15.

[71] Chen R. and Pignatello J.J. (1997). Role of quinone intermediates as electron shuttles in Fenton and photoassisted Fenton oxidations of aromatic compounds. *Environ. Sci. Technol.*, **31**, 2399–2406.

[72] Kavitha V. and Palanivelu K (2004). The role of ferrous ion in Fenton and photo-Fenton processes for the degradation of phenol. *Chemosphere*, **55**, 1235-1243.

[73] Lipczynska-Kochany E., Sprah G.and Harms S. (1995). Influence of some groundwater and surface waters constituents on the degradation of 4-chlorophenol by the Fenton reaction. *Chemosphere*, **30**, 9-20.

[74] Pignatello J.J. (1992). Dark and Photoassisted Fe^{3+}-Catalyzed Degradation of Chlorophenoxy Herbicides by Hydrogen Peroxide. *Environ. Sci. Technol.*, **26**, 944-951.

[75] Kiwi J., Lopez A. and Nadtochenko V. (2000). Mechanism and kinetics of the OH-radical intervention during Fenton oxidation in the presence of a significant amount of radical scavenger (Cl⁻). *Environ. Sci. Technol.*, **34**, 2162-2168.

[76] De Laat J., Truong Le G. and Legube B (2004). A comparative study of the effects of chloride, sulfate and nitrate ions on the rates of decomposition of H_2O_2 and organic compounds by $Fe(II)/H_2O_2$ and $Fe(III)/H_2O_2$. *Chemosphere*, **55**, 715-723.

[77] Maciel R., Sant'Anna G.L. and Dezotti M. (2004). Phenol removal from high salinity effluents using Fenton's reagent and photo-Fenton reactions. *Chemosphere*, **57**, 711-719.

[78] Zepp R.G., Faust B.C. and Hoigné J. (1992). Hydroxyl radical formation in aqueous reactions (pH 3-8) of iron(II) with hydrogen peroxide: The photo-Fenton reaction. *Environ. Sci. Technol.*, **26**, 313-319.

[79] Safarzadeh-Amiri A., Bolton J.R. and Carter S.R. (1996). Ferrioxalate-mediated solar degradation of organic contaminants in water. *Sol. Energy*, **56**, 439-444.

[80] Nogueira R.F.P., Trovó A.G. and Modé D.F. (2002). Solar photodegradation of dichloroacetic acid and 2,4-dichlorophenol using an enhanced photo-Fenton process. *Chemosphere*, **48**, 385–391.

[81] Paterlini W.C. and Nogueira R.F.P. (2005). Multivariate analysis of photo-Fenton degradation of the herbicides tebuthiuron, diuron and 2,4-D. *Chemosphere*, **58**, 1107-1116.

[82] Sun Y. and Pignatello J.J. (1992). Chemical treatment of pesticide wastes. Evaluation of Fe(III) chelates for catalytic hydrogen peroxide oxidation of 2,4-D at circumneutral pH. *J. Agric. Food Chem.*, **40**, 322-327.

[83] Sun, Y. and Pignatello J.J. (1993). Activation of hydrogen peroxide by iron(III) chelates for abiotic degradation of herbicides and insecticides in water. *J. Agric. Food Chem.*, **41**, 308-312.

[84] Braun A.M., Maurette M.-T. and Oliveros E. (1991). Photochemical technology. Wiley, Chichester.

[85] David F., David P.G. (1976). Photoredox chemistry of iron(3) chloride and iron(3) perchlorate in aqueous media. A comparative study. *J. Phys. Chem.*, **80**, 579-583.

[86] Cooper G.D., DeGraff B.A. (1971). On the photochemistry of the ferrioxalate system. *J. Phys. Chem.*, **75**, 2897-2902.

[87] Hatchard C.G., Parker C.A. (1956). A sensitive chemical actinometer II. Potassium ferrioxalate as a standard chemical actinometer. *Proc. Roy. Soc.*, **A235**, 518-536.

[88] Ononye A.I.,. McIntosh A.R. and Bolton J.R. (1986). Mechanism of the photochemistry of p-benzoquinone in aqueous solutions. 1. Spin trapping and flash photolysis electron paramagnetic resonance studies. *J. Phys. Chem.*, **90**, 6266-6270.

[89] Bishop D.F., Stern G., Fleischmann M. and Marshall L.S. (1968). Hydrogen peroxide catalytic oxidation of refractory organics in municipal waste waters. *Ind. Eng. Chem. Process Des. & Dev.*, **7**, 110-117.

[90] Lipczynska-Kochany E. (1991). Novel Method for a Photoanalytic Degradation of 4-Nitrophenol in Homogenous Aqueous Solution. *Environ. Technol.*, **12**, 87-92.

[91] Lipczynska-Kochany E. (1992). Degradation of Nitrobenzene and Nitrophenols by Means of AOP´s in Homogenous Phase: Photolysis in the Presence of Hydrogenperoxide versus the Fenton Reaction. *Chemosphere*, **24**, 1369-1380.

[92] Sun Y. and Pignatello J.J. (1993). Photochemical reactions involved in the total mineralization of 2,4-D by $Fe^{3+}/H_2O_2/UV$. *Environ. Sci. Technol.*, **27**, 304-310.

[93] Ruppert G., Bauer R. and Heisler G. (1993). The Photo-Fenton Reaction - an Effective Photochemical Wastewater Treatment Process. *J. Photochem. Photobiol. A: Chem.*, **73**, 75-78.

[94] Fallmann H., Krutzler T., Bauer R., Malato S. and Blanco J. (1999). Detoxification of pesticide containing effluents by solar driven Fenton process. *Z. Phys. Chemie*, **213**, 67-74.

[95] Huston P.L. and Pignatello J.J. (1999). Degradation of selected pesticide active ingredients and commercial formulations in water by the photo-assisted Fenton reaction. *Water Res.*, **33**, 1238-1246.

[96] Hincapié M., Maldonado M.I., Oller I., Gernjak W., Sánchez-Pérez J. A., Ballesteros M. M. and Malato S. (2005). Solar photocatalytic degradation and detoxification of EU priority substances. *Catal. Today*, **101**, 203-210.

[97] Malato S., Blanco J., Vidal A., Alarcón D., Maldonado M. I., Cáceres J. and Gernjak W. (2003). Applied studies in solar photocatalytic detoxification: an overview. *Sol. Energy*, **75**, 329-336.

[98] Pera-Titus M., García-Molina V., Baños M.A., Giménez J. and Esplugas S. (2004) Degradation of chlorophenols by means of advanced oxidation proceses: a general review. *Appl. Catal. B: Environ.*, **47**, 219-256.

[99] Krutzler T., Fallmann H., Maletzky P., Bauer R., Malato S. and Blanco J. (1999). Solar driven degradation of 4-chlorophenol. *Catal. Today*, **54**, 321-327.

[100] Herrera F., Pulgarin C., Nadtochenko V. and Kiwi J. (1998). Accelerated photo-oxidation of concentrated p-coumaric acid in homogeneous solution. Mechanistic studies, intermediates and precursors formed in the dark. *Appl. Catal. B: Environ.*, **17**, 141-156.

[101] Pérez-Estrada L., Maldonado M.I., Gernjak W., Agüera A., Fernández-Alba A.R., Ballesteros M.M. and Malato S. (2005) .Decomposition of diclofenac by solar driven photocatalysis at pilot-plant scale. *Catal. Today*, **101**, 219-226.

[102] Arslan-Alaton I. and Gurses F. (2004). Photo-Fenton and photo-Fenton-like oxidation of Procaine Penicillin G formulation effluent. *J. Photochem. Photobio. A: Chem.*, **165**, 165-175.

[103] Sigman, M. E., Buchanan, A.C., "Application of advanced oxidation process technologies to extremely high TOC containing aqueous solutions", J. Adv. Oxid. Technol. 2, 415-423 (1997).

[104] Gernjak W., Maldonado M.I., Malato S., Cáceres J., Krutzler T., Glaser A. and Bauer R. (2004). Pilot-Plant Treatment of Olive Mill Wastewater (OMW) by Solar TiO$_2$ Photocatalysis and Solar Photo-Fenton. *Sol. Energy*, **77**, 567-572.

[105] Sarria V., Parra S., Adler N., Péringer P., Benitez N. and Pulgarin, C. (2002). Recent developments in the coupling of photoassisted and aerobic biological processes for the treatment of biorecalcitrant compounds. *Catal. Today*, **76**, 301-315.

[106] Sarria V., Deront M., Péringer P. and Pulgarín C. (2003). Degradation of biorecalcitrant dye precursor present in industrial wastewater by a new integrated iron(III) photoassisted-biological treatment. *Appl. Catal. B: Environ.*, **40**, 231-246.

[107] Scott J.P. and Ollis D.F. (1995). Integration of chemical and biological oxidation processes for water treatment: Review and recommendations. *Environ. Prog.*, **14**, 88-103.

[108] Esplugas S. and Ollis D.F. (1997). Economic aspects of integrated (chemical + biological) processes for water treatment. *J. Adv. Oxid. Technol.*, **1**, 197-202.

[109] Oliveros E., Legrini O., Hohl M., Müller T. and Braun A.M. (1997). Industrial waste water treatment: large scale development of a light-enhanced Fenton reaction. *Chem. Eng. Proc.*, **36**, 397-405.

[110] Göb S., Oliveros E., Bossmann S.H., Braun A.M., Nascimento C.A.O. and Guardani R. (2001). Optimal experimental design and artificial neural networks applied to the photochemically enhanced Fenton reaction. *Water Sci. Technol.*, **44(5)**, 339-345.

[111] Torrades F., Pérez M., Mansilla H.D. and Peral J. (2003). Experimental design of Fenton and photo-Fenton reactions for the treatment of cellulose bleaching effluents. *Chemosphere*, **53**, 1211-1220.

[112] Sarria V., Kenfack S., Guillod O. and Pulgarin C. (2003). An innovative coupled solar-biological system at field pilot scale for the treatment of biorecalcitrant pollutants. *J. Photoch. Photobio. A*, **159**, 89-99.

[113] Sagawe G., Lehnard A., Lubber M., Rochendorf G. and Bahnemann D. (2001). The insulated solar Fenton hybrid process: fundamental investigations. *Helv. Chim. Acta*, **84**, 3742-3759.

[114] Feng W. and Nansheng D. (2000). Photochemistry of hydrolytic iron (III) species and photoinduced degradation of organic compounds. *Chemosphere*, **41**, 1137-1147.

[115] Bozzi A., Yuranova T., Lais P. and Kiwi J.(2005). Degradation of industrial waste waters on Fe/C-fabrics. Optimization of the solution parameters during reactor operation. *Water Res.*, **39**, 1441-1450.

[116] Maletzky P., Bauer R., Lahnsteiner J. and Pouresmael B. (1999). Immobilisation of iron ions on nafion(R) and its applicability to the photo-Fenton method. *Chemosphere*, **38**, 2315-2325.

[117] Martínez F., Calleja G., Melero J.A. and Molina R. (2005). Heterogeneous photo-Fenton degradation of phenolic aqueous solutions over iron-containing SBA-15 catalyst. *Appl. Catal. B: Environ.*, **60**, 185-194.

[118] Box G.E.P., Hunter W.G. and Hunter J.S. (1978). Statistics for Experimenters: An Introduction to Design, Data Analysis, and Model Building. Wiley, New York.

[119] Wu C.F.J. and Hamada M. (2000). Experiments: Planning, Analysis, and Parameter Design Optimization. Wiley, New York.

[120] Doehlert D.H. (1970). Uniform Shell Designs. *J. Roy. Stat. Soc.*, **C19**, 231-239.

[121] Yates F. (1937). The design and analysis of factorial experiments. *Imp. Bur. Soil Sci.* Techn. Comm. 35.

[122] Hair J.F., Anderson R.E., Tatham R.L. and Black W.C. (1998). Multivariate Data Analysis. Prentice Hall International, New Jersey.

[123] Lohninger H. (1999). Teach/Me Data Analysis. Springer-Verlag, Berlin-New York-Tokyo.

[124] Rossetti G.H., Albizzati E.D. and Alfano O.M. (2004). Modeling of a flat-plate solar reactor. Degradation of formic acid by the photo-Fenton reaction. *Sol. Energy*, **77**, 461-470.

[125] Zupan J. and Gasteiger J. (1993). Neural Networks for Chemists: An Introduction. VCH, Weilheim.

[126] Nascimento C.A.O., Oliveros E. and Braun A.M. (1994). Neural network modelling for photochemical processes. *Chem. Eng. Proc.*, **33**, 319–324.

[127] Ogunnaike B.A. and Harmon Ray W. (1994). Process Dynamics, Modeling, and Control. Oxford University Press, New York.

[128] Coughanowr D.R. (1991). Process Systems Analysis and Control. 2nd Ed. McGraw-Hill, Boston.

[129] Åström K.J. and Hägglund T. (1996). PID Control. In: Levine, W.S. (ed.). The Control Handbook. CRC/IEEE Press, Boca Raton, Florida. 198-209.

[130] Hägglund T. and Åström K.J. (1996). Automatic Tuning of PID Controllers. In: Levine, W.S. (ed.). The Control Handbook. CRC/IEEE Press, Boca Raton, Florida. 817-826.

[131] Syracuse Research Coorportation. The Physical Properties Database. Available from: http://www.syrres.com/esc/databases.htm (30.11.2005).

[132] Pelizzetti E., Minero C., Carlin V., Vincenti M., Pramauro E. and Doici M. (1992). Identification of Photocatalytic Degradation Pathways of 2-Cl-s-Triazine Herbicides and Detection of their Decomposition Intermediates. *Chemosphere*, **24**, 891-910.

[133] McLoughlin O.A., Kehoe S.C., McGuigan K., Duffy E.F., Al Touati F., Gernjak W., Oller Alberola I., Malato Rodríguez S. and Gill L.W. Solar disinfection of contaminated water: a comparison of three small-scale reactors. *Sol. Energy*, **77**, 657-664.

[134] Kipp & Zonen CUV3 broadband radiometer instruction manual. Available from www.kippzonen.com (30.11.2005).

[135] APHA, AWWA, WEF (1998). Standard Methods for the Examination of Water and Waste Water. 20th Edition. United Book Press Inc., Maryland.

[136] Atkins P.W. and de Paula J. (2001). Atkins' Physical Chemistry. 7th Ed. Oxford University Press, Oxford.

[137] Lide D.R. (Ed.). (1996). Handbook of Chemistry and Physics. 77th Ed. 1996-1997. CRC Press, Boca Raton, Florida.

[138] Bates R.G. (1973). Determination of pH. Theory and Practice. 2nd Ed. Wiley, New York.

[139] Goswami D.Y., Sharma S.K., Mathur G.D. and Jotshi C.K. (1997). Techno-Economic Analysis of Solar Detoxification Systems. *J. Sol. Energ.-T ASME*, **119**, 108-113.

[140] Bolton J.R., Bircher K.G., Tumas W. and Tolman C.A. (2001). Figures-of-merit for the technical development and application of advanced oxidation technologies for both, electric- and solar driven systems. *Pure Appl. Chem.*, **73(4)**, 627-637.

[141] Teel A.L. and Watts R.J. (2002). Degradation of carbon tetrachloride by modified Fenton's reagent. *J. Haz. Mat.*, **94**, 179-189.

[142] Arnold S.M., Hickey W.J. and Harris R.F. (1995). Degradation of atrazine by Fenton's reagent: condition optimisation and product quantification. *Environ. Sci. Technol.*, **29**, 2083-2089.

[143] Hincapié M., Peñuela G., Maldonado M.I., Malato O., Fernández-Ibañez P., Oller I., Gernjak W. and Malato S. (2006). Degradation of pesticides in water using solar Advanced Oxidation Processes. *Appl. Catal. B: Environ.*, in press.

[144] Maletzky P. and Bauer R. (1998). The photo-Fenton method – Degradation of nitrogen containing organic compounds. *Chemosphere*, **37**, 899-909.

[145] Malato S., Blanco J., Maldonado M.I., Fernández P., Alarcon D., Collares M., Farinha J. and Correia J. (2004). Engineering of solar photocatalytic collectors. *Sol. Energy*, **77**, 513-524.

[146] Peñuela G.A. and Barceló D. (1996). Comparative degradation kinetics of alachlor in water by photocatalysis with $FeCl_3$, TiO_2 and photolysis, studied by solid-phase disk extraction followed by gas chromatographic techniques. *J. Chromatog. A*, **754**, 187-195.

[147] Fernández-Alba A.R., Hernando D., Agüera A., Cáceres J. and Malato S. (2002). Toxicity assays: a way for evaluating AOPs efficiency. *Water Res.*, **36**, 4255-4262.

[148] Malato S., Cáceres J., Fernández-Alba A.R., Piedra L., Hernando M.D., Agüera A. and Vial J. (2003). Photocatalytic Treatment of Diuron by Solar Photocatalysis: Evaluation of Main Intermediates and Toxicity. *Environ. Sci. Technol.*, **37**, 2516-2524.

[149] Lu M.C., Chen J.N. and Chang C.P. (1999). Oxidation of dichlorvos with hydrogen peroxide using ferrous iron as catalyst. *J. Hazard. Mater. B*, **65**, 277-288.

[150] Fallmann H. (1999). Der Einsatz von Sonnelicht zur Abwasserreinigung mit dem Photo-Fenton Verfahren. Dissertation, Vienna University of Technology.

[151] Měšťánková H., Mailhot G., Jirkovský J., Krýsa J. and Bolte M. (2005). Mechanistic approach of the combined (iron–TiO_2) photocatalytic system for the degradation of pollutants in aqueous solution: an attempt of rationalisation. *Appl. Catal. B: Environ.*, **57**, 257-265.

[152] Měštánková H., Krýsa J., Jirkovský J., Mailhot G., Bolte M. (2005). The influence of Fe(III) speciation on supported TiO_2 efficiency: example of monuron photocatalytic degradation. *Appl. Catal. B: Environ.*, **58**, 185-191.

[153] Pérez-Estrada L., Malato S., Gernjak W., Agüera A., Thurman M., Ferrer I. and Fernández-Alba A.R. (2005). Photo-Fenton degradation of Diclofenac: Identification of Main Intermediates and Degradation Pathway. *Env. Sci. Technol.*, **39**, 8300-8306.

[154] Berenguel M., Rodríguez F., Acién F.D and García J.L. (2004). Model predictive control of pH in tubular photobioreactors. *J. Proc. Control*, **14**, 377-387.

7 Index of Tables

8 Index of Figures

9 Index of Abbreviations

9.1 Abbreviations

ACN	acetonitrile
ALC	alachlor
AM	Air Mass
AOP	Advanced Oxidation Process
ATZ	atrazine
BAT	Best Available Technology
CAS	Chemical Abstracts Services Registry Number
cf.	confer
CIEMAT	Centro de Investigaciones Energéticas, Medioambientales y Tecnológicas
CPC	Compound Parabolic Collector
CFVP	chlorfenvinphos
DAQ	Data Acquisition
DCE	1,2-dichloroethane
DCM	dichloromethane
DIU	diuron
DO	Dissolved Oxygen
DOC	Total Dissolved Organic Carbon
EDC	Endocrine Disrupting Chemical
e.g.	"exempli gratia" – for example
Eq., Eqs.	equation(s)
et al.	"et alia" – and others
etc.	etcetera
ETAP	Environmental Technologies Action Plan
EU	European Union
exp.	experiment
F value	Fisher's value
HPLC-UV	High Performance Liquid Chromatography with UV/Vis detection
i.e.	"id est" – that is
IC	Ion Chromatography
IPPC	Integrated Pollution Prevention and Control Directive

IPR	isoproturon
IUPAC	International Union of Pure and Applied Chemistry
LDR	Logistic Dose Response
LIN	lindane
LMCT	ligand-to-metal charge transfer
MLR	Multiple Linear Regression
NBCS	Non-Biodegradable Chlorinated Solvents
4-NP	4-nonylphenol
ORP	Oxidation-Reduction Potential
p.A.	pro analysi
PC	Personal Computer
PCP	pentachlorophenol
PPCP	Pharmaceutical or Personal Care Product
pH	"potentia hydrogenii" – pH value
PHS	Priority Hazardous Substance as classified by WFD
PID	proportional-integral-derivative
PS	Priority Substance as classified by WFD
PSA	Plataforma Solar de Almería
PTC	Parabolic Trough Concentrator
RSM	Response Surface Methodology
SCADA	Supervisory Control and Data Acquisition
SMARTS	Simple Model of the Atmospheric Radiative Transfer of Sunshine
TC	Total Carbon
TCM	trichloromethane (chloroform)
TIC	Total Inorganic Carbon
TOC	Total Organic Carbon
UV	Ultraviolet
UV/Vis	Ultraviolet/Visible light
vs.	versus
WFD	Water Framework Directive

9.2 Nomenclature and symbols

9.2.1 Roman letters

"		inch, 1" = 0.0254 m
A	[m^2]	solar collector area; Ampere
A_{CM}	[m^2 h kg^{-1}]	Collector area per mass
$A_{CM}^{50\%DOC}$	[m^2 h kg^{-1}]	Collector area per mass at 50% degradation of DOC^i
$A_{CM}^{80\%DOC}$	[m^2 h kg^{-1}]	Collector area per mass at 80% degradation of DOC^i
AU	[m]	Astronomic Unit, sun-earth distance
c	[mg L^{-1}; mM]	concentration
c^i	[mg L^{-1}; mM]	initial concentration
c(t)		feedback controller command signal in process control
c$_{Fe}$	[mg L^{-1}; mM]	iron concentration
d(t)		disturbances on the system in process control
DOC^i	[mg L^{-1}]	initial DOC concentration
E°	[V]	Oxidation Potential vs. the Standard Hydrogen Electrode
g		gram
h	[J s]	Planck's constant, h = 6.626 10^{-34} J s; hour
hν		photon
$H_2O_2^i$	[mg L^{-1}]	initial hydrogen peroxide concentration
$H_2O_2^{50\%DOC}$	[mg L^{-1}, mM]	H_2O_2 needed to degrade 50% of the initial DOC
$H_2O_2^{80\%DOC}$	[mg L^{-1}, mM]	H_2O_2 needed to degrade 80% of the initial DOC
$H_2O_2^{theor}$	[mg L^{-1}, mM]	theoretical stoichiometric amount of H_2O_2 needed for complete pollutant mineralisation
I_B	[W m^{-2}]	direct beam radiation
$I_{Bn\lambda}$	[W m^{-2}]	spectral direct beam radiation on a surface normal to the sun's rays
I_D	[W m^{-2}]	diffuse radiation
I_G	[W m^{-2}]	global radiation
$I^o_{G,UV}$	[W m^{-2}]	standard global UV irradiance at PSA of 30 W m^{-2}
$I_{G,UV}(t)$	[W m^{-2}]	global UV irradiance
$I_{on\lambda}$	[W m^{-2} nm^{-1}]	spectral extraterrestrial direct beam radiation
J		Joule

k		reaction rate constant
K		equilibrium constant
K	[mg L^{-1}]	static gain of a system towards a control action
K_{OW}		octanol-water partition coefficient
K_S		equilibrium solubility constant of a salt
K_c		proportional gain in a PID controller
kWh		kilowatt-hour, 1 kWh = 3600 kJ
L		litre; ligand
m		metre
M	[mol L^{-1}]	molar, mole per litre
min		minute
Pa		Pascal, pressure unit
Q	[kJ L^{-1}]	accumulated UV radiation energy in reaction solution
$Q^{50\%DOC}$	[kJ L^{-1}]	Q needed to degrade 50% of the initial DOC
$Q^{80\%DOC}$	[kJ L^{-1}]	Q needed to degrade 80% of the initial DOC
rad		radiant degree
s		second; Laplace transformation of t
t	[s]	time
T	[ºC]	temperature
t_{30W}	[min]	normalised illumination time
$t_{30W}^{50\%DOC}$	[min]	t_{30W} needed to degrade 50% of the initial DOC
$t_{30W}^{80\%DOC}$	[min]	t_{30W} needed to degrade 80% of the initial DOC
t_r	[s]	system delay of the gauge response to the control action
$T_{a\lambda}$	[-]	Transmittance coefficient for aerosol extinction
$T_{g\lambda}$	[-]	Transmittance coefficient for uniformly mixed gases
$T_{n\lambda}$	[-]	Transmittance coefficient for absorption by NO_2
$T_{o\lambda}$	[-]	Transmittance coefficient for absorption by O_3
$T_{R\lambda}$	[-]	Transmittance coefficient for Rayleigh scattering
$T_{w\lambda}$	[-]	Transmittance coefficient for water vapour absorption
u(t)		process input variable; deliberate action of the actuator on the system in process control
V		Volt
V_{ill}	[L]	illuminated volume inside the solar collector
V_{tot}	[L]	total volume of pilot-plant

W		Watt
w/v		weight per volume
w/w		weight per weight
$X_{H_2O_2}^{50\%DOC}$	[-]	H_2O_2 consumption mass ratio to degrade 50% of DOC[i]
$X_{H_2O_2}^{80\%DOC}$	[-]	H_2O_2 consumption mass ratio to degrade 80% of DOC[i]
y(t)		process output variable in process control
$y_d(t)$		set-point of process output variable in process control

9.2.2 Greek letters

α	[rad]	sun altitude
β	[rad]	inclination of an inclined surface with respect to a horizontal plane
γ	[rad]	the orientation of an inclined surface with respect to the azimuth angle ψ
Γ	[rad]	day angle
δ	[rad]	declination with respect to the equatorial plane
δ	[-]	the damping coefficient of an oscillation in control
Δ		a difference
ε	[L mol^{-1} cm^{-1}]	molar extinction coefficient
$\varepsilon(t)$		error function; deviation from set-point in process control
$\varepsilon_a(t)$		actuator error function in antireset windup PID control
$\eta_{H_2O_2}^{80\%DOC}$	[-]	stoichiometric efficiency of H_2O_2 consumption to degrade 80% of the initial DOC
θ_z	[rad]	zenith angle
λ	[m]	wavelength
ν	[s^{-1}]	frequency
τ_D	[s]	derivative time constant in a PID controller
τ_I	[s]	integral time in a PID controller
τ_t	[s]	tracking time in a antireset windup PID controller
ψ	[rad]	azimuth angle
ω	[rad]	hour angle
ω_n	[rad s^{-1}]	the natural oscillation frequency of a system in control

10 Curriculum vitae

ADDRESS C. San Juan Bosco Nº63-4A, E-04005 Almería, Spain.
Mobile phone: +34 / 686 624 707
E-mail: Wolfgang.Gernjak@PSA.ES

DATE of BIRTH June, 29th 1974 in Salzburg, Austria

MARITAL STATUS Single

NATIONALITY Austrian

PROFESSIONAL CAREER

Since Sept. 2002 **External Scientific Staff**

Solar Chemistry Group, Plataforma Solar de Almería, Spain

Responsibilities / Achievements:

♦ **Planning and Management of R+D projects**
♦ **Planning & Execution of R+D testing programmes**
♦ **Participation in** 4 EU & 1 Spanish **R+D projects,** all related with wastewater treatment and drinking water disinfection
♦ **Laboratory Quality Management** (equipped with GC-MS, HPLC-UV, LC-IC, TOC analyser, etc.)
♦ **Set-up of Pilot-Plant** for Integrated Solar Advanced Oxidation Process – Aerobic Biological Treatment
♦ **20 scientific articles,** in peer-reviewed journals, **2 book chapters** and **33 communications** to international congresses

September 2001 – July 2002 **Assistant to the CRM Project Manager**

Market Development MM, Coca Cola Beverages GmbH, Austria

Responsibilities / Achievements:

♦ **Project Management of SFA project**
♦ Implementation of **Sales Force Support Tools**
♦ Development of **Market Analysis Tools**
♦ **Communication interface** between Management, Sales Force and IT department

September 2000 – July 2001 **External Scientific Staff**

Solar Chemistry Group, Plataforma Solar de Almería, Spain

Responsibilities / Achievements:

♦ **Planning & Execution of R+D testing programmes**
♦ **Participation in** 2 EU **R+D projects,** both related with Wastewater treatment

March – July 2000	**Assistant to the Market Development Manager**
August – Sept. 1999	***Market Development MM, Coca Cola Beverages GmbH, Austria***
July – August 1998	

Responsibilities / Achievements:

- ♦ **Market analysis** and **Universe building**
- ♦ Development of supporting tools for the Sales Force

EDUCATION

Since Oct. 2002	Ph.D. studies at the *University of Natural Resources and Applied Life Sciences, Vienna*. Provisional working title of Ph.D.: "Solar Photo-Fenton Treatment for Wastewater Containing Priority Substances. Influence of Process Parameters and Process Control Options". Expected completion April 2006.
Oct. 1995 – May 2002	Studies of Technical Chemistry, branch of study Analytical and Physical Chemistry, at the *Vienna University of Technology*, achieved Austrian academic title Diplomingenieur (Austrian equivalent to MSc.). Graduated with distinction.
Oct. 1992 – Sept. 1995	Studies of German and Roman Philology, subject Spanish at the *Paris Lodron University of Salzburg*
June 1992	Passed Austrian Matura (corresponding to A-Levels) with distinction

LANGUAGES

- ♦ German, native language
- ♦ English, fluent, oral and written
- ♦ Spanish, fluent, oral and written
- ♦ French, basic

SKILLS

- ♦ Result oriented, passionate
- ◆ Good teamworker
- ◆ Empathetic communication style
- ◆ Very good analytical thinking and planning abilities
- ◆ Self-critical
- ◆ Project MM skills (international R+D and private company experience)
- ◆ Excellent computer skills (MS Office, several statistical and programming software)
- ◆ Basic knowledge in accounting

INTERESTS

Travelling, getting to know to new people and ideas, languages, literature, sports (badminton, squash, cycling, swimming)